# INTERACTIONS BETWEEN PODOCYTES, MESANGIAL CELLS, AND GLOMERULAR ENDOTHELIAL CELLS IN GLOMERULAR DISEASES

EDITED BY: John D. Imig, Xueying Zhao, Ahmed A. Elmarakby and Tengis Pavlov
PUBLISHED IN: Frontiers in Pharmacology, Frontiers in Physiology and Frontiers in Medicine

**frontiers** Research Topics

## About Frontiers

Frontiers is more than just an open-access publisher of scholarly articles: it is a pioneering approach to the world of academia, radically improving the way scholarly research is managed. The grand vision of Frontiers is a world where all people have an equal opportunity to seek, share and generate knowledge. Frontiers provides immediate and permanent online open access to all its publications, but this alone is not enough to realize our grand goals.

## Frontiers Journal Series

The Frontiers Journal Series is a multi-tier and interdisciplinary set of open-access, online journals, promising a paradigm shift from the current review, selection and dissemination processes in academic publishing. All Frontiers journals are driven by researchers for researchers; therefore, they constitute a service to the scholarly community. At the same time, the Frontiers Journal Series operates on a revolutionary invention, the tiered publishing system, initially addressing specific communities of scholars, and gradually climbing up to broader public understanding, thus serving the interests of the lay society, too.

## Dedication to Quality

Each Frontiers article is a landmark of the highest quality, thanks to genuinely collaborative interactions between authors and review editors, who include some of the world's best academicians. Research must be certified by peers before entering a stream of knowledge that may eventually reach the public - and shape society; therefore, Frontiers only applies the most rigorous and unbiased reviews.
Frontiers revolutionizes research publishing by freely delivering the most outstanding research, evaluated with no bias from both the academic and social point of view. By applying the most advanced information technologies, Frontiers is catapulting scholarly publishing into a new generation.

## What are Frontiers Research Topics?

Frontiers Research Topics are very popular trademarks of the Frontiers Journals Series: they are collections of at least ten articles, all centered on a particular subject. With their unique mix of varied contributions from Original Research to Review Articles, Frontiers Research Topics unify the most influential researchers, the latest key findings and historical advances in a hot research area! Find out more on how to host your own Frontiers Research Topic or contribute to one as an author by contacting the Frontiers Editorial Office: frontiersin.org/about/contact

# INTERACTIONS BETWEEN PODOCYTES, MESANGIAL CELLS, AND GLOMERULAR ENDOTHELIAL CELLS IN GLOMERULAR DISEASES

Topic Editors:
**John D. Imig,** Medical College of Wisconsin, United States
**Xueying Zhao,** Morehouse School of Medicine, United States
**Ahmed A. Elmarakby,** Augusta University, United States
**Tengis Pavlov,** Henry Ford Health System, United States

# Table of Contents

# Editorial: Interactions Between Podocytes, Mesangial Cells, and Glomerular Endothelial Cells in Glomerular Diseases

John D. Imig[1]*, Xueying Zhao[2], Ahmed A. Elmarakby[3] and Tengis Pavlov[4]

[1] Drug Discovery Center, Medical College of Wisconsin, Milwaukee, WI, United States, [2] Department of Physiology, Morehouse School of Medicine, Atlanta, GA, United States, [3] Department of Oral Biology and Diagnostic Sciences, Augusta University, Augusta, GA, United States, [4] Division of Hypertension and Vascular Research, Henry Ford Health System, Detroit, MI, United States

**Editorial on the Research Topic**

**Interactions Between Podocytes, Mesangial Cells, and Glomerular Endothelial Cells in Glomerular Diseases**

## INTRODUCTION

The complex mechanism by which kidneys fail and progress to end stage renal disease (ESRD) involves renal hemodynamics, glomerular function, and tubular function. A progressive decline in glomerular filtration (GFR) to ESRD ultimately requires dialysis and kidney transplantation (Foley and Collins, 2007). All types of glomerular cells including podocytes that maintain the filtration barrier, mesangial cells that have contractile properties, parietal epithelial cells that serve as podocyte progenitors and glomerular endothelial cells that respond to changes in shear stress and plasma constituents maintain proper glomerular function (Daehn and Duffield, 2021). During renal diseases these glomerular cells and cell interactions become dysfunctional (Daehn and Duffield, 2021). Glomerular diseases are common and include minimal change disease, focal segmental glomerulosclerosis, membranous nephropathy, and lupus nephritis.

This Research Topic captures changes in glomerular cell types resulting in progressive decline in GFR to ESRD. Research publications span cell signaling, animal studies, disease pathology studies, renal hemodynamics, and glomerular function. The Research Topic contains ten contributions that demonstrate the exciting investigations on interactions between podocytes, mesangial cells, and glomerular endothelial cells in glomerular diseases.

## GLOMERULAR MODELING

The complexity of the glomerulus and glomerular filtration barrier has led to modeling that considers the functions of the different cell types. A review article provides an update on the ever-expanding research efforts to model glomerular function (Ebefors et al.). This wave of new modeling technologies includes glomerulus-on-a-chip, three dimensional microfluidic models, and organoids that can enable better predictions of cell-to-cell interactions in the glomerulus. The continuous development of better modeling of the glomerulus is sure to accelerate discoveries that will lead to better therapeutics for glomerular diseases.

# IMMUNOGLOBULIN A (IGA) AND MEMBRANOUS NEPHROPATHY

Four original research articles to the Research Topic tackle IgA and membranous nephropathy. A major complexity to glomerular diseases is that multiple diseases can occur at the same time in patients. The combination of IgA nephropathy and minimal change were the focus of a retrospective patient cohort study (Li et al.). The findings of this study revealed that low levels of plasma galactose deficient IgA1 (GdIgA1), IgG antiglycan autoantibodies were found in patients with combined IgA nephropathy and minimal change disease (Li et al.). The plasma from these IgA nephropathy and minimal change patients resulted in a weaker inflammatory response when added to mesangial cells than plasma from IgA nephropathy patients (Li et al.). A second study evaluated plasma from IgA nephropathy patients and podocyte injury (Jia et al.). Angiopoietin-like protein 4 (Angptl4) levels in IgA nephropathy patients correlated with podocyte injury (Jia et al.). The next two studies evaluated traditional Chinese medicines on nephropathy. The ability for modified Huangqi decoction (MHCD) to reduce IgA nephropathy in rats was determined (Chang et al.). MHCD reduced proteinuria, decreased mesangial cell hyperplasia and matrix expansion, and increased podocyte number in IgA nephropathy rats (Chang et al.). A study in patients with refractory idiopathic membranous nephropathy demonstrated that Shulifenxiao treatment for up to 2 years had a favorable safety profile, increased the remission rate, and improved glomerular function (Cui et al.). These studies highlight factors that contribute to damaging glomerular cells in nephropathies and potential therapies that target glomerular cells to combat nephropathies.

# VASCULAR ENDOTHELIAL GROWTH FACTOR INHIBITION AND GLOMERULAR TOXICITY

Vascular endothelial growth factor (VEGF) inhibition on glomerular function is the topic in two articles that are published in this Research Topic. VEGF inhibitors are given systemically to treat cancers and intravitreally for age-related macular degeneration and diabetic retinopathy (Hanna et al.; Jankiewicz et al.). A hypothesis and theory article puts forth evidence that intravitreally administered VEGF inhibitors can cause thrombotic microangiopathy and acute kidney injury (Hanna et al.). This supports the concept that glomerular disease needs to be monitored in patients receiving in intravitreally administered VEGF inhibitors (Hanna et al.). Next, the ability for a dual soluble epoxide hydrolase (sEH) and cyclooxygenase-2 (COX-2) inhibitor, PTUPB to combat hypertension and glomerular injury during systemic administration of the VEGF and multikinase inhibitor sorafenib is demonstrated (Jankiewicz et al.). PTUPB was able to decrease glomerular permeability and improve podocyte and mesangial cell function in rats administered sorafenib (Jankiewicz et al.). Taken together, the glomerular damage induced by VEGF inhibitors needs to be monitored; however, novel therapies to mitigate the glomerular damage are on the horizon.

# OTHER GLOMERULAR DISEASES

Various aspects of kidney and glomerular damage are the focus of a review and two scientific studies published in this Research Topic. Hyperuricaemia which occurs due to alterations in urate production and excretion was the focus of a review article (Sun et al.). Urate transporters in the kidney provide a mechanism for therapies to lower urate levels in hyperuricaemia (Sun et al.). Glomerular nephropathy can be induced by environmental factors falling under the responsibility of occupational safety and health. Trichloroethylene is solvent widely used for degreasing metal, parts cleaning and exposure to this chemical exceeds 20,000 industry and warehouse workers every year in China. Wang and colleagues report signs of renal insufficiency in six patients with occupational medicamentosa-like dermatitis due to TCE. To study mechanisms of renal toxicity of TCE, the authors administer trichloroethylene in Freund's complete adjuvant to Balb/c mice (Wang et al.). The sensitized animals exhibit ultrastructural damage and loss of podocytes, plus increased plasma BUN and creatinine. The involvement of mTOR/cathepsin-L hyperactivity in TCE-induced renal damage is demonstrated by a series of rapamycin treatments and histopathological analyses (Wang et al.). Nephrology patients develop extrarenal abnormalities due to uremia, vitamin D deficiency, electrolyte imbalance and other complications. Hemodialysis brings additional risks—access complications and use of anticoagulants. As a result, dialysis patients exhibit systemic vascular damage and inflammation which erodes the glycocalyx layer. Kusuzawa et al. present a single-center study featuring whether syndican-1, a polysaccharide component of glycocalyx, can be used as a marker of endothelial injury in patients on dialysis. The authors analyze syndican-1 level in relation to the procedure settings, fluid removal, and use of anticoagulants and conclude that assessment of syndican-1 can be used in the selection of treatment and limiting endothelial injury (Kusuzawa et al.).

# CONCLUSIONS

The Research Topic *Interactions between podocytes, mesangial cells, and glomerular endothelial cells in glomerular diseases* demonstrates the need for a better understanding of mechanisms that contribute to glomerular function and damage. This collection of ten articles demonstrates that glomerular diseases are diverse and include different glomerular cell types and their interactions. Therefore, there is great need for a better understanding of these glomerular cell types in diseases to allow for the development of effective therapies to combat glomerular diseases.

## AUTHOR CONTRIBUTIONS

JI conceived the content and drafted the manuscript. JI, XZ, AE, and TP revised and approved the final manuscript. All authors contributed to the article and approved the submitted version.

## REFERENCES

Daehn, I. S., and Duffield, J. S. (2021). The glomerular filtration barrier: a structural target for novel kidney therapies. *Nat. Rev. Drug Discov.* 20, 770–788. doi: 10.1038/s41573-021-00 242-0

Foley, R. N., and Collins, A. J. (2007). End-stage renal disease in the United States: an update from the United States Renal Data System. *J. Am. Soc. Nephrol.* 18, 2644–2648. doi: 10.1681/ASN.200702 0220

**Conflict of Interest:** The authors declare that the research was conducted in the absence of any commercial or financial relationships that could be construed as a potential conflict of interest.

## FUNDING

**frontiers**
in Medicine

# Thrombotic Microangiopathy and Acute Kidney Injury Induced After Intravitreal Injection of Vascular Endothelial Growth Factor Inhibitors VEGF Blockade-Related TMA After Intravitreal Use

Ramy M. Hanna[1]*, Ngoc-Tram Tran[2], Sapna S. Patel[2], Jean Hou[3], Kenar D. Jhaveri[4], Rushang Parikh[4], Umut Selamet[5], Lena Ghobry[6], Olivia Wassef[7], Marina Barsoum[8], Vanesa Bijol[9], Kamyar Kalantar-Zadeh[1], Alex Pai[1], Alpesh Amin[10], Baruch Kupperman[11] and Ira B. Kurtz[7,12]

[1] Division of Nephrology, Department of Medicine, University of California (UC) Irvine School of Medicine, Orange, CA, United States, [2] Division of Nephrology, Department of Medicine, Long Beach Memorial Medical Center, Long Beach, CA, United States, [3] Department of Pathology and Laboratory Medicine, Cedars Sinai Medical Center, Los Angeles, CA, United States, [4] Division of Kidney Diseases and Hypertension, Donald and Barbara Zucker School of Medicine at Hofstra/Northwell, Great Neck, NY, United States, [5] Division of Renal Medicine, Department of Internal Medicine, Brigham and Women's Hospital, Boston, MA, United States, [6] School of Public Health, University of Pittsburgh, Pittsburgh, PA, United States, [7] Division of Nephrology, Department of Medicine, University of California, Los Angeles, Los Angeles, CA, United States, [8] Keck School of Science and Technology, School of Pharmacy, Chapman University, Orange, CA, United States, [9] Department of Pathology, Donald and Barbara Zucker School of Medicine at Hofstra/Northwell, Great Neck, NY, United States, [10] Department of Medicine, University of California (UC) Irvine, Orange, CA, United States, [11] Herbert Gavin Eye Institute, Department of Ophthalmology, University of California (UC) Irvine, Irvine, CA, United States, [12] Brain Research Institute, University of California Los Angeles (UCLA), Los Angeles, CA, United States

Vascular endothelial growth factor (VEGF) inhibition can cause worsening hypertension, proteinuria, chronic kidney injury, and glomerular disease. Thrombotic microangiopathy (TMA) and other nephrotic disorders have been reported with systemic VEGF blockade. These same agents are given intravitreally for age-related macular degeneration (AMD) and diabetic retinopathy (DR), albeit at lower doses than those given for systemic indications. Systemic absorption of anti-VEGF agents when given intravitreally has been shown consistently along with evidence of significant intravascular VEGF suppression. While worsening hypertension has only been seen in some large-scale studies, case reports show worsening proteinuria and diverse glomerular diseases. These include TMA-associated lesions like focal and segmental glomerulosclerosis with collapsing features (cFSGS). In this paper, we report three cases of TMA likely associated with the use of intravitreal anti-VEGF therapy. These patients developed the signature lesion of VEGF blockade in a 6 to 11 month time frame after starting intravitreal VEGF inhibitors. The literature is reviewed showing similar cases. Intravitreal VEGF blockade may cause these adverse events in a hitherto unidentified subgroup of patients. Well-controlled prospective observational trials are needed to determine the event rate and identify which subgroups of patients are at increased risk. A registry for patients who develop worsening

hypertension, proteinuria exacerbation, and glomerular diseases from intravitreal VEGF blockade is proposed.

## INTRODUCTION

Vascular endothelial growth factor (VEGF) is intimately involved in the physiological function of the glomerulus. Endothelial cells rely on VEGF signaling as trophic signals and for control of diacylglycerol kinase epsilon (DAG-ε). DAG-ε can induce thrombosis if not tightly regulated (1–4). Podocytes rely on VEGF for cytoskeletal organization via nephrin, and trophic signaling is also mediated in podocyte cells via VEGF signaling (autocrine or otherwise) (1). This signaling system interacts with Rel-A (REL-associated protein) and prevents upregulation of renin–angiotensin–aldosterone signaling (RAAS) via the pro-inflammatory nuclear factor kappa B (NF-κB). Tyrosine kinase pathways interact with C-Maf-inducing protein (C-MIP) (1, 2, 5, 6). The blockade of this critical system has various pharmacological applications, namely, the inhibition of angiogenesis. As such, VEGF inhibition has served as a cornerstone of adjunct chemotherapeutic effects for blockage of angiogenesis, limiting tumor growth (1–3, 5, 7).

As a result of the clinical success of these agents, anti-VEGF treatments were adapted for intravitreal usage for patients with neovascularization. Age-related macular degeneration (AMD), diabetic macular edema (DME), and central retinal vein obstruction became amenable to pharmacotherapy (8, 9). Systemic blockade of VEGF leads to several well-known side effects (10–12). These include worsening hypertension, *de novo* proteinuria, renal limited thrombotic microangiopathy (TMA), and various other causes of nephrotic syndrome (13, 14).

The US Food and Drug Administration (FDA) never approved bevacizumab for intravitreal use but did approve aflibercept (Eylea®) and ranibizumab (Lucentis®) for intravitreal use. The label inserts state that the serum drug levels with intravitreal injections were 200-fold lower than the levels achieved by systemic administration, and thus, VEGF inhibition would be minimal (15, 16). However, data published by Avery et al. showed that intravitreal absorption could be significant (at or above 50% inhibitory concentration) and result in significant inhibition of systemic VEGF for days to weeks after intravitreal injections (8, 9, 17, 18).

Avery et al., Jampol et al., Rogers et al., and Zehetner et al. showed that intravitreal injections of VEGF inhibitors caused significant depletion of circulating systemic VEGF levels (8, 9, 17–21). The search for the clinical consequences of this observed VEGF depletion has been ongoing since these results were published. Various studies showed worsening blood pressure and hematological changes (22, 23). Recently, various groups found differences in mortality and post cardiovascular and cerebrovascular event mortality and morbidity (22–26) [though the results are not all in agreement (27–29)].

Glassman et al. and Kameda et al. did not find obvious population-wide effects of acute kidney injury (AKI) after intravitreal VEGF injections. There was also no evidence that all patients had worsening of proteinuria category between Kidney Disease Improving Global Outcomes (KDIGO) A1 to A3 (30, 31). A1 patients tended to stay in the A1 category and A3 patients tended to stay in A3. Bagheri et al. showed a positive change in hypertension, systemic VEGF levels, hemoglobin, and platelets, and though not statistically significant, 45% of patients showed worsening proteinuria after intravitreal bevacizumab (22). It is increasingly clear that a subgroup of patients may be experiencing these changes, and many factors are involved in modulating the response in a given patient.

Many confounding factors exist like vitreal absorption, total dose of drug, and genetics of response to VEGF blockade (1, 2). We present three cases of clear TMA with rapid decline of renal function in diabetic, hypertensive patients. These changes are clinically observed to occur after introduction of intravitreal VEGF inhibitors for the indication of diabetic retinopathy (DR). These cases demonstrate clearly that glomerular pathologies can be superimposed on a background of kidney disease due to diabetic nephropathy. See **Table 1**.

## METHODS

Documented (written) informed consent was obtained from the individuals in cases 1–3 for the publication of any potentially identifiable images or data included in this article; we endeavored to have no identifying information to be used in this report.

### Case 1

A 56 year-old Caucasian male with a history of type 2 diabetes mellitus with an elevated hemoglobin A1c (8.1%) (reference range: <5.7%) is reported. He has a history of moderate hypertension and chronic kidney disease with a serum creatinine of 0.9 mg/dl (reference range: 0.7–1 mg/dl) in 4/2018 [estimated glomerular filtration rate (eGFR) = 96 ml/min] (reference range: 90–120 ml/min). He was referred to nephrology care for proteinuria. The patient was diagnosed with DR and diabetic nephropathy with a urine microalbumin-to-creatinine ratio of 360 mg of albumin per gram of creatinine noted in early 2019 (reference range: <30 μg/mg or mg/g). When he first presented to care in late 2018/early 2019, he had not taken any non-steroidal anti-inflammatory agents and was only on proton pump inhibitor (pantoprazole), which was then switched to a histamine receptor 2 antagonist (ranitidine) after a short duration of use.

He complained of progressively blurry vision and was seen by an ophthalmologist, after which he was started on intravitreal

| References | N | Age | Gender | Agent | Pathology on biopsy |
|---|---|---|---|---|---|
| Hanna et al. (2) | 4 | 53-82 | F,F,F,M | Bev and Ran | Biopsy proven MCD, 45% increased proteinuria (NS), worsening HTN, Increased platelets |
| Nobakht et al. (4) | 1 | 96 | F | LucBevAflib | Biopsy proven CFSGS |
| Bagheri et al. (22) [study] | 18/40 | 60.3 ±9.2y | 33F, 7M | Bev | 45% of patients with increased proteinuria |
| Rasier et al. (23) [study] | 82 | 67.2 ± 5.2 | 44F, 38M | Bev | Significant increase in SBP and DBP |
| Chenugpasitporn et al. (32) | 2 | 56,67 | M, M | Bev | Biopsy proven MCD. Biopsy proven TMA |
| Diabetic Retinopathy Clinical Research Network et al. (33) | 3 | NR | NR | Bev | Decreased eGFR |
| Georgalas et al. (34) | 2 | 51/68 | F,M | Ran & Bev | Decreased eGFR |
| Jamrozy-Witkowska et al. (35) | 1 | NR | NR | NR | Decreased eGFR |
| Kenworthy et al. (36) | 1 | 88 | F | Bev | Increased Proteinuria |
| Khneizer (37) | 1 | 74 | M | Bev | Biopsy proven MGN |
| Morales et al. (38) | 1 | 56 | M | Ran | Increased Proteinuria, biopsy proven DN |
| Pelle et al. (39) | 1 | 77 | F | Ran | Biopsy proven TMA |
| Perez-Valdivia et al. (40) | 1 | 54 | M | Bev | Biopsy proven MCD relapse |
| Sato et al. (41) | 1 | 16 | F | Bev | Biopsy proven MCD relapse |
| Tran (42) | 1 | 51 | M | Bev | Biopsy proven AIN |
| Touzani et al. (43) | 1 | 72 | M | Bev | Biopsy proven TMA |
| Yen and Zhang (44) | 1 | 56 | M | Bev | Biopsy proven Endotheliosis/TMA changes |
| Hanna et al. (45) | 1 | 38 | F | BevRan | Worsening HTN and proteinuria, lessened with Ran use vs. Bev |
| Shye et al. (46) | 3 | 58 | M | Bev | Decreased eGFR, Biopsy proven CFSGS and AIN, and biopsy proven AIN |
| Chung et al. (47) [study] | 53 | 59.8 average age | 31F, 29M | Bev | Significant worsening in proteinuria after bevacizumab in already proteinuric patients |
| (Phadke-Hanna) (UR) | 1 | 74 | M | RanAflib | Biopsy proven CFSGS with TMA |
| (Hanna) CC | 3 | 56,43,77 | F, F, M | Bev x 2, Aflib x 1 | Chronic TMA x 2, FSGS, Endotheliosis/Chronic TMA |

*Aflib, aflibercept; AIN, allergic interstitial nephritis; Bev, bevacizumab; CC, current case; CFSGS, collapsing focal and segmental sclerosis; DBP, diastolic blood pressure; eGFR, estimated glomerular filtration rate; F, female; FSGS, focal and segmental sclerosis; HTN, hypertension; M, male; MCD, minimal change disease; MGN, membranous glomerulonephritis; N, number; NS, not significant; Ran, ranibizumab; SB, systolic blood pressure; TMA, thrombotic microangiopathy, UR, under review.*

VEGF inhibitor therapy in late 2018 to 1/2019. Intravitreal injections of bevacizumab (1.25 mg) were given in each eye (2.5 mg injected total) every 2 months until 7/2019 when he had a more severe episode of recurrent macular edema. This necessitated switching the anti-VEGF regimen to a monthly interval. This was also deemed necessary due to the development of possible early central retinal vein occlusion. According to this dosing schedule, the patient received a total of 20 mg bevacizumab between both eyes throughout 2019 [1.25 mg OU 1/2019 (2.5 mg), 1.25 mg OU 3/2019 (2.5 mg), 1.25 mg OU 5/2019 (2.5 mg), 1.25 mg OU 7/2019 (2.5 mg), 1.25 mg OU 8/2019 (2.5 mg), 1.25 mg OU 9/2019 (2.5 mg), 1.25 mg OU 10/2019 (2.5 mg), 1.25 mg OU 11/2019 (2.5 mg)].

Early in 2019, the patient's serum creatinine rose to 1.44 mg/dl and then 1.86 mg/dl by 4/2019 (reference range: 0.7–1 mg/dl). In the latter half of 2019, the patient presented to nephrology with severely increased blood pressure, first in 9/2019 with a blood pressure of 214/107 mmHg and again in 10/2019 with a blood pressure of 236/108 mmHg; dyspnea; and severely worsened bilateral lower-extremity edema. At this time, the patient had an elevated serum creatinine of 3.6 mg/dl, as well as a microalbumin/creatinine ratio of >600 μg/mg (reference range: <30 μg/mg or mg/g) (none on baseline in 2018 and 359 μg/mg in

04/2019). A 24-h urine protein collection revealed that the patient had nephrotic range proteinuria with a total of 6.5 g of protein per day (reference range: <80 mg/24 h). Hypoalbuminemia had greatly worsened to 2.8 g/dl from a baseline of 3.8 g/dl in 4/2018 (reference range: 3.4–5.4 g/L). The patient's severe hypertension prompted admission for blood pressure control. After the patient's hypertension was controlled, a kidney biopsy was obtained given the rapid onset of renal dysfunction, worsening proteinuria, and accelerated hypertension (**Figure 1**).

From the biopsy samples, 33 glomeruli were identified, four of which were globally sclerotic. Three glomeruli contained lesions of segmental sclerosis characterized by luminal obliteration by insudates, foam cells, and lipid, with focal adherence to Bowman's capsule (**Figure 2A**). The glomeruli were normal in size with predominantly single-contoured capillary basement membranes with segmental double contours (**Figure 2B**) and patent capillary lumina. Mesangial areas showed diffuse and focal nodular expansion by matrix material with segmental mesangiolysis and microaneurysm formation. Few glomeruli displayed variable ischemic changes. No crescents or necrotizing features were present. There was moderate parenchymal scarring with mild interstitial inflammation. Arteries displayed moderate intimal fibrosis, and

**FIGURE 1** | Trend of lab values over time in a patient with diabetic retinopathy treated with bevacizumab and subsequent thrombotic microangiopathy. Bev, bevacizumab; Cr, creatinine; dl, deciliter; eGFR, estimated glomerular filtration rate; mg, milligram; ml, milliliter; min, minute.
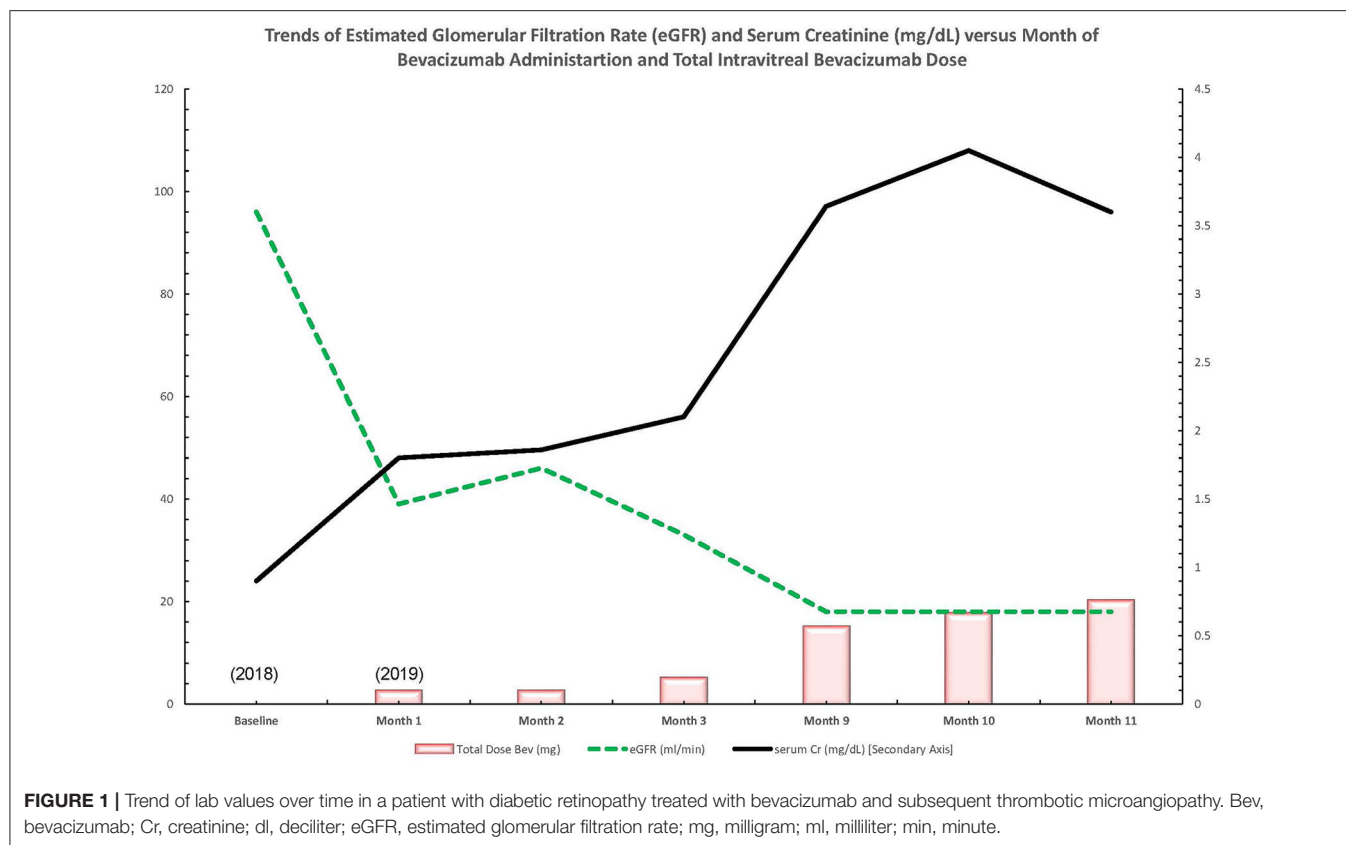
arterioles showed prominent afferent and efferent hyalinization. Immunofluorescence was negative for significant glomerular immune complex deposition.

Electron microscopy revealed glomerular basement membranes with normal trilaminar structure and global thickening (up to 1,440 nm). Segmentally, there was mild electron lucent, subendothelial widening with segmental glomerular basement membrane duplication and mesangial cell interposition. Focally within these areas, there was accumulation of flocculent and electron lucent debris with mild layering of new basement membrane material (**Figure 2C**). Mesangial areas were expanded by matrix material, and there was ∼50% podocyte foot process effacement. The pathological findings showed a renal TMA in a background of diabetic nephropathy.

With the diagnosis of TMA, review of peripheral blood smears and laboratory parameters was undertaken. Peripherally, there were no schistocytes, and vitamin B12 level was 571 pg/ml (reference range: 300–950 pg/ml). ADAMTS13 was 117% of reference range activity (reference range: 50–160%). Severe ADAMTS13 deficiency was <5–10%. This ruled out any ADAMTS13 deficiency/thrombotic thrombocytopenic purpura. No diarrhea was noted, suggesting that there was no typical hemolytic uremic syndrome or evidence for the presence of Shiga toxin (reference range: undetectable). Platelets remained in normal range (reference range: 150,000–450,000/uL) despite hemoglobin level decline over the course of the year. Serum VEGF level on intravitreal anti-VEGF therapy was 34 pg/ml,

which is near the lower limit of the reference range (reference range: 31–310 pg/ml). The presentation did not seem to fit the classical systemic presentation of an atypical hemolytic uremic syndrome but rather seemed to conform to a renal limited TMA as the biopsy suggested.

The patient's serum creatinine worsened to a level of 3.6–3.64 mg/dl (reference range: 0.7–1 mg/dl) a year after presentation. Intravitreal injections were discussed with the patient as a possible cause for TMA, but as of now, they are being continued due to the patient's severe visual impairment. The patient is now preparing for hemodialysis. **Table 2** summarizes lab value trends for cases 1–3.

## Case 2

A 43 year-old female with a history of type 2 diabetes mellitus had a subacute decline of her kidney function over 6 months, which was faster than expected for typical diabetic nephropathy. The treating physician noted that this occurred after the initiation of intravitreal bevacizumab. Her initial serum creatinine was reported only as normal, but her final serum creatinine was reported as 3.6 mg/dl (reference range: 0.7–1 mg/dl) with a eGFR < 30 ml/min (stage IV CKD, G4, A3) (reference range: 90–120 ml/min). She had >3 g/day of proteinuria (reference range: <80 mg/day).

Given the standard bevacizumab dose of 1.25–2.5 mg every month, the estimated total dose she was exposed to is estimated to be up to 7.5–15 mg intravitreally over
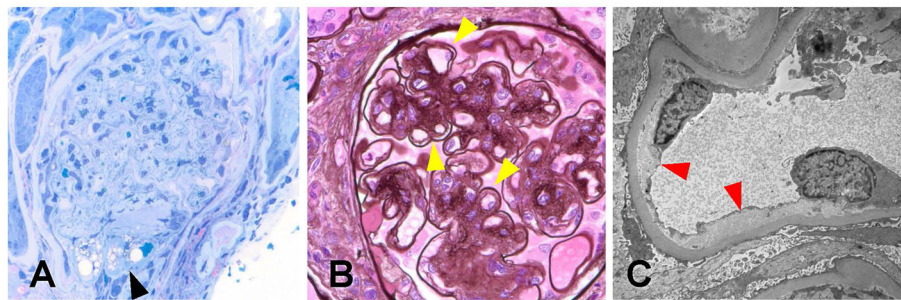
**FIGURE 2 |** Biopsy findings in patient 1 with diabetic retinopathy and nephropathy treated with bevacizumab and subsequent thrombotic microangiopathy. **(A)** One glomerulus showed segmental luminal obliteration by insudates and lipid, with adherence to Bowman's capsule consistent with segmental glomerulosclerosis (arrowhead, methylene blue stain, 400×). **(B)** Few glomeruli demonstrated segmental duplication of glomerular basement membranes (arrowhead, Jones methenamine silver stain, 400×). **(C)** Ultrastructural analysis revealed segmental subendothelial electron lucent widening, with very early duplication of basement membrane material (arrowheads, 20,000×). The light and ultrastructural findings were consistent with chronic thrombotic microangiopathy.

**TABLE 2 |** A1c, glycated hemoglobin; ADAMTS13, a disintegrin and metalloproteinase thrombospondin motif #1, member # 13; B12 cyanocobalamin; dL, BL, baseline; deciliter; eGFR, estimated glomerular filtration rate; g, gram; L, liter; min, minute; mL, milliter; VEGF, vascular endothelial growth factor; VEGFi, VEGF inhibitor; uL, microliter.

| Lab value | Case 1 BL | Case 1 Post-VEGFi | Case 2 BL | Case 2 Post-VEGFi | Case 3 BL | Case 3 post VEGFi |
|---|---|---|---|---|---|---|
| Age | 56 | | 43 | | 77 | |
| Gender | Male | | Female | | Female | |
| Identified ethnicity | Caucasian | | Hispanic | | Guyanese | |
| Total Dose of VEGFi | 20 mg Bevacizumab (2018–2020) | | 7.5–15 mg bevacizumab | | Ranibizumab (unknown quantity), 28 mg of aflibercept given | |
| Time frame of AKI in relation to initiation or changes to intravitreal VEGFi | 2 years after starting bevacizumab 1 year after increasing frequency of injections | | 6 months after bevacizumab initiation | | Year after changing from ranibizumab to aflibercept | |
| Serum Creatinine (mg/dL) | 0.9 (2018) | 1.8–3.6 (2019) | Normal | 3.6 (2019) | 1 (2019) | 1.4 (2020) |
| eGFR (ml/min) | 96 (2018) | 54–18 (2019) | Not reported | 25–30 (2019) | 51 (2019) | 37 (2020) |
| Hemoglobin (g/dL) | 13 (2018) | 7.7–11.1 (2019) | Not reported | Not reported | Normal (2019) | Normal (2020) |
| Platelets (/uL) | 256,000(2018) | 210–248,000 (2019) | Not reported | Not reported | Normal (2019) | Normal (2020) |
| Albumin (g/L) | 3.8 (1/2019) | 3.4 to 2.8 (11/2019) | Not reported | Not reported | Normal (2019) | Normal (2020) |
| Hemoglobin A1C (%) | 10.4 (1/2019) | 6.4–6.6 (11/2019) | Not reported | Not reported | 5–5.7% (2019) | 5–5.7% (2020) |
| Systolic blood pressure (mmHg) | 134–177 (every 2–month VEGF inhibitor) | 177–236 (every 1–month VEGF inhibitor eye injections) | 150–160 (2019) | 150–160 (2019) | Normal (2019) | 150 (2020) |
| Diastolic blood pressure (mmHg) | 74–86 (every 2–month VEGF inhibitor) | 74–108 (every 1–month VEGF inhibitor eye injections) | 90 (2019) | 90 (2019) | Normal (2019) | 100 (2020) |
| 24 hour urine total protein (g/day) | Not reported | 6.5 (10/2/2019) | Not reported | >3 (2019) | Not reported (2019) | 0.8 (2020) |
| Urine microalbumin/Creatinine ratio (mcg/mg or mg/g) | 360 | >600 (9–11/2019) | Not reported | Not reported | <30 (2019) | 800 (2020) |
| Serum VEGF level (pg/mL) | Not reported | 34 (11/2019) | Not reported | Not reported | Not reported | Not reported |
| ADAMTS13 (%) | Not reported | 117(11/2019) | Not reported | Not reported | Not reported | Not reported |

6 months. She was noted to have accelerated worsening of her hypertension and nephrotic range proteinuria, but this was successfully controlled with blood pressure medications without improvement in her renal function. The worsening of blood pressure, proteinuria, and kidney function was noted to have occurred contemporaneously with initiating intravitreal bevacizumab for DR/DME. The

patient had moderate hypertension at 150–160 mmHg systolic blood pressure but did not have clinically apparent malignant hypertension.

The biopsy identified, overall, 29 glomeruli, eight of which were globally sclerotic. Glomeruli ranged in size from normal to enlarged with single-contoured capillary basement membranes and predominantly patent capillary lumina. One glomerulus

displayed segmental luminal obliteration by insudates and lipid. Immunofluorescence staining revealed prominent staining for fibrinogen within these arterioles (**Figure 3A**). Arteries displayed mild to moderate intimal fibrosis, and arterioles had muscular hypertrophy, insudates, and mucoid intimal thickening with luminal narrowing and endothelial cell swelling (**Figure 3B**). Mesangial areas displayed diffuse and nodular expansion by matrix material (**Figure 3C**). No crescents or necrotizing features were noted. There was severe parenchymal scarring with mild interstitial inflammation.

Electron microscopy revealed glomerular basement membranes with normal trilaminar structure and global thickening (up to 1,210 nm). Segmentally, there were subendothelial lucencies with flocculent material as well as segmental mesangial cell interposition with double-contour formation (**Figure 3D**). Podocytes displayed subtotal foot process effacement. This suggested endothelial injury, a chronic TMA, and concomitant secondary focal and segmental sclerosis due to VEGF blockade. **Table 2** summarizes lab value trends for cases 1–3.

## Case 3

A 77 year-old Guyanese female was referred to nephrology for worsening hypertension and proteinuria. She had had known type 1 diabetes mellitus for over 20 years with known DR and retinal vein disease. She also had a history of hypertension for the last 15 years well controlled on single-agent enalapril 10 mg once a day. She had prior urinalysis done yearly that showed trace protein. In the last few months, she was noticed to have increasing proteinuria of 800 mg over 24 h and worsening hypertension requiring enalapril to be increased to 20 mg twice daily and addition of amlodipine 10 mg daily. In addition, her kidney function had worsened from a serum creatinine of baseline 1.0 mg/dl (reference range: 0.7–1 mg/dl) (eGFR = 51 ml/min; reference range: 90–120 ml/min) to 1.4 mg/dl (eGFR = 37 ml/min). Her physical exam was consistent with a blood pressure of 150/100 mmHg and 1+ lower-extremity edema. Her medication list revealed no nephrotoxic agent and no herbal medications.

Her serological testing was negative for anti-nuclear antibody (ANA) (reference range: <1:20), lupus serologies (reference range: not detected), paraprotein workup (reference range: not detected), and anti-neutrophil cytoplasmic antibody (ANCA) and phospholipase A2 receptor antibody (reference range: not detected). Cell counts (white blood cells, hemoglobin, and platelets) were all within normal limits. Her complements were within normal range, lactate dehydrogenase was normal, and there was no decrease noted in haptoglobin. Her repeat urinary spot protein/creatinine ratio was 0.8. Her hemoglobin A1c had been in the 5.5–7% range (reference range: <5.7%) in the last few years. On further questioning, she mentioned she had been receiving ranibizumab for her DME for 4 years. In the last 1 year, she was switched to aflibercept 2 mg every 4 weeks for each eye, intravitreal for the first 3 months and then every 8 weeks following, leading to a total dose of 28 mg. As a result, a kidney biopsy was performed.
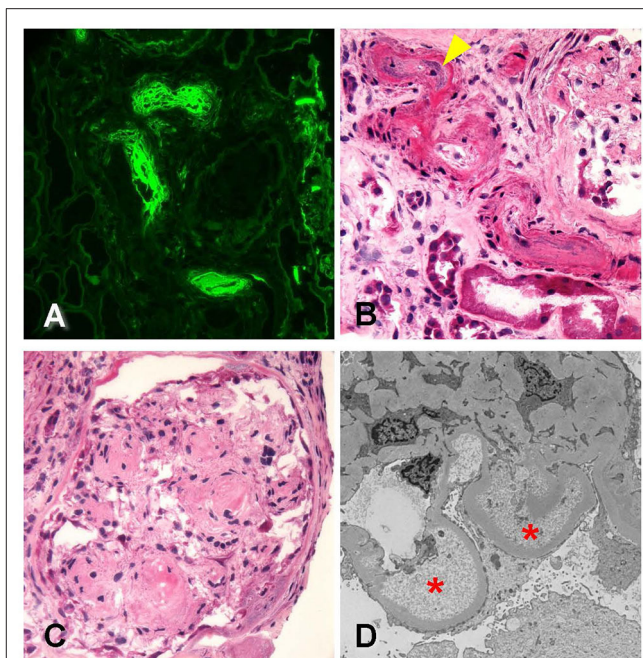


**FIGURE 3 |** Biopsy findings in patient 2 with diabetic retinopathy and nephropathy treated with bevacizumab and subsequent thrombotic microangiopathy. **(A)** Immunofluorescence microscopy revealed scattered arterioles which displayed strong amorphous intraluminal and vessel wall staining for fibrinogen (400×). **(B)** Examination of hematoxylin–eosin (H&E)-stained sections from the frozen tissue demonstrated that the fibrin staining corresponded with changes of arteriopathy, including mucoid intimal thickening (arrowhead) and considerable luminal narrowing, consistent with acute thrombotic microangiopathy (400×). **(C)** Glomeruli showed changes of diffuse and nodular diabetic glomerulosclerosis (600×). **(D)** Ultrastructural analysis revealed glomerular basement membranes which showed prominent subendothelial electron lucent widening with accumulation of flocculent debris (20,000×). Overall, the findings were consistent with acute thrombotic microangiopathy.

The biopsy was dominated by chronic changes, in the setting of severe arterial sclerosis [**Figure 4A**, periodic acid–Schiff (PAS) stain, 200×]. A large subcapsular scar containing 15 globally sclerosed glomeruli was found in one of the biopsy cores. Outside of this scar, there were up to 10 glomeruli, often revealing irregular thickening and segmental remodeling of the capillary loops, with occasional double-contour formation (**Figure 4B**, PAS stain, 400×, yellow arrowheads). The mesangium revealed mild expansion by matrix, without well-developed Kimmelstiel–Wilson nodules. Overall, there was about 40–50% tubular atrophy and interstitial fibrosis in this biopsy sample. No active glomerular or interstitial inflammation was noted. On immunofluorescence microscopy, no immune-type deposits were present, but there was dull reactivity for fibrin along the glomerular capillary walls [**Figure 4C**, fibrinogen fluorescein isothiocyanate (FITC) stain, 200×]. Glomerular capillary walls often revealed subendothelial widening by electron lucent material on electron microscopy (**Figure 4D**, 10,000×, red arrowheads).
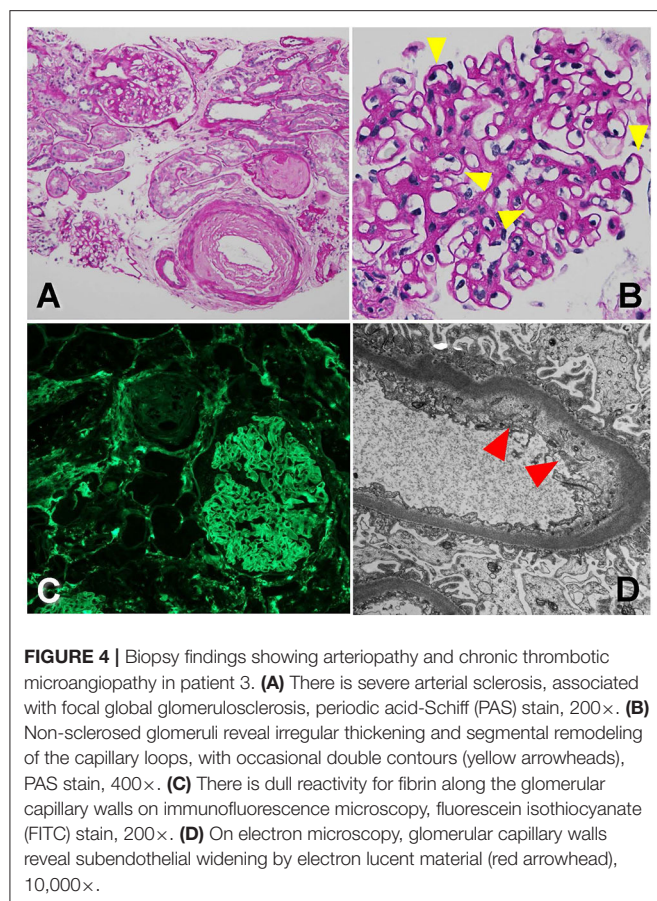
FIGURE 4 | Biopsy findings showing arteriopathy and chronic thrombotic microangiopathy in patient 3. (A) There is severe arterial sclerosis, associated with focal global glomerulosclerosis, periodic acid-Schiff (PAS) stain, 200×. (B) Non-sclerosed glomeruli reveal irregular thickening and segmental remodeling of the capillary loops, with occasional double contours (yellow arrowheads), PAS stain, 400×. (C) There is dull reactivity for fibrin along the glomerular capillary walls on immunofluorescence microscopy, fluorescein isothiocyanate (FITC) stain, 200×. (D) On electron microscopy, glomerular capillary walls reveal subendothelial widening by electron lucent material (red arrowhead), 10,000×.

Given signs of only early diabetic nephropathy on the kidney biopsy and with most of the changes noted to be related to endothelial and vascular damage, we attributed the findings to the anti-VEGF therapy this patient was exposed to over the last few years. The change in renal function and proteinuria timely fit with the initiation of aflibercept, and therefore, reverting back to the initial treatment (ranibizumab) for her DME was prudent. After discussion with the patient's treating retina specialists, she was taken off aflibercept and returned back to ranibizumab intravitreal treatment. **Table 2** summarizes lab value trends for cases 1–3.

## FDA ADVERSE REPORT SYSTEM EVENTS

In addition to reviewing the published literature, we also reviewed the US FDA adverse event reporting system (FAERS) quarterly legacy data file (first quarter of 2010 to second quarter of 2019) for both aflibercept (Eylea®) and ranibizumab (Lucentis®) since the years they were approved specifically for intravitreal indications. Bevacizumab was not reviewed given the mixed results it would provide with use on oncology patients. The adverse event terms queried were proteinuria, renal failure acute, AKI, hypertension, thrombocytopenia nephritis, and TMA. **Table 3** summarizes the data from the FAERS. Hypertension is the most common renal adverse event reported; other notable side effects include proteinuria. Few cases of TMA have been reported to the FDA from both agents. There are more cases reported of ranibizumab over aflibercept given the approval data of the latter being in 2016. Interestingly, most events happened in male patients for unknown reasons.

## DISCUSSION

There are 26 published cases showing worsening hypertension, proteinuria, and glomerular disease after intravitreal VEGF inhibition (2, 4, 32–46). Our group has published nine cases (2, 4, 45, 46). There are three more in this case series and one more under review. In total, there are 30 known cases demonstrating systemic toxicity after intravitreal VEGF inhibitor injections (2, 4, 32–46). See **Table 1**.

The cases presented in this manuscript show renal limited TMA in patients with poorly controlled diabetes and hypertension. The pattern of injury is exactly what is expected with VEGF blockade systemically. The timeline of initiation or increased dosing of intravitreal VEGF blockade fit the timeline of renal injury and proteinuria exacerbation, and this is what suggested the diagnosis clinically. The finding of pathognomonic lesions of VEGF blockade on kidney biopsy confirmed our clinical suspicion.

Other TMA presentations after intravitreal VEGF blockade in the literature are reviewed in **Table 1** (4, 32, 39, 42, 43, 46) along with other published evidence (2, 4, 32–46). Other glomerular lesions such as collapsing glomerulopathy have been associated with intravitreal anti-VEGF agents as well (2, 4). cFSGS is a TMA-associated lesion that has been noted in conjunction with TMA presentations as was seen in case 2 in this series (48).

Tying the pathophysiology with mechanism, evidence of absorption, evidence of VEGF depletion, and clear biopsy findings has made these cases valuable. An important clinical lesson from these cases is that diabetic nephropathy *per se* cannot be invoked to account for an abrupt rise in serum creatinine. In addition, the secondary glomerular findings such as TMA and collapsing glomerulopathy are not features of diabetic nephropathy. It is likely that these renal pathological changes occur preferentially in proteinuric, hypertensive patients with preexisting renal disease. This is similar to preeclampsia, a naturally occurring disease model that approximates the pharmacologic phenomenon of VEGF blockade (49). This model of differential susceptibility to VEGF depletion has been suggested by a recently conducted South Korean study, showing that patients with more proteinuria at baseline were more likely to experience worsening proteinuria after intravitreal VEGF injections (47).

The FAERS database analysis suggests that hypertension might be the most common renal adverse event reported (**Table 3**). This is important as it might be the first sign of a systemic endothelial injury as seen with other anti-VEGF agents in the oncology literature.

These cases are extremely challenging to diagnose, and it is useful to consider the role of intravitreal VEGF blockade in every diabetic patient. The clinician needs to have a high index of suspicion to consider this diagnosis. The meticulous

**TABLE 3 |** Review of FDA FAERS for adverse events affecting Kidney by gender for Lucentis (ranibizumab) and Eylea (aflibercept).

| Name of Medication | Reaction | Male ($N$ = 101) $n$ (%) | Female ($N$ = 160) $n$ (%) | Missing ($N$ = 144) $n$ (%) | Overall ($N$ = 405) $n$ (%) |
|---|---|---|---|---|---|
| Aflibercept (m = 97) | Hypertension | 5 (4.95) | 20 (12.50) | 52 (36.11) | 77 (19.01) |
| | Proteinuria | 5 (4.95) | 0 (0.00) | 6 (4.17) | 11 (2.72) |
| | Thrombocytopenia | 0 (0.00) | 0 (0.00) | 6 (4.17) | 6 (1.48) |
| | Renal Injury | 0 (0.00) | 0 (0.00) | 2 (1.39) | 2 (0.49) |
| | Thrombotic Microangiopathy | 0 (0.00) | 0 (0.00) | 1 (0.69) | 1 (0.25) |
| Ranibizumab(m = 308) | Hypertension | 75 (74.26) | 130 (81.25) | 68 (47.22) | 273 (67.41) |
| | Thrombocytopenia | 7 (6.93) | 8 (5.00) | 3 (2.08) | 18 (4.44) |
| | Thrombotic Microangiopathy | 4 (3.96) | 0 (0.00) | 4 (2.78) | 8 (1.98) |
| | Renal Injury | 3 (2.97) | 1 (0.63) | 1 (0.69) | 5 (1.23) |
| | Proteinuria | 2 (1.98) | 1 (0.63) | 1 (0.69) | 4 (0.99) |

-Adverse events reported as (Renal Failure, Renal Impairment, Renal Failure Acute, Renal Injury, Nephritis) presented as one group (RENAL INJURY).
-Percentage(%)= n/N* 100.

**TABLE 4 |** When to Consider Intravitreal VEGF Toxicity, Referral to Nephrology.

- Rapid worsening of renal function (25% rise in BUN, Cr over short time)
- Unexplained changes in blood pressure (>20 mmHg over short time)
- Rapid or unexpected change in proteinuria (>25% rise over short time)
  - If any of above occur: Check urinalysis, Urine protein to Creatinine ratio, Refer to nephrology
  - If suspicion of intravitreal anti VEGF renal toxicity: consider decreasing dose, change to lower potency VEGF inhibitors (like ranibizumab)

mcg, micrograms; TMA, thrombotic microangiopathy.

measurement of urine protein and albumin in addition to monitoring blood pressure changes is needed to document the effect of VEGF depletion on the kidney. Specialty consultation with a nephrologist in case of abrupt changes in renal parameters and monitoring patients receiving these agents closely are prudent recommendations.

**Table 4** details clinical clues that raise the suspicion that intravitreal VEGF inhibition may be leading to renal or systemic toxicity. Recommendations for referral to specialty nephrology care are also listed in **Table 4**. They are a rise in serum blood urea nitrogen and creatinine by 25% or more acutely, an increase in blood pressure by 20 mmHg acutely, and an increase in urine protein-to-creatinine ratio by 25% or more after initiating intravitreal VEGF blockade (1).

There are comprehensive reviews that highlight the lesions and clinical manifestations seen after intravitreal VEGF blockade (1, 2). The utility of this report is to document three examples of the prototypical renal lesions resulting from systemic VEGF blockade in patients receiving VEGF inhibitors intravitreally. Currently, the only known risk factors for worsening hypertension and proteinuria after intravitreal VEGF injection are preexisting hypertension and proteinuria at baseline.

There is no specific guidance regarding the treatment of intravitreal VEGF inhibitor-associated glomerular lesions at this time. In our experience, oral corticosteroids for treatment of cFSGS lesions induced while patients were getting intravitreal VEGF blockade were not uniformly successful. Given the emerging evidence of efficacy of complement blockade in some

secondary forms of TMA/atypical hemolytic uremic syndrome, use of complement factor 5 blockade may be a therapeutic option (50).

Ultimately, DR and AMD can lead to irreversible visual deterioration and blindness (1). Intravitreal VEGF blockade in ameliorating these diseases has been important. It is important to note that the rate of renal events occurring with intravitreal VEGF blockade requires further study. We acknowledge the importance of intravitreal VEGF blockade but propose that patients receiving intravitreal VEGF blockade require close monitoring (1). If there are concerns regarding renal sequelae after intravitreal VEGF blockade, prompt referral to nephrological care is crucial (1). The importance of the ophthalmologist and retina specialists, who are closely monitoring patients with retinal pathology, cannot be overstated. A registry to track these events can suggest how common the events are, and controlled observational trials following pharmacokinetic data would be helpful. A new era of ophthalmological and nephrological collaboration in research and patient care is clearly needed to fully investigate the systemic risks of intravitreal VEGF blockade.

## DATA AVAILABILITY STATEMENT

The original contributions presented in the study are included in the article, further inquiries can be directed to the corresponding author/s.

## ETHICS STATEMENT

Documented (written) informed consent was obtained from the individuals in cases 1–3, for the publication of any potentially identifiable images or data included in this article.

## AUTHOR CONTRIBUTIONS

RH: lead writing of case series. N-TT: contributed to case 1. SP: contributed to case 2. JH: pathology to case 2. KJ: contributed to case 3. RP: ERAS search. US: contributed to introduction. LG, OW, MB, KK-Z, AP, and AA: editing of

manuscript. VB: pathology of case 3. BK: editing of manuscript from ophthalmology perspective. IK: senior author. All authors contributed to the article and approved the submitted version.

## REFERENCES

1. Hanna RM, Barsoum M, Arman F, Selamet U, Hasnain H, Kurtz I. Nephrotoxicity induced by intravitreal vascular endothelial growth factor inhibitors: emerging evidence. *Kidney Int.* (2019) 96:572–80. doi: 10.1016/j.kint.2019.02.042

2. Hanna RM, Lopez E, Hasnain H, Selamet U, Wilson J, Youssef PN, et al. Three patients with injection of intravitreal vascular endothelial growth factor inhibitors and subsequent exacerbation of chronic proteinuria and hypertension. *Clin Kidney J.* (2018) 12:92–100. doi: 10.1093/ckj/sfy060

3. Hanna RM, Lopez E, Wilson J, Barathan S, Cohen AH. Minimal change disease onset observed after bevacizumab administration. *Clin Kidney J.* (2016) 9:239–44. doi: 10.1093/ckj/sfv139

4. Nobakht N, Nguyen HA, Kamgar M, Abdelnour L, Rastogi A, Hanna RM. Development of collapsing focal and segmental glomerulosclerosis in a patient receiving intravitreal vascular endothelial growth factor blockade. *Kidney Int Rep.* (2019) 4:1508–12. doi: 10.1016/j.ekir.2019.07.019

5. Hanna RM, Selamet U, Hasnain H, El-Masry M, Saab S, Wallace WD, et al. Development of focal segmental glomerulosclerosis and thrombotic microangiopathy in a liver transplant patient on sorafenib for hepatocellular carcinoma: a case report. *Transplant Proc.* (2018) 50:4033–7. doi: 10.1016/j.transproceed.2018.07.020

6. Ollero M, Sahali D. Inhibition of the VEGF signalling pathway and glomerular disorders. *Nephrol Dial Transplant.* (2015) 30:1449–55. doi: 10.1093/ndt/gfu368

7. Hanna RM, Yanny B, Barsoum M, Mikhail M, Al-Baghdadi M, Rastogi A, et al. Everolimus worsening chronic proteinuria in patient with diabetic nephropathy post liver transplantation. *Saudi J Kidney Dis Transpl.* (2019) 30:989–94. doi: 10.4103/1319-2442.265481

8. Avery RL, Castellarin AA, Steinle NC, Dhoot DS, Pieramici DJ, See R, et al. Systemic pharmacokinetics following intravitreal injections of ranibizumab, bevacizumab or aflibercept in patients with neovascular AMD. *Br J Ophthalmol.* (2014) 98:1636–41. doi: 10.1136/bjophthalmol-2014-305252

9. Avery RL, Castellarin AA, Steinle NC, Dhoot DS, Pieramici DJ, See R, et al. Systemic pharmacokinetics and pharmacodynamics of intravitreal aflibercept, bevacizumab, and ranibizumab. *Retina.* (2017) 37:1847–58. doi: 10.1097/IAE.0000000000001493

10. Izzedine H. Anti-VEGF cancer therapy in nephrology practice. *Int J Nephrol.* (2014) 2014:143426. doi: 10.1155/2014/143426

11. Izzedine H, Brocheriou I, Deray G, Rixe O. Thrombotic microangiopathy and anti-VEGF agents. *Nephrol Dial Transplant.* (2007) 22:1481–2. doi: 10.1093/ndt/gfl565

12. Izzedine H, Sene D, Hadoux J, Gharbi C, Bourry E, Massard C, et al. Thrombotic microangiopathy related to anti-VEGF agents: intensive versus conservative treatment? *Ann Oncol.* (2011) 22:487–90. doi: 10.1093/annonc/mdq743

13. Eremina V, Jefferson JA, Kowalewska J, Hochster H, Haas M, Weisstuch J, et al. VEGF inhibition and renal thrombotic microangiopathy. *N Engl J Med.* (2008) 358:1129–36. doi: 10.1056/NEJMoa0707330

14. Hayman SR, Leung N, Grande JP, Garovic VD. VEGF inhibition, hypertension, and renal toxicity. *Curr Oncol Rep.* (2012) 14:285–94. doi: 10.1007/s11912-012-0242-z

15. Eylea FDA package Insert. (2011).

16. Lucentis FDA package Insert. (2012).

17. Avery RL. What is the evidence for systemic effects of intravitreal anti-VEGF agents, and should we be concerned? *Br J Ophthalmol.* (2014) 98(Suppl. 1):i7–10. doi: 10.1136/bjophthalmol-2013-303844

18. Avery RL, Gordon GM. Systemic safety of prolonged monthly anti-vascular endothelial growth factor therapy for diabetic macular edema: a systematic review and meta-analysis. *JAMA Ophthalmol.* (2016) 134:21–9. doi: 10.1001/jamaophthalmol.2015.4070

19. Jampol LM, Glassman AR, Liu D, Aiello LP, Bressler NM, Duh EJ, et al. Plasma vascular endothelial growth factor concentrations after intravitreous anti-vascular endothelial growth factor therapy for diabetic macular edema. *Ophthalmology.* (2018) 125:1054–63. doi: 10.1016/j.ophtha.2018.05.003

20. Rogers CA, Scott L, Reeves BC, Downes S, Lotery AJ, Dick AD, Chakravarthy U. Serum vascular endothelial growth factor levels in the IVAN trial; relationships with drug, dosing, and systemic serious adverse events. *Ophthalmol Retina.* (2018) 2:118–27. doi: 10.1016/j.oret.2017.05.015

21. Zehetner C, Kralinger MT, Modi YS, Waltl I, Ulmer H, Kirchmair R, et al. Systemic levels of vascular endothelial growth factor before and after intravitreal injection of aflibercept or ranibizumab in patients with age-related macular degeneration: a randomised, prospective trial. *Acta Ophthalmol.* (2015) 93:e154–9. doi: 10.1111/aos.12604

22. Bagheri S, Dormanesh B, Afarid M, Sagheb MM. Proteinuria and renal dysfunction after intravitreal injection of bevacizumab in patients with diabetic nephropathy: a prospective observational study. *Galen Med J.* (2018) 7:e1299. doi: 10.22086/gmj.v0i0.1299

23. Rasier R, Artunay O, Yuzbasioglu E, Sengul A, Bahcecioglu H. The effect of intravitreal bevacizumab (avastin) administration on systemic hypertension. *Eye.* (2009) 23:1714–8. doi: 10.1038/eye.2008.360

24. Hanhart J, Comaneshter DS, Freier Dror Y, Vinker S. Mortality in patients treated with intravitreal bevacizumab for age-related macular degeneration. *BMC Ophthalmol.* (2017) 17:189. doi: 10.1186/s12886-017-0586-0

25. Hanhart J, Comaneshter DS, Freier-Dror Y, Vinker S. Mortality associated with bevacizumab intravitreal injections in age-related macular degeneration patients after acute myocardial infarct: a retrospective population-based survival analysis. *Graefes Arch Clin Exp Ophthalmol.* (2018) 256:651–63. doi: 10.1007/s00417-018-3917-9

26. Hanhart J, Comaneshter DS, Vinker S. Mortality after a cerebrovascular event in age-related macular degeneration patients treated with bevacizumab ocular injections. *Acta Ophthalmol.* (2018) 96:e732–9. doi: 10.1111/aos.13731

27. Lee K, Yang H, Lim H, Lew HM. A prospective study of blood pressure and intraocular pressure changes in hypertensive and nonhypertensive patients after intravitreal bevacizumab injection. *Retina.* (2009) 29:1409–17. doi: 10.1097/IAE.0b013e3181b21056

28. Risimic D, Milenkovic S, Nikolic D, Simeunovic D, Jaksic V, Stojkovic M, et al. Influence of intravitreal injection of bevacizumab on systemic blood pressure changes in patients with exudative form of age-related macular degeneration. *Hellenic J Cardiol.* (2013) 54:435–40.

29. Starr MR, Dalvin LA, AbouChehade JE, Damento GM, Garcia MD, Shah SM, et al. Classification of strokes in patients receiving intravitreal anti-vascular endothelial growth factor. *Ophthalm Surg Lasers Imaging Retina.* (2019) 50:e140–57. doi: 10.3928/23258160-20190503-14

30. Glassman AR, Liu D, Jampol LM, Sun JK, Diabetic Retinopathy Clinical Research N. Changes in blood pressure and urine albumin-creatinine ratio in a randomized clinical trial comparing aflibercept, bevacizumab, and

ranibizumab for diabetic macular edema. *Invest Ophthalmol Vis Sci.* (2018) 59:1199–205. doi: 10.1167/iovs.17-22853

31. Kameda Y, Babazono T, Uchigata Y, Kitano S. Renal function after intravitreal administration of vascular endothelial growth factor inhibitors in patients with diabetes and chronic kidney disease. *J Diabetes Investig.* (2018) 9:937–9. doi: 10.1111/jdi.12771

32. Cheungpasitporn W, Chebib FT, Cornell LD, Brodin ML, Nasr SH, Schinstock CA, et al. Intravitreal antivascular endothelial growth factor therapy may induce proteinuria and antibody mediated injury in renal allografts. *Transplantation.* (2015) 99:2382–6. doi: 10.1097/TP.0000000000000750

33. Diabetic Retinopathy Clinical Research Network, Scott IU, Edwards AR, Beck RW, Bressler NM, Chan CK, et al. A phase II randomized clinical trial of intravitreal bevacizumab for diabetic macular edema. *Ophthalmology.* (2007) 114:1860–7. doi: 10.1016/j.ophtha.2007.05.062

34. Georgalas I, Papaconstantinou D, Papadopoulos K, Pagoulatos D, Karagiannis D, Koutsandrea C. Renal injury following intravitreal anti-VEGF administration in diabetic patients with proliferative diabetic retinopathy and chronic kidney disease–a possible side effect? *Curr Drug Saf.* (2014) 9:156–8. doi: 10.2174/1574886309666140211113635

35. Jamrozy-Witkowska A, Kowalska K, Jankowska-Lech I, Terelak-Borys B, Nowosielska A, Grabska-Liberek I. [Complications of intravitreal injections– own experience]. *Klin Oczna.* (2011) 113:127–31.

36. Kenworthy J-A, Davis J, Chandra V, Clark JB, Desmond M. Worsening proteinuria following intravitreal anti-VEGF therapy for diabetic macular edema. *J VitreoRetinal Dis.* (2019) 3:54–6. doi: 10.1177/2474126418815823

37. Khneizer G. A-TA, bastani B Self limited membranous nephropathy after intravitreal nephropathy after intravitreal bevacizumab therapy for age related macular degeneration. *J Nephropathol.* (2017) 6:134–7. doi: 10.15171/jnp.2017.23

38. Morales E, Moliz C, Gutierrez E. Renal damage associated to intravitreal administration of ranibizumab. *Nefrologia.* (2017) 37:653–5. doi: 10.1016/j.nefroe.2017.10.007

39. Pelle G, Shweke N, Duong Van Huyen JP, Tricot L, Hessaine S, Fremeaux-Bacchi V, et al. Systemic and kidney toxicity of intraocular administration of vascular endothelial growth factor inhibitors. *Am J Kidney Dis.* (2011) 57:756–9. doi: 10.1053/j.ajkd.2010.11.030

40. Perez-Valdivia MA, Lopez-Mendoza M, Toro-Prieto FJ, Cabello-Chaves V, Toro-Ramos M, Martin-Herrera MC, et al. Relapse of minimal change disease nephrotic syndrome after administering intravitreal bevacizumab. *Nefrologia.* (2014) 34:421–2. doi: 10.3265/Nefrologia.pre2014.Mar.12388

41. Sato T, Kawasaki Y, Waragai T, Imaizumi T, Ono A, Sakai N, et al. Relapse of minimal change nephrotic syndrome after intravitreal bevacizumab. *Pediatr Int.* (2013) 55:e46–8. doi: 10.1111/ped.12017

42. Tran T. Intravitreal VEGF inhibitor causing allergic interstitial nephritis. *AJKD.* (2017) 69:A99. doi: 10.1053/j.ajkd.2017.02.339

43. Touzani F, Geers C, Pozdzik A. Intravitreal injection of Anti-VEGF antibody induces glomerual endothelial cells injury. *Case Rep Nephrol.* (2019) 2019:2919080. doi: 10.1155/2019/2919080

44. Yen W, Zhang Pl. *Intravitreal Injection of Avastin (IIA) Over Time Can Be Associated with Thrombotic Microangiopathy (TMA) in the Native Kidney. ASN Kidney Week.* Washington, DC: fJASN (2019).

45. Hanna RM, Abdelnour L, Hasnain H, Selamet U, Kurtz I. Intravitreal bevacizumab-induced exacerbation of proteinuria in diabetic nephropathy, and amelioration by switching to ranibizumab. *SAGE Open Med Case Rep.* (2020) 8:2050313X20907033. doi: 10.1177/2050313X20907033

46. Shye M, Hanna RM, Patel SS, Tram-Tran N, Hou J, Mccannel C, et al. Worsening proteinuria and renal function after intravitreal vascular endothelial growth factor blockade for diabetic proliferative retinopathy. *Clin Kidney J.* (2020) sfaa049. doi: 10.1093/ckj/sfaa049

47. Chung YR, Kim YH, Byeon HE, Jo DH, Kim JH, Lee K. Effect of a single intravitreal injection of bevacizumab on proteinuria in patients with diabetes. *Tranls Vis Sci Technol.* (2020) 9:805. doi: 10.1167/tvst.9.4.4

48. Buob D, Decambron M, Gnemmi V, Frimat M, Hoffmann M, Azar R, et al. Collapsing glomerulopathy is common in the setting of thrombotic microangiopathy of the native kidney. *Kidney Int.* (2016) 90:1321–31. doi: 10.1016/j.kint.2016.07.021

49. Thadhani R, Hagmann H, Schaarschmidt W, Roth B, Cingoez T, Karumanchi SA, et al. Removal of soluble fms-like tyrosine kinase-1 by dextran sulfate apheresis in preeclampsia. *J Am Soc Nephrol.* (2016) 27:903–13. doi: 10.1681/ASN.2015020157

50. Hanna RM, Barsoum M, Vandross A, Kurtz I, Burwich R. Atypical hemolytic uremic syndrome and complement blockade: established and emerging uses of complement inhibition. *Curr Opin Nephrol Hypertens.* (2019) 28:278–87. doi: 10.1097/MNH.0000000000000499

# The Study of Angptl4-Modulated Podocyte Injury in IgA Nephropathy

Sha Jia[1,2,3,4,5,6†], Xiaofeng Peng[1,2,3,4,5†], Ludan Liang[1,2,3,4,5], Ying Zhang[1,2,3,4,5], Meng Li[1,2,3,4,5], Qin Zhou[1,2,3,4,5], Xiujin Shen[1,2,3,4,5], Yucheng Wang[1,2,3,4,5], Cuili Wang[1,2,3,4,5], Shi Feng[1,2,3,4,5], Jianghua Chen[1,2,3,4,5], Pingping Ren[1,2,3,4,5*] and Hong Jiang[1,2,3,4,5*]

[1] Kidney Disease Center, The First Affiliated Hospital, College of Medicine, Zhejiang University, Hangzhou, China, [2] Key Laboratory of Nephropathy, Hangzhou, China, [3] Kidney Disease Immunology Laboratory, The Third-Grade Laboratory, State Administration of Traditional Chinese Medicine of China, Hangzhou, China, [4] Key Laboratory of Multiple Organ Transplantation, Ministry of Health of China, Beijing, China, [5] Institute of Nephropathy, Zhejiang University, Hangzhou, China, [6] Dongyang Women & Children Hospital, Dongyang, China

**Background:** Increasing evidence shows that Angptl4 affects proteinuria in podocytes injured kidney disease, however, whether there is a relationship between Angptl4 and IgA nephropathy (IgAN) has not been studied yet.

**Methods:** Plasma and urine samples were obtained from 71 patients with IgAN and 61 healthy controls. Glomeruli from six renal biopsy specimens (three IgAN patients and three healthy controls) were separated by RNA-Seq. Differentially expressed genes (DEGs) related to podocytes and Angptl4 between IgAN patients and healthy controls were performed using the Limma package. Gene set enrichment analysis was used to determine whether there was a statistically significant difference between the two groups. STRING was used to create a protein-protein interaction network of DEGs. Association analysis between Angptl4 levels and clinical features of IgAN was performed.

**Results:** Thirty-three podocyte-related and twenty-three Angpt4-related DEGs were found between IgAN patients and healthy controls. By overlapping the genes, *FOS* and *G6PC* were found to be upregulated in IgAN patients, while *MMP9* was downregulated in IgAN patients. Plasma and urine Angptl4 levels were closely related to the degree of podocyte injury and urine protein, but not to the protein-creatine ratio.

**Conclusion:** Our findings show that Angptl4 levels in plasma and urine are related to podocyte damage and, therefore, may be a promising tool for assessing the severity of IgAN patients to identify and reverse the progression to ESRD.

Keywords: Angptl4, podocyte, immunoglobulin A nephropathy, RNA-Seq, progression

## INTRODUCTION

Immunoglobulin A nephropathy (IgAN), which is characterized by galactose-deficient IgA deposits in the glomerular mesangium, is the most prevalent type of glomerulonephritis worldwide (Suzuki et al., 2011; Wyatt and Julian, 2013). IgAN is one of the major causes of end-stage renal disease (ESRD), proteinuria, and hypertension. Reduced glomerular filtration rates are often used to assess its prognosis in clinical practice (Floege and Feehally, 2013). Nevertheless, a new indicator that would provide meaningful information about the diagnosis of IgAN and the effects of its treatment is still needed.

It is generally thought that mesangial cells play a dominant role in the pathogenesis of IgAN, but since mesangial-podocytic-tubular crosstalk has been proposed, emerging evidence shows that the role of podocytes in IgAN should not be underestimated (Hishiki et al., 2001; Faul et al., 2007; Lai, 2012; Fukuda et al., 2015; Leung et al., 2018). Podocytes possess numerous foot processes, surround glomerular capillaries, and serve as the last barrier to renal filtration (Greka and Mundel, 2012). Foot process effacement is a hallmark of podocyte injury, which leads to proteinuria and glomerulosclerosis (Lemley et al., 2002; Hara et al., 2007).

Angiopoietin-like protein 4 (Angptl4), an inhibitor of lipoprotein lipase (Yoshida et al., 2002), has been the focus of many studies examining novel mechanisms of proteinuria in recent years (Clement et al., 2011, 2014; Li et al., 2015; Ma et al., 2015). A previous study indicated that increased secretion of Angptl4 with a high isoelectric point (pI) by podocytes leads to proteinuria and foot process effacement in humans, and experimentally, minimal change disease (MCD) (Clement et al., 2011). However, circulating Angptl4 with a neutral pI, which is mainly secreted by adipose tissue and liver, reduces proteinuria by binding to αvβ5 integrin on the glomerular endothelium (Clement et al., 2014). Our previous study also observed an important role of Angptl4 in podocyte injury-associated nephropathy (Chen et al., 2013). However, the changes in Angptl4 expression levels in IgAN have not yet been investigated.

To more easily diagnose and evaluate the severity of IgAN, it is vital to find novel and non-invasive biomarkers. In this study, we attempted to use RNA sequencing of glomeruli separated from biopsy tissues of IgAN patients and healthy controls to explore the potential functions of Angptl4 in IgAN. We further confirmed the relationship between Angptl4 expression and IgAN in clinical samples.

## MATERIALS AND METHODS

### Study Population

All procedures in this study involved human participants in accordance with the Declaration of Helsinki. The study was approved by the Ethical Committee of the Zhejiang University College of Medicine, First Affiliated Hospital. All subjects (patients and healthy controls) provided written informed consent for blood, urine, or tissue collection. Seventy-one adult patients with biopsy-proven idiopathic IgAN were included in the IgAN group, and 60 live renal transplant donors were included in the healthy control group. The IgAN group was further divided into two groups according to electron microscopy results: one group consisted of 37 patients with foot process fusion, and the other group consisted of 34 patients without foot process fusion.

### Tissue Samples

Plasma and urine samples were collected at the time of kidney biopsy before treatment. Laser-captured microdissected glomeruli were obtained from the kidney biopsy tissues of three IgAN patients and three healthy controls for RNA sequencing. Dissection of the glomeruli under the microscope was performed according to a previously described protocol (Jiang et al., 2008). In short, the glomeruli were dissected with sharp forceps under a stereoscopic electron microscope. The small tubules, except for the medullary thick ascending limb of Henle's loop, were removed. All the steps were carried out in an albumin-rich saline solution (0.1%) at 4°C. Dissection was completed within 120 min of the kidney biopsy. The studies on human samples were conducted according to the Declaration of Helsinki.

### Library Preparation for Sequencing

RNA was extracted from the glomeruli after dissection. The RNA concentration and purity were determined using a Qubit® 2.0 fluorometer (Qubit® RNA Analysis Kit, Life Technologies, California, United States) and NanoPhotometer® (Implen, California, United States), respectively. A 1% agarose gel was used to assess RNA degradation and contamination. The RNA Nano 6000 Assay Kit of the Agilent Bioanalyzer 2100 system (Agilent Technologies, CA, United States) was used to assess RNA integrity.

A total of 3 μg of RNA per sample was used as the input material for the RNA sample preparations. The sequencing libraries were generated using the NEBNext® Ultra™ RNA Library Prep Kit for Illumina® (NEB, United States) following the manufacturer's instructions, and index codes were added to label the sequences of each sample. Briefly, mRNA was purified from total RNA using poly T oligo-conjugated magnetic beads. Fragmentation was conducted using divalent cations under an elevated temperature in NEBNext First-Strand Synthesis Reaction Buffer (five times). Synthesis of the first-strand and second-strand cDNA was carried out using a random hexamer primer, M-MuLV Reverse Transcriptase (RNaseH-), DNA Polymerase I, and RNase H. The remaining overhangs were converted to blunt ends through exonuclease/polymerase activities. After the 3′ terminus of the DNA fragments was adenylated, ligation of the NEBNext adaptor with a hairpin loop structure was performed to prepare for hybridization. To select cDNA fragments of 150–200 bp in length, the library fragments were purified with the AMPure XP system (Beckman Coulter, Beverly, MA, United States). Then, 3 μL of USER Enzyme (NEB, United States) was incubated with size-selected and adaptor-ligated cDNA at 37°C for 15 min, followed by 5 min at 95°C before PCR. Then, PCR was carried out with Phusion High-Fidelity DNA polymerase, universal PCR primers, and Index (X) Primer. Finally, the PCR products were purified on the AMPure XP system, and the library quality was assessed using the Agilent Bioanalyzer 2100 system.

### Clustering and Sequencing (Novogene Experimental Department)

The clustering of the index-coded samples was carried out on a cBot Cluster Generation System with the TruSeq SR Cluster Kit v3-cBot-HS (Illumina). All processes were conducted according

to the manufacturer's instructions. The sequencing of the library was conducted on the basis of an Illumina HiSeq 2000/2500 platform to generate 150/100/50 bp paired/single-end reads.

## Bioinformatics Analysis

FastQC and Trimmoatic were used to assess the quality of the raw sequencing reads and to clean the sequencing adaptor sequences at both ends of the raw reads. Clean reads were mapped using STAR to the human genome hg19. Gene expression was calculated, and the identification of differentially expressed genes (DEGs) was conducted using Cuffdiff 2 with a $q$-value $< 0.05$. Functional annotation and pathway enrichment analysis with DAVID were conducted. Polysearch2 and another web server that supports text mining from Medline and PubMed were used to search for Angptl4-related or podocyte-related genes. After the extraction of the related genes, a relevance score was calculated and converted to a Z-score. Then, the genes with Z-scores above 1 were selected for subsequent analysis. IgAN-related genes were searched by literature mining from the PubMed database.

## Measurement of the Concentration of Angptl4 in Plasma and Urine From Patients With IgAN

Plasma and urine samples were collected from IgAN patients and enzyme-linked immunosorbent assay (ELISA) was used to determine and compare the concentration of Angptl4 in the different samples. The characteristics of Angptl4 expression were analyzed and combined with the electron microscopy observation results and urinary protein levels.

## ELISA

The Angptl4 levels in plasma and urine were analyzed using commercial immunoassay kits (Angiopoietin-Like protein 4 Human ELISA, BioVendor, Human IgG4 Platinum ELISA, eBioscience) according to the manufacturer's instructions.

## Measurement of Podocyte Injury by Electron Microscopy

Renal cortical and medullary tissues from IgAN patients and healthy controls were minced into 1 mm$^3$ pieces and processed for electron microscopy using standard protocols. Ultrathin sections (80–90 nm) were prepared for examination and imaging with an Olympus transmission electron microscope (Tecnai, Tokyo, Japan).

## Statistical Analyses

Statistical analyses were carried out using GraphPad Prism software (version 8.3.0). All data are presented as the mean $\pm$ SEM. Analysis of the differences in Angptl4 expression was conducted by one-way ANOVA with Dunnett's *post hoc* test using GraphPad. The one-sample Kolmogorov–Smirnov test was used to assess for normal distribution of the data. Relationships between the Angptl4 levels and clinical parameters were examined using Pearson correlation analysis when normally distributed; otherwise, the Spearman rank test was

used. All $P$-values were two-tailed, and significance was defined as $P < 0.05$.

# RESULTS

## Demographic Characteristics of the IgAN Patients and Healthy Controls

The clinical data of the patients and controls are shown in **Table 1**. Clinical parameters, such as serum albumin (g/L), serum creatinine ($\mu$mol/L), 24-hour urine protein excretion (g/day), and protein-creatinine ratio (g/g), were examined at the time of renal biopsy. No significant differences in age or sex were observed among the three groups. The patients in the IgAN with and without podocyte injury groups presented with a mean serum creatinine level of $187.22 \pm 20.61$ and $95.94 \pm 5.97$ $\mu$mol/L, and a mean serum albumin level of $35.20 \pm 0.98$ and $37.89 \pm 1.25$ g/L, respectively ($P < 0.05$ compared with the healthy controls). The controls had no proteinuria and presented with a mean serum albumin level of $44.26 \pm 0.26$ g/L.

## Gene Expression Analysis by RNA-Seq

We used STRING to analyze protein interactions and screened DEGs that were directly or indirectly related to Angptl4. The red and blue colors in the heatmap depict higher and lower gene expression, respectively. The official gene names are given, the test values of the IgAN patients and the controls are listed. The fold changes indicate the relative alteration in the IgAN value compared to the control value, and the log$_2$ value of the fold change is shown. A positive log$_2$ (fold change) indicated upregulation in the disease group, and a negative log$_2$ (fold change) indicated downregulation in the disease group. The glomerular expression levels of 33 transcripts related to podocytes and 23 transcripts correlated with Angptl4 (**Figures 1A,B**).

**TABLE 1** | Characteristics of individuals included in the study.

| | IgAN | | Control (*n* = 61) |
|---|---|---|---|
| | IgAN with podocyte injury (*n* = 37) | IgAN without podocyte injury (*n* = 34) | |
| Age (years) | $42.89 \pm 1.78$ | $45.44 \pm 2.15$ | $45.49 \pm 1.29$ |
| Sex (male/female) | 23/14 | 20/14 | 45/16 |
| Serum albumin (g/L) | $35.20 \pm 0.98^*$ | $37.89 \pm 1.25^*$ | $44.26 \pm 0.26$ |
| Scr ($\mu$mol/L) | $187.22 \pm 20.61^*$ | $95.94 \pm 5.97^*$ | $72.92 \pm 1.30$ |
| 24 UP (g/day) | $3.06 \pm 0.40$ | $1.35 \pm 0.48$ | |
| P/C (g/g) | $1.23 \pm 0.26$ | $1.60 \pm 0.35$ | |
| Oxford evaluation | | | |
| M1 | 12 | 7 | |
| E1 | 2 | 3 | |
| S1 | 32 | 20 | |
| T1 or T2 | 11 | 5 | |

*Scr, serum creatinine; 24 UP, 24-hour urine protein excretion; P/C, protein: creatinine ratio. The data are shown as the mean $\pm$ SEM. *$P < 0.05$ versus the control.*
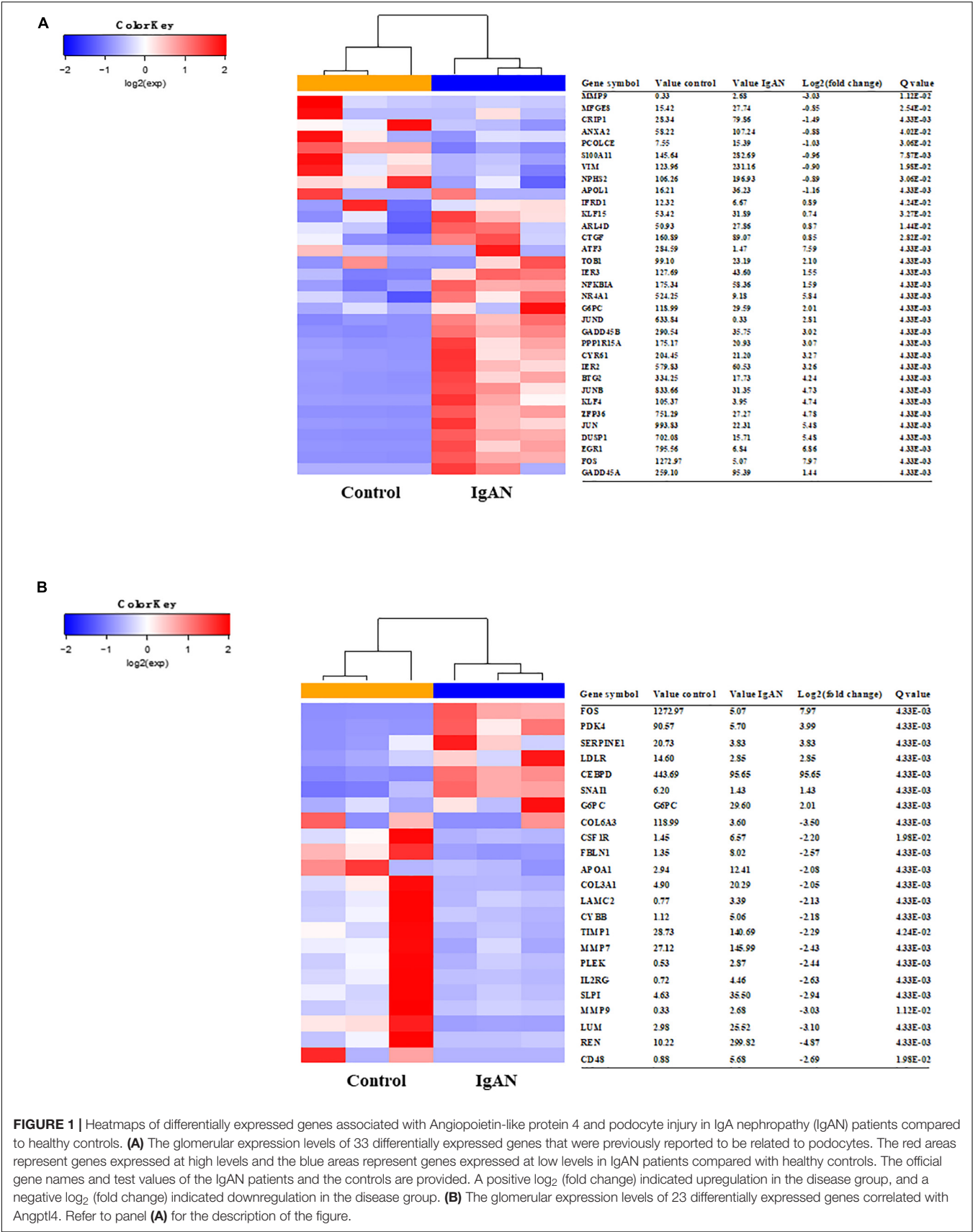
**FIGURE 1 |** Heatmaps of differentially expressed genes associated with Angiopoietin-like protein 4 and podocyte injury in IgA nephropathy (IgAN) patients compared to healthy controls. **(A)** The glomerular expression levels of 33 differentially expressed genes that were previously reported to be related to podocytes. The red areas represent genes expressed at high levels and the blue areas represent genes expressed at low levels in IgAN patients compared with healthy controls. The official gene names and test values of the IgAN patients and the controls are provided. A positive log$_2$ (fold change) indicated upregulation in the disease group, and a negative log$_2$ (fold change) indicated downregulation in the disease group. **(B)** The glomerular expression levels of 23 differentially expressed genes correlated with Angptl4. Refer to panel **(A)** for the description of the figure.

## Gene Set Enrichment Analysis of Angptl4

GSEA 3.0 software was used to analyze the Angptl4 gene enrichment results. The Angptl4 gene participated in seven enriched sets, which were statistically significantly different between the IgAN group and the control group. The transcripts of three genes, FOS, G6PC, and MMP9, were simultaneously included in the Angptl4-related and podocyte-related genes (**Figure 2A**). Two of these genes, namely, FOS and G6PC, were upregulated in the disease group, whereas MMP9 was downregulated in the disease group (**Figure 2B**). STRING was used to depict the protein-protein interaction network of Angptl4, FOS, G6PC, and MMP9 with several DEGs selected from among the Angptl4-related or podocyte-related genes (**Figure 2C**).

## Angptl4 in Plasma and Urine

Plasma Angptl4 levels were significantly lower in IgAN patients than in normal controls. The expression of Angptl4 in plasma was decreased in the IgAN without podocyte injury patients compared with the normal controls ($1.75 \pm 0.06$ versus $2.12 \pm 0.05$, ****$P < 0.0001$). The plasma Angptl4 level in the IgAN with podocyte injury patients was also significantly lower than that in the controls ($1.59 \pm 0.09$ versus $2.12 \pm 0.05$, ****$P < 0.0001$). There were no significant differences between the IgAN without podocyte injury and IgAN in podocyte injury patients (**Figure 3A**). The Angptl4 expression level in urine was significantly higher in IgAN patients than in normal controls. Urine Angptl4 expression was increased in the IgAN without podocyte injury patients compared with the normal controls ($1.64 \pm 0.14$ versus $0.36 \pm 0.03$, ****$P < 0.0001$). The urine Angptl4 level in the IgAN with podocyte injury patients was also significantly higher than that in the controls ($1.93 \pm 0.17$ versus $0.36 \pm 0.03$, ****$P < 0.0001$). Similarly, no significant difference was observed between the IgAN without podocyte injury and IgAN in podocyte injury patients (**Figure 3B**). In the IgAN patients, there was a significant correlation between the levels of urine protein and the levels of plasma Angptl4 or urine Angptl4 ($p = 0.022$, $p = 0.032$, respectively) (**Figures 3C,D**). Plasma Angptl4 or urine Angptl4 levels were positively correlated with urine protein levels ($r = 0.310$, $p = 0.022$; $r = 0.340$, $p = 0.032$, respectively). There was no significant correlation between the urine protein-creatinine ratio and plasma Angptl4 or urine Angptl4 levels (**Figures 3E,F**).

## Relationship of Plasma and Urine Angptl4 Levels With Podocyte Injury

Among the 37 IgAN patients with podocyte injury, there were 28 patients with focal fusion of the foot process (<70%) and 9 patients with diffuse fusion of the foot process (≥70%). Representative electron microscopy images of IgAN patients with or without podocyte foot process effacement are shown in **Figures 4A,B**. The plasma Angptl4 levels in the focally fused group and the diffusely fused group were significantly lower than those in the controls

($1.71 \pm 0.09$ versus $1.99 \pm 0.04$, *$P < 0.05$; $1.22 \pm 0.17$ versus $1.99 \pm 0.04$, **$P < 0.01$, respectively). There were no significant differences between the focally fused group and the diffusely fused group (**Figure 4C**). The Angptl4 level in the urine of the focally fused group was significantly higher than that in the control group ($1.84 \pm 0.19$ versus $0.82 \pm 0.08$, ***$P < 0.001$; $2.19 \pm 0.38$ versus $0.82 \pm 0.08$, *$P < 0.05$, respectively). Similarly, there were no significant differences between the focally fused group and the diffusely fused group (**Figure 4D**).

## DISCUSSION

A total of 20–40% of IgAN patients progress to ESRD by 20 years after biopsy, which significantly contributes to the population of patients with ESRD (Wyatt and Julian, 2013). Although progress has been made in understanding the pathogenesis of IgAN, predicting exactly which patients will progress to ESRD or how quickly they will progress remains a challenge. To identify the trend of the severe progression of patients as early as possible, to provide individualized and accurate treatment, and to delay the course of the disease has always been the aim of our research.

Proteinuria is one of the most important factors for assessing the risk of disease progression in patients with IgAN. Podocyte injury plays an important role in proteinuria during the severe progression of IgAN. Our previous studies found that Angptl4 affects podocytes and is much more sensitive and significant than circulating antibodies against PLA2R, a possible marker of idiopathic MN disease progression (Chen et al., 2013). Whether Angptl4 is related to podocyte damage in the progression of IgAN is the focus of this study.

Our previous studies found that the plasma level of LL-37, which is one of the ageing markers we identified (Jiang et al., 2008), is associated with the progression of human IgAN (Lu et al., 2014). Through bioinformatics analysis, we searched for aging-related genes that are also related to IgAN and found that JUN and FOS play an important role in the severe progression of IgAN, especially in the progression of fibrosis (Jiang et al., 2016). However, understanding and reversing the progression to the fibrotic stage early in this process remains a challenge.

In this study, we found that FOS, MMP9, and G6PC are hub genes that are related to both Angptl4 and podocytes through overlapping genes. FOS is an AP-1 transcription factor. Increased expression of AP-1 activates the RAAS system (Cao et al., 2013), which subsequently results in IgAN. MMP-9 is a member of the matrix metalloproteinases (MMPs) and an important regulator of the extracellular matrix. MMP-9 plays a role in the decomposition of the mesangial matrix and mediates the recovery from pathogenic processes (Sekiuchi et al., 2012). G6PC (glucose-6-phosphatase catalytic subunit) is one of the three glucose-6-phosphatase catalytic subunit-encoding genes in humans. Mutations in this gene result in glycogen storage disease type I (GSD1), which is
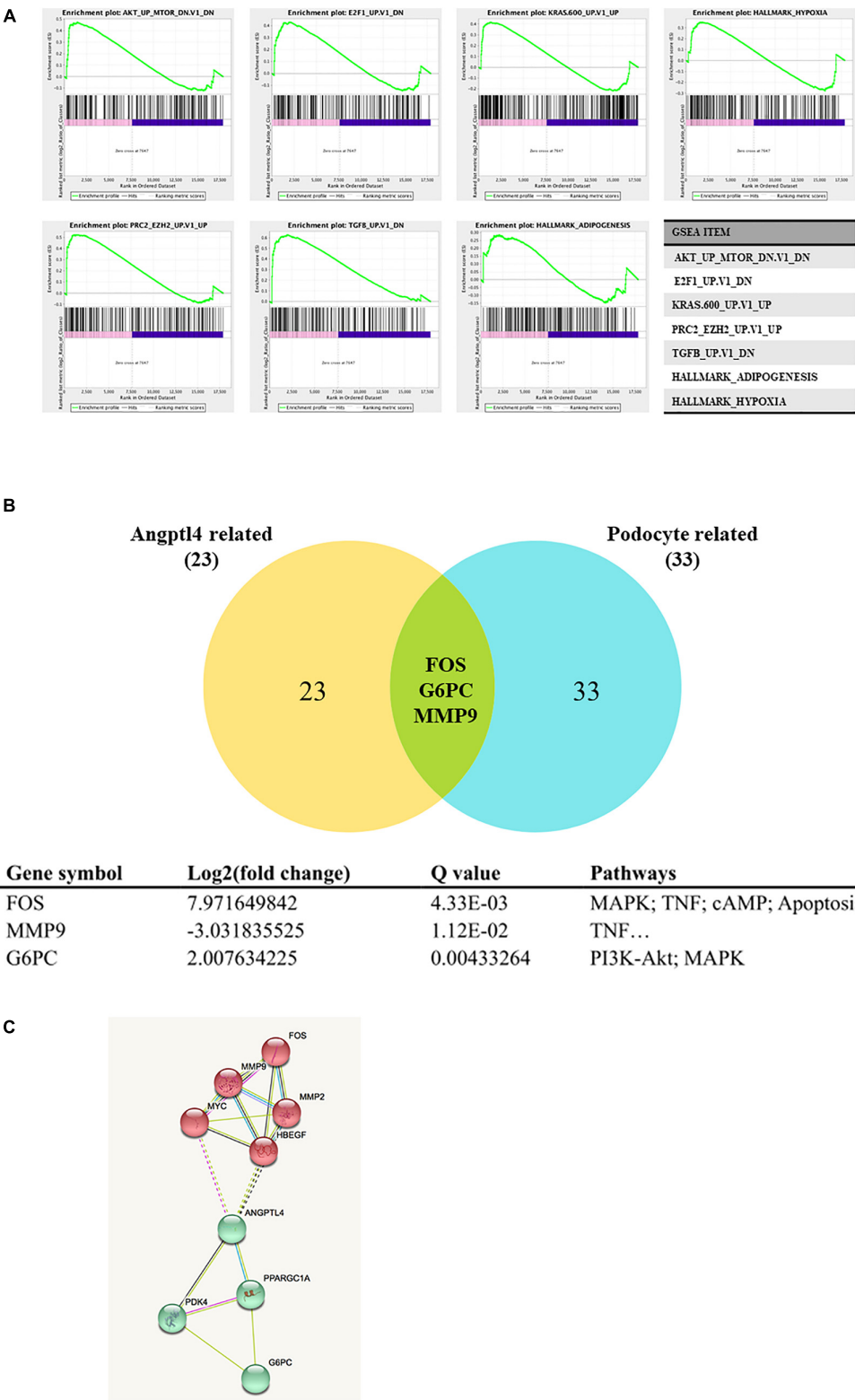
**FIGURE 2 |** Gene set enrichment analysis of Angiopoietin-like protein 4. **(A)** The Angptl4 gene participated in 7 enriched sets that were statistically significantly different between the IgA nephropathy (IgAN) group and the control group. **(B)** The transcripts of three genes, namely, *FOS*, *G6PC*, and *MMP9*, were simultaneously included in the Angptl4-related and podocyte-related genes. Two of these genes, namely, *FOS* and *G6PC*, were upregulated in the disease group, whereas *MMP9* was downregulated in the disease group. **(C)** The depiction of the network of Angptl4, *FOS*, *G6PC*, and *MMP9* with several differentially expressed genes selected from among the Angptl4-related or podocyte-related genes by STRING.

**FIGURE 3** | Angiopoietin-like protein 4 levels in plasma and urine. **(A,B)** The expression of Angptl4 in plasma and urine was detected in IgA nephropathy (IgAN) without podocyte injury patients ($n = 34$), IgAN with podocyte injury patients ($n = 37$), and normal controls ($n = 61$) by enzyme-linked immunosorbent assay. **(C,D)** The relationship between urine protein (g/L) and Angptl4 expression in plasma and urine was analyzed in IgAN patients ($n = 61$). **(E,F)** The relationship between the urine protein-creatinine ratio (g/g) and Angptl4 expression in plasma and urine was analyzed in IgAN patients ($n = 61$). The data are expressed as the mean ± SEM. \*\*\*$P < 0.001$ compared with the normal controls.

characterized by an ectopic accumulation of lipids in the liver and kidneys. Laure et al. showed that in K. G6pc$^{-/-}$ mice, the renin-angiotensin system was activated, which caused increased Tgf-β1 expression, thereby activating epithelial-mesenchymal transition and subsequent fibrosis development (Clar et al., 2014).

To verify the potential roles of Angptl4 in IgAN, correlation analyses between Angptl4 levels and clinical features were performed. We found that the plasma and urine Angptl4 levels were strongly correlated with the degree of IgAN podocyte damage, which implies that Angptl4 may be a potential factor for evaluating IgAN progression in the future. Clement et al. (2011) showed that Angptl4 in urine is derived from a low-sialylated, high-pI, pro-proteinuric form that is secreted by podocytes, and its increase causes massive proteinuria. In this study, we also found that Angptl4 in urine is positively correlated
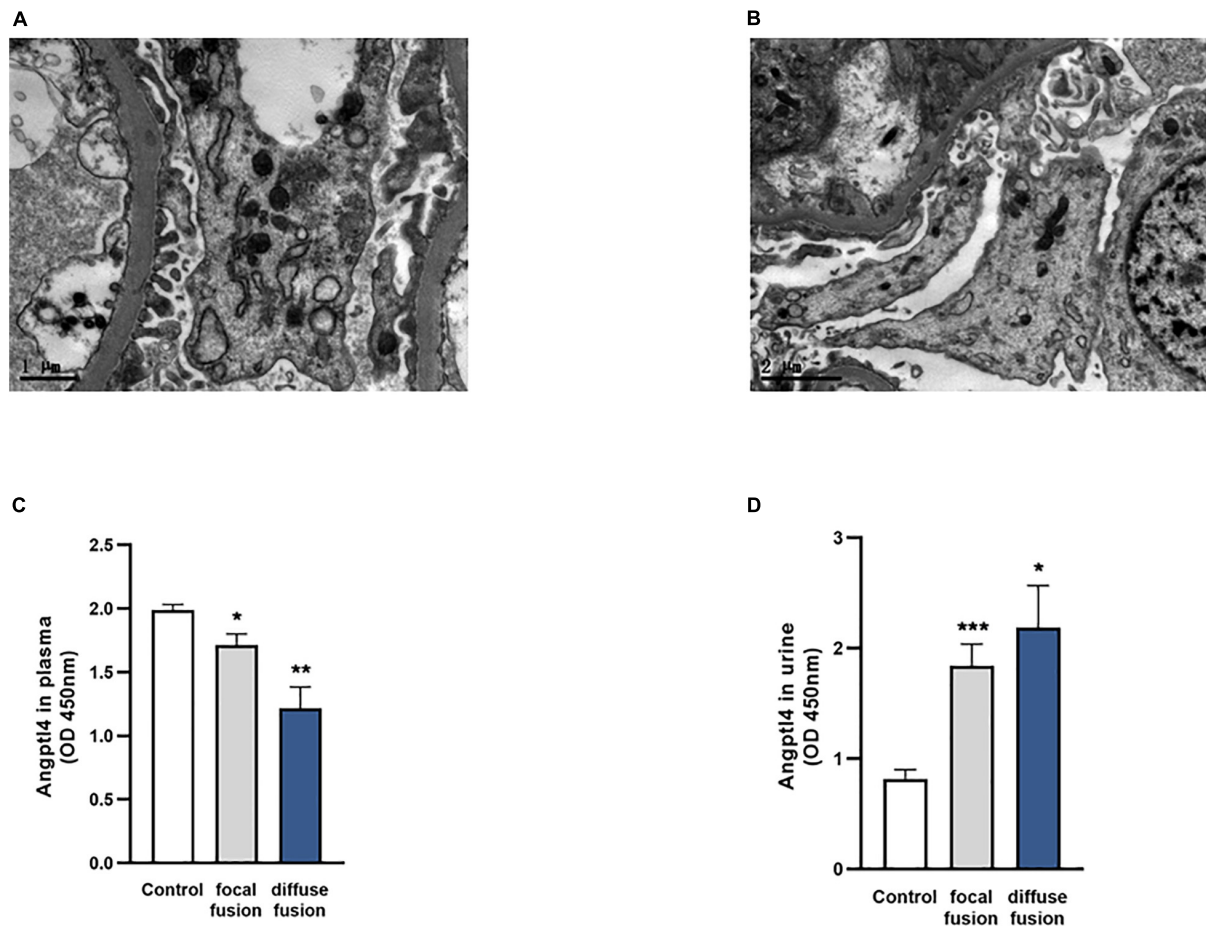
**FIGURE 4 |** Analysis of podocyte foot process effacement in the two patient groups and the control group. **(A)** Electron microscopy image of no podocyte foot process effacement in the IgA nephropathy (IgAN) patients without podocyte group. **(B)** Electron microscopy image of podocyte foot process effacement in the IgAN patients with podocyte group (scale bar = 1 or 2 $\mu$m). **(C,D)** The expression of plasma and urinary Angptl4 in IgAN patients with podocyte foot process focal effacement ($n = 28$), diffuse effacement ($n = 9$), and controls (healthy and IgAN patients without podocyte injury) ($n = 95$). The data are expressed as the mean $\pm$ SEM. *$P < 0.05$, **$P < 0.01$, and ***$P < 0.001$ compared with the controls.

with urine protein content. In contrast, in our experiment, Angptl4 in plasma was positively correlated with urine protein content, and (Clement et al., 2014) found that Angptl4 in plasma reduced proteinuria by binding to $\alpha v \beta 5$ integrin. However, protein-creatinine ratio is not related to Angptl4 expression in plasma or urine.

In conclusion, the present study aimed to explore the possible functions of Angptl4 in IgAN progression. Three hub genes were screened via multiple-microarray analysis, and these genes may become potential targets for the diagnosis and treatment of IgAN in the future. However, this study has some limitations, as Angptl4 has an effect on podocyte damage in many kidney diseases, it is not specific to IgAN, and the size of biopsies of patients with IgAN used for expression was small. The underlying mechanism of podocyte damage is unclear. We further need to explore whether there is a connection between Angptl4 and the mechanism of telomere damage in aging, and we must conduct more thorough research regarding the molecular mechanism.

## DATA AVAILABILITY STATEMENT

The sequencing data is deposited in the BioProject database (accession: PRJNA669346).

## ETHICS STATEMENT

The studies involving human participants were reviewed and approved by Ethical Committee of the Zhejiang University College of Medicine, the First Affiliated Hospital. The patients/participants provided their written informed consent to participate in this study.

## AUTHOR CONTRIBUTIONS

SJ planned and conducted the project, collected the data, and wrote the manuscript. XP supplemented the project, analyzed the

data, and wrote the manuscript. LL conducted the bioinformatics analysis. YZ and ML collected the sample. QZ conducted the IgAN pathologic diagnosis. XS conducted the Angptl4 experiment. YW processed the sample with the help of CW and SF. HJ designed and arranged the project with the help of JC and PR. HJ and PR provided the clinical support.

## REFERENCES

Cao, W., Xu, J., Zhou, Z. M., Wang, G. B., Hou, F. F., and Nie, J. (2013). Advanced oxidation protein products activate intrarenal renin-angiotensin system via a CD36-mediated, redox-dependent pathway. *Antioxid. Redox Signal.* 18, 19–35. doi: 10.1089/ars.2012.4603

Chen, W. Q., Zhang, Y., Jiang, H., Li, H., Li, X. Y., Yang, X., et al. (2013). Podocyte-related proteins in membranous nephropathy progression. *Chin. Med. J.* 126, 3782–3783.

Clar, J., Gri, B., Calderaro, J., Birling, M. C., Hérault, Y., Smit, G. P. A., et al. (2014). Targeted deletion of kidney glucose-6 phosphatase leads to nephropathy. *Kidney Int.* 86, 747–756. doi: 10.1038/ki.2014.102

Clement, L. C., Avila-Casado, C., Mace, C., Soria, E., Bakker, W. W., Kersten, S., et al. (2011). Podocyte-secreted angiopoietin-like-4 mediates proteinuria in glucocorticoid-sensitive nephrotic syndrome. *Nat. Med.* 17, 117–122. doi: 10.1038/nm.2261

Clement, L. C., Mace, C., Avila-Casado, C., Joles, J. A., Kersten, S., and Chugh, S. S. (2014). Circulating angiopoietin-like 4 links proteinuria with hypertriglyceridemia in nephrotic syndrome. *Nat. Med.* 20, 37–46. doi: 10.1038/nm.3396

Faul, C., Asanuma, K., Yanagida-Asanuma, E., Kim, K., and Mundel, P. (2007). Actin up: regulation of podocyte structure and function by components of the actin cytoskeleton. *Trends Cell Biol.* 17, 428–437. doi: 10.1016/j.tcb.2007.06.006

Floege, J., and Feehally, J. (2013). Treatment of IgA nephropathy and Henoch-Schonlein nephritis. *Nat. Rev. Nephrol.* 9, 320–327. doi: 10.1038/nrneph. 2013.59

Fukuda, A., Sato, Y., Iwakiri, T., Komatsu, H., Kikuchi, M., Kitamura, K., et al. (2015). Urine podocyte mRNAs mark disease activity in IgA nephropathy. *Nephrol. Dial. Transplant.* 30, 1140–1150. doi: 10.1093/ndt/gfv104

Greka, A., and Mundel, P. (2012). Cell biology and pathology of podocytes. *Annu. Rev. Physiol.* 74, 299–323. doi: 10.1146/annurev-physiol-020911-153238

Hara, M., Yanagihara, T., and Kihara, I. (2007). Cumulative excretion of urinary podocytes reflects disease progression in IgA nephropathy and Schonlein-Henoch purpura nephritis. *Clin. J. Am. Soc. Nephrol.* 2, 231–238. doi: 10.2215/CJN.01470506

Hishiki, T., Shirato, I., Takahashi, Y., Funabiki, K., Horikoshi, S., and Tomino, Y. (2001). Podocyte injury predicts prognosis in patients with iga nephropathy using a small amount of renal biopsy tissue. *Kidney Blood Press Res.* 24, 99–104. doi: 10.1159/000054214

Jiang, H., Liang, L., Qin, J., Lu, Y., Li, B., Wang, Y., et al. (2016). Functional networks of aging markers in the glomeruli of IgA nephropathy: a new therapeutic opportunity. *Oncotarget* 7, 33616–33626. doi: 10.18632/oncotarget.9033

Jiang, H., Schiffer, E., Song, Z., Wang, J., Zurbig, P., Thedieck, K., et al. (2008). Proteins induced by telomere dysfunction and DNA damage represent biomarkers of human aging and disease. *Proc. Natl. Acad. Sci. U.S.A.* 105, 11299–11304. doi: 10.1073/pnas.0801457105

Lai, K. N. (2012). Pathogenesis of IgA nephropathy. *Nat. Rev. Nephrol.* 8, 275–283. doi: 10.1038/nrneph.2012.58

Lemley, K. V., Lafayette, R. A., Safai, M., Derby, G., Blouch, K., Squarer, A., et al. (2002). Podocytopenia and disease severity in IgA nephropathy. *Kidney Int.* 61, 1475–1485. doi: 10.1046/j.1523-1755.2002.00269.x

Leung, J. C. K., Lai, K. N., and Tang, S. C. W. (2018). Role of mesangial-podocytic-tubular cross-talk in IgA nephropathy. *Semin. Nephrol.* 38, 485–495. doi: 10.1016/j.semnephrol.2018.05.018

Li, J. S., Chen, X., Peng, L., Wei, S. Y., Zhao, S. L., Diao, T. T., et al. (2015). Angiopoietin-Like-4, a potential target of tacrolimus, predicts earlier podocyte injury in minimal change disease. *PLoS One* 10:e0137049. doi: 10.1371/journal.pone.0137049

Lu, Y. Y., Yang, X., Chen, W. Q., Ju, Z. Y., Shou, Z. F., Jin, J., et al. (2014). Proteins induced by telomere dysfunction are associated with human IgA nephropathy. *J. Zhejiang Univ. Sci. B* 15, 566–574. doi: 10.1631/jzus.B1300115

Ma, J., Chen, X., Li, J. S., Peng, L., Wei, S. Y., Zhao, S. L., et al. (2015). Upregulation of podocyte-secreted angiopoietin-like-4 in diabetic nephropathy. *Endocrine* 49, 373–384. doi: 10.1007/s12020-014-0486-5

Sekiuchi, M., Kudo, A., Nakabayashi, K., Kanai-Azuma, M., Akimoto, Y., Kawakami, H., et al. (2012). Expression of matrix metalloproteinases 2 and 9 and tissue inhibitors of matrix metalloproteinases 2 and 1 in the glomeruli of human glomerular diseases: the results of studies using immunofluorescence, in situ hybridization, and immunoelectron microscopy. *Clin. Exp. Nephrol.* 16, 863–874. doi: 10.1007/s10157-012-0633-3

Suzuki, H., Kiryluk, K., Novak, J., Moldoveanu, Z., Herr, A. B., Renfrow, M. B., et al. (2011). The pathophysiology of IgA nephropathy. *J. Am. Soc. Nephrol.* 22, 1795–1803. doi: 10.1681/ASN.2011050464

Wyatt, R. J., and Julian, B. A. (2013). IgA nephropathy. *N. Engl. J. Med.* 368, 2402–2414. doi: 10.1056/NEJMra1206793

Yoshida, K., Shimizugawa, T., Ono, M., and Furukawa, H. (2002). Angiopoietin-like protein 4 is a potent hyperlipidemia-inducing factor in mice and inhibitor of lipoprotein lipase. *J. Lipid Res.* 43, 1770–1772. doi: 10.1194/jlr.C200010-JLR200

**frontiers**
in Pharmacology

# Herbal Medicine "Shulifenxiao" Formula for Nephrotic Syndrome of Refractory Idiopathic Membranous Nephropathy

Hailan Cui[1], Frank Qiang Fu[2,3†], Baoli Liu[4], Wei Jing Liu[2,5]* and Yu Ning Liu[2]*

[1]Beijing Changping Hospital of Traditional Chinese Medicine, Beijing, China, [2]Renal Research Institution of Beijing University of Chinese Medicine, Key Laboratory of Chinese Internal Medicine of Ministry of Education and Beijing and Dongzhimen Hospital, Beijing University of Chinese Medicine, Beijing, China, [3]School of Chinese Materia Medica, Beijing University of Chinese Medicine, Beijing, China, [4]Beijing Hospital of Traditional Chinese Medicine Affiliated to Capital Medical University, Beijing, China, [5]Zhanjiang Key Laboratory of Prevention and Management of Chronic Kidney Disease, Guangdong Medical University, Zhanjiang, China

**OPEN ACCESS**

**Background:** Treatment for adult patients with refractory idiopathic membranous nephropathy (RIMN) by conventional immunosuppressive regimens is not satisfactory. This study aims to evaluate the effectiveness of Chinese herbal medicine, Shulifenxiao formula, as a promising regimen.

**Methods:** A total of 31 RIMN patients resistant to corticosteroid or immunosuppressive agents were retrospectively analyzed. Shulifenxiao treatment lasted a minimum of 12°months in all patients and extended to 24°months in 11 patients. The primary outcomes [the complete remission (CR) and partial remission (PR)] and secondary outcomes (the serum creatinine and estimated glomerular filtration rate (eGFR) levels) were measured at 6, 12, 18, and 24°months.

**Results:** The data provided an average follow-up of $21 \pm 9.16$°months from baseline. The remission was attained in 25/31 patients (80.7%: CR 29.0% and PR 51.6%) at 12°months and in 10/11 patients (90.9%: CR 54.6% and PR 36.4%) at 24°months, respectively. Proteinuria reduced from 6.02 g/d at baseline to 0.98 g/d at 12°months ($p < 0.001$) and to 0.27 g/d at 24°months ($p = 0.003$); serum albumin increased from 28 g/L to 37.2 g/L at 12°months ($p < 0.001$) and to 41.3 g/L at 24°months ($p = 0.003$); eGFR improved from 100.25 ml/min/1.73 m$^2$ to 118.39 ml/min/1.73 m$^2$ at 6°months ($p < 0.001$) and finally to 111.62 ml/min/1.73 m$^2$ at 24°months ($p = 0.008$). Only two patients developed subsequent relapse.

**Abbreviations:** ACEI, angiotensin converting enzyme inhibitors; ALT, alanine aminotransferase; ANOVA, one-way analysis of variance; ARB, angiotensin II receptor antagonist; AST, aspartate transaminase; CKD, chronic kidney disease; CR, complete remission; CsA, cyclosporine A; CTX, cyclophosphamide; DBP, diastolic blood pressure; eGFR, estimated glomerular filtration rate; ESRD, end-stage renal disease; IMN, idiopathic membranous nephropathy; KDIGO, kidney disease improving global outcomes; MMF, mycophenolate mofetil; MN, membranous nephropathy; MZR, mizoribine; NR, nonremission; PR, partial remission; PRED, prednisone; RIMN, refractory idiopathic membranous nephropathy; SBP, systolic blood pressure; TAC, tacrolimus; TCM, traditional Chinese medicine.

**Conclusion:** Shulifenxiao formula as a clinical cocktail therapy serves as an alternative therapeutic option for steroid and immunosuppressant-resistant RIMN patients, with a favourable safety profile, though further studies are warranted.

**Clinical Trial registration:** http://www.chictr.org.cn, Chinese Clinical Trials Registry [ChiCTR1800019351].

Keywords: Chinese herbal medicine, nephrotic syndrome, refractory membranous nephropathy, retrospective analysis, shulifenxiao formula



GRAPHICAL ABSTRACT |
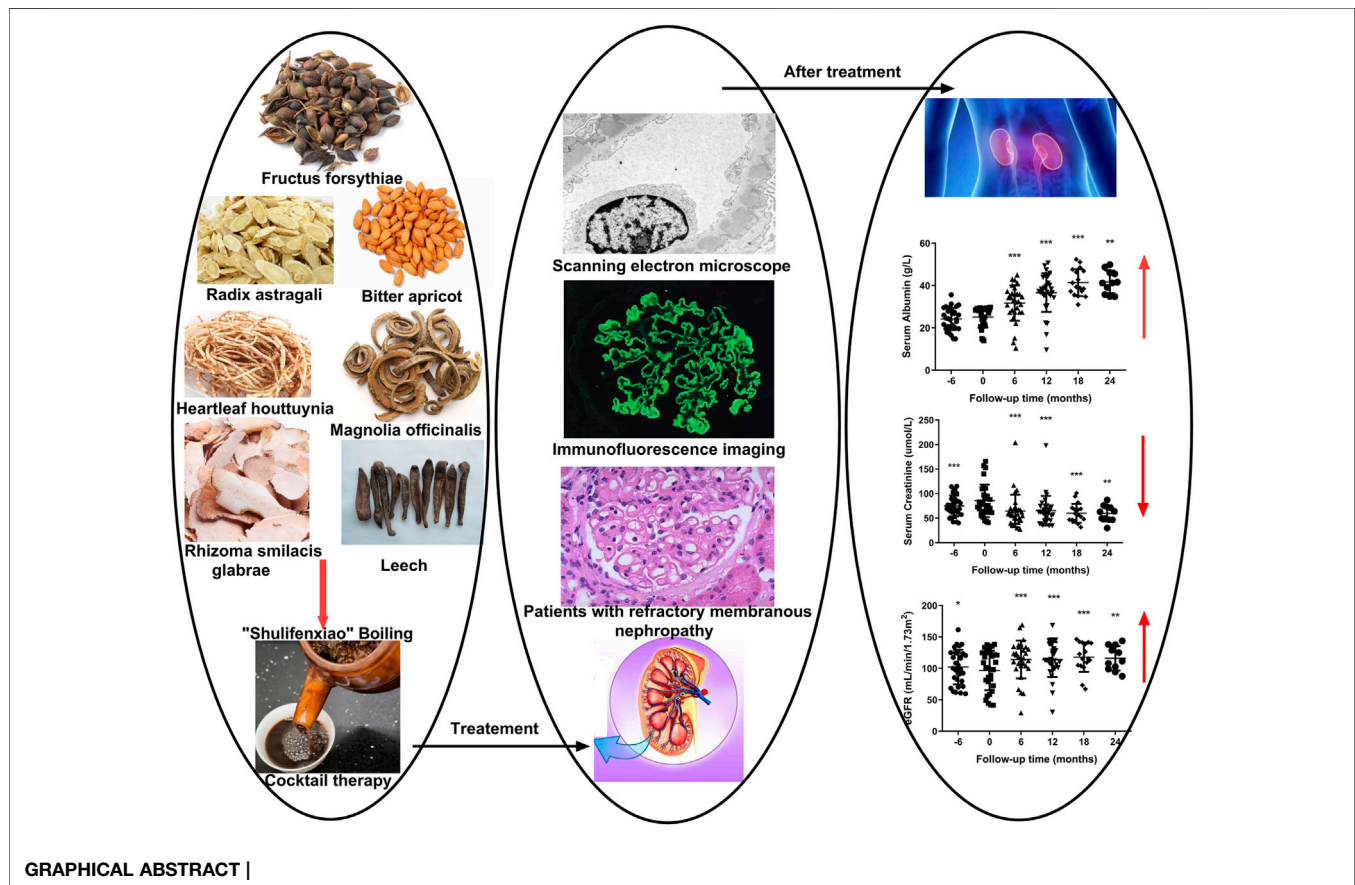
# INTRODUTION

Membranous nephropathy (MN) is one of the most common causes of nephrotic syndrome in adults. Approximately 75% of MN cases are idiopathic (Glassock, 2010). Over the past few years, most MN patients have received glucocorticoid in combination with an alkylating agent, or received calcineurin inhibitor, according to the 2012 guidelines of kidney disease improving global outcomes (KDIGO). These regimens significantly improve the clinical remission rate and renal survival rate of idiopathic membranous nephropathy (IMN). Nevertheless, nearly 30% of patients fail to respond to the conventional immunosuppressive therapies and eventually develop end-stage renal disease (ESRD) or

complications related to nephrotic syndrome (Du Buf-Vereijken et al., 2005; Couser, 2017). Therefore, refractory idiopathic MN (RIMN) is proposed to refer to MN cases resistant to steroids and general immunosuppressive agents (Iida et al., 2000; Chen et al., 2013; Sengupta et al., 2013). Treatment of RIMN is a significant challenge because traditional immunosuppressive agents appear to be unsuccessful and show obvious side effects. Alternative therapeutic agents to treat RIMN are an urgent need.

Based on the traditional theories of Traditional Chinese Medicine (TCM), TCM treatment has been done on humans for thousands of years with using the formula of natural herbal medicines. Up to now, TCM has accumulated rich experience in treating various kidney diseases and holds great potential for providing effective treatments for

MN. Recently, existing preclinical and clinical evidence has supported the effectiveness of TCM in treating IMN. TCM treatment reduces proteinuria, improves serum albumin, and thereby prevents the progress of IMN and avoids side effects caused by long-term applications of immunosuppressive agents (Chen et al., 2013; Zhang et al., 2014; Xiao et al., 2018). Combination of TCM and Western medicine has proven to improve the outcome of MN.

Despite this, very few high-quality studies testing the efficacy of TCM in adult RIMN patients are available. This may be due to the difficulty in formulating a control group. So many of the current studies are small single arm studies or case reports, with the observation periods ranging from half a year to one year (Chen, 2016; Zhang et al., 2017). Therefore, for RIMN patients, the possible benefits of TCM remain undetermined.

Medicinal "Shulifenxiao" is an herbal treatment for qi-deficiency, a damp-heat syndrome of RIMN. It has been used for nearly 30 years as an empirical treatment, first devised by Professor Liu Yuning. We have found "Shulifenxiao" formula has a significant clinical effect on the treatment of MN, and so in 2014, we started the clinical data collect of MN patients receiving "Shulifenxiao" treatment to establish a database for MN analysis. Here, we conducted a retrospective study aimed to evaluate the efficacy, recurrence, and safety of the TCM Shulifenxiao formula in patients with RIMN who are resistant to conventional immunosuppressive regimens.

## MATERIALS AND METHODS

### Patients

This was a retrospective case-series study. The outpatient records of adult patients with histologically proven membranous nephropathy in Dongzhimen Hospital affiliated to Beijing University of Chinese Medicine (Beijing, China) from January 2014 to June 2017 were screened (n = 157) (**Figure 1**). Only patients with the following criteria were included: 1) Histologically proven idiopathic membranous nephropathy; 2) Patients who did not respond to corticosteroid and immunosuppressive agents and remained in nephrotic syndrome (proteinuria≥3.5 g/d, serum albumin<30 g/L) even after 6 months of regular immunosuppressive therapy, such as prednisone (PRED), cyclophosphamide (CTX), cyclosporine A (CsA), tacrolimus (TAC), and mycophenolate mofetil (MMF); 3) eGFR > 30 ml/min/1.73 m$^2$. 4) The follow-up period >1 year with an interval between visits of <3 months or >4 visit times per year.

31 patients were found to be eligible for the retrospective analysis.

### Intervention

All eligible patients were treated with a consecutive Shulifenxiao formula (a formula of TCM), which is made of seven Chinese herbs. Medicines was provided by the pharmacy department of Dongzhimen Hospital, and was orally administered 30 min after breakfast and supper (200 ml, bid). All patients were treated with angiotensin-converting enzyme inhibitors (ACEI) or angiotensin II receptor antagonist (ARB). If the patient's blood pressure remained >130/80 mmhg, appropriate calcium channel blockers were added to



**FIGURE 1** | Flow chart of the patient selection process.
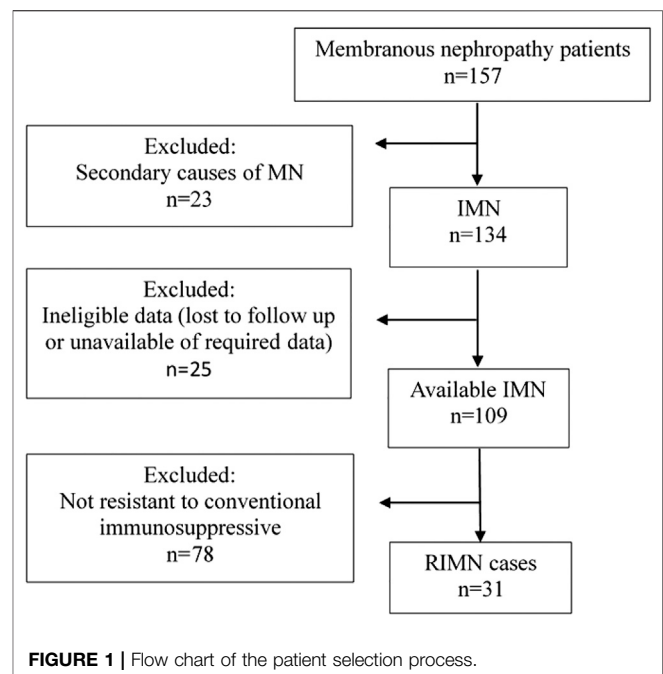
stabilize blood pressure. Treatment lasted for a minimum of 12 months in all patients. Clinical and laboratory data at 6 months prior to Shulifenxiao treatment, baseline, 6th, 12th, 18th, and 24th months after Shulifenxiao treatment were analyzed. All adverse events recorded during follow-up were also analyzed.

### Outcome Measures

The primary outcomes were attainment of complete and partial remission and changes in proteinuria and serum albumin. Complete remission (CR) was defined as a reduction of proteinuria to <0.3 g/d and serum albumin >35 g/L; Partial remission (PR) was defined as level of proteinuria decline to <3.5 g/day but minimum >0.3 g/day and at least 50% reduction from baseline with a serum albumin concentration of at least 30 g/L; Nonremission (NR) was defined as a reduction of proteinuria <50% or proteinuria >3.5 g/d. Relapse was defined as an increased proteinuria >3.5 g/d in consecutive analyses in patients with CR or PR. Any relapse was considered as an endpoint of the study. If no relapse was observed prior to the latest visit, June 30, 2018, was designated as the endpoint. Secondary outcomes included changes in serum creatinine and eGFR levels at each time point.

### Statistical Analysis

Statistical analysis was performed with SPSS 20.0 (version 20.0; SPSS, Chicago, IL, United States). Values are given as mean ± standard deviation for normal distribution variables, and median with interquartile range for abnormal distribution continuous variables. The *t*-test was used for comparisons of the means of two normal distributed quantitative variables. One-way analysis of variance (ANOVA) was used for comparisons of the means of multiple normal distributed quantitative variables. For anomaly distributed qualitative variables, a paired nonparametric test was used. A *p* value < 0.05 was considered to be statistically significant.

**TABLE 1** | Characteristics of patients at baseline.

| Characteristics | Baseline ($n$ = 31) |
|---|---|
| Gender [$n$ (male/female)] | 23/8 |
| Age (years) | 44 (28–53) |
| Duration of disease (months) | 12 (8–36) |
| Systolic BP (mmHg) | 128.77 ± 11.88 |
| Diastolic BP (mmHg) | 77.9 ± 9.1 |
| Histology grading of membranous nephropathy ($n$ [%]) stage I | 13 (41.9) |
| Stage II | 10 (32.3) |
| Stage III | 2 (6.5) |
| Non-typical membranous nephropathy | 6 (19.3) |
| Proteinuria (g/d) | 6.02 (5.13–8.8) |
| **Proteinuria Group [$n$ (%)]** | |
| 4–8 g/d | 22 (71) |
| >8 g/d | 9 (29) |
| Serum Albumin (g/L) | 28 (21.8–28.9) |
| Serum Creatinine (umol/L) | 78 (61.9–97.2) |
| eGFR (mL/min/1.73 m$^2$) | 100.24 (72.73–124.7) |
| **eGFR Group [$n$ (%)]** | |
| >90 ml/min/1.73 m$^2$ | 18 (58.0) |
| 60–90 ml/min/1.73 m$^2$ | 7 (22.6) |
| <60 ml/min/1.73 m$^2$ | 6 (19.4) |
| ACEI [$n$ (%)] | 20 (64.5) |
| ARB [$n$ (%)] | 11 (35.5) |

*Results are presented as mean ± standard deviation, median with inter-quartile range, or number of patients (percentage).*

# RESULTS

## General Information

Characteristics of the 31 patients at baseline are listed in **Table 1**. All patients were treated with Shulifenxiao formula for a minimum of 12°months. Of these, 17 patients had complete clinical and laboratory data for 18°months of treatment, and 11 patients had complete data of 24°months of treatment. The average follow-up time was 21 ± 9.16°months. Other diseases associated with MN include 11 patients with hypertension, 1 with diabetes, 6 with hyperlipidemia, 1 with hyperuricemia, and 2 with coronary heart disease. The previous immunosuppressive agents used in the 31 patients were shown in **Table 2**.

## Primary Outcomes

The partial and complete remission rates increased gradually with the extension of treatment time (**Figure 2A**). The remission rate was 45.2% (14/31; CR 6.5% and PR 38.7%) at 6°months, 80.7% at 12°months (25/31; CR 29.0% and PR 51.6%), and 90.9% at 24°months (10/11; CR 54.6% and PR 36.4%). The average length from treatment initiation to PR was 7.32 ± 3.61°months, while to CR was 12.38 ± 4.73°months. Notably, two (6.45%) patients presented relapse within 24°months. One patient who achieved CR at 6°months relapsed at 12°months (due to a urinary tract infection). Another PR patient relapsed at 24°months (due to an upper respiratory infection), which indicated the end of the follow-up.

The changes in proteinuria and serum albumin levels in RIMN patients are illustrated in **Figures 2B,C**. The proteinuria

levels decreased drastically from 6.02 (5.13–8.80)°g/d at baseline to 0.98 (0.27–2.41)°g/d at 12°months ($p < 0.001$) and further to 0.27 (0.1–1.34)°g/d at 24°months ($p = 0.003$). Meanwhile, serum albumin gradually increased from 28 (21.8–28.9)°g/L at baseline to 37.2 (35.2–43.7)°g/L at 12°months ($p < 0.001$) and to 41.3 (35.8–46.1)°g/L at 24°months ($p = 0.003$). Levels of both test indices showed a significant difference between baseline and different post-treatment time points.

It is well known that MN has a high spontaneous remission rate (Saito et al., 2017), and it can be concluded that some patients achieve spontaneous remission. In order to exclude such potential spontaneous remission cases, we reviewed the proteinuria and

**TABLE 2** | The previous immunosuppressive agents used in patients.

| Previous treatment regimen | Samples | Percentage (%) |
|---|---|---|
| PRED, CTX | 6 | 19.35 |
| CsA | 3 | 9.68 |
| CsA, PRED | 6 | 19.35 |
| CsA, TAC | 1 | 3.23 |
| CsA, PRED, TAC | 1 | 3.23 |
| TAC | 4 | 12.90 |
| PRED, TAC | 3 | 9.68 |
| PRED, CTX, CsA | 3 | 9.68 |
| PRED, CTX, TAC | 1 | 3.23 |
| PRED, TAC, MMF | 2 | 6.45 |
| PRED, CsA, MMF | 1 | 3.23 |

*CsA, cyclosporine A; CTX, cyclophosphamide; MMF, mycophenolate mofetil; PRED, prednisone; TAC, tacrolimus.*
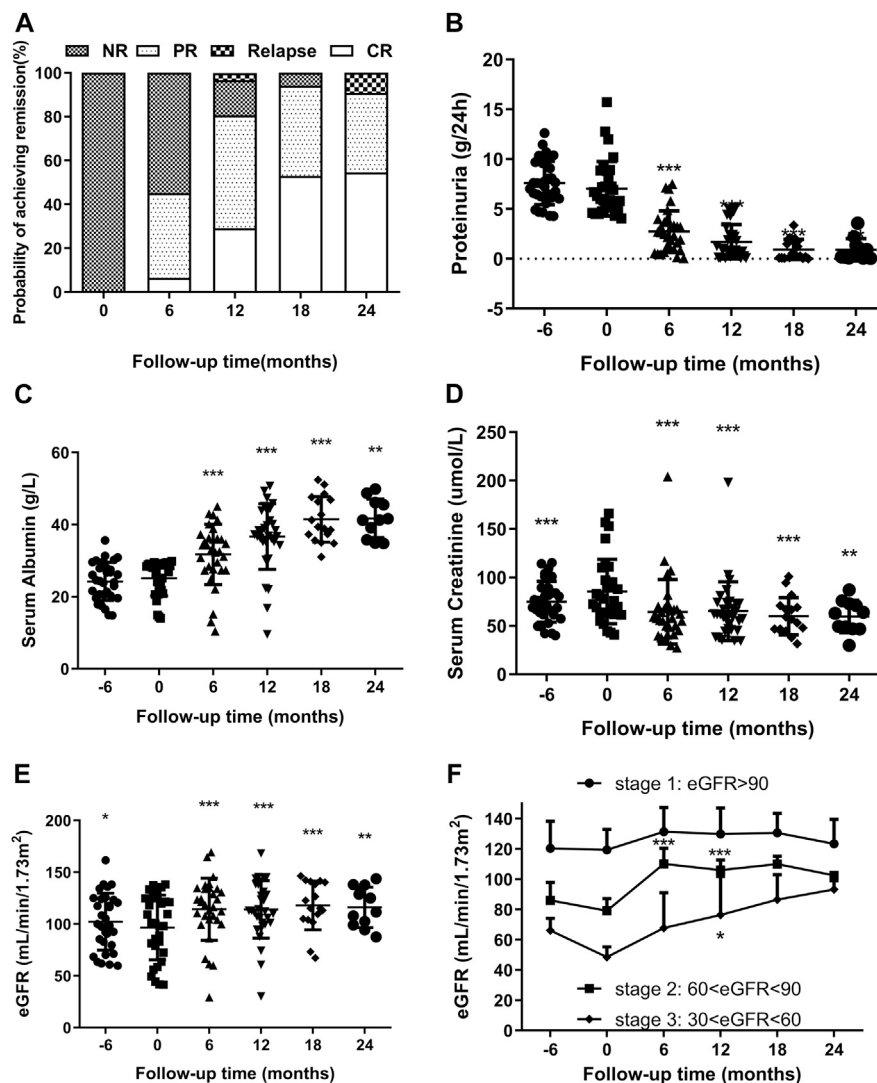
**FIGURE 2 | (A)**. Remission and relapse rates of RIMN paitients with follow-up time (in months after starting Shulifenxiao formula therapy). **(B,C)** Changes of proteinuria and serum albumin levels (median with inter-quartile ranges) with follow-up time in RIMN patients (–6°months means 6°months before Shulifenxiao therapy). The values of each time point were compared to the baseline (0°months), and the $p$ values were evaluated by paired non-parametric test. *$p$ values < 0.05, **$p$ values < 0.01, ***$p$ values < 0.001. **(D,E)** The changes of serum creatinine and eGFR levels (median with interquartile ranges) with follow-up time in RIMN patients. **(F)**. The changes of eGFR levels (mean ± standard deviation) in RIMN patients of three stages with follow-up time (–6°months means 6°months before Shulifenxiao therapy). The values of each time point were compared to one's own baseline. The $p$ values of **(D,E)** were evaluated by a paired non-parametric test, and the $p$ values of **(F)** were evaluated by one-way ANOVA test.*$p$ values < 0.05, **$p$ values < 0.01, ***$p$ values < 0.001.

serum albumin levels 6°months prior to the TCM treatment. Data showed that there were no significant changes in these levels in the prior 6°months ($p > 0.05$).

## Secondary Outcomes
Another important finding of this study was the reduction in serum creatinine. Although the level of serum creatinine increased from 6°months prior to TCM treatment ($p < 0.001$), it decreased remarkably from 78 (61.99–7.2)°g/L at baseline to 58 (45.23–68)°g/L at 6°months ($p < 0.001$) and continued to fluctuate smoothly until reaching 63 (47–73)°g/L at 24°months ($p = 0.003$) (**Figure 2D**). Simultaneously, eGFR significantly increased from

100.25 (72.37–124.70) at baseline to 118.39 (104.09–133.86)°ml/min/1.73 m$^2$ at 6°months ($p < 0.001$) and finally to 111.62 (99.01–137.83)°ml/min/1.73 m$^2$ at 24°months ($p = 0.008$) (**Figure 2E**).

Next, we observed changes in eGFR values. To the best of our knowledge, according to the KDOQI clinical guidelines, chronic kidney disease (CKD) can be classified into different stages (Levey 2003): Stage 1: kidney damage with normal or increased GFR (≥90 ml/min/1.73 m)$^2$; Stage 2: kidney damage with mild decreased GFR (60–89 ml/min/1.73 m)$^2$; Stage 3: moderately decreased GFR (30–59 ml/min/1.73 m)$^2$; Stage 4: severely decreased GFR (15–29 ml/min/1.73 m)$^2$; Stage 5: kidney failure

with GFR <15 ml/min/1.73 m$^2$ or dialysis required. As shown in **Figure 2F**, although there was no significant difference from baseline ($p > 0.05$), eGFR values in stage 1 were still on the rose after treatment. Interestingly, the eGFR values of the stage 2 group were statistically enhanced from 79.14 ± 8.63 ml/min/ 1.73 m$^2$ at baseline to 110.16 ± 11.14 ml/min/1.73 m$^2$ at 6°months, and reached 106.02 ± 7.22 ml/min/1.73 m$^2$ at 12°months, and a significant difference was observed compared to baseline ($p < 0.001$). A similar trend was observed in the group of CKD stage 3: the eGFR values increased from 48.58 ± 7.34 ml/min/1.73 m$^2$ at baseline to 67.85 ± 25.27 ml/min/1.73 m$^2$ at 6°months ($p = 0.167$), and to 76.39 ± 27.92 ml/min/1.73 m$^2$ at 12 months ($p = 0.04$). Since there were fewer than 5 cases in stages 2 and 3 during the 18th and 24th°month, we did not compare them. From the above results, it can be seen that Shulifenxiao formula treatment can improve the glomerular filtration rate, especially in patients with low eGFR.

## Safety

Over the follow-up time of 31 patients, liver function, routine blood tests, and blood pressure in all the patients indicated no significant changes from baseline after the intervention (**Table 3**). No severe adverse events were reported. Only one patient developed nausea, and another patient developed vomiting, but both were transient and the symptoms resolved after 2 weeks.

## DISCUSSION

The treatment for adult patients with RIMN who are resistant to standard immunosuppressive therapies remains a therapeutic challenge. The efficacy and safety profile of conventional treatments like steroids, CTX, CsA, TAC is not always satisfactory as revealed by recent studies. W. Chen et al. (Chen et al., 2013) reported a benefit of combining TAC with prednisone in treating 14 adults Chinese RIMN patients, that remission was attained in 11/14 patients (78.6%: CR 35.7% and PR 42.9%) at the end of follow-up. T. Saito et al. (Saito et al., 2017) treated 19 patients with Mizoribine (MZR) in combination with prednisolone, and CR was attained in only 10/19 (52.6%) patients after more than 2°years of treatment. F.B. Cortazar et al. (Cortazar et al., 2017) reported a higher remission rate in a study combining low-dose rituximab with oral

cyclophosphamide, and an accelerated prednisone taper in treating 15 consecutive IMN patients (including 8 RIMN patients), in which 100% of patients achieved PR and 93% of patients achieved CR at a median time of 2 and 13°months respectively. Regardless of their fair or good efficacy, these therapies have serious adverse events, sometimes with fatal consequences. Therefore, in China, many RIMN patients turn to traditional Chinese medicine (TCM) for alternative therapy. In this study, we retrospectively reviewed the efficacy and safety of Shulifenxiao formula in 31 adult RIMN patients who did not response to 6°months conventional immunosuppressant therapies.

In this study, we excluded cases with spontaneous remission potentials by confirming no changes in the proteinuria, serum albumin levels of all patients from 6°months prior TCM treatment to the baseline. After Shulifenxiao treatment, a significant decrease in proteinuria from 6.02 g/d at baseline to 0.27 g/d at 24°months and an upward trend in serum albumin level was achieved. Previous studies have suggested that patients with proteinuria of 0.3–1.0 g/d showed a favourable prognosis almost equal to CR (Shiiki et al., 2004; Saito et al., 2014), and patients with PR had a similar average GFR decline as those with CR (Troyanov et al., 2004). From this viewpoint, we can consider that most participants of this study achieved remission within 2°years of treatment, which is cross verified with the results in the remission rate. Obviously, Shulifenxiao formula has shown a promising effect in inducing remission in the refractory patients and relatively low relapse rate.

Persistence of nephrotic syndrome in MN portends a poor prognosis, with a considerably high risk of a GFR decline rate of 10 ml/min/1.73 m$^2$, and a 29% ESRD risk rate (Troyanov et al., 2004), therefore long-term immunosuppressive therapies are used. However, these therapies do not always induce remission and may cause significant adverse effects. The calcineurin inhibitor (CsA and TAC) directly affects renal function and cause nephrotoxicity and hypertension. Therefore, under these treatments, improvement of proteinuria and protection of renal function seems to be a trade-off process. Notably, Shulifenxiao formula appeared to show significant benefits in increasing eGFR levels, especially in CKD stage 2: The eGFR values increased from 79.14 to 110.16 ml/min/1.73 m$^2$ at 6°months ($p < 0.001$). These findings suggest that Shulifenxiao formula can improve renal function by significantly increasing eGFR, which is important for long-term prognosis.

In the present study, no severe adverse events were observed. Liver function, routine blood tests and blood pressure in all patients indicated no significant changes between baseline and post-treatment time points. Only two patients developed nausea or vomiting, both of which were mild and easily controlled. This is clearly an exciting outcome for RIMN patients who have to take long-term immunosuppressants, most of which are associated with serious adverse events. Compared to these conventional drugs, Shulifenxiao formula seems to be a safe and beneficial solution for long-term use.
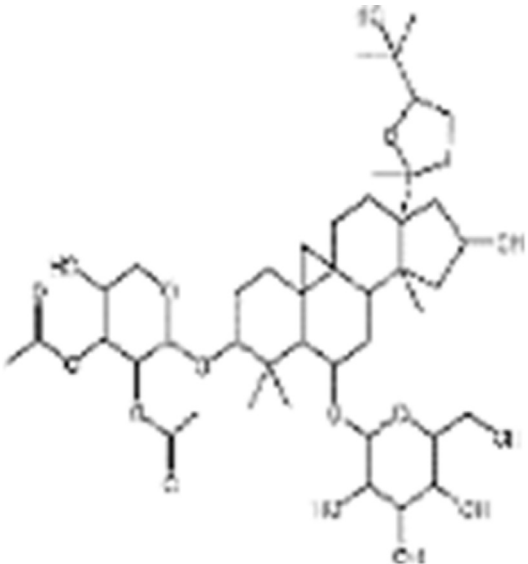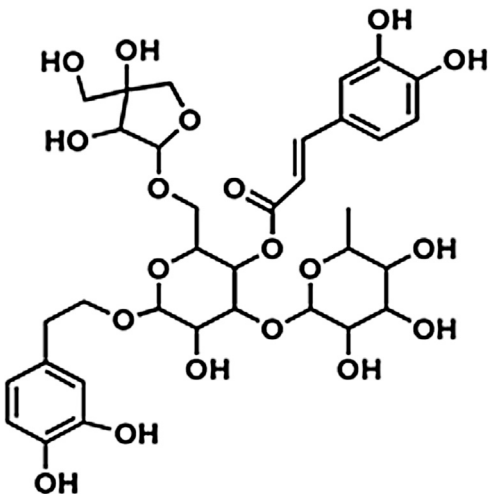
The mechanism of action for herbal medicines have been studied, and their effects are mainly related to anti-inflammation, antioxidation, antifibrosis, immune system

**TABLE 3** | Side effects of patients at baseline and the last follow-up of the study.

| Characteristics | Baseline | Last follow-up | p |
|---|---|---|---|
| ALT (U/L) | 19.11 ± 8.20 | 18.47 ± 6.21 | 0.536 |
| AST (U/L) | 18.95 ± 8.75 | 18.04 ± 5.36 | 0.603 |
| Total bilirubin (umol/L) | 8.68 ± 2.92 | 8.87 ± 3.29 | 0.799 |
| White blood cell (×109/L) | 7.48 ± 2.45 | 7.26 ± 1.29 | 0.608 |
| Hemoglobin (g/L) | 132.87 ± 15.22 | 133.61 ± 12.83 | 0.574 |
| Platelet count (×10$^9$/L) | 243.39 ± 64.32 | 243.45 ± 55.74 | 0.989 |
| SBP (mm Hg) | 128.77 ± 11.88 | 127.13 ± 8.90 | 0.17 |
| DBP (mm Hg) | 77.90 ± 9.10 | 76.94 ± 7.66 | 0.22 |
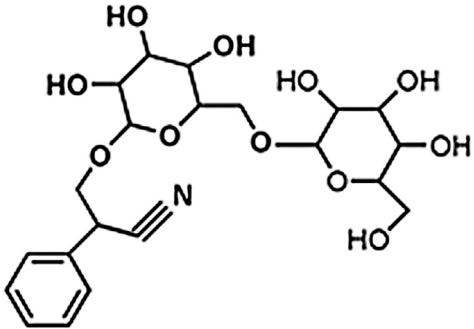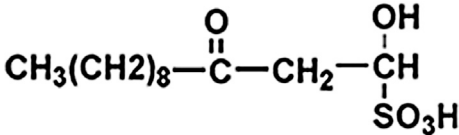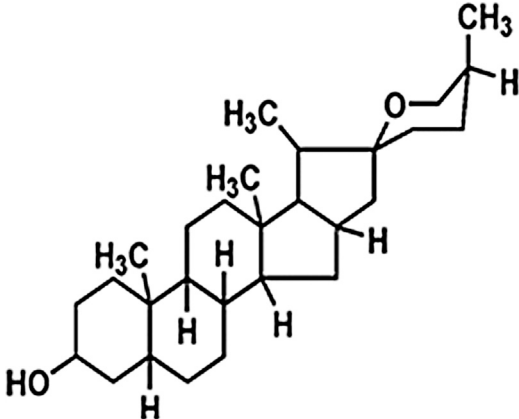
*ALT, alanine aminotransferase; AST, aspartate transaminase; DBP; diastolic blood pressure; SBP, systolic blood pressure.*

**TABLE 4** | Medicinal ingredients of Shulifenxiao formula.

| Crude drug name | Part used | (g) | Main chemicals | Chemical structure | Pharmacological activity | Clinical impacts to this kidney disease |
|---|---|---|---|---|---|---|
| Radix Astragali | Root | 60 | Saponin | | To improve immunity | Improve immunity, protect vascular endothelium, inhibit mesangial cell multiplication, encourage the metabolism of body liquid, improve hemorheological targets, protect podocytes, and reduce renal interstitial fibrosis and glomerular sclerosis |
| Fructus forsythiae | Fruit | 15 | Forsythin | | Antibacterial anti-inflammatory | It can effectively block the TLR4 signaling pathway and further by blocking the expression of inflammatory factors induced by lipopolysaccharide |
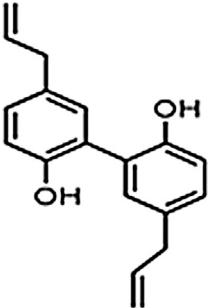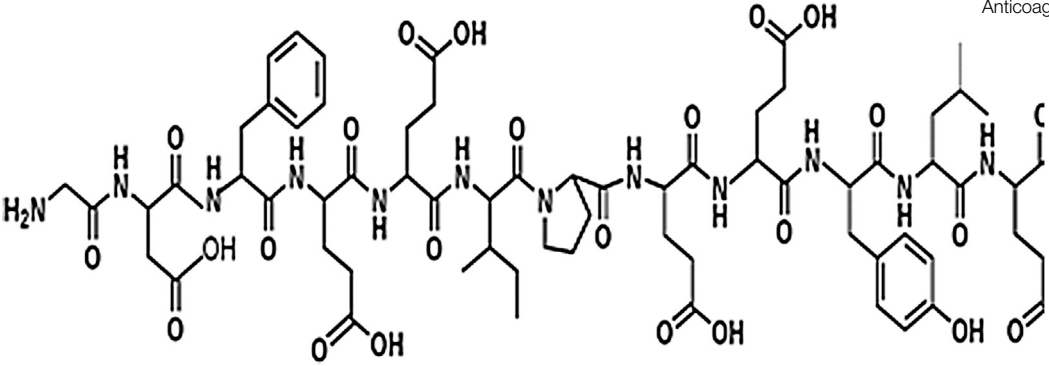
(Continued on following page)

**TABLE 4 |** (*Continued*) Medicinal ingredients of Shulifenxiao formula.

| Crude drug name | Part used | (g) | Main chemicals | Chemical structure | Pharmacological activity | Clinical impacts to this kidney disease |
|---|---|---|---|---|---|---|
| Bitter Apricot | Seed | 12 | Amygdalin | | Expectorant and anti-inflammatory | To increase the activity of type I collagenase in renal fibroblast cells in order to reduce the expression of type I collagen protein, that would further inhibit the proliferation of human renal fibroblast cells or would promote renal fibroblast apoptosis |
| Heartleaf Houttuynia | Whole | 30 | Houttuyfonate | | Antibacterial anti-inflammatory | Effective antibacterial, antiviral, enhance the body's immunity, diuresis (Good for peeing), and lower blood pressure |
| Magnolia Officinalis | Bark | 15 | Smilax saponins | | To improve immunity and anti-inflammatory | It has a muscle relaxation effect; it lowers blood pressure, anti-pathogenic microorganisms, anti-tumor; also, anti-platelet |

(Continued on following page)

34

**TABLE 4 |** (*Continued*) Medicinal ingredients of Shulifenxiao formula.

| Crude drug name | Part used | (g) | Main chemicals | Chemical structure | Pharmacological activity | Clinical impacts to this kidney disease |
|---|---|---|---|---|---|---|
| Rhizoma smilacis glabrae | Root | 30 | Magnolol | | Antibacterial | Anti-inflammatory, analgesic, antibacterial, antioxidant |
| Leech | Whole | 9 | Hirudin | | Anticoagulant | Anticoagulation, anti-thrombosis, to reduce the deposition of fibrin-related antigen in the glomerulus in order to reduce the proliferation of mesangial cells and glomerular sclerosis |

**FIGURE 3 |** Shulifenxiao formula as clinical cocktail therapy has the potential to reduce proteinuria and attenuate kidney injury through these mechanisms.
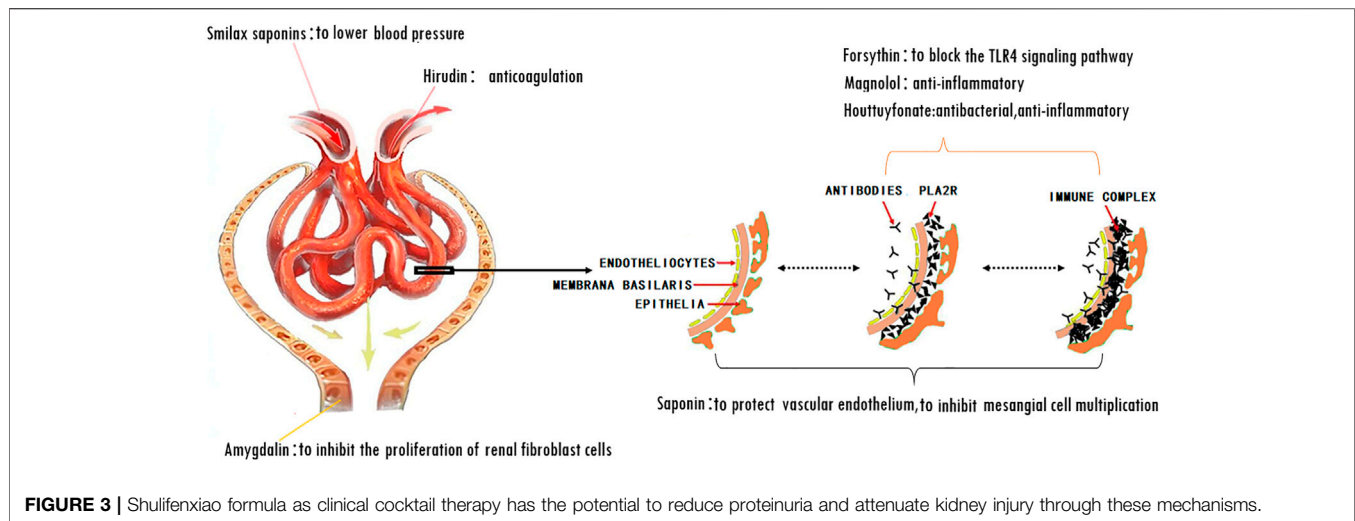
regulation, anticoagulation, and improvement of metabolic disturbance (Zhang et al., 2014; Ren et al., 2017; Wojcikowski et al., 2006). There are 7 Chinese herbal medicines in the Shulifenxiao formula (**Table 4**). One such component is Saponin in *Astragalus* which can improve immunity, protect vascular endothelium, inhibit mesangial cell multiplication, encourage the metabolism of body liquid, improve hemorheological targets, protect podocytes, and reduce renal interstitial fibrosis and glomerular sclerosis (Wang et al., 2017). Forsythin in Forsythia can effectively block the TLR4 signaling pathway and further by blocking the expression of inflammatory factors induced by lipopolysaccharide (Toba et al., 1991). Amygdalin in Bitter Apricot can increase the activity of type I collagenase in renal fibroblast cells in order to reduce the expression of type I collagen protein, that would further inhibit the proliferation of human renal fibroblast cells or would promote renal fibroblast apoptosis (Zhao and el al., 2020). Houttuyfonate in Houttuynia cordata has effective antibacterial, antiviral, enhance the body's immunity, diuresis (Good for peeing), and lower blood pressure (Wang et al., 2010). Smilax saponins in Magnolia Officinalis has the Anti-inflammatory, analgesic, antibacterial, antioxidant (Wang, 2014). Hirudin in Leech has the anticoagulation, anti-thrombosis, to reduce the deposition of fibrin-related antigen in the glomerulus in order to reduce the proliferation of mesangial cells and glomerular sclerosis (Ren et al., 2019) (**Table 4**). Cocktail therapy contains a combination of different medicines, taken by HIV/AIDS patients to improve health. Chinese officials currently administer cocktail therapy for treatment of HIV and COVID-19 (Schimt et al., 1996). The superior antiproteinuric and renoprotective effects of Shulifenxiao formula on RIMN may be related to multifactorial effects. These studies suggest that the Shulifenxiao formula as clinical cocktail therapy has the potential to reduce proteinuria and attenuate kidney injury through these mechanisms (**Figure 3**).

Our study has the advantages and innovation as this is the first report or information about "Herbal Medicine "Shulifenxiao" therapy for Nephrotic Syndrome of Refractory Idiopathic Membranous Nephropathy" in the world. Most of the previous clinical studies of TCM were the research of IMN and they compared the differences of the efficacy and safety between TCM and traditional immunosuppressant. There were few studies of RIMN. Our study focusses on RIMN, and we strictly selected the patients with nephrotic syndrome after 6 months of treatment with a standardized immunosuppressant regimen.

The major limitation of this study is that it is a retrospective single-centre study, with a limited number of patients, and lacking a parallel control group. As a matter of fact, In China, before most MN patients came to our hospital for the herbal medicine therapy, patients suffering from MN have previously received conventional treatment such as immunosuppressant or hormone therapy. Some patients cannot sustain the side effects of immunologic therapy or ineffective treatment options, and so they prefer to accept to the herbal medicine treatment. Based on real-world conditions and patients' preference for herbal treatment, all patients were treated with traditional herbal medicine, with no patients treated with immunosuppressant or hormones therapy only. This made it difficult to formulate a control group. Therefore, the statistical results must be interpreted with caution in this setting. Meanwhile, randomized controlled trials with long-term follow-up are needed in the future to establish Shulifenxiao formula as an evidence-based treatment option for RIMN patients.

## CONCLUSION

In this study, patients with refractory membranous nephropathy were treated with Shulifenxiao cocktail therapy. After treatment, it was observed that patient urine protein content decreased, plasma albumin levels increased, clinical remission rate was significantly increased, and patient's renal function was improved.

Shulifenxiao formula as clinical cocktail therapy serves as an alternative therapeutic option for steroid and general immunosuppressant-resistant RIMN patients, with a favourable safety profile, though studies with larger sample sizes and longer follow-ups are warranted. When seeking new RIMN treatment, we believe herbal medicine therapy should be considered.

## DATA AVAILABILITY STATEMENT

The raw data supporting the conclusion of this article will be made available by the authors, without undue reservation.

## ETHICS STATEMENT

The studies involving human participants were reviewed and approved by the Ethics Committee of Dongzhimen Hospital Affiliated to Beijing University of Chinese Medicine. The patients/participants provided their written informed consent to participate in this study. Written informed consent was obtained from the individual(s) for the publication of any potentially identifiable images or data included in this article. Consent to publish from the participant to report individual patient data has been obtained from each participant.

## AUTHOR CONTRIBUTIONS

YL and WL conceived the trial and obtained research funding. HC and WL designed the study and wrote the study protocol. HC and FF collected clinical data and conducted the statistical analysis and wrote the manuscript, BL contributed to the refinement of the study protocol. WL, YL, and FF critically revised the manuscript. All authors read and approved the final manuscript.

## FUNDING

## SUPPLEMENTARY MATERIAL

The Supplementary Material for this article can be found online at: https://www.frontiersin.org/articles/10.3389/fphar.2021.675406/full#supplementary-material

## REFERENCES

Chen, W., Liu, Q., Ji, Y., Liu, Z., Yu, X., Liao, Y., et al. (2013). Outcomes of Tacrolimus Therapy in Adults with Refractory Membranous Nephrotic Syndrome: a Prospective, Multicenter Clinical Trial. *Am. J. Med. Sci.* 345 (2), 81–87. doi:10.1097/maj.0b013e31824ce676

Chen, X. (2016). Clinical Observation on Curative Effect of Primary Nephrotic Syndrome Treated with Jiawei Fangji Huangqi Tang and its Effects on Serum IL-10 and TNF-α. *J. Traditional Med. Sci. Tech.* 4, 393–395.

Chen, Y., Deng, Y., Ni, Z., Chen, N., Chen, X., Shi, W., et al. (2013). Efficacy and Safety of Traditional Chinese Medicine (Shenqi Particle) for Patients with Idiopathic Membranous Nephropathy: a Multicenter Randomized Controlled Clinical Trial. *Am. J. Kidney Dis.* 62 (6), 1068–1076. doi:10.1053/j.ajkd.2013.05.005

Cortazar, F. B., Leaf, D. E., Owens, C. T., Laliberte, K., Pendergraft, W. F., and Niles, J. L. (2017). Combination Therapy with Rituximab, Low-Dose Cyclophosphamide, and Prednisone for Idiopathic Membranous Nephropathy: a Case Series. *BMC Nephrol.* 18, 44. doi:10.1186/s12882-017-0459-z

Couser, W. G. (2017). Primary Membranous Nephropathy. *Clin. J. Am. Soc. Nephrol.* 12, 983–997. doi:10.2215/cjn.11761116

Du Buf-Vereijken, P. W. G., Branten, A. J. W., and Wetzels, J. F. M. (2005). Idiopathic Membranous Nephropathy: Outline and Rationale of a Treatment Strategy. *Am. J. Kidney Dis.* 46, 1012–1029. doi:10.1053/j.ajkd.2005.08.020

Glassock, R. J. (2010). The Pathogenesis of Idiopathic Membranous Nephropathy: A 50-Year Odyssey. *Am. J. Kidney Dis.* 56 (1), 157–167. doi:10.1053/j.ajkd.2010.01.008

Iida, H., Naito, T., Sakai, N., and Aoki, S. (2000). Effect of Cyclosporine Therapy on Idiopathic Membranous Nephropathy Presented with Refractory Nephrotic Syndrome. *Clin. Exp. Nephrol.* 4 (1), 81–85. doi:10.1007/s101570050068

Ren, X. D., Zhang, Y. W., Wang, X. P., et al. (2017). Effects of Dangguibuxue Decoction on Rat Glomerular Mesangial Cells Cultured under High Glucose Conditions. *Bmc Complement. Altern. Med.* 17 (1), 283. doi:10.1186/s12906-017-1774-4

Ren, S.-H., Liu, Z.-J., Cao, Y., Hua, Y., Chen, C., Guo, W., et al. (2019). A Novel Protease-Activated Receptor 1 Inhibitor from the Leech Whitmania Pigra. *Chin. J. Nat. Med.* 17 (8), 591–599. doi:10.1016/S1875-5364(19)30061-5

Saito, T., Iwano, M., Iwano, M., Matsumoto, K., Mitarai, T., Yokoyama, H., et al. (2017). Mizoribine Therapy Combined with Steroids and Mizoribine Blood Concentration Monitoring for Idiopathic Membranous Nephropathy with Steroid-Resistant Nephrotic Syndrome. *Clin. Exp. Nephrol.* 21, 961–970. doi:10.1007/s10157-016-1340-2

Saito, T., Iwano, M., Iwano, M., Matsumoto, K., Mitarai, T., Yokoyama, H., et al. (2014). Significance of Combined Cyclosporine–prednisolone Therapy and Cyclosporine Blood Concentration Monitoring for Idiopathic Membranous Nephropathy with Steroid-Resistant Nephrotic Syndrome: a Randomized Controlled Multicenter Trial. *Clin. Exp. Nephrol.* 18, 784–794. doi:10.1007/s10157-013-0925-2

Schmit, J. C., Cogniaux, J., Hermans, P., Van Vaeck, C., Sprecher, S., Van Remoortel, B., et al. (1996). Multiple Drug Resistance to Nucleoside Analogues and Nonnucleoside Reverse Transcriptase Inhibitors in an Efficiently Replicating Human Immunodeficiency Virus Type 1 Patient Strain. *J. Infect. Dis.* 174 (5), 962–968. doi:10.1093/infdis/174.5.962

Sengupta, U., Kumar, V., Yadav, A. K., et al. (2013). Infusion of Autologous Bone Marrow Mononuclear Cells Leads to Transient Reduction in Proteinuria in Treatment Refractory Patients with Idiopathic Membranous Nephropathy. *BMC Nephrol.* 14 (1), 262. doi:10.1186/1471-2369-14-262

Shiiki, H., Saito, T., Saito, T., Nishitani, Y., Mitarai, T., Yorioka, N., et al. (2004). Prognosis and Risk Factors for Idiopathic Membranous Nephropathy with Nephrotic Syndrome in Japan. *Kidney Int.* 65, 1400–1407. doi:10.1111/j.1523-1755.2004.00518.x

Toba, T., Nagashima, S., and Adachi, S. (1991). Is Lactose Really Present in Plants? *J. Sci. Food Agric.* 54, 305–308. doi:10.1002/jsfa.2740540217

Troyanov, S., Wall, C. A., Scholey, J. W., Miller, J. A., and Cattran, D. C. Toronto Glomerulonephritis Registry Group (2004). Idiopathic Membranous Nephropathy: Definition and Relevance of a Partial Remission. *Kidney Int.* 66, 1199–1205. doi:10.1111/j.1523-1755.2004.00873.x

Wang, L., Cui, X., Cheng, L., Yuan, Q., Li, T., Li, Y., et al. (2010). Adverse Events to Houttuynia Injection: A Systematic Review. *J. Evidence-Based Med.* 3 (3), 168–176. doi:10.1111/j.1756-5391.2010.01091.x

Wang, L., et al. (2014). Natural Product Agonists of Peroxisome Proliferator-Activated Receptor Gamma (PPARγ): a Review. *Biochem. Pharmacol.* 92 (1), 73–89. doi:10.1016/j.bcp.2014.07.018

Wang, T., Xuan, X., Li, M., Gao, P., Zheng, Y., Zang, W., et al. (2017). Retraction Note: *Astragalus* Saponins Affect Proliferation, Invasion and Apoptosis of Gastric Cancer BGC-823 Cells. *Diagn. Pathol.* 12, 67. doi:10.1186/s13000-017-0657-9

Wojcikowski, K., Johnson, D. W., and Gobe, G. (2006). Herbs or Natural Substances as Complementary Therapies for Chronic Kidney Disease: Ideas for Future Studies. *J. Lab. Clin. Med.* 147, 160–166. doi:10.1016/j.lab.2005.11.011

Xiao, J., Yang, Y., Zhu, Y., Qin, Y., Li, Y., Fu, M., et al. (2018). Efficacy and Safety of Traditional Chinese Medicine on Nonerosive Reflux Disease: A Meta-Analysis of Randomized Controlled Trials. *Evidence-Based Complement. Altern. Med.* 2018, 1–13. doi:10.1155/2018/1505394

Zhang, H., Zhao, T., Gong, Y., Dong, X., Zhang, W., Sun, S., et al. (2014). Attenuation of Diabetic Nephropathy by Chaihuang-Yishen Granule through Anti-inflammatory Mechanism in Streptozotocin-Induced Rat Model of Diabetics. *J. Ethnopharmacology* 151, 556–564. doi:10.1016/j.jep.2013.11.020

Zhang, K., Dong, P., Yuxia, Q. I., et al. (2017). *Clinical Observation on Jiawei Fangjihuangqitang on the Treatment of Primary Nephrotic Syndrome in Adults.* Beijing: China Health Standard Management.

Zhang, L., Li, P., Xing, C.-y., Zhao, J.-y., He, Y.-n., Wang, J.-q., et al. (2014). Efficacy and Safety of Abelmoschus Manihot for Primary Glomerular Disease: A Prospective, Multicenter Randomized Controlled Clinical Trial. *Am. J. Kidney Dis.* 64 (1), 57–65. doi:10.1053/j.ajkd.2014.01.431

Zhao, X., et al. (2020). Research Progress on Anti - Fibrosis Mechanism of Amygdalin. *CHINESE ARCHIVES TRADITIONAL CHINESE MEDICINE* 30–10. doi:10.13193/j.issn.1673-7717.2020.10.025

**Conflict of Interest:** The authors declare that the research was conducted in the absence of any commercial or financial relationships that could be construed as a potential conflict of interest.

# Modeling the Glomerular Filtration Barrier and Intercellular Crosstalk

Kerstin Ebefors[1†], Emelie Lassén[2†], Nanditha Anandakrishnan[2], Evren U. Azeloglu[2] and Ilse S. Daehn[2*]

[1]Department of Physiology, Institute of Neuroscience and Physiology, Sahlgrenska Academy, University of Gothenburg, Gothenburg, Sweden, [2]Division of Nephrology, Department of Medicine, Icahn School of Medicine at Mount Sinai, New York, NY, United States

The glomerulus is a compact cluster of capillaries responsible for blood filtration and initiating urine production in the renal nephrons. A trilaminar structure in the capillary wall forms the glomerular filtration barrier (GFB), composed of glycocalyx-enriched and fenestrated endothelial cells adhering to the glomerular basement membrane and specialized visceral epithelial cells, podocytes, forming the outermost layer with a molecular slit diaphragm between their interdigitating foot processes. The unique dynamic and selective nature of blood filtration to produce urine requires the functionality of each of the GFB components, and hence, mimicking the glomerular filter *in vitro* has been challenging, though critical for various research applications and drug screening. Research efforts in the past few years have transformed our understanding of the structure and multifaceted roles of the cells and their intricate crosstalk in development and disease pathogenesis. In this review, we present a new wave of technologies that include glomerulus-on-a-chip, three-dimensional microfluidic models, and organoids all promising to improve our understanding of glomerular biology and to enable the development of GFB-targeted therapies. Here, we also outline the challenges and the opportunities of these emerging biomimetic systems that aim to recapitulate the complex glomerular filter, and the evolving perspectives on the sophisticated repertoire of cellular signaling that comprise the glomerular milieu.

Keywords: glomerular filtration barrier, crosstalk, *in vitro*, podocyte, glomerular endothelial cell, 3D model

"*A model is a lie that helps you see the truth*" – Dr. Howard Skipper

## INTRODUCTION

The glomerular filtration barrier (GFB) is a highly specialized interface responsible for blood filtration that is charge and size selective. While its functionality and integrity are maintained by a constant interaction between glomerular endothelial cells (GECs), the glomerular basement membrane (GBM), and podocytes (Rennke et al., 1975; Rennke and Venkatachalam, 1979), they are also influenced by the milieu and dynamics of the renal blood flow. In glomerular diseases, this barrier loses functional integrity, allowing the passage

of macromolecules and cells, and results in morphological changes, increasing the risk of long-term kidney damage that ultimately leads to kidney failure (USRDS, 2020). This is a growing worldwide health problem that accounts for a substantial economic burden (Honeycutt et al., 2013). Although the etiologies differ among glomerular diseases, damage to the GFB often has the same clinical manifestations, proteinuria or hematuria, and impaired glomerular filtration rate (GFR).

The interconnectivity and structural complexity of the GFB have favored the use of experimental *in vivo* models, where these traits are preserved. Using rodent models is regarded as the gold standard in GFB research. Mice have been used extensively to study the GFB, given the advantage that the complexity of the GFB microenvironment can be fully recapitulated, that there are several available genetically defined strains and the relative ease of single gene targeting (Becker and Hewitson, 2013). Also, transgenic lines with fluorescent reporters in different glomerular cell types provide visual readout and have been useful for determining the origins and fate of glomerular cells *in vivo* (Hackl et al., 2013). There are however significant challenges with mimicking human disease in animals, as many models do not completely recapitulate human disease manifestations and instead allow only for studies of certain disease aspects (Becker and Hewitson, 2013). However, the use of animal models is of particular importance for pharmacodynamics and pharmacokinetics testing, where the effects of pharmaceutical interventions can be examined at the systemic level to determine drug safety and efficacy before entering human trials.

The use of transgenic zebrafish strains is growing as a vertebrate model for GFB research (Zhou and Hildebrandt, 2012; Hansen et al., 2020) and has proven to be a useful tool to investigate glomerular disease development and the effects of drugs on GFB (Schiffer et al., 2015; Müller-Deile et al., 2019). Although studies in zebrafish are more time- and cost-efficient compared with rodent models, there are some inherent caveats. It can for instance be difficult to detect proteinuria or the clearance of specific markers of interest in the urine due to the surrounding water volume. Also, zebrafish have numerous duplicate genes (Woods et al., 2000), which complicates the generation of knockout strains, and they also have the ability to regenerate nephrons *de novo* after injury. Other limitations include the need for microinjections to the dorsal aorta and cardinal vein for certain drugs, which limits throughput. Altogether, animal work can be expensive, has limited throughput, and poses challenges for studying intricate crosstalk between the cells in the glomerulus. Therefore, there is a need for microphysiological systems that can recapitulate the form and function of the GFB and offer a controlled environment for studies of isolated pathological events. Current model systems range from simple to physiologically complex and offer opportunities for examining specific mechanisms involved in the maintenance as well as damage to the GFB (**Table 1**). Here, we review and discuss some of the current and future experimental *in vitro* model systems for studying the GFB.

# THE FUNCTIONAL BARRIER
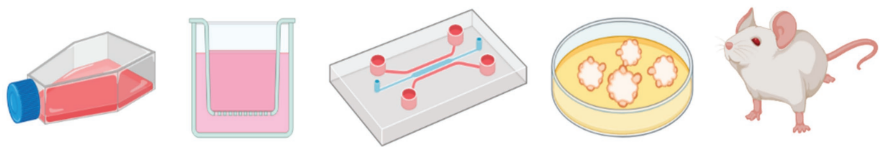
The glomerulus is the filtering part of the nephron (**Figure 1A**) and consists of three different cell types: podocytes (visceral epithelial cells), GECs, and mesangial cells. The filtrate from the glomerulus enters the Bowman's capsule as pre-urine before reabsorption and secretion in the tubular system. Glomerular cells are highly specialized and interdependent, with fenestrated GECs covering the luminal surface of glomerular capillaries, in direct contact with the blood. Podocytes tightly wrap around the glomerular capillary vessels, with interdigitating foot processes bridged by a slit diaphragm (**Figure 1B**). GECs and podocytes share a common extracellular matrix (ECM), the glomerular basement membrane (GBM), and together, they form the GFB (**Figure 1C**). Between the capillaries are contractile mesangial cells surrounded by their ECM, providing structural support to the glomerular tuft (Brenner et al., 1978).

The GFB function relies on its three layers: podocytes, GBM, and GECs (**Figure 1C**). Podocytes are terminally differentiated epithelial cells that form the architectural backbone of the GFB anchored to the GBM through transmembrane receptors, such as integrins (e.g., integrin α3 and laminin β2) and dystroglycan, and cover the outer aspect of the glomerular capillary (Pozzi et al., 2008; Meyrier, 2011). They have specialized projections that interdigitate to form the slit diaphragm, a key element in the GFB (Perico et al., 2016). The slit diaphragm proteins (e.g., nephrin and podocin) anchor to the cytoskeleton at the plasma membrane and form bridging structures between the interdigitating podocyte projections (foot processes; Kestila et al., 1998; Boute et al., 2000). Additional proteins that maintain slit diaphragm proteins, such as CD2AP, play vital roles in GFB maintenance. Podocytes are essential in GFB function, underscored by the discovery of pathogenic mutations to proteins involved in maintaining podocyte structure that are causal to proteinuric forms of kidney disease (Vivante and Hildebrandt, 2016; Li et al., 2020a).

The GBM is formed by secreted products from both podocytes and endothelial cells during glomerulogenesis (St John and Abrahamson, 2001). Its role in the barrier function is highlighted by genetic studies showing that mutations in key components of GBM; encoding laminin-α5 and *COL4A5*, or recessive *COL4A3/4*, results in basement membrane nephropathy due to the absence or inadequate assembly of all collagen chains. These mutations contribute to the development of nephrotic syndrome in pediatric patients and Alport syndrome, respectively (Tryggvason et al., 1993; Kashtan, 1999; Quinlan and Rheault, 2021).

Glomerular endothelial cells are highly specialized cells with fenestrae and a charged luminal endothelial surface layer, or glycocalyx, that is composed of negatively charged networks of proteoglycans, glycoproteins, and glycolipids (Ballermann, 2007; Fogo and Kon, 2010; Haraldsson and Nystrom, 2012; Khramova et al., 2021) that together with the GBM contribute to the maintenance of a charge-selective barrier which is important to restrain albumin from the glomerular filtrate (Jeansson et al., 2009; Singh et al., 2011; Öberg and Rippe, 2013; Boels et al., 2016; **Figure 1C**). GEC dysfunction can initiate and contribute to GFB breakdown (Haraldsson et al., 2008; Haraldsson and Nystrom, 2012; Sun et al., 2013; Daehn, 2018). In addition, activated podocytes have been shown to influence endothelial

**TABLE 1 |** Comparison of *in vivo* and *in vitro* models currently used or under development for studies of the glomerular filtration barrier (GFB).



| | In vitro | | | | In vivo |
| --- | --- | --- | --- | --- | --- |
| | 2D monolayer | Static co-culture | Microfluidic co-culture | Spheroids organoids | Animal models |
| All GFB cell types (Nishinakamura, 2019) | No | No | No | No | Yes |
| GBM (Slater et al., 2011; Chew and Lennon, 2018; Hale et al., 2018; Petrosyan et al., 2019) | No | Limited | Limited | Limited | Yes |
| Glycocalyx (Singh et al., 2007; Petrosyan et al., 2019; Koning et al., 2020) | Limited | Limited | Yes | Limited | Yes |
| Allows cell differentiation (relevant phenotype; Musah et al., 2017; Bao et al., 2018; Nishinakamura, 2019; Veissi et al., 2020) | No | No | Limited | Limited | Yes |
| Permselectivity (Li et al., 2016; Petrosyan et al., 2019; Li et al., 2020b) | No | Yes | Yes | Limited | Yes |
| Recapitulation of microenvironment (Huh et al., 2013; Bhatia and Ingber, 2014; Veissi et al., 2020) | No | Limited | Limited | Limited | Yes |
| Controlled microenvironment (Anandakrishnan and Azeloglu, 2020) | Yes | Yes | Yes | Yes | No |
| Shear stress (Slater et al., 2012; Musah et al., 2017; Yang et al., 2017; Homan et al., 2019) | No | Limited | Yes | Limited | Yes |
| Bidirectional crosstalk (Li et al., 2016; Casalena et al., 2020; Veissi et al., 2020) | No | Yes | Yes | Limited | Yes |
| Material of human origin (Little and Takasato, 2015; Musah et al., 2017; Anandakrishnan and Azeloglu, 2020) | Yes | Yes | Yes | Yes | No |
| High throughput (Boreström et al., 2018; Anandakrishnan and Azeloglu, 2020) | Yes | Limited | Limited | Limited | No |
| Development of personalized/precision medicine (Anandakrishnan and Azeloglu, 2020) | Yes | Yes | Yes | Yes | No |
| Timeline for experiment | Short | Short | Long | Long | Long |

glycocalyx remodeling and loss in experimental FSGS and *in vitro* (Ebefors et al., 2019). In diabetic kidney disease, GEC dysfunction and glycocalyx damage represent initiating steps in diabetic albuminuria in humans and in experimental models (Zhao et al., 2006; Satchell and Tooke, 2008; Yuen et al., 2012; Dogne et al., 2016; Lassen and Daehn, 2020).

Importantly, bidirectional signaling enables cells in the glomeruli to function effectively, where podocytes control GEC growth and survival *via* crosstalk of paracrine vascular endothelial growth factor alpha (VEGFA and VEGF-R; Sison et al., 2010; Jeansson et al., 2011). Crosstalk also exists between endothelial and mesangial cells (PDGF-B and PDGFR-β) and between podocytes and mesangial cells (CCL21 and CCR7; Vaughan and Quaggin, 2008; Schlondorff and Banas, 2009). Hence, all components contribute to the overall structure and function of this complex barrier, and model systems that can recapitulate *in vivo* biology and microenvironment would provide a platform for studying cell crosstalk and feedback regulation and open up the new therapeutic strategies specifically targeting the GFB.

## Modeling the Glomerular Filtration Barrier

The unique environment and complex interactions between the specialized cells in the GFB make modeling glomerular disease particularly challenging. Podocytes are a key target cell for injury in the evolution of segmental sclerosis lesions of proteinuric diseases, and their morphology is critical for glomerular filtration. However, once isolated, podocytes rapidly dedifferentiate and lose their specialized morphology, making it difficult to study their function *in vitro*. Immortalized mouse and human podocyte cell lines have played a fundamental role in advancing podocyte research, but they lack defined foot processes as well as slit diaphragms. Efforts have been made to improve podocytes in culture to more closely recapitulate their *in vivo* phenotypic characteristics. By modulating the ECM, which affects most aspects of cellular behavior, researchers have established that growing primary rat podocytes in the presence of heparin and all-trans retinoic acid on laminin-coated plates resulted in podocytes with primary processes that further bifurcated and interdigitated with adjacent cells (Yaoita et al., 2018). Growing podocytes in

**FIGURE 1 |** Schematic drawing of a single nephron and glomerulus, a glomerular capillary vessel, and the glomerular filtration barrier (GFB). **(A)** A single nephron comprising the blood-filtering glomerulus, enveloped by Bowman's capsule that connects to the proximal tubule at the start of the urine-modifying tubular system. **(B)** The luminal surface of the glomerular capillary vessel is covered by glomerular endothelial cells (GECs), while podocytes wrap around the outside of the vessel with primary and foot processes (FT), forming an interdigitated pattern. Neighboring FPs are bridged by the slit diaphragm, one of the several essential components for glomerular permselectivity. The blood is filtered over this capillary barrier, and the pre-urine produced is forwarded from the Bowman's capsule into the lumen of the proximal tubule. **(C)** The schematic cross section of the GFB displays the GEC fenestrae attached to the basement membrane (BM) and covered luminally by glycoproteins, proteoglycans, and glycosaminoglycans of the glycocalyx, important for maintaining the charge selectivity of the GFB. On the opposite side of the BM, the podocyte FPs are attached. The FPs interlink by slit diaphragm proteins, such as nephrin and podocin, are important for the restriction of albumin by the GFB. The arrow shows the direction of plasma filtration over the barrier.

a gelatin microbial transglutaminase platform tuned to the stiffness of healthy glomeruli promoted the differentiation and maturation response of podocytes (Hu et al., 2017). Other approaches involve culturing podocytes on nanoporous surfaces with grooves. This method showed that podocytes were better differentiated, had organized actin cytoskeleton stress fibers, and developed vinculin-positive focal adhesions (Zennaro et al., 2016). Microscale curvature surfaces have also been shown to promote podocyte differentiation *in vitro* (Korolj et al., 2018). By growing podocytes on topographic substrates, the authors showed augmented nephrin expression and structured F-actin arrangement within cells. The curved surfaces promoted process formation with interdigitation and improved barrier function compared to podocytes grown on flat substrates (Korolj et al., 2018). Bioengineered surfaces that artificially induce branch formation have been developed by growing podocytes on a 3D geometry that mechanically enforces the arborization of individual podocytes (Ron et al., 2017). The formation of peripheral projections showed increased slit diaphragm proteins (nephrin, podocin, and NEPH1) and synaptopodin, as well as actinin-4 cross-linked actin stress fibers properly localized within these peripheral processes. In addition to observing slit diaphragm-like cell-cell junctions, the authors also demonstrated that on these surfaces, podocytes had a significant increase in expression of genes related to podocyte function, hence a more mature physiological phenotype (Ron et al., 2017). The next steps are already underway involving the derivation and generation of human pluripotent stem cells into podocyte-like cells (Yaoita et al., 2018; Ge et al., 2020). These will be instrumental for future studies and high-content screening for podocentric therapies, and for integration into more complex model systems discussed below.

There are also challenges in obtaining, culturing, and maintaining GECs *in vitro*. GECs differ in anatomy to most other endothelial cells in the body and are defined by their fenestrations, which are important for the function of the filtration barrier (Satchell and Braet, 2009; Fogo and Kon, 2010). The fenestrations lack diaphragm but are covered with a glycocalyx. Mimicking GEC function *in vitro* has been challenging as they lose fenestrations in culture. This may be due to their dependence on podocyte-derived growth factors for their viability through intercellular crosstalk and interactions with the GBM. However, the very first human glomerular endothelial cell (GEnC) line, developed by Satchell et al. (2006), was shown to have fenestrations in response to VEGF, and over the years, it has proved to be a useful tool in GFB research, including in studies of glomerular cell interactions (Boor et al., 2010; Byron et al., 2014). The importance of VEGF-C on GEC monolayer permeability has been demonstrated through the measurement of trans-endothelial electrical resistance (TEER) as an indicator of the integrity of GEC's intercellular junctions (Ramnath and Satchell, 2020) and the passage of fluorescence-labeled BSA (Foster et al., 2008). The authors found that VEGF-C increased TEER and limited albumin passage, in contrast to the effect of VEGF-A, suggesting that these podocyte-derived growth factors regulate the permeability of GECs in the GFB (Foster et al., 2008). Although quantification of the glomerular endothelial glycocalyx *in vivo* has been achieved by direct labeling or indirect measurements (Hjalmarsson et al., 2004; Dane et al., 2015), measuring the glycocalyx in cultured GECs has been challenging due to the nature of this invisible layer. Recently, atomic force microscope elastography was used to successfully measure 3D biomechanical properties of the glycocalyx on murine GECs through direct contact by deflection of a cantilever, without

exposing cultured cells to fixation or staining procedures that alter the fragile structure (Ebefors et al., 2019). An additional requirement of GECs function is fluid flow, which is absent in monocultures, leading to loss of the influence of shear stress on cell shape and signal transduction that is present under physiological conditions (Ballermann et al., 1998). One shear stress-inducible transcription factor is Krüppel-like factor 2 (KLF2; Lee et al., 2006), an important regulator of hemodynamic signals in endothelial cells that has been shown to be dysregulated in diabetic kidney disease. Importantly, the endothelial cell-specific knockout of KLF2 results in worsened endothelial cell and podocyte injury in an experimental model of type 1 diabetes (Zhong et al., 2014).

In addition to the challenges of providing a favorable biophysical environment for glomerular cells, ideal models of the GFB should allow for adjustment of the GFR, given that hyperfiltration occurs under physiological conditions, such as during pregnancy, and is commonly observed in DKD, polycystic kidney disease, and sickle-cell anemia (Helal et al., 2012; Cheung and Lafayette, 2013). A physiological decline in GFR is conversely associated with advancing age (Musso and Oreopoulos, 2011). Hence, adjustable GFR is an important consideration for the physiological relevance of *in vitro* GFB models that can be addressed by using microfluidic devices. Innovative tools are still needed to account for tubuloglomerular feedback (TGF) that is regulated *via* macula densa cells in the distal tubule and the myogenic response (Vallon, 2003). TGF has mostly been studied *in vivo* due to the challenges of studying the intricate signaling between these cells *in vitro*.

Despite some of the challenges mentioned, *in vitro* models are making substantial progress as an alternative or complement to *in vivo* experimental models for mechanistic studies of the GFB components and intercellular crosstalk. In the following sections, we review the recent developments in this evolving field.

# STUDYING GLOMERULAR CELL CROSSTALK

Two-dimensional (2D) cultures are a simple culture system to study glomerular cell-specific effects, as they provide screening of large numbers of conditions and treatments that would otherwise not be possible *in vivo* (**Table 1**). To study glomerular crosstalk, conditioned medium transfer is necessary when using 2D cultures. Despite the inherent limitations of 2D cultures, this system allows to chronologically separate cellular signaling events of pathogenic stimuli that ultimately lead to cell and/or organ dysfunction.

There are different strategies used for the conditioned medium transfer, and these have been well described by Hanspal et al. in the context of amyotrophic lateral sclerosis research (Hanspal et al., 2017). The simplest strategy consists of whole medium transfer from one monoculture to another in separate culture vessels. There can also be an intermediate step of extraction or enrichment of specific media components before medium transfer to the acceptor cell culture. Insights from this approach have provided evidence for the pathologic effects of the milieu in women with preeclampsia, where factors including

endothelin-1 from GECs exposed to the serum from patients with preeclampsia resulted in shedding of nephrin from podocytes cell surface *via* endothelin receptor A after media transfer (Collino et al., 2008). Another study utilized the transfer of purified exosomes from high glucose-treated GECs to podocytes and found that TGFβ mRNA, carried by the extracellular vesicles, contributed to podocyte dedifferentiation epithelial-mesenchymal transition (Wu et al., 2017). The authors found the same mechanism of exosomes containing TGFβ mRNA to contribute to mesangial cell proliferation and matrix production through a similar experimental setup, as well as through tail-vain injections of the purified exosomes from high glucose-treated GECs in C57BL/6 mice (Wu et al., 2016). Furthermore, the studies of TGFβ-containing exosomes by another group supported the involvement of these extracellular vesicles in glomerular crosstalk following high glucose stimulation (Wang et al., 2018b). Exosomes have emerged as a novel vector for cell-cell communication in the kidney, and they are beginning to be recognized more and more as a critical player in the pathogenesis of kidney disease and decline in renal function.

Co-culture of two or more cell types offers increased complexity over monocultures when studying glomerular crosstalk. Open microfluidics systems allow simultaneous paracrine signaling between two separated cell populations by sharing culture medium and hence allow for exchange of soluble factors and transient signals (Zhang et al., 2020). In transwell systems, two distinct cell types are separated by a porous membrane (Hanspal et al., 2017), where a bidirectional exchange of signaling molecules can occur with or without direct cell-cell contact (**Table 1**). Li and colleagues demonstrated the applicability of their co-culture model of the GFB for studies of drug testing and intracellular signaling, using murine podocytes and GECs on opposite sides of a collagen IV-coated polyethylene terephthalate membrane (Li et al., 2016). More recently, the same research group successfully exchanged the murine glomerular cells for human immortalized GECs and podocytes, and reported an increase in albumin leak after exposure to sera from patients with recurrent FSGS, compared to genetic or non-recurrent forms (Li et al., 2020b). Casalena et al. have demonstrated that both high glucose and serum from diabetic mice susceptible to developing diabetic kidney disease disrupt mitochondrial function and cause oxidative stress in GECs. Interestingly, the transfer of factors released by the stressed GECs mediated podocyte cell death in transwell co-cultures, as well as in media exchange (Casalena et al., 2020). Given that bi-directional communication can still occur while cells are physically separated, this approach allows for subsequent interrogation of cell-specific responses. This approach has also been used to define podocyte-to-GEC-to-podocyte crosstalk in the pathogenesis of FSGS by shedding light on the role molecules, such as endothelin-1/endothelin receptor type A-mediated glomerular endothelial cell dysfunction, which was shown to be required for podocyte depletion and progression of glomerulosclerosis (Daehn et al., 2014).

Exposure of GECs to laminar shear forces found *in vivo* adds physiological relevance to the transwell co-culture model of the GFB. Studies by Slater et al. used both conditioned medium transfer and co-culture of human GECs and podocytes to investigate how ERK5 activation and KLF2 transcription

(associated with endothelial cell shear stress in large vessels) affected the glomerular microvasculature (Slater et al., 2012). Their findings demonstrated the existence of intercellular signaling from GECs exposed to chronic laminar shear stress that affects podocytes. In another study by the same research group, GECs and podocytes were co-cultured on opposite sides of a polycaprolactone/electrospun collagen membrane to closer mimic the GBM, which was shown to enable cell-cell contact (Slater et al., 2011). Differences in between the conditioned medium transfer and the co-culture settings suggest that spatial separation between crosstalking cell types is an important consideration.

The models described so far provide robust high-throughput, high-content reductionist assay systems. They have provided a wealth of information on the fundamental biological and disease processes of the GFB. Nevertheless, they provide a limited physiological context of the filtration barrier. Since there is growing awareness of the interconnections between cells and the ECM surrounding them, there is substantial effort by the community to develop model systems that can better reflect the complex microenvironment cells encounter in a tissue.

## 3D Culture Models of the GFB

Organs-on-a-chip have been developed for complex organs such as liver (Beckwitt et al., 2018), heart (Agarwal et al., 2013), gut (Kim et al., 2012; Kim and Ingber, 2013), lungs (Huh et al., 2010, 2012), and brain (Moreno et al., 2015). The goal has not been to mimic the whole organs, but rather to study complex parts of an organ in a more physiological context. In the renal field, chips for modeling the proximal tubules (Jang et al., 2013; Hoppensack et al., 2014; Wilmer et al., 2016) as well as the filtration barrier are being developed. An ideal model of the GFB would include cell-to-cell and cell-to-ECM interactions, biomimetic micromechanical properties, shear flow, oxygen and nutrient/waste exchange, and a functional permselective filtration barrier. In the last decade, the development of microfluidic platforms that allow co-culture of cells under flow (Bhatia and Ingber, 2014) and stretch (Huh et al., 2013) has emerged (**Table 1**) and these continue to evolve. Here, we describe some examples.

To study the effect of hypertension on the filtration barrier, Zhou et al. developed a glomerulus-on-a-chip using murine immortalized GECs and podocytes. The cells were separated in the chip by a polycarbonate membrane coated with basement membrane extracts, and the authors increased the flow in the upper channel of the chip harboring the GECs (Zhou et al., 2016). Increasing the mechanical force led to cell damage, loss of junctions, and changes to the cell's cytoskeleton, leading to increased leakage (Zhou et al., 2016). In an *in vitro* model of diabetic kidney disease, Wang et al. developed a glomerulus-on-a-chip using glomeruli isolated from rats. The chip consisted of five channels, a capillary in the middle and collection channels on the outside, with the channels in between filled with gel. Isolated glomeruli were injected in the capillary channel and allowed to attach for the cells to spread and form a barrier under flow. GECs and podocytes were identified by CD31 and synaptopodin staining, respectively. High glucose treatment enhanced the permeability to proteins and increased reactive oxygen species production and podocyte detachment (Wang et al., 2017). Musah et al. developed a glomerulus-on-a-chip with fluidics and strain by using vacuum channels on the side of the channel harboring the GECs and podocytes (Musah et al., 2017). The authors developed podocytes derived from human induced pluripotent stem cells (iPSCs) and used them in combination with human GECs separated by a porous polydimethylsiloxane membrane coated with laminin. The mechanical strain was shown to increase the expression of nephrin and secretion of VEGF-A by the podocytes. Albuminuria and podocyte damage were observed with adriamycin treatment, underscoring the resemblance to the *in vivo* setting (Musah et al., 2017). These models however lack GBM; hence, Petrosyan et al. developed a glomerulus-on-a-chip without an artificial membrane between GECs and podocytes (Petrosyan et al., 2019). The authors allowed both cell types to interact and to generate a layer of ECM components. Human GECs and podocytes were obtained from the same donor; cells were separated by collagen I and eventually formed a basement membrane between the cell layers. GECs were further shown to develop a glycocalyx layer. The cells could be maintained in the chip for at least a month, enabling long-term experiments. Exposure of chips to puromycin aminonucleoside induced podocyte injury and loss of permselectivity for albumin. Adding serum from patients with membranous nephropathy (MN) resulted in albumin leakage, which was prevented by treatment with α-MSH. Using podocytes derived from a patient with Alport syndrome rendered improper filtration, supporting the chips potential for the use in personalized medicine (Petrosyan et al., 2019).

Given that the glomerulus *in situ* has a complex structure with intricate microvascular capillary networks in a unique geometry that could play a role in the development and function of podocytes (Falkenberg et al., 2017), there have been significant efforts to generate 3D models with complex microvascular networks using 3D bioprinting technology. Rayner et al. demonstrated the use of a multiphoton microscopy-guided 3D printing technique to generate perfusable vascular networks with diameters as small as 10 μm (Rayner et al., 2021). They further demonstrate bioprinting of a glomerular-like microvascular network that supports endothelial lumen formation; however, they still require the incorporation of podocytes and mesangial cells to recapitulate the glomerular physiology and to study cell-cell crosstalk. Other developments include the glomerulus-on-a-plate, recently developed by using a microfluidic topographical hollow fiber (Xie et al., 2020). This system uses a tubular-like perfusable channel to seed GECs in a glomerulus-like knot with microconvex topography, filled with hydrogel and covered with murine podocytes. The fibers were mounted in specialized 96-well plates with inlet and outlet wells allowing flow to be applied by either gravity or syringe pump. Perfusing the lumen with albumin showed no leakage of over the barrier, while small molecules could readily pass. However, adriamycin treatment was shown to increase the passage of BSA over the barrier, but only mildly damaged podocytes (Xie et al., 2020).

Current GFB 3D culture model technologies have a number of drawbacks, such as recirculating instead of a continuous flow, long culture times to achieve fully confluent layers, lack of a basement membrane, and limited throughput. However, these models still hold great promise for improving our understanding of glomerular crosstalk and their potential use for personalized and precision medicine. In the future, chips where cells can form a basement membrane without separating gels or man-made membranes will emerge, and the inclusion of mesangial cells, pericytes, and parietal epithelial cells to the chips would enable all the intricate signaling which takes place in the glomerulus.

## Scaffold-Free 3D Cultures

Scaffold-free 3D cultures are anchorage-independent models that rely on the self-aggregation of cells in specialized culture plates with ultra-low attachment coating that promotes spheroid formation. Multicellular spheroids have been shown to recapitulate physiological characteristics of tissues and tumors with regard to cell-cell contact, and allow for natural cell-ECM interactions (Sutherland, 1988). Glomeruloid spheres have been developed using human mesenchymal stem cells, HUVECs, and HEKs (Abe et al., 2019). These spheroids expressed several podocyte markers and were stable for at least 5 days. Adding serum from patients with FSGS resulted in the collapse of the spheres (Abe et al., 2019). In 2020, Cho et al. demonstrated a novel pressure-assisted network for droplet accumulation method for high-throughput generation of uniform microtissues. As a proof of principle, they generated glomerulus-like microtissues using immortalized mouse podocytes and mesenchymal stem cells (Cho et al., 2020). More recently, Sobreiro-Almeida et al. observed that the addition of retinoic acid to an organotypic model of human renal progenitor cells resulted in spheroids with a preferential glomerular differentiation. Using a hanging drop culture technique to form spheroids, they showed that these spheroids remain viable over a period of 28 days and display an elevated expression of *PAX2* and *NPHS1* in the presence of retinoic acid. Further, co-culture with microvascular endothelial cells resulted in more compact organization of the spheroids (Sobreiro-Almeida et al., 2021).

These scaffold-free 3D cultures are not barrier models, and many questions remain: in particular, about the composition of the spheres. And improvement in oxygenation through integration of endothelial cells has not been examined in this setting. Today's glomeruloid spheres can provide insights for podocyte-ECM interactions and can be adapted to medium- or high-throughput screening assays. There is still the need for culture optimization to enhance reproducibility of spheroids in culture and to study GFB components, while maintaining a small enough size for sufficient nutrient exchange. However, this area of research is moving fast, and we will undoubtedly see advances in the years to come.

## Organoids

Attempts to fully culture organs *in vitro* have led to the development of organoids, self-organized 3D aggregations of cells. Over the last few years, these developments have provided researchers the

opportunity to establish near-physiological models to study human development and diseases. Organoids can be derived from embryonic stem cells or iPSCs. The kidney is an anatomically complex organ with numerous different cell types, which makes it difficult to get organoids containing all renal structures including a functional filtration barrier. As of today, organoids are premature, and as such, they do not represent ideal modeling systems for studies of the GFB; however, they hold promise to be so in the future.

Embryonic kidneys are divided into the metanephric mesenchyme and the ureteric bud. Nephron progenitor cells in the metanephric mesenchyme are the origin of the glomeruli, Bowman's capsule, and the renal tubules, and stromal progenitor cells give rise to interstitial cells. The ureteric bud is the origin of the collecting ducts. During development, intricate signaling leads to differentiation of cells and the formation of a mature kidney. In order to form kidney organoids, this signaling needs to be applied to embryonic or pluripotent stem cells. With this in mind, the development of differentiation protocols for embryonic and iPSCs toward renal cells (Xia et al., 2013; Taguchi et al., 2014; Takasato et al., 2014) was rapidly followed by the first reports of kidney organoids (Morizane et al., 2015; Takasato et al., 2015). Kidney organoids have been characterized *via* single-cell sequencing and have been found to contain developing podocytes, parietal epithelial cells, tubular cells, collecting ducts, and interstitial and stromal cells. Missing or underrepresented cells with current methods are GECs, mesangial cells, principal and intercalated cells (Czerniecki et al., 2018; Wu et al., 2018; Combes et al., 2019), and immune cells. Although glomerulus-like structures are formed, they mainly consist of early podocytes, and these have the potential to be explored further to study podocytopathies (Sharmin et al., 2016; Kim et al., 2017; Hale et al., 2018). Hale et al. describe a protocol for kidney organoids from iPSCs and compared the expression to human immortalized podocyte cell lines. Podocytes derived from organoids were shown to have an improved expression profile, as well as a GBM (Hale et al., 2018). Genetic modifications targeting podocytes have also been used in kidney organoids to explore congenital nephrotic syndrome (Kim et al., 2017; Hale et al., 2018; Tanigawa et al., 2018). In addition, to better study the GFB, improvements in methods that promote maturation and vascularization of the organoids have been reported recently, such as culturing kidney organoids on millifluidic chips (Homan et al., 2019), or transplantation of human kidney organoids into the subcapsular of mouse kidneys (van den Berg et al., 2018). In the latter, the authors demonstrated an improvement in the formation of a GBM with the development of a fenestrated endothelium in glomeruli (van den Berg et al., 2018). By modulating biophysical cues, such as ECM stiffness, Garreta et al. were able to accelerate kidney organoid generation from iPSCs (Garreta et al., 2019). They showed that implantation of kidney organoids into chick chorioallantoic membrane (CAM) resulted in vascularization of the organoids within 5 days. They further generated soft hydrogels that display similar mechanical properties as CAM to study if soft substrates drive kidney organoid generation compared to stiffer substrates. They observed that soft matrix environment resulted in kidney organoids that display similar protein expression as a fetal human kidney. Although the kidney organoids still are embryonic in development and need an *in vivo* environment for vascularization,

further characterization of the role of substrate stiffness can improve kidney organoid differentiation. Another limitation of the current organoid systems is the heterogeneity and batch-to-batch variation during initial formation and maturation. To address this, Dr. Little's group have employed two different approaches for scaling up the generation of kidney organoids with less heterogeneity and higher reproducibility. Kumar et al. demonstrated a method to scale up the generation of kidney micro-organoids in suspension culture (Kumar et al., 2019). Using this method, they were able to generate 8,000–10,000 kidney micro-organoids in an even size range. These organoids are less than 200–300 μm in final size, much smaller compared to standard organoids, which allows efficient nutrient diffusion to the core of the organoids. However, they showed limited utility with respect to extended long-term cultures due to the absence of vascularization. Lawlor et al. employed extrusion bioprinting method to plate cell aggregates that mature into kidney organoids, which partially eliminates organoid heterogeneity and enables scaling up of throughput (Lawlor et al., 2021). Using this technique, they were able to generate 200 organoids in 10 min. In addition to reducing variability, extrusion bioprinting can also be used to alter the conformation of the organoids, to generate a spheroid or a rectangular cell aggregate patch based on the extruding tip movement. The authors observe that the rectangular conformation yielded a greater number of nephron units compared to the spheroid conformation (Lawlor et al., 2021), which with further improvements may be useful for the development of transplantable kidney tissues.

Despite the many challenges that still remain for organoids to fully resemble mature human kidneys, including less off targets cells as described in detail in the review by Geuens et al. (2020), organoid biobanks as repository for drug screening and development are emerging (Calandrini et al., 2020) and have the potential for applications in precision medicine.

## FUTURE PERSPECTIVE

The lack of specific treatments for diseases of the GFB is a worldwide health issue. The need for new explorative *in vitro* models is paramount to elucidate the intricate signaling of cells in the GFB. Today, there is greater recognition that components of the GFB work as an integrated functional unit. As more and more new tools become available, such as iPSCs in culture and 3D model systems, we shall look to integrate these human-relevant *in vitro* models with data-driven and mechanistic modeling as well as artificial intelligence-driven methods that can assist with *in silico* drug discovery and modeling (Azeloglu et al., 2014),

which will inevitably streamline time-consuming and costly experiments. As we gain our understanding on other aspects that influence GFB function, such as tubuloglomerular crosstalk (Tasnim and Zink, 2012; Wang et al., 2018a), opportunities to "plug-in" modules will provide insights from the whole nephron's perspective and even distant organ crosstalk. Together with the increasingly quantitative precision medicine approaches that can collate and combine clinical data with genomic information, these joint efforts can help guide the design of novel drug candidates and move the field toward the common goal of treating patients with better therapies for diseases of the GFB.

## CONCLUSION

As these experimental model systems continue to evolve and improve in terms of their physiological context and throughput, model systems have a huge potential to help unravel the molecular mechanisms of GFB breakdown and the pathogenic crosstalk signaling that may drive disease. These developments should minimize the use of animal models and accelerate discoveries by enabling the platforms for personalized and precision medicine to lower drug-induced adverse events, and identify new targets for treatments of kidney diseases that affect the filtration barrier.

## AUTHOR CONTRIBUTIONS

Conceptualization by KE, EL and ID. KE, EL, NA, EA and ID wrote the manuscript. All authors contributed to the article and approved the submitted version.

## FUNDING

## ACKNOWLEDGMENTS

## REFERENCES

Abe, H., Sakurai, A., and Ochi, A. (2019). Induction of steady-state glomeruloid sphere by self-assembly from human embryonic kidney cells. *Biochem. Biophys. Res. Commun.* 508, 654–659. doi: 10.1016/j.bbrc.2018.11.160

Agarwal, A., Goss, J. A., Cho, A., McCain, M. L., and Parker, K. K. (2013). Microfluidic heart on a chip for higher throughput pharmacological studies. *Lab Chip* 13, 3599–3608. doi: 10.1039/c3lc50350j

Anandakrishnan, N., and Azeloglu, E. U. (2020). Kidney tissue engineering for precision medicine. *Nat. Rev. Nephrol.* 16, 623–624. doi: 10.1038/s41581-020-00355-6

Azeloglu, E. U., Hardy, S. V., Eungdamrong, N. J., Chen, Y., Jayaraman, G., Chuang, P. Y., et al. (2014). Interconnected network motifs control podocyte morphology and kidney function. *Sci. Signal.* 7:ra12. doi: 10.1126/scisignal.2004621

Ballermann, B. J. (2007). Contribution of the endothelium to the glomerular permselectivity barrier in health and disease. *Nephron Physiol.* 106, 19–25. doi: 10.1159/000101796

Ballermann, B. J., Dardik, A., Eng, E., and Liu, A. (1998). Shear stress and the endothelium. *Kidney Int. Suppl.* 67, S100–S108. doi: 10.1046/j.1523-1755.1998.06720.x

Bao, Y.-W., Yuan, Y., Chen, J.-H., and Lin, W.-Q. (2018). Kidney disease models: tools to identify mechanisms and potential therapeutic targets. *Zool. Res.* 39, 72–86. doi: 10.24272/j.issn.2095-8137.2017.055

Becker, G. J., and Hewitson, T. D. (2013). Animal models of chronic kidney disease: useful but not perfect. *Nephrol. Dial. Transplant.* 28, 2432–2438. doi: 10.1093/ndt/gft071

Beckwitt, C. H., Clark, A. M., Wheeler, S., Taylor, D. L., Stolz, D. B., Griffith, L., et al. (2018). Liver 'organ on a chip'. *Exp. Cell Res.* 363, 15–25. doi: 10.1016/j.yexcr.2017.12.023

Bhatia, S. N., and Ingber, D. E. (2014). Microfluidic organs-on-chips. *Nat. Biotechnol.* 32, 760–772. doi: 10.1038/nbt.2989

Boels, M. G., Avramut, M. C., Koudijs, A., Dane, M. J., Lee, D. H., van der Vlag, J., et al. (2016). Atrasentan reduces albuminuria by restoring the glomerular endothelial glycocalyx barrier in diabetic nephropathy. *Diabetes* 65, 2429–2439. doi: 10.2337/db15-1413

Boor, P., van Roeyen, C. R., Kunter, U., Villa, L., Bucher, E., Hohenstein, B., et al. (2010). PDGF-C mediates glomerular capillary repair. *Am. J. Pathol.* 177, 58–69. doi: 10.2353/ajpath.2010.091008

Boreström, C., Jonebring, A., Guo, J., Palmgren, H., Cederblad, L., Forslöw, A., et al. (2018). A CRISP(e)R view on kidney organoids allows generation of an induced pluripotent stem cell–derived kidney model for drug discovery. *Kidney Int.* 94, 1099–1110. doi: 10.1016/j.kint.2018.05.003

Boute, N., Gribouval, O., Roselli, S., Benessy, F., Lee, H., Fuchshuber, A., et al. (2000). NPHS2, encoding the glomerular protein podocin, is mutated in autosomal recessive steroid-resistant nephrotic syndrome. *Nat. Genet.* 24, 349–354. doi: 10.1038/74166

Brenner, B. M., Hostetter, T. H., and Humes, H. D. (1978). Molecular basis of proteinuria of glomerular origin. *N. Engl. J. Med.* 298, 826–833. doi: 10.1056/NEJM197804132981507

Byron, A., Randles, M. J., Humphries, J. D., Mironov, A., Hamidi, H., Harris, S., et al. (2014). Glomerular cell cross-talk influences composition and assembly of extracellular matrix. *J. Am. Soc. Nephrol.* 25, 953–966. doi: 10.1681/ASN.2013070795

Calandrini, C., Schutgens, F., Oka, R., Margaritis, T., Candelli, T., Mathijsen, L., et al. (2020). An organoid biobank for childhood kidney cancers that captures disease and tissue heterogeneity. *Nat. Commun.* 11:1310. doi: 10.1038/s41467-020-15155-6

Casalena, G. A., Yu, L., Gil, R., Rodriguez, S., Sosa, S., Janssen, W., et al. (2020). The diabetic microenvironment causes mitochondrial oxidative stress in glomerular endothelial cells and pathological crosstalk with podocytes. *Cell Commun. Signal* 18:105. doi: 10.1186/s12964-020-00605-x

Cheung, K. L., and Lafayette, R. A. (2013). Renal physiology of pregnancy. *Adv. Chronic Kidney Dis.* 20, 209–214. doi: 10.1053/j.ackd.2013.01.012

Chew, C., and Lennon, R. (2018). Basement membrane defects in genetic kidney diseases. *Front. Pediatr.* 6:11. doi: 10.3389/fped.2018.00011

Cho, C. Y., Chiang, T. H., Hsieh, L. H., Yang, W. Y., Hsu, H. H., Yeh, C. K., et al. (2020). Development of a novel hanging drop platform for engineering controllable 3D microenvironments. *Front. Cell Dev. Biol.* 8:327. doi: 10.3389/fcell.2020.00327

Collino, F., Bussolati, B., Gerbaudo, E., Marozio, L., Pelissetto, S., Benedetto, C., et al. (2008). Preeclamptic sera induce nephrin shedding from podocytes through endothelin-1 release by endothelial glomerular cells. *Am. J. Physiol. Renal Physiol.* 294, F1185–F1194. doi: 10.1152/ajprenal.00442.2007

Combes, A. N., Zappia, L., Er, P. X., Oshlack, A., and Little, M. H. (2019). Single-cell analysis reveals congruence between kidney organoids and human fetal kidney. *Genome Med.* 11:3. doi: 10.1186/s13073-019-0615-0

Czernieck, S. M., Cruz, N. M., Harder, J. L., Menon, R., Annis, J., Otto, E. A., et al. (2018). High-throughput screening enhances kidney organoid differentiation from human pluripotent stem cells and enables automated multidimensional phenotyping. *Cell Stem Cell* 22, 929.e4–940.e4. doi: 10.1016/j.stem.2018.04.022

Daehn, I., Casalena, G., Zhang, T., Shi, S., Fenninger, F., Barasch, N., et al. (2014). Endothelial mitochondrial oxidative stress determines podocyte depletion in segmental glomerulosclerosis. *J. Clin. Invest.* 124, 1608–1621. doi: 10.1172/JCI71195

Daehn, I. S. (2018). Glomerular endothelial cells stress and cross-talk with podocytes in the development of diabetic kidney disease. *Front. Med.* 5:76. doi: 10.3389/fmed.2018.00076

Dane, M. J., van den Berg, B. M., Lee, D. H., Boels, M. G., Tiemeier, G. L., Avramut, M. C., et al. (2015). A microscopic view on the renal endothelial glycocalyx. *Am. J. Physiol. Renal Physiol.* 308, F956–F966. doi: 10.1152/ajprenal.00532.2014

Dogne, S., Rath, G., Jouret, F., Caron, N., Dessy, C., and Flamion, B. (2016). Hyaluronidase 1 deficiency preserves endothelial function and glycocalyx integrity in early streptozotocin-induced diabetes. *Diabetes* 65, 2742–2753. doi: 10.2337/db15-1662

Ebefors, K., Wiener, R. J., Yu, L., Azeloglu, E. U., Yi, Z., Jia, F., et al. (2019). Endothelin receptor-A mediates degradation of the glomerular endothelial surface layer via pathologic crosstalk between activated podocytes and glomerular endothelial cells. *Kidney Int.* 96, 957–970. doi: 10.1016/j.kint.2019.05.007

Falkenberg, C. V., Azeloglu, E. U., Stothers, M., Deerinck, T. J., Chen, Y., He, J. C., et al. (2017). Fragility of foot process morphology in kidney podocytes arises from chaotic spatial propagation of cytoskeletal instability. *PLoS Comput. Biol.* 13:e1005433. doi: 10.1371/journal.pcbi.1005433

Fogo, A. B., and Kon, V. (2010). The glomerulus–a view from the inside–the endothelial cell. *Int. J. Biochem. Cell Biol.* 42, 1388–1397. doi: 10.1016/j.biocel.2010.05.015

Foster, R. R., Slater, S. C., Seckley, J., Kerjaschki, D., Bates, D. O., Mathieson, P. W., et al. (2008). Vascular endothelial growth factor-C, a potential paracrine regulator of glomerular permeability, increases glomerular endothelial cell monolayer integrity and intracellular calcium. *Am. J. Pathol.* 173, 938–948. doi: 10.2353/ajpath.2008.070416

Garreta, E., Prado, P., Tarantino, C., Oria, R., Fanlo, L., Marti, E., et al. (2019). Fine tuning the extracellular environment accelerates the derivation of kidney organoids from human pluripotent stem cells. *Nat. Mater.* 18, 397–405. doi: 10.1038/s41563-019-0287-6

Ge, X., Zhang, T., Yu, X., Muwonge, A. N., Anandakrishnan, N., Wong, N. J., et al. (2020). LIM-nebulette reinforces podocyte structural integrity by linking actin and vimentin filaments. *J. Am. Soc. Nephrol.* 31, 2372–2391. doi: 10.1681/ASN.2019121261

Geuens, T., van Blitterswijk, C. A., and LaPointe, V. L. S. (2020). Overcoming kidney organoid challenges for regenerative medicine. *NPJ Regener. Med.* 5:8. doi: 10.1038/s41536-020-0093-4

Hackl, M. J., Burford, J. L., Villanueva, K., Lam, L., Susztak, K., Schermer, B., et al. (2013). Tracking the fate of glomerular epithelial cells in vivo using serial multiphoton imaging in new mouse models with fluorescent lineage tags. *Nat. Med.* 19, 1661–1666. doi: 10.1038/nm.3405

Hale, L. J., Howden, S. E., Phipson, B., Lonsdale, A., Er, P. X., Ghobrial, I., et al. (2018). 3D organoid-derived human glomeruli for personalised podocyte disease modelling and drug screening. *Nat. Commun.* 9:5167. doi: 10.1038/s41467-018-07594-z

Hansen, K. U. I., Siegerist, F., Daniel, S., Schindler, M., Iervolino, A., Blumenthal, A., et al. (2020). Prolonged podocyte depletion in larval zebrafish resembles mammalian focal and segmental glomerulosclerosis. *FASEB J.* 34, 15961–15974. doi: 10.1096/fj.202000724R

Hanspal, M. A., Dobson, C. M., Yerbury, J. J., and Kumita, J. R. (2017). The relevance of contact-independent cell-to-cell transfer of TDP-43 and SOD1 in amyotrophic lateral sclerosis. *Biochim. Biophys. Acta Mol. Basis Dis.* 1863, 2762–2771. doi: 10.1016/j.bbadis.2017.07.007

Haraldsson, B., and Nystrom, J. (2012). The glomerular endothelium: new insights on function and structure. *Curr. Opin. Nephrol. Hypertens.* 21, 258–263. doi: 10.1097/MNH.0b013e3283522e7a

Haraldsson, B., Nyström, J., and Deen, W. M. (2008). Properties of the glomerular barrier and mechanisms of proteinuria. *Physiol. Rev.* 88, 451–487. doi: 10.1152/physrev.00055.2006

Helal, I., Fick-Brosnahan, G. M., Reed-Gitomer, B., and Schrier, R. W. (2012). Glomerular hyperfiltration: definitions, mechanisms and clinical implications. *Nat. Rev. Nephrol.* 8, 293–300. doi: 10.1038/nrneph.2012.19

Hjalmarsson, C., Johansson, B. R., and Haraldsson, B. (2004). Electron microscopic evaluation of the endothelial surface layer of glomerular capillaries. *Microvasc. Res.* 67, 9–17. doi: 10.1016/j.mvr.2003.10.001

Homan, K. A., Gupta, N., Kroll, K. T., Kolesky, D. B., Skylar-Scott, M., Miyoshi, T., et al. (2019). Flow-enhanced vascularization and maturation of kidney organoids in vitro. *Nat. Methods* 16, 255–262. doi: 10.1038/s41592-019-0325-y

Honeycutt, A. A., Segel, J. E., Zhuo, X., Hoerger, T. J., Imai, K., and Williams, D. (2013). Medical costs of CKD in the Medicare population. *J. Am. Soc. Nephrol.* 24, 1478–1483. doi: 10.1681/ASN.2012040392

Hoppensack, A., Kazanecki, C. C., Colter, D., Gosiewska, A., Schanz, J., Walles, H., et al. (2014). A human in vitro model that mimics the renal proximal tubule. *Tissue Eng. Part C Methods* 20, 599–609. doi: 10.1089/ten.tec.2013.0446

Hu, M., Azeloglu, E. U., Ron, A., Tran-Ba, K. H., Calizo, R. C., Tavassoly, I., et al. (2017). A biomimetic gelatin-based platform elicits a pro-differentiation effect on podocytes through mechanotransduction. *Sci. Rep.* 7:43934. doi: 10.1038/srep43934

Huh, D., Kim, H. J., Fraser, J. P., Shea, D. E., Khan, M., Bahinski, A., et al. (2013). Microfabrication of human organs-on-chips. *Nat. Protoc.* 8, 2135–2157. doi: 10.1038/nprot.2013.137

Huh, D., Leslie, D. C., Matthews, B. D., Fraser, J. P., Jurek, S., Hamilton, G. A., et al. (2012). A human disease model of drug toxicity-induced pulmonary edema in a lung-on-a-chip microdevice. *Sci. Transl. Med.* 4:159ra147. doi: 10.1126/scitranslmed.3004249

Huh, D., Matthews, B. D., Mammoto, A., Montoya-Zavala, M., Hsin, H. Y., and Ingber, D. E. (2010). Reconstituting organ-level lung functions on a chip. *Science* 328, 1662–1668. doi: 10.1126/science.1188302

Jang, K. J., Mehr, A. P., Hamilton, G. A., McPartlin, L. A., Chung, S., Suh, K. Y., et al. (2013). Human kidney proximal tubule-on-a-chip for drug transport and nephrotoxicity assessment. *Integr. Biol.* 5, 1119–1129. doi: 10.1039/c3ib40049b

Jeansson, M., Bjorck, K., Tenstad, O., and Haraldsson, B. (2009). Adriamycin alters glomerular endothelium to induce proteinuria. *J. Am. Soc. Nephrol.* 20, 114–122. doi: 10.1681/ASN.2007111205

Jeansson, M., Gawlik, A., Anderson, G., Li, C., Kerjaschki, D., Henkelman, M., et al. (2011). Angiopoietin-1 is essential in mouse vasculature during development and in response to injury. *J. Clin. Invest.* 121, 2278–2289. doi: 10.1172/JCI46322

Kashtan, C. E. (1999). Alport syndrome: an inherited disorder of renal, ocular, and cochlear basement membranes. *Medicine* 78, 338–360. doi: 10.1097/00005792-199909000-00005

Kestila, M., Lenkkeri, U., Mannikko, M., Lamerdin, J., McCready, P., Putaala, H., et al. (1998). Positionally cloned gene for a novel glomerular protein–nephrin–is mutated in congenital nephrotic syndrome. *Mol. Cell* 1, 575–582. doi: 10.1016/S1097-2765(00)80057-X

Khramova, A., Boi, R., Fridén, V., Granqvist, A. B., Nilsson, U., Tenstad, O., et al. (2021). Proteoglycans contribute to the functional integrity of the glomerular endothelial cell surface layer and are regulated in diabetic kidney disease. *Sci. Rep.* 11:8487. doi: 10.1038/s41598-021-87753-3

Kim, H. J., Huh, D., Hamilton, G., and Ingber, D. E. (2012). Human gut-on-a-chip inhabited by microbial flora that experiences intestinal peristalsis-like motions and flow. *Lab Chip* 12, 2165–2174. doi: 10.1039/c2lc40074j

Kim, H. J., and Ingber, D. E. (2013). Gut-on-a-Chip microenvironment induces human intestinal cells to undergo villus differentiation. *Integr. Biol.* 5, 1130–1140. doi: 10.1039/c3ib40126j

Kim, Y. K., Refaeli, I., Brooks, C. R., Jing, P., Gulieva, R. E., Hughes, M. R., et al. (2017). Gene-edited human kidney organoids reveal mechanisms of disease in podocyte development. *Stem Cells* 35, 2366–2378. doi: 10.1002/stem.2707

Koning, M., van den Berg, C. W., and Rabelink, T. J. (2020). Stem cell-derived kidney organoids: engineering the vasculature. *Cell. Mol. Life Sci.* 77, 2257–2273. doi: 10.1007/s00018-019-03401-0

Korolj, A., Laschinger, C., James, C., Hu, E., Velikonja, C., Smith, N., et al. (2018). Curvature facilitates podocyte culture in a biomimetic platform. *Lab Chip* 18, 3112–3128. doi: 10.1039/C8LC00495A

Kumar, S. V., Er, P. X., Lawlor, K. T., Motazedian, A., Scurr, M., Ghobrial, I., et al. (2019). Kidney micro-organoids in suspension culture as a scalable source of human pluripotent stem cell-derived kidney cells. *Development* 146:dev172361. doi: 10.1242/dev.172361

Lassen, E., and Daehn, I. S. (2020). Molecular mechanisms in early diabetic kidney disease: glomerular endothelial cell dysfunction. *Int. J. Mol. Sci.* 21:9456. doi: 10.3390/ijms21249456

Lawlor, K. T., Vanslambrouck, J. M., Higgins, J. W., Chambon, A., Bishard, K., Arndt, D., et al. (2021). Cellular extrusion bioprinting improves kidney organoid reproducibility and conformation. *Nat. Mater.* 20, 260–271. doi: 10.1038/s41563-020-00853-9

Lee, J. S., Yu, Q., Shin, J. T., Sebzda, E., Bertozzi, C., Chen, M., et al. (2006). Klf2 is an essential regulator of vascular hemodynamic forces in vivo. *Dev. Cell* 11, 845–857. doi: 10.1016/j.devcel.2006.09.006

Li, A. S., Ingham, J. F., and Lennon, R. (2020a). Genetic disorders of the glomerular filtration barrier. *Clin. J. Am. Soc. Nephrol.* 15, 1818–1828. doi: 10.2215/CJN.11440919

Li, M., Alfieri, C. M., Morello, W., Cellesi, F., Armelloni, S., Mattinzoli, D., et al. (2020b). Assessment of increased glomerular permeability associated with recurrent focal segmental glomerulosclerosis using an in vitro model of the glomerular filtration barrier. *J. Nephrol.* 33, 747–755. doi: 10.1007/s40620-019-00683-2

Li, M., Corbelli, A., Watanabe, S., Armelloni, S., Ikehata, M., Parazzi, V., et al. (2016). Three-dimensional podocyte-endothelial cell co-cultures: assembly, validation, and application to drug testing and intercellular signaling studies. *Eur. J. Pharm. Sci.* 86, 1–12. doi: 10.1016/j.ejps.2016.02.013

Little, M. H., and Takasato, M. (2015). Generating a self-organizing kidney from pluripotent cells. *Curr. Opin. Organ Transplant.* 20, 178–186. doi: 10.1097/MOT.0000000000000174

Meyrier, A. (2011). Focal and segmental glomerulosclerosis: multiple pathways are involved. *Semin. Nephrol.* 31, 326–332. doi: 10.1016/j.semnephrol.2011.06.003

Moreno, E. L., Hachi, S., Hemmer, K., Trietsch, S. J., Baumuratov, A. S., Hankemeier, T., et al. (2015). Differentiation of neuroepithelial stem cells into functional dopaminergic neurons in 3D microfluidic cell culture. *Lab Chip* 15, 2419–2428. doi: 10.1039/C5LC00180C

Morizane, R., Lam, A. Q., Freedman, B. S., Kishi, S., Valerius, M. T., and Bonventre, J. V. (2015). Nephron organoids derived from human pluripotent stem cells model kidney development and injury. *Nat. Biotechnol.* 33, 1193–1200. doi: 10.1038/nbt.3392

Müller-Deile, J., Schenk, H., Schroder, P., Schulze, K., Bolaños-Palmieri, P., Siegerist, F., et al. (2019). Circulating factors cause proteinuria in parabiotic zebrafish. *Kidney Int.* 96, 342–349. doi: 10.1016/j.kint.2019.02.013

Musah, S., Mammoto, A., Ferrante, T. C., Jeanty, S. S. F., Hirano-Kobayashi, M., Mammoto, T., et al. (2017). Mature induced-pluripotent-stem-cell-derived human podocytes reconstitute kidney glomerular-capillary-wall function on a chip. *Nat. Biomed. Eng.* 1:0069. doi: 10.1038/s41551-017-0069

Musso, C. G., and Oreopoulos, D. G. (2011). Aging and physiological changes of the kidneys including changes in glomerular filtration rate. *Nephron Physiol.* 119(Suppl. 1), 1–5. doi: 10.1159/000328010

Nishinakamura, R. (2019). Human kidney organoids: progress and remaining challenges. *Nat. Rev. Nephrol.* 15, 613–624. doi: 10.1038/s41581-019-0176-x

Öberg, C. M., and Rippe, B. (2013). Quantification of the electrostatic properties of the glomerular filtration barrier modeled as a charged fiber matrix separating anionic from neutral Ficoll. *Am. J. Physiol. Renal Physiol.* 304, F781–F787. doi: 10.1152/ajprenal.00621.2012

Perico, L., Conti, S., Benigni, A., and Remuzzi, G. (2016). Podocyte-actin dynamics in health and disease. *Nat. Rev. Nephrol.* 12, 692–710. doi: 10.1038/nrneph.2016.127

Petrosyan, A., Cravedi, P., Villani, V., Angeletti, A., Manrique, J., Renieri, A., et al. (2019). A glomerulus-on-a-chip to recapitulate the human glomerular filtration barrier. *Nat. Commun.* 10:3656. doi: 10.1038/s41467-019-11577-z

Pozzi, A., Jarad, G., Moeckel, G. W., Coffa, S., Zhang, X., Gewin, L., et al. (2008). Beta1 integrin expression by podocytes is required to maintain glomerular structural integrity. *Dev. Biol.* 316, 288–301. doi: 10.1016/j.ydbio.2008.01.022

Quinlan, C., and Rheault, M. N. (2021). Genetic basis of type IV collagen disorders of the kidney. *Clin. J. Am. Soc. Nephrol.* 13:CJN.19171220. doi: 10.2215/cjn.19171220

Ramnath, R. D., and Satchell, S. C. (2020). Glomerular endothelial cells: assessment of barrier properties in vitro. *Methods Mol. Biol.* 2067, 145–151. doi: 10.1007/978-1-4939-9841-8_11

Rayner, S. G., Howard, C. C., Mandrycky, C. J., Stamenkovic, S., Himmelfarb, J., Shih, A. Y., et al. (2021). Multiphoton-guided creation of complex organ-specific microvasculature. *Adv. Healthc. Mater.* e2100031. doi: 10.1002/adhm.202100031 [Epub ahead of print].

Rennke, H. G., Cotran, R. S., and Venkatachalam, M. A. (1975). Role of molecular charge in glomerular permeability. Tracer studies with cationized ferritins. *J. Cell Biol.* 67, 638–646. doi: 10.1083/jcb.67.3.638

Rennke, H. G., and Venkatachalam, M. A. (1979). Glomerular permeability of macromolecules. Effect of molecular configuration on the fractional clearance of uncharged dextran and neutral horseradish peroxidase in the rat. *J. Clin. Invest.* 63, 713–717. doi: 10.1172/JCI109354

Ron, A., Azeloglu, E. U., Calizo, R. C., Hu, M., Bhattacharya, S., Chen, Y., et al. (2017). Cell shape information is transduced through tension-independent mechanisms. *Nat. Commun.* 8:2145. doi: 10.1038/s41467-017-02218-4

Satchell, S. C., and Braet, F. (2009). Glomerular endothelial cell fenestrations: an integral component of the glomerular filtration barrier. *Am. J. Physiol. Renal Physiol.* 296, F947–F956. doi: 10.1152/ajprenal.90601.2008

Satchell, S. C., Tasman, C. H., Singh, A., Ni, L., Geelen, J., von Ruhland, C. J., et al. (2006). Conditionally immortalized human glomerular endothelial cells expressing fenestrations in response to VEGF. *Kidney Int.* 69, 1633–1640. doi: 10.1038/sj.ki.5000277

Satchell, S. C., and Tooke, J. E. (2008). What is the mechanism of microalbuminuria in diabetes: a role for the glomerular endothelium? *Diabetologia* 51, 714–725. doi: 10.1007/s00125-008-0961-8

Schiffer, M., Teng, B., Gu, C., Shchedrina, V. A., Kasaikina, M., Pham, V. A., et al. (2015). Pharmacological targeting of actin-dependent dynamin oligomerization ameliorates chronic kidney disease in diverse animal models. *Nat. Med.* 21, 601–609. doi: 10.1038/nm.3843

Schlondorff, D., and Banas, B. (2009). The mesangial cell revisited: no cell is an island. *J. Am. Soc. Nephrol.* 20, 1179–1187. doi: 10.1681/ASN.2008050549

Sharmin, S., Taguchi, A., Kaku, Y., Yoshimura, Y., Ohmori, T., Sakuma, T., et al. (2016). Human induced pluripotent stem cell-derived podocytes mature into vascularized glomeruli upon experimental transplantation. *J. Am. Soc. Nephrol.* 27, 1778–1791. doi: 10.1681/ASN.2015010096

Singh, A., Friden, V., Dasgupta, I., Foster, R. R., Welsh, G. I., Tooke, J. E., et al. (2011). High glucose causes dysfunction of the human glomerular endothelial glycocalyx. *Am. J. Physiol. Renal Physiol.* 300, F40–F48. doi: 10.1152/ajprenal.00103.2010

Singh, A., Satchell, S. C., Neal, C. R., McKenzie, E. A., Tooke, J. E., and Mathieson, P. W. (2007). Glomerular endothelial glycocalyx constitutes a barrier to protein permeability. *J. Am. Soc. Nephrol.* 18, 2885–2893. doi: 10.1681/asn.2007010119

Sison, K., Eremina, V., Baelde, H., Min, W., Hirashima, M., Fantus, I. G., et al. (2010). Glomerular structure and function require paracrine, not autocrine, VEGF-VEGFR-2 signaling. *J. Am. Soc. Nephrol.* 21, 1691–1701. doi: 10.1681/ASN.2010030295

Slater, S. C., Beachley, V., Hayes, T., Zhang, D., Welsh, G. I., Saleem, M. A., et al. (2011). An in vitro model of the glomerular capillary wall using electrospun collagen nanofibres in a bioartificial composite basement membrane. *PLoS One* 6:e20802. doi: 10.1371/journal.pone.0020802

Slater, S. C., Ramnath, R. D., Uttridge, K., Saleem, M. A., Cahill, P. A., Mathieson, P. W., et al. (2012). Chronic exposure to laminar shear stress induces Kruppel-like factor 2 in glomerular endothelial cells and modulates interactions with co-cultured podocytes. *Int. J. Biochem. Cell Biol.* 44, 1482–1490. doi: 10.1016/j.biocel.2012.05.020

Sobreiro-Almeida, R., Melica, M. E., Lasagni, L., Romagnani, P., and Neves, N. M. (2021). Retinoic acid benefits glomerular organotypic differentiation from adult renal progenitor cells in vitro. *Stem Cell Rev. Rep.* doi: 10.1007/s12015-021-10128-8 [Epub ahead of print].

St John, P. L., and Abrahamson, D. R. (2001). Glomerular endothelial cells and podocytes jointly synthesize laminin-1 and -11 chains. *Kidney Int.* 60, 1037–1046. doi: 10.1046/j.1523-1755.2001.0600031037.x

Sun, Y. B., Qu, X., Zhang, X., Caruana, G., Bertram, J. F., and Li, J. (2013). Glomerular endothelial cell injury and damage precedes that of podocytes in adriamycin-induced nephropathy. *PLoS One* 8:e55027. doi: 10.1371/journal.pone.0055027

Sutherland, R. (1988). Cell and environment interactions in tumor microregions: the multicell spheroid model. *Science* 240, 177–184. doi: 10.1126/science.2451290

Taguchi, A., Kaku, Y., Ohmori, T., Sharmin, S., Ogawa, M., Sasaki, H., et al. (2014). Redefining the in vivo origin of metanephric nephron progenitors enables generation of complex kidney structures from pluripotent stem cells. *Cell Stem Cell* 14, 53–67. doi: 10.1016/j.stem.2013.11.010

Takasato, M., Er, P. X., Becroft, M., Vanslambrouck, J. M., Stanley, E. G., Elefanty, A. G., et al. (2014). Directing human embryonic stem cell differentiation towards a renal lineage generates a self-organizing kidney. *Nat. Cell Biol.* 16, 118–126. doi: 10.1038/ncb2894

Takasato, M., Er, P. X., Chiu, H. S., Maier, B., Baillie, G. J., Ferguson, C., et al. (2015). Kidney organoids from human iPS cells contain multiple lineages and model human nephrogenesis. *Nature* 526, 564–568. doi: 10.1038/nature15695

Tanigawa, S., Islam, M., Sharmin, S., Naganuma, H., Yoshimura, Y., Haque, F., et al. (2018). Organoids from nephrotic disease-derived iPSCs identify impaired NEPHRIN localization and slit diaphragm formation in kidney podocytes. *Stem Cell Rep.* 11, 727–740. doi: 10.1016/j.stemcr.2018.08.003

Tasnim, F., and Zink, D. (2012). Cross talk between primary human renal tubular cells and endothelial cells in cocultures. *Am. J. Physiol. Renal Physiol.* 302, F1055–F1062. doi: 10.1152/ajprenal.00621.2011

Tryggvason, K., Zhou, J., Hostikka, S. L., and Shows, T. B. (1993). Molecular genetics of Alport syndrome. *Kidney Int.* 43, 38–44. doi: 10.1038/ki.1993.8

USRDS (2020). *2020 USRDS Annual Data Report: Epidemiology of Kidney Disease in the United States.* United States Renal Data System. Bethesda, MD: National Institutes of Health, National Institute of Diabetes and Digestive and Kidney Diseases.

Vallon, V. (2003). Tubuloglomerular feedback and the control of glomerular filtration rate. *News Physiol. Sci.* 18, 169–174. doi: 10.1152/nips.01442.2003

van den Berg, C. W., Ritsma, L., Avramut, M. C., Wiersma, L. E., van den Berg, B. M., Leuning, D. G., et al. (2018). Renal subcapsular transplantation of PSC-derived kidney organoids induces neo-vasculogenesis and significant glomerular and tubular maturation in vivo. *Stem Cell Rep.* 10, 751–765. doi: 10.1016/j.stemcr.2018.01.041

Vaughan, M. R., and Quaggin, S. E. (2008). How do mesangial and endothelial cells form the glomerular tuft? *J. Am. Soc. Nephrol.* 19, 24–33. doi: 10.1681/ASN.2007040471

Veissi, S., Smeets, B., van den Heuvel, L. P., Schreuder, M. F., and Jansen, J. (2020). Nephrotic syndrome in a dish: recent developments in modeling in vitro. *Pediatr. Nephrol.* 35, 1363–1372. doi: 10.1007/s00467-019-4203-8

Vivante, A., and Hildebrandt, F. (2016). Exploring the genetic basis of early-onset chronic kidney disease. *Nat. Rev. Nephrol.* 12, 133–146. doi: 10.1038/nrneph.2015.205

Wang, J., Zhong, J., Yang, H. C., and Fogo, A. B. (2018a). Cross talk from tubules to glomeruli. *Toxicol. Pathol.* 46, 944–948. doi: 10.1177/0192623318796784

Wang, L., Tao, T., Su, W., Yu, H., Yu, Y., and Qin, J. (2017). A disease model of diabetic nephropathy in a glomerulus-on-a-chip microdevice. *Lab Chip* 17, 1749–1760. doi: 10.1039/C7LC00134G

Wang, Y. Y., Tang, L. Q., and Wei, W. (2018b). Berberine attenuates podocytes injury caused by exosomes derived from high glucose-induced mesangial cells through TGFβ1-PI3K/AKT pathway. *Eur. J. Pharmacol.* 824, 185–192. doi: 10.1016/j.ejphar.2018.01.034

Wilmer, M. J., Ng, C. P., Lanz, H. L., Vulto, P., Suter-Dick, L., and Masereeuw, R. (2016). Kidney-on-a-chip technology for drug-induced nephrotoxicity screening. *Trends Biotechnol.* 34, 156–170. doi: 10.1016/j.tibtech.2015.11.001

Woods, I. G., Kelly, P. D., Chu, F., Ngo-Hazelett, P., Yan, Y. L., Huang, H., et al. (2000). A comparative map of the zebrafish genome. *Genome Res.* 10, 1903–1914. doi: 10.1101/gr.10.12.1903

Wu, H., Uchimura, K., Donnelly, E. L., Kirita, Y., Morris, S. A., and Humphreys, B. D. (2018). Comparative analysis and refinement of human PSC-derived kidney organoid differentiation with single-cell transcriptomics. *Cell Stem Cell* 23, 869.e8–881.e8. doi: 10.1016/j.stem.2018.10.010

Wu, X., Gao, Y., Xu, L., Dang, W., Yan, H., Zou, D., et al. (2017). Exosomes from high glucose-treated glomerular endothelial cells trigger the epithelial-mesenchymal transition and dysfunction of podocytes. *Sci. Rep.* 7:9371. doi: 10.1038/s41598-017-09907-6

Wu, X. M., Gao, Y. B., Cui, F. Q., and Zhang, N. (2016). Exosomes from high glucose-treated glomerular endothelial cells activate mesangial cells to promote renal fibrosis. *Biol. Open* 5, 484–491. doi: 10.1242/bio.015990

Xia, Y., Nivet, E., Sancho-Martinez, I., Gallegos, T., Suzuki, K., Okamura, D., et al. (2013). Directed differentiation of human pluripotent cells to ureteric bud kidney progenitor-like cells. *Nat. Cell Biol.* 15, 1507–1515. doi: 10.1038/ncb2872

Xie, R., Korolj, A., Liu, C., Song, X., Lu, R. X. Z., Zhang, B., et al. (2020). H-FIBER: microfluidic topographical hollow fiber for studies of glomerular filtration barrier. *ACS Cent. Sci.* 6, 903–912. doi: 10.1021/acscentsci.9b01097

Yang, S. H., Choi, J. W., Huh, D., Jo, H. A., Kim, S., Lim, C. S., et al. (2017). Roles of fluid shear stress and retinoic acid in the differentiation of primary cultured human podocytes. *Exp. Cell Res.* 354, 48–56. doi: 10.1016/j.yexcr.2017.03.026

Yaoita, E., Yoshida, Y., Nameta, M., Takimoto, H., and Fujinaka, H. (2018). Induction of interdigitating cell processes in podocyte culture. *Kidney Int.* 93, 519–524. doi: 10.1016/j.kint.2017.06.031

Yuen, D. A., Stead, B. E., Zhang, Y., White, K. E., Kabir, M. G., Thai, K., et al. (2012). eNOS deficiency predisposes podocytes to injury in diabetes. *J. Am. Soc. Nephrol.* 23, 1810–1823. doi: 10.1681/ASN.2011121170

Zennaro, C., Rastaldi, M. P., Bakeine, G. J., Delfino, R., Tonon, F., Farra, R., et al. (2016). A nanoporous surface is essential for glomerular podocyte differentiation in three-dimensional culture. *Int. J. Nanomed.* 11, 4957–4973. doi: 10.2147/Ijn.S110201

Zhang, T., Lih, D., Nagao, R. J., Xue, J., Berthier, E., Himmelfarb, J., et al. (2020). Open microfluidic coculture reveals paracrine signaling from human kidney epithelial cells promotes kidney specificity of endothelial cells. *Am. J. Physiol. Renal Physiol.* 319, F41–F51. doi: 10.1152/ajprenal.00069.2020

Zhao, H. J., Wang, S., Cheng, H., Zhang, M. Z., Takahashi, T., Fogo, A. B., et al. (2006). Endothelial nitric oxide synthase deficiency produces accelerated nephropathy in diabetic mice. *J. Am. Soc. Nephrol.* 17, 2664–2669. doi: 10.1681/ASN.2006070798

Zhong, F., Chen, H., Wei, C., Zhang, W., Li, Z., Jain, M. K., et al. (2014). Reduced Kruppel-like factor 2 expression may aggravate the endothelial injury of diabetic nephropathy. *Kidney Int.* 87, 382–395. doi: 10.1038/ki.2014.286

Zhou, M., Zhang, X., Wen, X., Wu, T., Wang, W., Yang, M., et al. (2016). Development of a functional glomerulus at the organ level on a chip to mimic hypertensive nephropathy. *Sci. Rep.* 6:31771. doi: 10.1038/srep31771

Zhou, W., and Hildebrandt, F. (2012). Inducible podocyte injury and proteinuria in transgenic zebrafish. *J. Am. Soc. Nephrol.* 23, 1039–1047. doi: 10.1681/ASN.2011080776

# Function of Uric Acid Transporters and Their Inhibitors in Hyperuricaemia

Hao-lu Sun[1][†], Yi-wan Wu[1][†], He-ge Bian[1], Hui Yang[1], Heng Wang[2], Xiao-ming Meng[2]* and Juan Jin[1]*

[1]Department of Pharmacology, Anhui Medical University, Hefei, China, [2]Inflammation and Immune Mediated Diseases Laboratory of Anhui Province, Anhui Institute of Innovative Drugs, School of Pharmacy, Anhui Medical University, Hefei, China

Disorders of uric acid metabolism may be associated with pathological processes in many diseases, including diabetes mellitus, cardiovascular disease, and kidney disease. These diseases can further promote uric acid accumulation in the body, leading to a vicious cycle. Preliminary studies have proven many mechanisms such as oxidative stress, lipid metabolism disorders, and rennin angiotensin axis involving in the progression of hyperuricaemia-related diseases. However, there is still lack of effective clinical treatment for hyperuricaemia. According to previous research results, NPT1, NPT4, OAT1, OAT2, OAT3, OAT4, URAT1, GLUT9, ABCG2, PDZK1, these urate transports are closely related to serum uric acid level. Targeting at urate transporters and urate-lowering drugs can enhance our understanding of hyperuricaemia and hyperuricaemia-related diseases. This review may put forward essential references or cross references to be contributed to further elucidate traditional and novel urate-lowering drugs benefits as well as provides theoretical support for the scientific research on hyperuricemia and related diseases.

Keywords: uric acid, transporters, gene, hyperuricaemia, inhibitor

## INTRODUCTION

With lifestyle changes, hyperuricaemia has become common around the world. 85–90% of hyperuricaemia patients have no clinical features. This stage is asymptomatic hyperuricaemia. Over time, long-term high serum uric acid (SUA) may cause many complications. Current studies have shown that 1) anomalous high SUA level is likely to induce a series of cardiovascular diseases, and acts as an independent risk factor for cardiovascular diseases, including atherosclerosis, hypertension, and coronary heart disease (Edwards, 2009); 2) obesity can cause hyperuricaemia, further leading to lipid metabolism disorder and chronic diseases (Fernandes Silva et al., 2019; Jingzhe Han et al., 2019); 3) in patients with diabetes, high uric acid (UA) further damages pancreatic cells and worsens diabetic condition (Changgui Li and Chang, 2013; Yun-Hong Lu et al., 2020). In summary, hyperuricaemia has become a key risk factor for development of many serious diseases.

Hyperuricaemia occurs due to alterations in urate production or excretion. UA is the final metabolite of purines and mainly excreted in the body by the kidney and intestine. The kidney excretes about two-thirds while the gastrointestinal tract excretes one-third of the UA load (Jessica Maiuolo et al., 2016). Most UA is filtered from glomerular, while renal tubules reabsorption and secretion regulate the amount of urate excretion (Jessica Maiuolo et al., 2016). The proximal tubule is the site of UA reabsorption and excretion. About 90% UA is reabsorbed into blood (Jessica Maiuolo et al., 2016). Urate transporters are mostly located in the proximal tubules of the kidney and play key roles in reabsorption and excretion of UA. In this review, we discuss the molecular mechanisms of
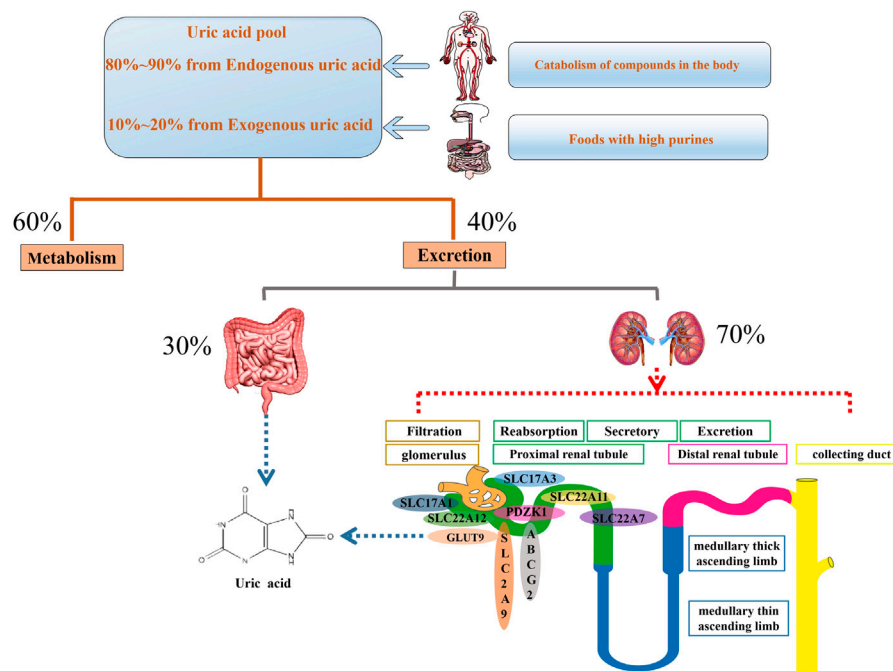
**FIGURE 1** | Mainly physiological progression of uric acid in the body. Serum uric acid is original from uptake of foods containing a high level of purines as well as catabolism of proteins and other compounds in the human body. About 60% uric acid involves in metabolism process and the rest of uric acid is excreted through the gut and urethra. Urethral excretion is the main way. A series of urate transporters including SLC and ABC transporters expressed in urethra, especially the proximal convoluted tubules, maintain urate homeostasis.

urate transports and their inhibitors on hyperuricaemia-associated diseases. This study not only shows that urate transports play considerable roles in the progression of hyperuricaemia-associated diseases but also indicates that they may be used as therapeutic targets.

# URIC ACID

At present, two sources of UA are recognized: 1) uptake of foods containing a high level of purines; 2) catabolism of proteins and other compounds in the human body. In long-term evolution, human UA kinase factors and a series of promoter gene mutations have caused humans to have higher UA levels than other mammals (**Figure 1**) (Edwards, 2009). Physiologically, it involves in many enzymes and hormones, such as xanthine oxidase, reproductive hormone, growth hormone, thyroid hormone, etc (Chengfu Xu et al., 2015; Liangshan Mu et al., 2018; Linqiang Ma et al., 2018; Shuang Liang et al., 2018). UA, as scavenger of oxygen radical, contributes to approximate 60% of plasma antioxidant activity and maintains the stability of blood pressure and antioxidant stress (Nieto et al., 2000; Wang et al., 2020). In addition, it prevents the oxidation of low-density lipoproteins and the inactivation of superoxide dismutase (Rudan et al., 2010). This antioxidant activity displays the protective roles of UA action under physiological environment. However, the abnormal UA level may be is correlative with many diseases.

# HYPERURICAEMIA

Hyperuricaemia is due to the broken balance between production and complex processes of secretion and reabsorption of UA (So and Thorens, 2010). A growing number of publications demonstrate that hyperuricaemia has been proved to be a risk for multiple diseases including gout, chronic kidney disease (CKD), cardiovascular diseases. Despite the importance of hyperuricaemia, the definition of hyperuricaemia remains inconclusive. Generally, abnormal SUA is higher in men than in women (Bardin and Richette, 2014). Hyperuricaemia is defined increased SUA as above 7 mg/dl in men and above 6 mg/dl in women in many studies (Zhu et al., 2011; Bardin and Richette, 2014)). High intake of purine-rich foods (such as alcohol) or those that can lead to increased purine levels (such as fructose) can also contribute to hyperuricaemia (Xiao et al., 2018; Go et al., 2019; Hoogerland et al., 2020). Genetic variations induced by multiple factors are also the key cause of hyperuricaemia (Guo et al., 2005; Mount and Mandal, 2019). Moreover, SUA concentration is negatively correlated with maximal oxygen uptake and positive correlation with carbon dioxide in patients with chronic heart failure (Leyva et al., 1997). Hypoxia leads to the accumulation of UA precursors and the activation of xanthine oxidase/dehydrogenase further increase the level of UA in the body (Hassoun et al., 1992). During hypoxia, glycolysis accelerates the production of UA in patients with heart failure (Swan et al., 1994). NO, an endothelial cell-derived relaxing factor produced by endothelial cells is another important factor

affecting uric acid. Decreased levels of NO are leading to increased UA and insulin resistance occurence (Cook et al., 2004; Gehr, 2004; So and Thorens, 2010). Chronic elevation of SUA level leads to the formation and deposition of monosodium urate (MSU) crystals leads to inflammatory reaction and tissue injury in many organs such as joint, kidney, and heart (Bardin and Richette, 2014). Together, the available information indicates that the regulation of UA level is complex and may explain the association with hyperuricaemia, gout, the metabolic syndrome, cardiovascular disease, and renal disease.

# HYPERURICAEMIA-RELATED DISEASES

## Gout

Strong epidemiological evidence demonstrates that the prevalence of gout is growing worldwide. Gout is a chronic disease caused by MSU crystal deposition, while hyperuricaemia is the major risk factor (Dalbeth et al., 2019). Over time, prolonged hyperuricaemia may result in more frequent and severe symptoms of gout (Dalbeth et al., 2019). In patients with established gout, elevated SUA is associated with increased risk of recurrent gout (Shiozawa et al., 2017). Despite advances in understanding the pathophysiology of gout, it remains common and challenging which may be associated with untimely treatment and lack of understanding about the role of urate-lowering therapy (Stamp and Dalbeth, 2019). For the treatment of gout, allopurinol remains the first-line urate-lowering therapy, with febuxostat regarded as an proper alternative in clinical practice (Stamp and Dalbeth, 2019). Lifestyle modification including reduced intake of purine-rich foods, weight loss, avoidance of fructose and alcohol has also been considered an vital aspect of gout management (Jeyaruban et al., 2016). Using available data, keeping the balance between excretion and overproduction of SUA is reasonable for prevention and management of gout.

## Chronic Kidney Disease (CKD)

Increasing evidence indicates that SUA is enhanced in patients with CKD (Liu et al., 2015). Epidemiological studies have reported the association between hyperuricaemia and CKD (Alobaidi et al., 2021). About 20–60% of patients with established gout have renal dysfunction (Kang et al., 2002). It is a risk marker and contributes to the development of glomerulosclerosis and interstitial fibrosis (Kang et al., 2002; Liu et al., 2015). Hyperuricaemia may aggravate kidney damage through RAS activation which is an important mediator of kidney disease progression or through developing hypertension by increasing salt sensitivity (Kang et al., 2002; Watanabe et al., 2002). Furthermore, it induces macrophage infiltration, renal tubular epithelial to mesenchymal transition, as well as an increased expression of inflammatory mediators (Balakumar et al., 2020). For the management of CKD, many investigations indicate that urate-lowering therapy slows and delays the development of CKD (Sonoda et al., 2011; Shi et al., 2012; Liu et al., 2015). In addition, these findings are contributed

to screen and manage individuals with an elevated risk of CKD development.

## Cardiovascular Diseases

Hyperuricaemia has been considered as not only a risk factor for human cardiovascular diseases such as myocardial infarction, hypertension, but also a co-variable of other known risk factors for cardiac deaths and coronary heart disease (Culleton et al., 1999; So and Thorens, 2010; Tian et al., 2021). In addition, hyperuricaemia is also demonstrated as an independent risk factor for cardiovascular mortality (Krishnan et al., 2008). It is reported that the risk of myocardial infarction enhances with higher cumulative UA. Early cumulative UA contributed more to myocardial infarction risk than later cumulative UA with the same overall cumulative exposure (Tian et al., 2021). UA further contributes to the development of hypertension in obesity (DeMarco et al., 2014). In a cross-sectional study of the association between hyperuricaemia, hypertension and ischemic stroke, higher risk is found even after full adjustment in participants with hyperuricaemia and hypertension (Sun et al., 2021). These findings highlight the importance of optimal SUA control in preventing cardiovascular diseases.

## Metabolic Syndrome

High UA level is found in patients with metabolic syndrome (Keskin et al., 2021). Insulin resistance can elevate UA by reducing renal urate clearance (Facchini et al., 1991). Increasing studies verify that insulin resistance is usually accompanied by an increased UA and high UA could induce insulin resistance (Bassanese et al., 2021; Jiao et al., 2021). While insulin resistance leads to a significant increase in the expression of urate transport-related proteins, an increase in urate reabsorption and an increase in SUA levels (Zhang et al., 2021). Therefore, hyperuricaemia and insulin resistance may promote each other. Reducing the expression of UA transporter proteins in the setting of insulin resistance down regulates blood UA levels (Zhang et al., 2021).

When cells are induced to differentiate into adipocytes, the physiological concentration of uric acid is further increased (So and Thorens, 2010). Hyperuricaemia in obese people is mainly caused by impaired renal uric acid clearance, not overproduction (Enomoto et al., 2002). This may be related to the mechanism of reactive oxygen species (ROS) production involving in NADPH oxidase activation (So and Thorens, 2010). Excretion of UA is inversely associated with leptin as a predictive marker for metabolic syndrome secreted by adipose tissue (Boden et al., 1997; Saad et al., 1998; D'Elia et al., 2020; Ghadge and Khaire, 2019). UA may also regulate leptin levels by changing leptin gene expression or decreasing leptin clearance (Fruehwald-Schultes et al., 1999). In conclusion, these findings suggest that some substances like leptin may involve in the crosstalk between metabolic syndrome and hyperuricaemia.

## Neurodegenerative Diseases

Hyperuricaemia displays an important causative effect in multiple diseases including gout, CKD, cardiovascular diseases. In contrast, it shows a protective role in neurodegenerative
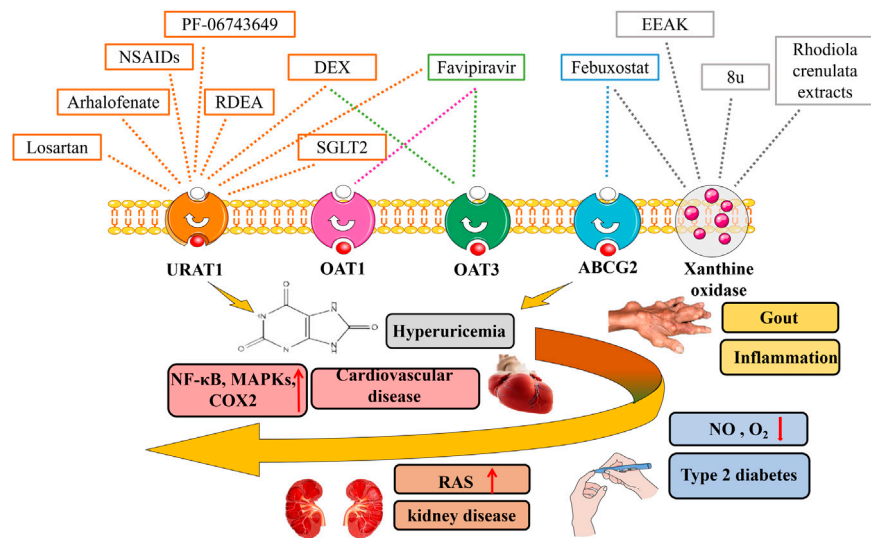
**FIGURE 2** | Urat-lowering drugs in hyperuricaemia-related diseases. Hyperuricaemia has been proven to be associated with multiple diseases including gout, chronic kidney disease, cardiovascular diseases, metabolic syndrome. The discovery of urate transporters provides new ideas for the development of drugs for the research of hyperuricaemia. In addition to urate transport inhibitors, xanthine oxidase inhibitors, SGLT2 inhibitors, as well as novel urat-lowering drugs like EEAK, Favipiravir, PF-06743649 have been summarized.

disorders such as Alzheimer's disease (Tana et al., 2018; Mandal and Mount, 2019). Previous studies indicate that reduced SUA levels in the body can lead to an increased risk of Alzheimer's disease, Parkinson's disease, multiple sclerosis, schizophrenia, and dementia (Ascherio et al., 2009; Du et al., 2016; Ye et al., 2016). These findings may be associated with the antioxidant effects that UA may display in neurodegenerative diseases (Tana et al., 2018). Controversially, there is conflicting evidence about SUA in cognitive decline in patients with vascular or mixed dementia (Tana et al., 2018). Hong et al. find a lower risk of developing vascular dementia in patients with established gout (Hong et al., 2015). However, Khan et al. did not find a significant association between them (Khan et al., 2016). One recent study indicates a significant risk of vascular or mixed dementia in patients with higher SUA (Latourte et al., 2018). Thus, UA may represent to be a complex mediator of influencing cognitive function in different dementia types. The specific contribution of UA on neurodegenerative disorders needs to be further clarified.

The strong association between SUA and cognition could be indicated also by the relationship between certain genetic abnormalities of the urate transporters and nerve injury. *SLC22A12* gene encoding for the urate transporter hURAT1 defects leads to primary renal hypouricemia characterized by increased UA excretion from a reduced reabsorption (Tana et al., 2018). Variations in *SLC2A9* gene, encoding the urate transporter GLUT9, are closely related to human cognition and neurodegenerative diseases (Houlihan et al., 2010; Mandal and Mount, 2019). ITM2B, a GLUT9-interacting protein, inhibited urate influx and stimulated urate efflux (Mandal and Mount, 2019). These data demonstrate that there may be some regulators

as potential molecular links between UA homeostasis and neurodegenerative disorders.

# URATE TRANSPORTERS AND GENETICS OF URATE TRANSPORTER PATHOLOGIES

A series of urate transporters including SLC and ABC transporters as well as several multispecific drug transporters (e.g., OAT1, OAT2, and ABCG2) maintain UA homeostasis (**Figure 2**) (Tomita et al., 2000; Edwards, 2009; Nigam and Bhatnagar, 2018). Over time, it has become apparent that altered urate transport, both in the gut and the kidneys, has a vital role in the pathogenesis of hyperuricaemia-associated diseases. Thus, the optimization of UA level can be regarded as a systemic issue. Recent studies have suggested that urate transporters mutations in genes and related sites directly affect urate reabsorption and excretion (Guo et al., 2005; Puig and Martínez, 2008). Compared with the modern environment, genetic factors on urate transporters have a larger effect on variation in serum urate concentrations (Major et al., 2018). Exploration of these transporters and related genes sites are important to regulate and achieve target serum urate (**Table 1**).

## *SLC* Transporters
### GLUT9 (*SLC2A9*)
GLUT9 encoded by *SLC2A9* gene is widely present in the proximal tubule in human kidney (Kimura et al., 2014). It has two splice variant isoforms, GLUT9a (540 amino acids encoded by 12 exons) and GLUT9b (512 amino acids encoded by 13 exons). In human, GLUT9a is expressed in the basolateral

membrane of proximal tubules of human kidney, whereas, GLUT9b is expressed at the apical membrane of the collecting duct (So and Thorens, 2010). GLUT9 initially identified as the glucose transporter serves acritical role in urate reabsorption (Ebert et al., 2017). Genetic inactivation in mice induces moderate hyperuricaemia and massive renal excretion of urate. Accumulating studies report that hypouriceamia has been associated with mutations in the *SLC2A9* gene. For example, L75R mutation and 36-kb deletion present in two different families of hypouriceamic patients; R198W, R380C, as well as P412R mutation are found in hypouriceamic patients, respectively (Anzai et al., 2008; Dinour et al., 2010; Kawamura et al., 2011).

## MCT9 (*SLC16A9*)

The human *SLC16* protein, also known as human monocarboxylic acid transporters (hMCTs), contains 14 members and mediates the transport of monocarboxylates through the plasma membrane (Futagi et al., 2020). MCTs are generally divided into two categories, the $H^+$-sensitive and $H^+$-non-sensitive transporters. MCT9 belongs to the latter and is ubiquitous with the highest expression level in the kidney and adrenal gland (Harst et al., 2010; Roshanbin et al., 2016; Console et al., 2020). *rs1171614* and *rs2242206* variants has been reported to be associated with SUA levels and the risk of kidney overload gout (Nakayama et al., 2013; Butler et al., 2021). At present, many members of the *SLC16* family have never been studied. Although MCT9 has been shown to be related to UA levels, its mechanism of action and location are still unclear. Further genetic and functional study of MCT9 is necessary.

## NPT1 (*SLC17A1*)

The *SLC17A1*, a membrane protein, is the first member of the SLC17 phosphate transporter family (Zhang et al., 2018). *SCL17A1* gene encoding NPT1 transports various substrates including UA (Chiba et al., 2015). A previous analysis shows that NPT1 mainly expressed in the kidney is localised to the apical membrane of the renal proximal tubule (JadeHollis-Moffatt et al., 2012; Chiba et al., 2015).

### Function of NPT1 (*SLC17A1*)

NPT1, weakly to moderately correlate with altered UA levels, mediates the absorption of UA when the plasma membrane is depolarised by high concentration of exogenous potassium (Bhatnagar et al., 2016). At the same time, NPT1 is conducive to the efflux of UA. When the cell membrane presents a negative potential phase, NPT1 mediates UA efflux (Chiba et al., 2015). NPT1 as a $Cl^-$-dependent urate transport, has two transportation activities, namely the of $Na^+$/phosphate co-transport; moreover, anion conductance is important to discriminate the mechanistic differences between the two activities and $\Delta\psi$-driven anion transport activity (Wright and Dantzler, 2004; Iharada et al., 2010).

### Mutation Loci of the NPT1 (*SLC17A1*) Gene

The study selects 545 Japanese men with gout as a model group and 1,115 healthy men as a normal control group to investigate mutations in the NPT1 *rs1165196* and *I269T* genes (Chiba et al., 2015). Functional analysis shows that NPT1 *rs1165196* variants significantly reduce the risk of renal under excretion gout and enhance the renal urate secretion (Chiba et al., 2015; Sakiyama et al., 2016). Interestingly, *rs1165196* variants have little effect onpatients with normal renal excretion (JadeHollis-Moffatt et al., 2012; Chiba et al., 2015; Sakiyama et al., 2016). *I269T* (a common missense variant of NPT1) mutations increase the maximum volume by increasing the turnover rate of the urate transport and output tomitigate gouty risk, but do not change NPT1 membrane expressions (Sakiyama et al., 2016). Compared with NPT1 wild type, *I269T* might have faster conformation changes leading to enhance renal urate export (Sakiyama et al., 2016).

## NPT4 (*SLC17A3*)

Human sodium phosphate co-transporter type 4 (NPT4/SLC17A3) is a multi-specific organic anion efflux transporter expressed in the kidneys and liver. NPT4 is located at the apical side of renal tubules, and functions as an apical voltage-driven urate efflux transporter, also known as NPT4-$Na^+$/phosphate co-transporter (Jutabha et al., 2010).

### Function of NPT4 (SLC17A3)

NPT4 plays an important role in the urate excretion and operates functionally with basolateral organic anion transporters 1/3 (OAT1/OAT3) (Jutabha et al., 2010; Riches et al., 2009; Polasek et al., 2010; Jutabha et al., 2011). SUA is taken up by OAT1/OAT3 into tubular cell, then intracellular UA is excreted by NPT4 into the urinary lumen (Møller and Sheikh, 1982; Pritchard and Miller, 1993; Jutabha et al., 2010).

### Mutation Loci of the NPT4 (SLC17A3) Gene

NPT4 variations have a greater effect on SUA concentration in women, have no close relationship with SUA in men (Jutabha et al., 2010). NPT4L and NPT4S are two splice variants of NPT4 (Polasek et al., 2010). NPT4L acts through the outlet channel of the proximal membrane of the renal proximal tubule. According to the voltage-driven promotion mechanism of NPT4L and its location on the proximal membrane of the proximal tubule, deeming NPT4 is the main channel for excretion of drugs and UA (Jutabha et al., 2010). Some reports have shown there were significant correlations between *rs9393672* and *rs942379* in NPT4 gene polymorphisms as well as changes in female SUA concentration (Jutabha et al., 2010; Riches et al., 2009).

## OAT1 (*SLC22A6*) and OAT3 (*SLC22A8*)

Both OAT1 (*SLC22A6*) and OAT3 (*SLC22A8*), as urate/dicarboxylate exchangers, are located on the basolateral side of the proximal tubule (So and Thorens, 2010). Previous studies find that knockout of OAT1 or OAT3 slightly reduces uricosuria, indicating that their essential function is urate excretion (Eraly et al., 2008).

## OAT2 (*SLC22A7*)

Members of the solute carrier 22A (*SLC22A*) family known as OATs, including OAT2, are expressed in various organs (Kimoto et al., 2018; Mathialagan et al., 2018). Among OATs, only OAT2

has a general expression pattern and is expressed in many tissues, such as the choroid plexus, liver, placenta, skeletal muscle, and kidney (Sager et al., 2018). In the kidney, OAT2 is located in the basolateral side of the proximal tubule for urate uptake transporter (Sakurai, 2013).

### Function of OAT2 (SLC22A7)

OAT2 is a transporter of several known exogenous drugs and endogenous compounds (Kimoto et al., 2018; Mathialagan et al., 2018). Urate and cGMP may be substrates of OAT1, OAT2, and OAT3 (Henjakovic et al., 2015). And OAT2 could take up urate from blood to the proximal tubular cell. However, different from the other two transporters, OAT2 is relatively independent and not associated with the pH of the body. A recent study has shown that OATs, especially OAT2, contribute to creatinine transport (Sager et al., 2018). Although existing evidence shows that OAT2 is mainly expressed in the kidney, but it also plays a role in the liver (Vildhede et al., 2018).

### Mutation Loci of the OAT2 (SLC22A7) Gene

Three quarters of OAT2 SNPs are found in men, and among the populations with these SNPs, the major allele frequencies of *C329T*, *G571A*, and *G1520A* were 0.94, 0.94, and 0.95, respectively (Xu et al., 2005). Three individuals (each with a non-synonymous SNP) are heterozygous at these loci, and originated from Sub-Saharan Africa (*C329T*), India-Pakistan (*G571A*), and Japan (*G1520A*) (Xu et al., 2005). OAT2 encodes a key renal solute transport protein, and genetic variations of *TBX2* are a determinant of CKD (Kato et al., 2015).

## OAT4 (*SLC22A11*)

Organic anion determines the transport of most renal tubules and the secretion or reabsorption of substances (Hagos et al., 2007). Members of OAT family have a main task of handling drug complexes or exogenous secretions (Wright and Dantzler, 2004; Anzai et al., 2006). OATs are expressed along the proximal tubules of the kidney and other marginal epithelia, such as the blood-brain barrier, choroid plexus, and placenta (Ugele et al., 2003). OAT4 is identified as an apical transporter in proximal tubule cells and only expressed in advanced primates, including humans (Hagos et al., 2007).

### Function of OAT4 (SLC22A11)

In addition to uric acid, OAT4 also promotes the absorption of high-affinity binding steroids such as estronesulfate (ES) or dehydroepian drosterone sulfate (Hagos et al., 2007). OAT4 can use chloride ion as the exchange anion of ES and uric acid (Roch-Ramel et al., 1994; Hagos et al., 2007). Physiologically, OAT4 guides the ion exchange of the proximal tubule through PAH/Cl$^-$, PAH/ES, and possibly PAH/UA to excrete UA (Hagos et al., 2007). In previous studies, after the removal of sodium or addition of the NHE3-specific inhibitor amiloride, the ES uptake of HEK293-OAT4 cells is significantly reduced, indicating that OAT4 transport may be coupled with the effect of NHE3 (Lang et al., 2003; Tom Nijenhuis et al., 2005). OAT4 interacts with NHE3 and sodium dicarboxylate transporter 1 to participate in the maintenance of intracellular $\alpha$-ketoglutarate (Hagos et al., 2007).

### Mutation Loci of the OAT4 (SLC22A11) Gene

*SLC22A11 rs2078267* is associated with gout in some Europeans (van der Harst et al., 2010; Flynn et al., 2013; Köttgen et al., 2013). Previous studies show that *rs218657*1 is associated with SUA levels in the Pacific Micronesian population of Kosrae (Kenny et al., 2011; Flynn et al., 2013). *rs17299124* gene mutation is related to gout in Southeast Asians patients. Another study indicates that *rs17300741*, a common variant of OAT4/*SLC22A11*, is associated with the renal under excretion type gout (Sakiyama et al., 2014).

## URAT1 (*SLC22A12*)

The *SLC22A12* gene encodes a transporter protein known as URAT1, which is a 553 amino acid protein that is 30% identical to rat organic cation transporter 1 at the amino acid level (Hosoyamada et al., 2004). URAT1 has been identified as a uric acid anion exchanger that affects UA homeostasis via urate reabsorption in human kidney (Enomoto et al., 2002; Zhou et al., 2010; Skwara et al., 2017; Misawa et al., 2020). It is expressed in the apical membrane of the proximal tubule of the human kidney (Hosoyamada et al., 2004).

### Function of URAT1 (SLC22A12)

URAT1 plays an important role in urate reabsorption in the kidney. Sodium hydrogen exchange regulator (NHERF) protein, which is abundantly expressed in the apical membrane transported by epithelial cells, such as renal proximal tubules and small intestine, interacts with mURAT1 and plays an important role in the regulation of uric acid transport in renal proximal tubule cells (Cunningham et al., 2007). NHERF-1 deficiency directly affects uric acid absorption (Cunningham et al., 2007). Human URAT1 has the C-terminal sequence of T-Q-F, and cell analysis revealed that hURAT1 can specifically bind with NHERF-3 (Hosoyamada et al., 2004; Cunningham et al., 2007). NHERF-1 has been shown to play an important role in determining the cellular distribution of mURAT1 (Cunningham et al., 2007). A possible mechanism is that NHERF-1 may act as a partner in a manner similar to the adaptor proteins CAL and CFTR, as a membrane retention signal for stabilising mURAT1 in the plasma membrane, assuming the interaction between NHERF-1 and CFTRNpt2a, or as the determinant of mURAT1 circulation to the plasma membrane (Shenolikar et al., 2002).

### Mutation Loci of the URAT1 (SLC22A12) Gene

Dysfunctional variants in URAT1 are considered as the major cause of hyperuricaemia (Zhu et al., 2021). *SLC22A12* produces a genetic variation that contributes to urate absorption and is a key factor in hyperuricaemia and gout (Toyoda et al., 2015; Tu et al., 2016). *SLC22A12 rs475688*(C/C) and p. N82N are reported to be significantly associated with gouty risk (Pavelcova et al., 2021). Interestingly, inactivating mutations in URAT1 have been shown to cause renal hypouricemia. Mutations in the *SLC22A12* gene can reduce SUA levels (Misawa et al., 2020). The results of this study shows that: 1) based on the serum levels of urate salt gene, the lack of *SLC22A12* was 10% more prominent in men than in women, and can be genetic (Misawa et al., 2020); 2) based on

urate absorption, some of the variants truncate a protein that may have a termination codon that leads to the loss of URAT1 function (Cha et al., 2019).

## ABCG2

The ATP binding cassette subfamily member 2 (ABCG2), a multi-specific transporter, is located on the apical membrane in tissues including kidney and intestine. It exerts a critical physiological effect in the excretion of UA in the kidney and intestine (Maliepaard et al., 2001; Yun-Hong Lu et al., 2020).

### Function of ABCG2

The export process of ABCG2 is ATP-dependent and unsaturated at the physiological concentration of UA, indicating that ABCG2 has high-capacity urate transport activity (Matsuo et al., 2009). ABCG2 dysfunction caused by common variants will significantly increase the risk of hyperuricaemia, and the reduction of extra renal urate excretion through dysfunctional ABCG2 is a common mechanism of hyperuricaemia (Ichida et al., 2012). One of the main causes of hyperuricaemia is not true overproduction of UA, but insufficient excretion of extra renal UA due to common ABCG2 dysfunction (Ichida et al., 2012). It exerts active roles in patients with CKD (Yano et al., 2014; Nigam, 2015; Bhatnagar et al., 2016). ABCG2 dysfunction enhances UA level and promotes renal dysfunction in CKD patients as well as systemic inflammatory responses (Bhatnagar et al., 2016; Cleophas et al., 2017).

In CKD, renal urate excretory mechanisms are compromised due to loss of renal function. In addition to transporting nucleotide analogues, ABCG2 is a vital transporter in intestinal UA excretion (Matsuo et al., 2009). Interestingly, renal urate excretion decrease but intestinal expression of ABCG2 increases, suggesting some sort of remote regulation of intestinal urate transport when renal transport is compromised. In CKD, intestinal ABCG2 becomes much more important, suggesting remote organ communication between the injured kidney and the intestine (Nigam and Bhatnagar, 2018).

### Mutation Loci of the ABCG2 Gene

To investigate ABCG2 gene mutations in hyperuricaemia patients, researching performed mutation analysis on all coding regions and intronexon boundaries of the ABCG2 gene in 90 Japanese patients with hyperuricaemia (Matsuo et al., 2009). The following six asynchronous mutations were found: *V12M*, *Q126X*, *Q141K*, *G268R*, *S441N*, and *F506SfsX4* (Matsuo et al., 2009). Among them, the allele frequency of *Q141K*, *V12M*, and *Q126X* is 31.9, 19.2, and 2.8% (Matsuo et al., 2009). ABCG2 gene mutation has a significant effect on UA, especially the amino acid substitution in *Q141K*, which leads to risk of hyperuricaemia and gout (Wen et al., 2015; Cleophas et al., 2017). At the same time, decrease in the amount of ABCG2 protein will inhibit *Q141K* activity (Kondo et al., 2004). In addition, ABCG2 *rs2231142* considered a risk allele for gout (Butler et al., 2021).

## PDZK1

Polyvalent PDZ domain 1 (PDZK) is a multi-domain protein containing four PDZ domain tubular cells observed in the apical membrane of the kidney proximal tubule. It is highly expressed at the apical membrane of tubular epithelial cells, and that most of the above-mentioned apical transporters have been reported to directly interact with PDZK1 (Prestin et al., 2017).

### Function of PDZK1

PDZK1 acts as a scaffold protein to regulate the activity of various transport proteins including URAT1 and NPT1 in the proximal tubules (Miyazaki et al., 2005; Lu et al., 2019). Using a yeast two-hybrid screen system, found that PDZK1 regulates the functional activity of URAT1 and enhances its UA reabsorption capacity (Anzai et al., 2004). Furthermore, PDZK1 might be an important upstream molecule of ABCG2, which changes its function in the small intestine (Lu et al., 2019). Soluble UA induced upregulation of ABCG2 expression and function in intestinal cell lines is dependent on PDZK1 at the transcriptional level (Lu et al., 2019). However, the correlation between PDZK1 and ABCG2 needs to be further investigated. SMCT1 (*SLC5A8*), a high-affinity lactate transport system that interacts with PDZK1, plays an important role in the reabsorption of urate in human kidney (Gopal et al., 2004; Miyauchi et al., 2004; Otsuka et al., 2019). *rs12129861* in PDZK1 is considered a risk allele for gout (Butler et al., 2021). According to previous studies, PDZK1 affects urate transporters and thus may have a certain effect on various transporters, but it is not yet possible to determine its specific mode of action.

## URATE-LOWERING DRUGS IN HYPERURICAEMIA-RELATED DISEASES

At present, there have been many studies on the traditional treatment of hyperuricaemia (Yang et al., 2018). The discovery of urates transporters provides new ideas for the development of drugs for the research of hyperuricaemia. In addition to urate transport inhibitors, xanthine oxidase inhibitors, as the most popular drug candidates, have attracted a lot of attention (**Figure 2**). Xanthine oxidoreductase is a rate-limiting enzyme catalyzing formation of UA by oxidative hydroxylation of hypoxanthine and xanthine in purine metabolism (Battelli et al., 2014). It plays a vital role in the production of hyperuricaemia and gout (Nakatani et al., 2021). We summarize advances in research on urate-lowering drugs including urate transporter inhibitors, xanthine oxidase inhibitors as well as novel urate-lowering drugs, and evaluate the effect of urate-lowering therapy on the rate of hyperuricaemia-related diseases.

### Urate Transporter Inhibitors
#### URAT1 Inhibitors
##### Arhalofenate

Arhalofenate, an emerging URAT1 inhibitor, is a dual-acting agent (Shahid and Singh, 2015). In addition to increasing uric acid excretion, it inhibits the production of IL-1β, thereby reducing the occurrence of flare gout (Dalbeth et al., 2014). Arhalofenate increases urate excretion by inhibiting the action of URAT1, which is one of its main effects (Shahid and Singh,

2015). The other main roles of arhalofenate are to activate AMPK, inhibit NF-κB and NLRP3 inflammasomes to promote the polarisation of anti-inflammatory macrophages, as well as significantly reduce UA-induced inflammation (Salminen et al., 2011; Wang et al., 2016). There are similar studies showing that arhalofenate acid activates AMPK in macrophages *in vitro*, inhibits the activation of NLRP3 inflammasomes, and reduces MSU-induced IL-1β production (Kim et al., 2016; McWherter et al., 2018). Moreover, arhalofenate acid activates AMPK downstream targets to participate in the regulation of mitochondrial function and maintain the function of mitochondrial crest (McWherter et al., 2018).

Colchicine can inhibit the release of IL-1β-induced MSU crystal deposition joints. Therefore, researchers believe that in the next few years, arhalofenate may become a substitute for colchicine (Shahid and Singh, 2015). In addition, arhalofenate lowers blood lipid and blood sugar levels in patients with hypertriglyceridaemia and diabetes. Owing to its effect on OAT4, it can reduce uric acid level in hypertensive patients treated with diuretics, and diuretics, especially thiazide drugs, and prevent hyperuricaemia (Shahid and Singh, 2015).

### Lesinurad

Lesinurad (RDEA594) is a selective inhibitor of URAT1 in the proximal tubules of the kidney (Shahid and Singh, 2015). RDEA594 through affects OAT4 relieve hyperuricaemia which caused by diuretics; however, lesinurad has no effect on other transport molecules, such as OAT1 and OAT3 (Shahid and Singh, 2015). RDEA594 in combination with XOI is a new treatment option considered for gout (Engel et al., 2017). Verinurad (RDEA3170), a new URAT1 inhibitor, demonstrates high potency in inhibiting URAT1 (Martin et al., 2018; Yue et al., 2019). *In vitro* studies have shown that three times the potency of benzbromarone and 100 times of probenecid effectiveness (Yue et al., 2019). RDEA3170 is currently in phase II clinical trials for the treatment of gout and asymptomatic hyperuricaemia (Yue et al., 2019).

### Losartan

Losartan, an angiotensin II receptor blocker (ARB), is confirmed to reduce SUA level (Matsumura et al., 2015; Bryant et al., 2021). It is due to its inhibition of urate/anion exchanger on the brush border membrane of renal proximal tubular epithelial cells (Enomoto et al., 2002; Iwanaga et al., 2007). The urate transporter URAT1 participates in the reabsorption of UA from lumen to cytoplasm along proximal tubules. Losartan lows the urate reabsorption by inhibitory activity of URAT1 in the range of clinically relevant concentrations (0.1–10 nm) (Iwanaga et al., 2007). These results suggest that losartan is effective inhibitors of URAT1, which may explain why patients taking losartan generally have low UA levels (Iwanaga et al., 2007). Intriguingly, UA level will restore at higher concentrations of losartan mainly due to trans-stimulation of these ARBs at higher concentrations (Iwanaga et al., 2007). Nevertheless, one recent study finds that the urate reduction is not a class effect of ARBs. Compared with multiple ARBs in

cluding candesartan, valsartan, azilsartan, eprosartan andirbesartan, only losartan has clear evidence of its ability to lower SUA level. This result suggests that for patients with hypertension and hyperuricaemia, losartan could be regarded as a first-line agent with irbesartan as an alternative when appropriate (Sutton Burke et al., 2020).

## Anti-inflammatory Drug
### Nonsteroidal Anti-inflammatory Drug (NSAIDs)
NSAIDs including aspirin and steroids are widely used for pain relief and inflammatory suppression during acute gout attacks (Enomoto et al., 2002; Ragab et al., 2017). Accumulating studies indicate that affect renal urate excretion in an inverse dose dependent manner. High dose aspirin is uricosuric, while low dose causes urate retention (Roch-Ramel et al., 1997; Enomoto et al., 2002). According to previous reports, the mechanism underlying dual effects of aspirin involve the renal urate transporter URAT1 (Choi et al., 2005; Zhang et al., 2014). High dose aspirin decreases SUA level by inhibiting URAT1, whereas low dose exerts urate retentive role through stimulating URAT1 (Zhang et al., 2014). Low dose of salicylate (75, 150, and 325 mg per day) reduces urinary urate excretion and contributes to gouty risk (Caspi et al., 2000). However, there was no significant change in SUA levels and urinary urate excretion in patients with gout who received 325 mg of aspirin daily combined with probenecid. Therefore, urate-lowering drugs (e.g., uricosuric agents orxanthine oxidase inhibitors) may reduce the effect of low-dose aspirin on hyperuricaemia (Harris et al., 2000; Zhang et al., 2014).

### Glucocorticoids
Glucocorticoids, such as dexamethasone (DEX), have been shown to increase xanthine oxidase activity in rats (Patel et al., 2014). Besides, DEX significantly increases the renal excretion of urate (Li et al., 2019). Many membrane transporters are involved in the urate reabsorption and secretion (Hyndman et al., 2016). During secretion by the renal tubules, SUA is absorbed by OAT1 and OAT3 to enter the renal tubule cells, and then enters urine through NPT1, NPT4, MRP4, BCRP, as well as other efflux transporters. Although DEX increases NPT1 and NPT4, it significantly reduces OAT3 expression in mouse kidney, which also shows the complex roles of DEX on urate absorption (Li et al., 2019). Nonetheless, compared to urate reabsorption, the tubular secretion is only a minor component of urine UA excretion. OAT10, GLUT9, and URAT1 are apically absorbed transporters of urate and play a crucial role in the urate reabsorption (Li et al., 2019). DEX had no effect on OAT10 and GLUT9, but significantly reduced the mRNA level of URAT1. Therefore, DEX-mediated increase in uric acid excretion is mainly due to the downregulation effect of URAT1 (Li et al., 2019).

## SGLT2 Inhibitors
The urine UA and SUA lowering effects of SGLT2 inhibitors are similar (Vallon and Thomson, 2017; Nespoux and Vallon, 2020). Researchers use SGLT2-, SGLT1-, URAT1-, and GLUT9-knockout mouse models to investigate the UA-lowering effect of the SGLT2 inhibitor canagliflozin, and show that the

**TABLE 1 |** Characteristics of Urate transporters.

| Transporter | Location in kidney | Mutation | Function of transporters |
|---|---|---|---|
| SLC2A9 (GLUT9) | Apical and basolateral membranes of the renal proximal tubule | R198W, R380C, P412R Anzai et al. (2008); Dinour et al. (2010); Kawamura et al. (2011) | Urate reabsorption |
| SLC16A9 (MCT9) | In the kidney and adrenal gland | rs1171614 Butler et al. (2021) rs2242206 Nakayama et al. (2013) | Related to UA levels |
| SLC17A1 (NPT1) | Apical membrane of the renal proximal tubule | rs1165196 Chiba et al. (2015); Sakiyama et al. (2016) I269T Sakiyama et al. (2016) | Urate absorption and efflux |
| SLC17A3 (NPT4) | Apical side of renal tubules | rs9393672 Sakiyama et al. (2016); Jutabha et al. (2010); Riches et al. (2009) rs942379 Sakiyama et al. (2016); Jutabha et al. (2010); Riches et al. (2009) | Urate excretion |
| SLC22A6 (OAT1) | Basolateral side of the proximal tubule | — — | Urate excretion |
| SLC22A7 (OAT2) | Mainly distributed in the kidney | C329T, G571A, G1520A Xu et al. (2005); Kato et al. (2015) | Urate secretion |
| SLC22A8 (OAT3) | In the basolateral side of the proximal tubule | — — | Urate excretion |
| SLC22A11 (OAT4) | Proximal tubules of the kidney and other marginal epithelia | rs2078267 Kenny et al. (2011); Flynn et al. (2013) rs2186571 Kenny et al. (2011); Flynn et al. (2013) rs17299124 Sakiyama et al. (2014) rs17300741 Sakiyama et al. (2014) | Urate reabsorption |
| SLC22A12 (URAT1) | Apical membrane of the proximal tubule | rs475688 Pavelcova et al. (2021) | Urate reabsorption |
| ABCG2 | Renal tubules and mesentery | V12M, Q126X, Q141K, G268R, S441N, and F506SfsX4 Matsuo et al. (2009) | Urate excretion |
| PDZK1 | Apical membrane of the kidney proximal tubule | rs12129861 Butler et al. (2021) | Regulate the transport and activity of various transport proteins in the proximal tubules |

mechanism of this effect involved intraluminal glucose transmission and inhibition of the proximal tubule urate transporter URAT1 (Novikov et al., 2019; Novikov et al., 2019). Insulin enhances the activity of URAT1. Therefore, the inhibition of SGLT2 may reduce the activity of URAT1 by enhancing luminal glucose transmission or lowering insulin levels, or SGLT2 and URAT1 may functionally interact in the proximal tubule, thereby inhibiting SGLT2 to partially suppress URAT1 (Novikov et al., 2019; Nespoux and Vallon, 2020). These SGLT2 inhibitors may also help protect mitochondrial function and tubular cell metabolism (Nespoux and Vallon, 2020). Preliminary studies in patients with T1DM and T2DM have shown that diabetes increases the urine ratio of lactobionate, and this may reflect the metabolic process of mitochondrial oxidation to glycolysis, which is reversed by SGLT2 inhibitors (Nespoux and Vallon, 2020).

## ABCG2 Inhibitors

Febuxostat is a common drug for the treatment of gout. Its main function is to inhibit xanthine oxidase. One study indicates that febuxostat exerts strong inhibitory effect on ABCG2 (Miyata et al., 2016). The researchers find that use of febuxostat reduces the efflux of many drugs mediated by ABCG2 and prolongs the action time of the drug in the body without increasing the level of UA. Further analysis show that the inhibitory effect of febuxostat on ABCG2 occurs both at clinical concentration *in vitro* and in mouse intestinal tract. It was also demonstrated that febuxostat can enhance the intestinal absorption of a substrate of ABCG2 (Yamasaki et al., 2008; Miyata et al., 2016). It is worth noting that febuxostat inhibits

ABCG2 more strongly than the two known ABCG2 inhibitors (Ko143 and elacrida), which means that febuxostat has not only advantages over these two inhibitors but also stronger in safety and ability than other ABCG2 inhibitor (Allen et al., 2002). However, decreased ABCG2 function may enhance the risk of hyperuricaemia, genetically. Thus, these findings suggest novel potential applications and risks in clinical use of febuxostat.

## Xanthine Oxidase Inhibitors
### Allopurinol

Allopurinol, a xanthine oxidase inhibitor, is one of first-line drugs for the management of gout (Stamp et al., 2016; Day et al., 2017; Coombs et al., 2021). Allopurinol has been used widely for many years, however, the reduction and maintenance of blood urate concentrations is often not achieved (Day et al., 2017). The main cause may be linked to intersubject variation in allopurinol pharmacokinetics and pharmacodynamics (Wright et al., 2013; Wright et al., 2016). In addition, recent studies report that high-dose allopurinol may induce severe cutaneous adverse drug reactions and liver injury. High drug-dosage also lead to high mortality in patients with CKD (Huang et al., 2021). Available findings suggest that the initial dosage of allopurinol should be low, particularly in patients with renal impairment. The dose should then be increased slowly until sufficient to dissolve MUS (Day et al., 2017).

### EEAK

The xanthine oxidase inhibitor tetrapeptide EEAK is identified from the skeletal myosin of tuna (Yu et al., 2021). Inhibitory peptides from tuna protein simulations indicate that traditional

hydrogen bond interactions, attractive charge interactions, and salt bridges play an important role in the interaction of EEAK with key residues of xanthine oxidase (eg, Glu802, Arg880, and Glu1261) (Yu et al., 2021). Overall, the current work strongly suggests that the tetrapeptide EEAK may be a promising compound as a natural inhibitor of xanthine oxidase for the control of gout and hyperuricaemia (Yu et al., 2021).

### Rhodiola Crenulata Extracts and Their Phytochemicals

Rhodiola crenulata is an important member of the genus Rhodiola, mainly distributed in northwest China. Previous studies have proved that the root of Rhodiola crenulata has beneficial properties, including scavenging active oxygen substances and anti-Alheimer's disease (Chen et al., 2012; Zhang et al., 2013). Researchers use fractional distillation techniques to separate four phytochemicals from Rhodiolarosea extract. These compounds are identified as 4′-hydroxyacetophenone (4-HAP), epicatechin-(4β,8)-epicatechingallate (B2-3′-O-gallate), red Sedum and *p*-tyrosol used mass spectrometry and nuclear magnetic resonance spectroscopy (Chu et al., 2014). These purified compounds are then evaluated for their inhibitory effects on xanthine oxidase activity and compared with known XO inhibitors (allopurinol). The results show that 4-HAP and B2-3′-O-gallate are effective xanthine oxidase inhibitors (Chu et al., 2014).

### 2-[4-Alkoxy-3-(1H-tetrazol-1-yl) phenyl]-6-oxo-1,6-dihydropyrimidine-5-carboxylic Acid Derivatives

The researchers in this study designed and synthesized a series of 2-[4-alkoxy-3-(1H-tetrazol-1-yl)phenyl]-6-oxo-1,6-dihydropyrimidine-5-carboxylic acid derivatives (8a-8z) and further evaluated their inhibitory effect on xanthine oxidase *in vitro* (Zhang et al., 2019). The results show that all test compounds (8a-8z) showed significant xanthine oxidase inhibitory efficacy (Zhang et al., 2019). Among them, compound 8u becomes the most effective xanthine oxidase inhibitor, with an IC50 value of 0.0288 mM, which is equivalent to febuxostat (IC50 ¼ 0.0236 mM) (Zhang et al., 2019). In addition, acute oral toxicity experiments in mice showed that compound 8u is non-toxic and can tolerate doses up to 2000 mg/kg (Zhang et al., 2019). Therefore, compound 8u may be a potentially effective xanthine oxidase inhibitor for the treatment of hyperuricaemia with low toxicity (Zhang et al., 2019).

## OTHER DRUGS THAT AFFECT UA LEVELS

### Favipiravir

Favipiravir is an antiviral agent that inhibits the RNA-dependent RNA polymerase of many RNA viruses (Furuta et al., 2017). Favipiravir is metabolized by aldehyde oxidase and xanthine oxidase to the inactive metabolite M1, which is excreted into urine. In the kidney, the processing of uric acid is regulated by the balance between proximal tubule reabsorption and renal tubule secretion. Favipiravir and M1 are moderate inhibitors of OAT1 and OAT3, which are involved in the excretion of uric acid in the kidney (Mishima et al., 2020). In addition, M1 enhances uric acid reabsorption through URAT1 in the proximal tubule of the kidney (Mishima et al., 2020). Therefore, it is believed that favipiravir reduces the excretion of urate in the urine, leading to increase the level of SUA (Mishima et al., 2020).

### PF-06743649

Some drugs under development have shown dual inhibitory effects on XOD and URAT1. But little information is available (Yue et al., 2019). Among of them, PF-06743649 is the first drug to enter clinical trials with dual effects on XOD and URAT1. PF-06743649 phase I clinical trials have been completed (Yue et al., 2019). Clinical studies have shown that PF-06743649 causes a large and rapid decrease in serum uric acid in healthy subjects and gout patients (Yue et al., 2019).

## CONCLUSION

NPT1, NPT4, ABCG2 expressed on the apical membrane and OAT1, OAT3 expressed on the basolateral membrane have been confirmed to contribute to the secretory transport of urate from proximal tubular epithelial cells into the tubule lumen (Cleophas et al., 2017). URAT1, GLUT9, OAT4 localized on the apical membrane are responsible for UA reabsorption from the tubule lumen to proximal tubule epithelial cells (Auberson et al., 2018; Wen et al., 2020). NPT1, URAT1, and OAT4 are known to bind to PDZK1 through their C-terminal PDZ domain. The metabolic disorder of UA mainly linked with abnormal urate transporters is an important cause of many diseases. In recent years, an increasing number of studies have shown that elucidating the urate transporters is essential to address the balance of urate homeostasis and hyperuricaemia-related diseases. In this review, eleven transporters and urate lowering drugs are summarized and evaluated.

Generally, asymptomatic hyperuricaemia is not an indication for treatment to lower the SUA level in persons with normal renal function. The recommended first line of urate-lowering therapy includes the xanthine oxidase inhibitors allopurinol and febuxostat by reducing urate. The novel uricosurics agent including lesinurad, arhalofenate, canagliflozin, xanthine oxidase inhibitor tetrapeptide EEAK, rhodiola crenulata, favipiravir, PF-06743649 increase renal urate excretion by inhibiting reabsorption. In sum, the exploration of the urate transports and inhibitors can enhance our understanding of hyperuricaemia and hyperuricaemia-related diseases. It may provide essential references or cross references to be contributed to further elucidate urate-lowering drugs benefits as well as provide theoretical support for the scientific research on hyperuricemia and related diseases.

## DATA AVAILABILITY STATEMENT

The raw data supporting the conclusions of this article will be made available by the authors, without undue reservation.

## AUTHOR CONTRIBUTIONS

## FUNDING

## ACKNOWLEDGMENTS

## REFERENCES

Allen, J. D., van Loevezijn, A., Lakhai, J. M., van der Valk, M., van Tellingen, O., Reid, G., et al. (2002). Potent and Specific Inhibition of the Breast Cancer Resistance Protein Multidrug Transporter *In Vitro* and in Mouse Intestine by a Novel Analogue of Fumitremorgin C. *Mol. Cancer Ther.* 1, 417–425.

Alobaidi, S., Dwid, N., Shikh Souk, K., Cheikh, M., Mandurah, A., Al-Khatib, K., et al. (2021). The Pattern of Allopurinol Prescription Among Chronic Kidney Disease Patients in a Tertiary Care Centre: A Single-Centre Experience. *Int. J. Gen. Med.* 14, 1141–1146. doi:10.2147/IJGM.S299723

Anzai, N., Miyazaki, H., Noshiro, R., Khamdang, S., Chairoungdua, A., Shin, H. J., et al. (2004). The Multivalent PDZ Domain-Containing Protein PDZK1 Regulates Transport Activity of Renal Urate-Anion Exchanger URAT1 via its C Terminus. *J. Biol. Chem.* 279, 45942–45950. doi:10.1074/jbc.M406724200

Anzai, N., Ichida, K., Jutabha, P., Kimura, T., Babu, E., Jin, C. J., et al. (2008). Plasma Urate Level Is Directly Regulated by a Voltage-Driven Urate Efflux Transporter URATv1 (SLC2A9) in Humans. *J. Biol. Chem.* 283, 26834–26838. doi:10.1074/jbc.C800156200

Anzai, N., Kanai, Y., and Endou, H. (2006). Organic Anion Transporter Family: Current Knowledge. *J. Pharmacol. Sci.* 100, 411–426. doi:10.1254/jphs.crj06006x

Ascherio, A., LeWitt, P. A., Xu, K., Eberly, S., Watts, A., Matson, W. R., et al. (2009). Urate as a Predictor of the Rate of Clinical Decline in Parkinson Disease. *Randomized Controlled Trial* 66, 1460–1468. doi:10.1001/archneurol.2009.247

Auberson, M., Stadelmann, S., Stoudmann, C., Seuwen, K., Koesters, R., Thorens, B., et al. (2018). SLC2A9 (GLUT9) Mediates Urate Reabsorption in the Mouse Kidney. *Pflugers Arch.* 470, 1739–1751. doi:10.1007/s00424-018-2190-4

Balakumar, P., Alqahtani, A., Khan, N. A., Mahadevan, N., and Dhanaraj, S. A. (2020). Mechanistic Insights into Hyperuricemia-Associated Renal Abnormalities with Special Emphasis on Epithelial-To-Mesenchymal Transition: Pathologic Implications and Putative Pharmacologic Targets. *Pharmacol. Res.* 161, 105209. doi:10.1016/j.phrs.2020.105209

Bardin, T., and Richette, P. (2014). Definition of Hyperuricemia and Gouty Conditions. *Curr. Opin. Rheumatol.* 26, 186–191. doi:10.1097/BOR.0000000000000028

Bassanese, G., Wlodkowski, T., Servais, A., Heidet, L., Roccatello, D., Emma, F., et al. (2021). The European Rare Kidney Disease Registry (ERKReg): Objectives, Design and Initial Results. *Orphanet J. Rare Dis.* 16, 251. doi:10.1186/s13023-021-01872-8

Battelli, M. G., Bolognesi, A., and Polito, L. (2014). Pathophysiology of Circulating Xanthine Oxidoreductase: New Emerging Roles for a Multi-Tasking Enzyme. *Biochim. Biophys. Acta* 1842, 1502–1517. doi:10.1016/j.bbadis.2014.05.022

Bhatnagar, V., Richard, E. L., Wu, W., Nievergelt, C. M., Lipkowitz, M. S., Jeff, J., et al. (2016). Analysis of ABCG2 and Other Urate Transporters in Uric Acid Homeostasis in Chronic Kidney Disease: Potential Role of Remote Sensing and Signaling. *Clin. Kideny J.* 9, 444–453. doi:10.1093/ckj/sfw010

Boden, G., Chen, X., Kolaczynski, J. W., and Polansky, M. (1997). Effects of Prolonged Hyperinsulinemia on Serum Leptin in Normal Human Subjects. *J. Clin. Invest* 100, 1107–1113. doi:10.1172/JCI119621

Bryant, C. E., Rajai, A., Webb, N. J. A., and Hogg, R. J. (2021). Effects of Losartan and Enalapril on Serum Uric Acid and GFR in Children with Proteinuria. *Pediatr. Nephrol.* doi:10.1007/s00467-021-05045-4

Butler, F., Alghubayshi, Ali., and Roman, Y. (2021). The Epidemiology and Genetics of Hyperuricemia and Gout across Major Racial Groups: A Literature Review and Population Genetics Secondary Database Analysis. *J. Pers Med.* 11, 231. doi:10.3390/jpm11030231

Caspi, D., Lubart, E., Graff, E., Habot, B., Yaron, M., and Segal, R. (2000). The Effect of Mini-Dose Aspirin on Renal Function and Uric Acid Handling in Elderly Patients. *ARTHRITIS RHEUMATOL.* 43, 103–108. doi:10.1002/1529-0131(200001)43:1<103::aid-anr13>3.0.co;2-c

Cha, D. H., Gee, H. Y., Cachau, R., Choi, J. M., Park, D., Jee, S. H., et al. (2019). Contribution of SLC22A12 on Hypouricemia and its Clinical Significance for Screening Purposes. *Sci. Rep-uk* 9, 14360. doi:10.1038/s41598-019-50798-6

Changgui Li, M.-C. H., and Chang, S-J. (2013). Metabolic Syndrome, Diabetes, and Hyperuricemia. *Curr. Opin. Rheumatol.* 25, 210–216. doi:10.1097/BOR.0b013e32835d951e

Chen, D., Fan, J., Wang, P., Zhu, L., Jin, Y., Peng, Y., et al. (2012). Isolation, Identification and Antioxidative Capacity of Water-Soluble Phenylpropanoid Compounds from Rhodiola Crenulata. *Food Chem.* 134, 2126–2133. doi:10.1016/j.foodchem.2012.04.011

Chengfu Xu, X. W., Xu, L., Weng, H., and Yan, M. (2015). Xanthine Oxidase in Non-alcoholic Fatty Liver Disease and Hyperuricemia: One Stone Hits Two Birds. *J. Hepatol.* 62, 1412–1419. doi:10.1016/j.jhep.2015.01.019

Chiba, T., Matsuo, H., Kawamura, Y., Nagamori, S., Nishiyama, T., Wei, L., et al. (2015). NPT1/SLC17A1 Is a Renal Urate Exporter in Humans and its Common Gain-Of-Function Variant Decreases the Risk of Renal Underexcretion Gout. *ARTHRITIS RHEUMATOL.* 67, 281–287. doi:10.1002/art.38884

Choi, H. K., Mount, D. B., and Reginato, A. M. (2005). Pathogenesis of Gout. *Ann. Intern. Med.* 143, 499–516. doi:10.7326/0003-4819-143-7-200510040-00009

Chu, Y-H., Chen, C-J., Wu, S-H., and Hsieh, J-F. (2014). Inhibition of Xanthine Oxidase by Rhodiola Crenulata Extracts and Their Phytochemicals. *J. Agric. Food Chem.* 62, 3742–3749. doi:10.1021/jf5004094

Cleophas, M. C., Joosten, L. A., Stamp, L. K., Dalbeth, N., Woodward, O. M., and Merriman, T. R. (2017). ABCG2 Polymorphisms in Gout: Insights into Disease Susceptibility and Treatment Approaches. *Pharmgenomics Pers Med.* 10, 129–142. doi:10.2147/PGPM.S105854

Console, L., Scalise, M., Mazza, T., Pochini, L., Galluccio, M., Giangregorio, N., et al. (2020). Carnitine Traffic in Cells. Link with Cancer. *Front Cell Dev Biol* 8, 583850. doi:10.3389/fcell.2020.583850

Cook, S., Hugli, O., Egli, M., Menard, B., Thalmann, S., Sartori, C., et al. (2004). Partial Gene Deletion of Endothelial Nitric Oxide Synthase Predisposes to Exaggerated High-Fat Diet-Induced Insulin Resistance and Arterial Hypertension. *Diabetes* 53, 2067–2072. doi:10.2337/diabetes.53.8.2067

Coombs, G. B., Akins, J. D., Patik, J. C., Vizcardo-Galindo, G. A., Figueroa-Mujica, R., Tymko, M. M., et al. (2021). Global Reach 2018: Nitric Oxide-Mediated Cutaneous Vasodilation Is Reduced in Chronic, but Not Acute, Hypoxia Independently of Enzymatic Superoxide Formation. *Free Radic. Biol. Med.* doi:10.1016/j.freeradbiomed.2021.06.005

Culleton, B. F., Larson, M. G., Kannel, W. B., and Levy, D. (1999). Serum Uric Acid and Risk for Cardiovascular Disease and Death: the Framingham Heart Study. *Ann. Intern. Med.* 131, 7–13. doi:10.7326/0003-4819-131-1-199907060-00003

Cunningham, R., Brazie, M., Kanumuru, S., Xiaofei, E., Biswas, R., Wang, F., et al. (2007). Sodium-hydrogen Exchanger Regulatory Factor-1 Interacts with Mouse Urate Transporter 1 to Regulate Renal Proximal Tubule Uric Acid Transport. *J. Am. Soc. Nephrol.* 18, 1419–1425. doi:10.1681/ASN.2006090980

D'Elia, L., Giaquinto, A., Cappuccio, F. P., Iacone, R., Russo, O., Strazzullo, P., et al. (2020). Circulating Leptin is Associated with Serum Uric Acid Level and its Tubular Reabsorption in a Sample of Adult Middle-Aged Men. *J. Endocrinol. Invest* 43, 587–593. doi:10.1007/s40618-019-01140-4

Dalbeth, N., Lauterio, T. J., and Wolfe, H. R. (2014). Mechanism of Action of Colchicine in the Treatment of Gout. *Clin. Ther.* 36, 1465–1479. doi:10.1016/j.clinthera.2014.07.017

Dalbeth, N., Choi, H. K., Joosten, L. A. B., Khanna, P. P., Matsuo, H., Perez-Ruiz, F., et al. (2019). *Gout. Nat. Rev. Dis. Primers* 5, 69. doi:10.1038/s41572-019-0115-y

Day, R. O., Kannangara, D. R., Stocker, S. L., Carland, J. E., Williams, K. M., and Graham, G. G. (2017). Allopurinol: Insights from Studies of Dose-Response Relationships. *Expert Opin. Drug Metab. Toxicol.* 13, 449–462. doi:10.1080/17425255.2017.1269745

DeMarco, V. G., Aroor, A. R., and Sowers, J. R. (2014). The Pathophysiology of Hypertension in Patients with Obesity. *Nat. Rev. Endocrinol.* 10, 364–376. doi:10.1038/nrendo.2014.44

Dinour, D., Gray, N. K., Campbell, S., Shu, X., Sawyer, L., Richardson, W., et al. (2010). Homozygous SLC2A9 Mutations Cause Severe Renal Hypouricemia. *J. Am. Soc. Nephrol.* 21, 64–72. doi:10.1681/ASN.2009040406

Du, N., Xu, D., Hou, X., Song, X., Liu, C., Chen, Y., et al. (2016). Inverse Association between Serum Uric Acid Levels and Alzheimer's Disease Risk. *Mol. Neurobiol.* 53, 2594–2599. doi:10.1007/s12035-015-9271-6

Ebert, K., Ludwig, M., Geillinger, K. E., Schoberth, G. C., Essenwanger, J., Stolz, J., et al. (2017). Reassessment of GLUT7 and GLUT9 as Putative Fructose and Glucose Transporters. *J. Membr. Biol.* 250, 171–182. doi:10.1007/s00232-016-9945-7

Edwards, N. L. (2009). The Role of Hyperuricemia in Vascular Disorders. *Curr. Opin. Rheumatol.* 21, 132–137. doi:10.1097/BOR.0b013e3283257b96

Engel, B., Just, J., Bleckwenn, M., and Weckbecker, K. (2017). Treatment Options for Gout. *Dtsch Arztebl Int.* 114, 215–222. doi:10.3238/arztebl.2017.0215

Enomoto, A., Kimura, H., Chairoungdua, A., Shigeta, Y., Jutabha, P., Cha, S. H., et al. (2002). Molecular Identification of a Renal Urate Anion Exchanger that Regulates Blood Urate Levels. *Nature* 417, 447–452. doi:10.1038/nature742

Eraly, S. A., Vallon, V., Rieg, T., Gangoiti, J. A., Wikoff, W. R., Gary, S., et al. (2008). Multiple Organic Anion Transporters Contribute to Net Renal Excretion of Uric Acid. *Physiol. Genomics* 33, 180–192. doi:10.1152/physiolgenomics.00207.2007

Facchini, F., Chen, Y. D., Hollenbeck, C. B., and Reaven, G. M. (1991). Relationship between Resistance to Insulin-Mediated Glucose Uptake, Urinary Uric Acid Clearance, and Plasma Uric Acid Concentration. *JAMA* 266, 3008–3011. doi:10.1001/jama.1991.03470210076036

Fernandes Silva, L., Vangipurapu, J., and Kuulasmaa, T. (2019). An Intronic Variant in the GCKR Gene Is Associated with Multiple Lipids. *Sci. Rep.* 9, 10240. doi:10.1038/s41598-019-46750-3

Flynn, T. J., Phipps-Green, A., JadeHollis-Moffatt, E., Merriman, M. E., Ruth, T., Montgomery, G., et al. (2013). Association Analysis of the SLC22A11 (Organic Anion Transporter 4) and SLC22A12 (Urate Transporter 1) Urate Transporter Locus with Gout in New Zealand Case-Control Sample Sets Reveals Multiple Ancestral-specific Effects. *Arthritis Res. Ther.* 15, 1–11. doi:10.1186/ar4417

Fruehwald-Schultes, B., Peters, A., Kern, W., Beyer, J., and Pfützner, A. (1999). Serum Leptin Is Associated with Serum Uric Acid Concentrations in Humans. *Metabolism* 48, 677–680. doi:10.1016/s0026-0495(99)90163-4

Furuta, Y., Komeno, T., and Nakamura, T. (2017). Favipiravir (T-705), a Broad Spectrum Inhibitor of Viral RNA Polymerase. *Proc. Jpn. Acad. Ser. B Phys. Biol. Sci.* 93, 449–463. doi:10.2183/pjab.93.027

Futagi, Y., Narumi, K., Furugen, A., Kobayashi, M., and Iseki, K. (2020). Molecular Characterization of the Orphan Transporter SLC16A9, an Extracellular pH- and Na Þ -sensitive Creatine Transporter. *Biochem. Biophys. Res. Commun.* 522, 539–544. doi:10.1016/j.bbrc.2019.11.137

Gehr, P. (2004). Swiss Medical Weekly Young Investigator's Award 2003: Clustering of Cardiovascular Risk Factors Mimicking the Human Metabolic Syndrome X in eNOS Null Mice. *Swiss Med. Wkly* 15, 267.

Ghadge, A. A., and Khaire, A. A. (2019). Leptin as a Predictive Marker for Metabolic Syndrome. *Cytokine* 121, 154735. doi:10.1016/j.cyto.2019.154735

Go, M. J., Jang, H. B., Park, S. I., Lee, H-J., and Cho, S. B. (2019). Chronic Heavy Alcohol Consumption Influences the Association between Genetic Variants of GCK or INSR and the Development of Diabetes in Men: A 12-year Follow-Up Study. *Scientific Rep.* 9, 20029. doi:10.1038/s41598-019-56011-y

Gopal, E., Fei, Y. J., Sugawara, M., Miyauchi, S., Zhuang, L., Martin, P., et al. (2004). Expression of Slc5a8 in Kidney and its Role in Na+-Coupled Transport of Lactate. *J. Biol. Chem.* 279, 44522–44532. doi:10.1074/jbc.M405365200

Guo, C-Y., Yang, Q., Cupples, L. A., and Levy, D. (2005). Genome-wide Search for Genes Affecting Serum Uric Acid Levels:the Framingham Heart Study. *METABOLISM* 54, 1435–1441. doi:10.1016/j.metabol.2005.05.007

Hagos, Y., Stein, D., Ugele, B., Burckhardt, G., and Bahn, A. (2007). Human Renal Organic Anion Transporter 4 Operates as an Asymmetric Urate Transporter. *J. Am. Soc. Nephrol.* 18, 430–439. doi:10.1681/ASN.2006040415

Harris, M., Bryant, L. R., Danaher, P., and Alloway, J. (2000). Effect of Low Dose Daily Aspirin on Serum Urate Levels and Urinary Excretion in Patients Receiving Probenecid for Gouty Arthritis. *J. Rheumatol.* 27, 2873–2876.

Harst, P. v. d., Bakker, S. J. L., de Boer, R. A., Wolffenbuttel, B. H. R., Johnson, T., Caulfield, M. J., et al. (2010). Replication of the Five Novel Loci for Uric Acid Concentrations and Potential Mediating Mechanisms. *Hum. Mol. Genet.* 19, 387–395. doi:10.1093/hmg/ddp489

Hassoun, P. M., Shedd, A. L., Lanzillo, J. J., Thappa, V., Landman, M. J., and Fanburg, B. L. (1992). Inhibition of Pulmonary Artery Smooth Muscle Cell Growth by Hypoxanthine, Xanthine, and Uric Acid. *Am. J. Respir. Cell Mol Biol* 6, 617–624. doi:10.1165/ajrcmb/6.6.617

Henjakovic, M., Hagos, Y., Krick, W., Burckhardt, G., and C Burckhardt, B. (2015). Human Organic Anion Transporter 2 Is Distinct from Organic Anion Transporters 1 and 3 with Respect to Transport Function. *Am. J. Physiol. Ren. Physiol* 309, F843–F851. doi:10.1152/ajprenal.00140.2015

Hong, J. Y., Lan, T. Y., Tang, G. J., Tang, C. H., Chen, T. J., and Lin, H. Y. (2015). Gout and the Risk of Dementia: a Nationwide Population-Based Cohort Study. *Arthritis Res. Ther.* 17, 139. doi:10.1186/s13075-015-0642-1

Hoogerland, J. A., Saeed, A, Hanna, W., Heegsma, J, Derks, T. G. J., van der Veer, E., et al. (2020). Klaas Nico Faber, Glycogen Storage Disease Type 1a Is Associated with Disturbed Vitamin A Metabolism and Elevated Serum Retinol Levels. *Hum. Mol. Genet.* 29, 264–273. doi:10.1093/hmg/ddz283

Hosoyamada, M., Ichida, K., Enomoto, A., Hosoya, T., and Endou, H. (2004). Function and Localization of Urate Transporter 1 in Mouse Kidney. *J. Am. Soc. Nephrol.* 15, 261–268. doi:10.1097/01.asn.0000107560.80107.19

Houlihan, L. M., Wyatt, N. D., Harris, S. E., Hayward, C., Gow, A. J., Marioni, R. E., et al. (2010). Variation in the Uric Acid Transporter Gene (SLC2A9) and Memory Performance. *Hum. Mol. Genet.* 19, 2321–2330. doi:10.1093/hmg/ddq097

Huang, Y-S., Wu, C-Y., Chang, T-T., Peng, C-Y., Lo, G-H., Hsu, C-W., et al. (2021). Drug-induced Liver Injury Associated with Severe Cutaneous Adverse Drug Reactions: A Nationwide Study in Taiwan. *Liver Int.* doi:10.1111/liv.14990

Hyndman, D., Liu, S., and Miner, J. N. (2016). Urate Handling in the Human Body. *Curr. Rheumatol. Rep.* 18, 34. doi:10.1007/s11926-016-0587-7

Ichida, K., Matsuo, H., Takada, T., Nakayama, A., Murakami, K., Shimizu, T., et al. (2012). Decreased Extra-renal Urate Excretion Is a Common Cause of Hyperuricemia. *Nat. Commun.* 3, 764. doi:10.1038/ncomms1756

Iharada, M., Miyaji, T., Fujimoto, T., Miki, H., Anzai, N., Omote, H., et al. (2010). Type 1 Sodium-dependent Phosphate Transporter (SLC17A1 Protein) Is a Cl(-)-dependent Urate Exporter. *J. Biol. Chem.* 285, 26107–26113. doi:10.1074/jbc.M110.122721

Iwanaga, T., Sato, M., Maeda, T., Ogihara, T., and Tamai, I. (2007). Concentration-dependent Mode of Interaction of Angiotensin II Receptor Blockers with Uric Acid Transporter. *J. Pharmacol. Exp. Ther.* 320, 211–217. doi:10.1124/jpet.106.112755

JadeHollis-Moffatt, E., Phipps-Green, A J., Chapman, B., Jones, G. T., van Rij, A., Gow, P. J., et al. (2012). The Renal Urate Transporter SLC17A1 Locus: Confirmation of Association with Gout. *Arthritis Res. Ther.* 14, R92. doi:10.1186/ar3816

Jessica Maiuolo, F. O., Gratteri, S., Muscoli, C., and Mollace, V. (2016). Regulation of Uric Acid Metabolism and Excretion. *Int. J. Cardiol.* 15, 8–14. doi:10.1016/j.ijcard.2015.08.109

Jeyaruban, A., Soden, M., and Larkins, S. (2016). General Practitioners' Perspectives on the Management of Gout: a Qualitative Study. *Postgrad. Med. J.* 92, 603–607. doi:10.1136/postgradmedj-2015-133920

Jiao, Z., Chen, Y., Xie, Y., Li, Y., and Li, Z. (2021). Metformin Protects against Insulin Resistance Induced by High Uric Acid in Cardiomyocytes via AMPK Signalling Pathways In Vitro and In Vivo. J. Cell Mol Med. doi:10.1111/jcmm.16677

Jingzhe Han, X. S., Lu, S., Ji, G., Xie, Y., and Wu, H. (2019). Adolescent Hyperuricemia with Lipid StorageMyopathy: A Clinical Study. Med. Sci. Monit. 25, 9103–9111. doi:10.12659/MSM.918841

Jutabha, P., Anzai, N., Kitamura, K., Taniguchi, A., Kaneko, S., Yan, K., et al. (2010). Human Sodium Phosphate Transporter 4 (hNPT4/SLC17A3) as a Common Renal Secretory Pathway for Drugs and Urate. J. Biol. Chem. 285, 35123–35132. doi:10.1074/jbc.M110.121301

Jutabha, P., Anzai, N., Wempe, M. F., Wakui, S., Endou, H., and Sakurai, H. (2011). Apical Voltage-Driven Urate Efflux Transporter NPT4 in Renal Proximal Tubule. Nucleosides Nucleotides Nucleic Acids 30, 1302–1311. doi:10.1080/15257770.2011.616564

Kang, D. H., Nakagawa, T., Feng, L., Watanabe, S., Han, L., Mazzali, M., et al. (2002). A Role for Uric Acid in the Progression of Renal Disease. J. Am. Soc. Nephrol. 13, 2888–2897. doi:10.1097/01.asn.0000034910.58454.fd

Kato, N., Loh, M., Takeuchi, F., Verweij, N., Wang, X., Zhang, W., et al. (2015). Trans-ancestry Genome-wide Association Study Identifies 12 Genetic Loci Influencing Blood Pressure and Implicates a Role for DNA Methylation. Nat. Genet. 47, 1282–1293. doi:10.1038/ng.3405

Kawamura, Y., Matsuo, H., Chiba, T., Nagamori, S., Nakayama, A., Inoue, H., et al. (2011). Pathogenic GLUT9 Mutations Causing Renal Hypouricemia Type 2 (RHUC2). Nucleosides Nucleotides Nucleic Acids 30, 1105–1111. doi:10.1080/15257770.2011.623685

Kenny, E. E., Kim, M., Gusev, A., Lowe, J. K., Salit, J., Smith, J. G., et al. (2011). Increased Power of Mixed Models Facilitates Association Mapping of 10 Loci for Metabolic Traits in an Isolated Population. Hum. Mol. Genet. 20, 827–839. doi:10.1093/hmg/ddq510

Keskin, H., Cadirci, K., Gungor, K., Karaaslan, T., Usta, T., Ozkeskin, A., et al. (2021). Association between TSH Values and GFR Levels in Euthyroid Cases with Metabolic Syndrome. Int. J. Endocrinol. 2021, 8891972. doi:10.1155/2021/8891972

Khan, A. A., Quinn, T. J., Hewitt, J., Fan, Y., and Dawson, J. (2016). Serum Uric Acid Level and Association with Cognitive Impairment and Dementia: Systematic Review and Meta-Analysis. Age (Dordr) 38, 16. doi:10.1007/s11357-016-9871-8

Kim, M. J., Yoon, J. H., and Ryu, J. H. (2016). Mitophagy: a Balance Regulator of NLRP3 Inflammasome Activation. BMB Rep. 49, 529–535. doi:10.5483/bmbrep.2016.49.10.115

Kimoto, E., Mathialagan, S., Tylaska, L., Niosi, M., Lin, J., Carlo, A. A., et al. (2018). Organic Anion Transporter 2 Mediated Hepatic Uptake Contribute to the Clearance of High Permeability–Low Molecular Weight Acid and Zwitterion Drugs: Evaluation Using 25 Drugs. JPET 1, 1–40. doi:10.1124/jpet.118.252049

Kimura, T., Takahashi, M., Yan, K., and Sakurai, H. (2014). Expression of SLC2A9 Isoforms in the Kidney and Their Localization in Polarized Epithelial Cells. PLoS One 9, e84996. doi:10.1371/journal.pone.0084996

Kondo, C., Suzuki, H., Itoda, M., Ozawa, S., Sawada, J-i., Kobayashi, D., et al. (2004). Kazunori Mine, Kenji Ohtsubo, Yuichi Sugiyama, Functional Analysis of SNPs Variants of BCRP/ABCG2. Pharm. Res. 21, 1895–1903. doi:10.1023/b:pham.0000045245.21637.d4

Köttgen, A., Albrecht, E., Teumer, A., Vitart, V., Krumsiek, J., Hundertmark, C., et al. (2013). Genome-wide Association Analyses Identify 18 New Loci Associated with Serum Urate Concentrations. Nat. Genet. 45, 145–154. doi:10.1038/ng.2500

Krishnan, E., Svendsen, K., Neaton, J. D., Grandits, G., Kuller, L. H., and Group, M. R. (2008). Long-term Cardiovascular Mortality Among Middle-Aged Men with Gout. Arch. Intern. Med. 168, 1104–1110. doi:10.1001/archinte.168.10.1104

Lang, K., Wagner, C., Haddad, G., Burnekova, O., and Geibel, J. (2003). Intracellular pH Activates Membrane-Bound Na(+)/H(+) Exchanger and Vacuolar H(+)-ATPase in Human Embryonic Kidney (HEK) Cells. Cell Physiol Biochem 13, 257–262. doi:10.1159/000074540

Latourte, A., Soumare, A., Bardin, T., Perez-Ruiz, F., Debette, S., and Richette, P. (2018). Uric Acid and Incident Dementia over 12 Years of Follow-Up: a Population-Based Cohort Study. Ann. Rheum. Dis. 77, 328–335. doi:10.1136/annrheumdis-2016-210767

Leyva, F., Anker, S., Swan, J. W., Godsland, I. F., Wingrove, C. S., Chua, T. P., et al. (1997). Serum Uric Acid as an Index of Impaired Oxidative Metabolism in Chronic Heart Failure. Eur. Heart 18, 858–865. doi:10.1093/oxfordjournals.eurheartj.a015352

Li, G., Han, L., Ma, R., Saeed, K., Xiong, H., Klaassen, C. D., et al. (2019). Glucocorticoids Increase Renal Excretion of Urate in Mice by Downregulating Urate Transporter 1. Drug Metab. Dispos 47, 1343–1351. doi:10.1124/dmd.119.087700

Liangshan Mu, J. P., Yang, L., Chen, Q., Chen, Y., Teng, Y., Wang, P., et al. (2018). Association between the Prevalence of Hyperuricemia and Reproductive Hormones in Polycystic Ovary Syndrome. Reprod. Biol. Endocrinol. 25, 104. doi:10.1186/s12958-018-0419-x

Linqiang Ma, J. H., Li, J., Yang, Y., Zhang, L., Zou, L., Gao, R., et al. (2018). Bisphenol A Promotes Hyperuricemia via Activating Xanthine Oxidase. FASEB J. 32, 1007–1016. doi:10.1096/fj.201700755R

Liu, N., Wang, L., Yang, T., Xiong, C., Xu, L., Shi, Y., et al. (2015). EGF Receptor Inhibition Alleviates Hyperuricemic Nephropathy. J. Am. Soc. Nephrol. 26, 2716–2729. doi:10.1681/ASN.2014080793

Lu, X., Chen, M., Shen, J., Xu, Y., and Wu, H. (2019). IL-1β Functionally Attenuates ABCG2 and PDZK1 Expression in HK-2 Cells Partiallythrough NF-κb Activation. Cell Biol. Int. 43, 279–289. doi:10.1002/cbin.11100

Major, T. J., Topless, R. K., Dalbeth, N., and Merriman, T. R. (2018). Evaluation of the Diet Wide Contribution to Serum Urate Levels: Meta-Analysis of Population Based Cohorts. BMJ 363, k3951. doi:10.1136/bmj.k3951

Maliepaard, M., Scheffer, G. L., Faneyte, I. F., van Gastelen, M. A., Pijnenborg, A. C., Schinkel, A. H., et al. (2001). Subcellular Localization and Distribution of the Breast Cancer Resistance Protein Transporter in Normal Human Tissues. Cancer Res. 61, 3458–3464.

Mandal, A. K., and Mount, D. B. (2019). Interaction between ITM2B and GLUT9 Links Urate Transport to Neurodegenerative Disorders. Front Physiol. 10, 1323. doi:10.3389/fphys.2019.01323

Martin, K., Hall, J., Gillen, M., Yang, X., Shen, Z., Lee, C., et al. (2018). Pharmacokinetics, Pharmacodynamics, and Tolerability of Concomitant Multiple Dose Administration of Verinurad (RDEA3170) and Allopurinol in Adult Male Subjects with Gout. J. Clin. Pharmacol. 58, 1214–12222. doi:10.1002/jcph.1119

Mathialagan, S., Costales, C., Tylaska, L., Kimoto, E., Vildhede, A., Johnson, J., et al. (2018). In Vitro studies with Two Human Organic Anion Transporters: OAT2 and OAT7. Xenobiotica 48, 1037–1049. doi:10.1080/00498254.2017.1384595

Matsumura, K., Arima, H., Tominaga, M., Ohtsubo, T., Sasaguri, T., Fujii, K., et al. (2015). Effect of Losartan on Serum Uric Acid in Hypertension Treated with a Diuretic: the COMFORT Study. Clin. Exp. Hypertens. 37, 192–196. doi:10.3109/10641963.2014.933968

Matsuo, H., Takada, T., Ichida, K., Nakamura, T., Nakayama, A., Ikebuchi, Y., et al. (2009). Common Defects of ABCG2, a High-Capacity Urate Exporter, Cause Gout: A Function-Based Genetic Analysis in a Japanese Population. Sci. Transl Med. 1, 5ra11. doi:10.1126/scitranslmed.3000237

McWherter, C., Choi, Y. J., Serrano, R. L., Mahata, S. K., Terkeltaub, R., and Liu-Bryan, R. (2018). Arhalofenate Acid Inhibits Monosodium Urate crystal-induced Inflammatory Responses through Activation of AMP-Activated Protein Kinase (AMPK) Signaling. Arthritis Res. Ther. 20. doi:10.1186/s13075-018-1699-4

Misawa, K., Hasegawa, T., Mishima, E., Jutabha, P., Ouchi, M., Kojima, K., et al. (2020). Contribution of Rare Variants of the SLC22A12 Gene to the Missing Heritability of Serum Urate Levels. Genetics 1, 1–32. doi:10.1534/genetics.119.303006

Mishima, E., Anzai, N., Miyazaki, M., and Abe, T. (2020). Uric Acid Elevation by Favipiravir, an Antiviral Drug. Tohoku J. Exp. Med. 251, 87–90. doi:10.1620/tjem.251.87

Miyata, H., Takada, T., Toyoda, Y., Matsuo, H., Ichida, K., and Suzuki, H. (2016). Identification of Febuxostat as a New Strong ABCG2 Inhibitor: Potential Applications and Risks in Clinical Situations. Front Pharmacol. 7, 1–12. doi:10.3389/fphar.2016.00518

Miyauchi, S., Gopal, E., Fei, Y. J., and Ganapathy, V. (2004). Functional Identification of SLC5A8, a Tumor Suppressor Down-Regulated inColon Cancer, as a Na+-Coupled Transporter for Short-Chain Fatty Acids. J. Biol. Chem. 279, 13293–13296. doi:10.1074/jbc.C400059200

Miyazaki, H., Anzai, N., Ekaratanawong, S., Sakata, T., Jung, H., Jutabha, P., et al. (2005). Modulation of Renal Apical Organic Anion Transporter 4 Function by Two PDZ Domain-Containing Proteins. J. Am. Soc. Nephrol. 16, 3498–3506. doi:10.1681/ASN.2005030306

Møller, J. V., and Sheikh, M. I. (1982). Renal Organic Anion Transport System: Pharmacological, Physiological, and Biochemical Aspects. *Pharmacol. Rev.* 34, 315–358.

Mount, D. B., and Mandal, A. K. (2019). Interaction between ITM2B and GLUT9 Links Urate Transport to Neurodegenerative Disorders. *Front Physiol.* 10, 1323. doi:10.3389/fphys.2019.01323

Nakatani, S., Ishimura, E., Murase, T., Nakamura, T., Nakatani, A., Toi, N., et al. (2021). Plasma Xanthine Oxidoreductase Activity Associated with Glycemic Control in Patients with Pre-dialysis Chronic Kidney Disease. *Kidney Blood Press Res.* 3, 1–9. doi:10.1159/000516610

Nakayama, A., Matsuo, H., Shimizu, T., Ogata, H., Takada, Y., Nakashima, H., et al. (2013). Common Missense Variant of Monocarboxylate Transporter 9 (MCT9/SLC16A9) Gene Is Associated with Renal Overload Gout, but Not with All Gout Susceptibility. *Hum. Cell* 26, 133–136. doi:10.1007/s13577-013-0073-8

Nespoux, J., and Vallon, V. (2020). Renal Effects of SGLT2 Inhibitors: an Update. *Curr. Opin. Nephrol. Hypertens.* 29, 190–198. doi:10.1097/MNH.0000000000000584

Nieto, C. I. F. J., Gross, M. D., Comstock, G. W., and Cutler, R. G. (2000). Uric Acid and Serum Antioxidant Capacity: a Reaction to Atherosclerosis? *Atherosclerosis* 148, 131–139. doi:10.1016/s0021-9150(99)00214-2

Nigam, S. K., and Bhatnagar, V. (2018). The Systems Biology of Uric Acid Transporters: the Role of Remote Sensing and Signaling. *Curr. Opin. Nephrol. Hypertens.* 27, 305–313. doi:10.1097/MNH.0000000000000427

Nigam, S. K. (2015). What Do Drug Transporters Really Do? *Nat. Rev. Drug Discov.* 14, 29–44. doi:10.1038/nrd4461

Novikov, A., Fu, Y., Huang, W., Freeman, B., Patel, R., van Ginkel, C., et al. (2019). SGLT2 Inhibition and Renal Urate Excretion: Role of Luminal Glucose, GLUT9, and URAT1. *Am. J. Physiol. Ren. Physiol* 316, F173–F185. doi:10.1152/ajprenal.00462.2018

Otsuka, Y., Furihata, T., Nakagawa, K., Ohno, Y., Reien, Y., Ouchi, M., et al. (2019). Sodium-coupled Monocarboxylate Transporter 1 Interacts with the RING finger- and PDZ Domain-Containing Protein PDZRN3. *J. Physiol. Sci.* 69, 635–642. doi:10.1007/s12576-019-00681-w

Patel, R., Williams-Dautovich, J., and Cummins, C. L. (2014). Minireview: New Molecular Mediators of Glucocorticoid Receptor Activity in Metabolic Tissues. *Mol. Endocrinol.* 28, 999–1011. doi:10.1210/me.2014-1062

Pavelcova, K., Bohata, J., Pavlikova, M., Bubenikova, E., Pavelka, K., and Stiburkova, B. (2021). Evaluation of the Influence of Genetic Variants of SLC2A9 (GLUT9) and SLC22A12 (URAT1) on the Development of Hyperuricemia and Gout. *J. Clin. Med.* 9, 2510.

Polasek, O., Jeroncić, I., Mulić, R., Klismanic, Z., Pehlić, M., Zemunik, T., et al. (2010). Common Variants in SLC17A3 Gene Affect Intra-personal Variation in Serum Uric Acid Levels in Longitudinal Time Series. *CROAT. MED. J.* 285, 2010. doi:10.3325/cmj.2010.51.32

Prestin, K., Hussner, J., Ferreira, C., Seibert, I., Breitung, V., Zimmermann, U., et al. (2017). Regulation of PDZ Domain-Containing 1 (PDZK1) Expression by Hepatocyte Nuclear Factor-1α (HNF1α) in Human Kidney. *Am. J. Physiol. Ren. Physiol* 313, F973–F983. doi:10.1152/ajprenal.00650.2016

Pritchard, J. B., and Miller, D. S. (1993). Mechanisms Mediating Renal Secretion of Organic Anions and Cations. *Physiol. Rev.* 73, 765–796. doi:10.1152/physrev.1993.73.4.765

Puig, J. G., and Martínez, M. A. (2008). Hyperuricemia, Gout and the Metabolic Syndrome. *Curr. Opin. Rheumatol.* 20, 187–191. doi:10.1097/BOR.0b013e3282f4b1ed

Ragab, G., Elshahaly, M., and Bardin, T. (2017). Gout: An Old Disease in New Perspective - A Review. *J. Adv. Res.* 8, 495–511. doi:10.1016/j.jare.2017.04.008

Riches, P. L., Wright, A. F., and Ralston, S. H. (2009). Recent Insights into the Pathogenesis of Hyperuricaemia and Gout. *Hum. Mol. Genet. Medline* 18, R177–R184. doi:10.1093/hmg/ddp369

Roch-Ramel, F., Guisan, B., and Diezi, J. (1997). Effects of Uricosuric and Antiuricosuric Agents on Urate Transport in Human brush-border Membrane Vesicles. *J. Pharmacol. Exp. Ther.* 280, 839–845.

Roch-Ramel, F., Werner, D., and Guisan, B. (1994). Transport in Brush-Border Membrane of Human Kidney. *Am. J. Physiol.* 266, F797–F805. doi:10.1152/ajprenal.1994.266.5.F797

Roshanbin, S., Lindberg, F. A., Lekholm, E., Eriksson, M. M., Perland, E., Åhlund, J., et al. (2016). Histological Characterization of Orphan Transporter MCT14 (SLC16A14) Shows Abundant Expression in Mouse CNS and Kidney. *BMC Neurosci.* 17, 43. doi:10.1186/s12868-016-0274-7

Rudan, I, Wright, A. F., Hastie, N. D., and Campbell, H. (2010). A 'complexity' of Urate Transporters. *Kidney Int.* 78, 446–452. doi:10.1038/ki.2010.206

Saad, M. F., Khan, A., Sharma, A., Michael, R., Riad-Gabriel, M. G., Boyadjian, R., et al. (1998). Physiological Insulinemia Acutely Modulates Plasma Leptin. *Diabetes* 47, 544–549. doi:10.2337/diabetes.47.4.544

Sager, G., Smaglyukova, N., and Fuskevaag, O-M. (2018). The Role of OAT2 (SLC22A7) in the Cyclic Nucleotide Biokinetics of Human Erythrocytes. *J. Cell Physiol* 233, 5972–5980. doi:10.1002/jcp.26409

Sakiyama, M., Matsuo, H., Nagamori, S., Ling, W., Kawamura, Y., Nakayama, A, et al. (2016). Expression of a Human NPT1/SLC17A1 Missense Variant Which Increases Urate Export. *NUCLEOS NUCLEOT NUCL.* 35, 536–542. doi:10.1080/15257770.2016.1149192

Sakiyama, M., Matsuo, H., Shimizu, S., Nakashima, H., Nakayama, A., Chiba, T., et al. (2014). A Common Variant of Organic Anion Transporter 4 (OAT4/SLC22A11) Gene Is Associated with Renal Underexcretion Type Gout. *Drug Metab. Pharmacokinet.* 29, 208–210. doi:10.2133/dmpk.dmpk-13-nt-070

Sakurai, H. (2013). Urate Transporters in the Genomic Era. *Curr. Opin. Nephrol. Hypertens.* 22, 545–550. doi:10.1097/MNH.0b013e328363ffc8

Salminen, A., Hyttinen, J. M., and Kaarniranta, K. (2011). AMP-activated Protein Kinase Inhibits NF-Kb Signaling and Inflammation: Impact on Healthspan and Lifespan. *J. Mol. Med. (Berl)* 89, 667–676. doi:10.1007/s00109-011-0748-0

Shahid, H., and Singh, J. A. (2015). Investigational Drugs for Hyperuricemia. *Expert Opin. Investig. Drugs* 24, 1013–1030. doi:10.1517/13543784.2015.1051617

Shenolikar, S., Voltz, J. W., Minkoff, C. M., Wade, J. B., and Weinman, E. J. (2002). Targeted Disruption of the Mouse NHERF-1 Gene Promotes Internalization of Proximal Tubule Sodium-Phosphate Cotransporter Type IIa and Renal Phosphate Wasting. *Proc. Natl. Acad. Sci. U S A.* 99, 11470–11475. doi:10.1073/pnas.162232699

Shi, Y., Chen, W., Jalal, D., Li, Z., Chen, W., Mao, H., et al. (2012). Clinical Outcome of Hyperuricemia in IgA Nephropathy: a Retrospective Cohort Study and Randomized Controlled Trial. *Kidney Blood Press Res.* 35, 153–160. doi:10.1159/000331453

Shiozawa, A., Szabo, S. M., Bolzani, A., Cheung, A., and Choi, H. K. (2017). Serum Uric Acid and the Risk of Incident and Recurrent Gout: A Systematic Review. *J. Rheumatol.* 44, 388–396. doi:10.3899/jrheum.160452

Shuang Liang, D. Z., Qi, J., Song, X., and Jiang, X. (2018). Reduced Peak Stimulated Growth Hormone Is Associated with Hyperuricemia in Obese Children and Adolescents. *Sci. Rep.* 21, 7931. doi:10.1038/s41598-018-26276-w

Skwara, P., Schömig, E., and Gründemann, D. (2017). A Novel Mode of Operation of SLC22A11: Membrane Insertion of Estrone Sulfate versus Translocation of Uric Acid and Glutamate. *Biochem. Pharmacol.* 15, 74–82. doi:10.1016/j.bcp.2016.12.020

So, A., and Thorens, B. (2010). Uric Acid Transport and Disease. *J. Clin. Invest* 120, 1791–1799. doi:10.1172/JCI42344

Sonoda, H., Takase, H., Dohi, Y., and Kimura, G. (2011). Uric Acid Levels Predict Future Development of Chronic Kidney Disease. *Am. J. Nephrol.* 33, 352–357. doi:10.1159/000326848

Stamp, L. K., Chapman, P. T., and Palmer, S. C. (2016). Allopurinol and Kidney Function: An Update. *Joint Bone Spine* 83, 19–24. doi:10.1016/j.jbspin.2015.03.013

Stamp, L. K., and Dalbeth, N. (2019). Prevention and Treatment of Gout. *Nat. Rev. Rheumatol.* 15, 68–70. doi:10.1038/s41584-018-0149-7

Sun, P., Chen, M., Guo, X., Li, Z., Zhou, Y., Yu, S., et al. (2021). Combined Effect of Hypertension and Hyperuricemia on Ischemic Stroke in a Rural Chinese Population. *BMC Public Health* 21, 776. doi:10.1186/s12889-021-10858-x

Sutton Burke, E. M., Kelly, T. C., Shoales, L. A., and Nagel, A. K. (2020). Angiotensin Receptor Blockers Effect on Serum Uric Acid-A Class Effect? *J. Pharm. Pract.* 33, 874–881. doi:10.1177/0897190019866315

Swan, J. W., Walton, C., Godsland, I. F., Clark, A. L., Coats, A. J., and Oliver, M. F. (1994). Insulin Resistance in Chronic Heart Failure. *Eur. Heart J.* 15, 1528–1532. doi:10.1093/oxfordjournals.eurheartj.a060425

Tana, C., Ticinesi, A., Prati, B., Nouvenne, A., and Meschi, T. (2018). Uric Acid and Cognitive Function in Older Individuals. *Nutrients* 10, 975 doi:10.3390/nu10080975

Tian, X., Wang, A., Wu, S., Zuo, Y., Chen, S., Zhang, L., et al. (2021). Cumulative Serum Uric Acid and its Time Course Are Associated with Risk of Myocardial Infarction and All-Cause Mortality. *J Am Heart Assoc.*, e020180. doi:10.1161/JAHA.120.020180

Tom NijenhuisVallon, V., Annemietevan der Kemp, W. C. M., Johannes, L., Hoenderop, Joost. G. J., and Bindels, R. J. M. (2005). Enhanced Passive Ca2+ Reabsorption and Reduced Mg2+ Channel Abundance Explains Thiazide-Induced Hypocalciuria and Hypomagnesemia. *J. Clin. Invest* 115, 1651–1658. doi:10.1172/JCI24134

Tomita, M., Mizuno, S., Yamanaka, H., Hosoda, Y., Sakuma, K., Matuoka, Y., et al. (2000). Does Hyperuricemia Affect Mortality? A Prospective Cohort Study of Japanese Male Workers. *J. Epidemiol.* 10, 403–409. doi:10.2188/jea.10.403

Toyoda, Y., Takada, T., Saito, H., Hirata, H., Ota-Kontani, A., Kobayashi, N., et al. (2015). Inhibitory Effect of Citrus Flavonoids on the *In Vitro* Transport Activity of Human Urate Transporter 1 (URAT1/SLC22A12), a Renal Reabsorber of Urate. *Npj Sci. Food* 4, 1–4.

Tu, H. P., Chung, C. M., Min-Shan Ko, A., Lee, S. S., Lai, H. M., Lee, C. H., et al. (2016). Additive Composite ABCG2, SLC2A9 and SLC22A12 Scores of High-Risk Alleles with Alcohol Use Modulate Gout Risk. *J. Hum. Genet.* 61, 803–810. doi:10.1038/jhg.2016.57

Ugele, B., MarieSt-Pierre, V., and Pihusch, M. (2003). Andrew Bahn, Peer Hantschmann, Characterization and Identification of Steroid Sulfate Transporters of Human Placenta. *Am. J. Physiol. Endocrinol. Metab.* 284, E390–E398. doi:10.1152/ajpendo.00257.2002

Vallon, V., and Thomson, S. C. (2017). Targeting Renal Glucose Reabsorption to Treat Hyperglycaemia: the Pleiotropic Effects of SGLT2 Inhibition. *Diabetologia* 60, 215–225. doi:10.1007/s00125-016-4157-3

van der Harst, P., Bakker, S. J., de Boer, R. A., and Wolffenbuttel, B. H. (2010). Replication of the Five Novel Loci for Uric Acid Concentrations and Potential Mediating Mechanisms. *Hum. Mol. Genet.* 19, 387–395. doi:10.1093/hmg/ddp489

Vildhede, A., Kimoto, E., Rodrigues, A. D., and Varma, M. V. S. (2018). Quantification of Hepatic Organic Anion Transport Proteins OAT2 and OAT7 in Human Liver Tissue and Primary Hepatocytes. *Mol. Pharm.* 15, 3227–3235. doi:10.1021/acs.molpharmaceut.8b00320

Wang, X., Wen, X., and Kong, J. (2020). Recent Progress on Uric Acid Detection: A Review. *Crit. Rev. Anal Chem.* 50, 359–375. doi:10.1080/10408347.2019.1637711

Wang, Y., Viollet, B., Terkeltaub, R., and Liu-Bryan, R. (2016). AMP-activated Protein Kinase Suppresses Urate crystal-induced Inflammation and Transduces Colchicine Effects in Macrophages. *Ann. Rheum. Dis.* 75, 286–294. doi:10.1136/annrheumdis-2014-206074

Watanabe, S., Kang, D. H., Feng, L., Nakagawa, T., Kanellis, J., Lan, H., et al. (2002). Uric Acid, Hominoid Evolution, and the Pathogenesis of Salt-Sensitivity. *Hypertension* 40, 355–360. doi:10.1161/01.hyp.0000028589.66335.aa

Wen, C. C., Yee, S. W., Liang, X., Hoffmann, T. J., Kvale, M. N., Banda, Y., et al. (2015). Genome-wide Association Study Identifies ABCG2 (BCRP) as an Allopurinol Transporter and a Determinant of Drug Response. *Clin. Pharmacol. Ther.* 97, 518–525. doi:10.1002/cpt.89

Wen, S., Wang, D., Yu, H., Liu, M., Chen, Q., Bao, R., et al. (2020). The Time-Feature of Uric Acid Excretion in Hyperuricemia Mice Induced by Potassium Oxonate and Adenine. *Int. J. Mol. Sci.* 21. doi:10.3390/ijms21155178

Wright, D. F., Duffull, S. B., Merriman, T. R., Dalbeth, N., Barclay, M. L., and Stamp, L. K. (2016). Predicting Allopurinol Response in Patients with Gout. *Br. J. Clin. Pharmacol.* 81, 277–289. doi:10.1111/bcp.12799

Wright, D. F., Stamp, L. K., Merriman, T. R., Barclay, M. L., Duffull, S. B., and Holford, N. H. (2013). The Population Pharmacokinetics of Allopurinol and Oxypurinol in Patients with Gout. *Eur. J. Clin. Pharmacol.* 69, 1411–1421. doi:10.1007/s00228-013-1478-8

Wright, S. H., and Dantzler, W. H. (2004). Molecular and Cellular Physiology of Renal Organic Cation and Anion Transport. *Physiol. Rev.* 84, 987–1049. doi:10.1152/physrev.00040.2003

Xiao, Y., Yang, X., Liu, K., Jiao, X., Lin, X., Wang, Y., et al. (2018). Prevalence of Hyperuricemia Among the Chinese Population of the Southeast Coastal Region and Association with Single Nucleotide Polymorphisms in Urate-Anion Exchanger Genes: SLC22A12, ABCG2 and SLC2A9. *Mol. Med. Rep.* 18, 3050–3058. doi:10.3892/mmr.2018.9290

Xu, G., Bhatnagar, V., Wen, G., Hamilton, B. A., Eraly, S. A., and Nigam, S. K. (2005). Analyses of Coding Region Polymorphisms in Apical and Basolateral Human Organic Anion Transporter (OAT) Genes [OAT1 (NKT), OAT2, OAT3, OAT4, URAT (RST)]. *Kidney Int.* 68, 1491–1499. doi:10.1111/j.1523-1755.2005.00612.x

Yamasaki, Y., Ieiri, I., Kusuhara, H., Sasaki, T., Kimura, M., Tabuchi, H., et al. (2008). Pharmacogenetic Characterization of Sulfasalazine Disposition Based on NAT2 and ABCG2 (BCRP) Gene Polymorphisms in Humans. *Clin. Pharmacol. Ther.* 84, 95–103. doi:10.1038/sj.clpt.6100459

Yang, X., Xiao, Y., Liu, K., and Jiao, X. (2018). Prevalence of Hyperuricemia Among the Chinese Population of the Southeast Coastal Region and Association with Single Nucleotide Polymorphisms in Urate-Anion Exchanger Genes: SLC22A12, ABCG2 and SLC2A9. *Mol. Med. Rep.* 18, 3050–3058. doi:10.3892/mmr.2018.9290

Yano, H., Tamura, Y., Kobayashi, K., Tanemoto, M., and Uchida, S. (2014). Uric Acid Transporter ABCG2 Is Increased in the Intestine of the 5/6 Nephrectomy Rat Model of Chronic Kidney Disease. *Clin. Exp. Nephrol.* 18, 50–55. doi:10.1007/s10157-013-0806-8

Ye, B. S., Lee, W. W., Ham, J. H., Lee, J. J., Lee, P. H., and Sohn, Y. H. (2016). Does Serum Uric Acid Act as a Modulator of Cerebrospinal Fluid Alzheimer's Disease Biomarker Related Cognitive Decline? *Eur. J. Neurol.* 23, 948–957. doi:10.1111/ene.12969

Yu, Z., Kan, R., Wu, S., Guo, H., Zhao, W., Ding, L., et al. (2021). Xanthine Oxidase Inhibitory Peptides Derived from Tuna Protein: Virtual Screening, Inhibitory Activity, and Molecular Mechanisms. *J. Sci. Food Agric.* 101, 1349–1354. doi:10.1002/jsfa.10745

Yue, D., Tong, Z., Ai, W., Zalloum, W. A., Kang, D., Wu, T., et al. (2019). Novel Urate Transporter 1 (URAT1) Inhibitors: a Review of Recent Patent Literature (2016–2019). *Expert Opin. Ther. Pat* 29, 871–879. doi:10.1080/13543776.2019.1676727

Yun-Hong Lu, Y.-P. C., Li, T., Han, F., Li, C-J., Li, X-Y., Xue, M., et al. (2020). Empagliflozin Attenuates Hyperuricemia by Upregulation of ABCG2 via AMPK/AKT/CREB Signaling Pathway in Type 2 Diabetic Mice. *Int. J. Biol. Sci.* 16, 529–542. doi:10.7150/ijbs.33007

Zhang, B., Dai, X., Bao, Z., Mao, Q., Duan, Y., Yang, Y., et al. (2019). Targeting the Subpocket in Xanthine Oxidase: Design, Synthesis, and Biological Evaluation of 2-[4-Alkoxy-3-(1h-Tetrazol-1-Yl) Phenyl]-6-Oxo-1,6-Dihydropyrimidine-5-Carboxylic Acid Derivatives. *Eur. J. Med. Chem.* 181, 11159. doi:10.1016/j.ejmech.2019.07.062

Zhang, J., Zhen, Y-f., Pu-Bu-Ci-RenSong, L-g., Kong, W-n., Shao, T-m., et al. (2013). Salidroside Attenuates Beta Amyloid-Induced Cognitive Deficits via Modulating Oxidative Stress and Inflammatory Mediators in Rat hippocampus. *Behav. Brain Res.* 244, 70–81. doi:10.1016/j.bbr.2013.01.037

Zhang, L., Huang, S-M., Reynolds, K., Madabushi, R., and Zineh, I. (2018). Transporters in Drug Development: Scientific and Regulatory Considerations. *Clin. Pharmacol. Ther.* 104, 793–796. doi:10.1002/cpt.1214

Zhang, X., Nie, Q., Zhang, Z., Zhao, J., Zhang, F., Wang, C., et al. (2021). Resveratrol Affects the Expression of Uric Acid Transporter by Improving Inflammation. *Mol. Med. Rep.* 24. doi:10.3892/mmr.2021.12203

Zhang, Y., Neogi, T., Chen, C., Chaisson, C., Hunter, D. J., and Choi, H. (2014). Low-dose Aspirin Use and Recurrent Gout Attacks. *Ann. Rheum. Dis.* 73, 385–390. doi:10.1136/annrheumdis-2012-202589

Zhou, F., Zhu, L., Cui, P. H., Church, W. B., and Murray, M. (2010). Functional Characterization of Nonsynonymous Single Nucleotide Polymorphisms in the Human Organic Anion Transporter 4 (hOAT4). *Br. J Pharmacol* 159, 419–427. doi:10.1111/j.1476-5381.2009.00545.x

Zhu, C., Sun, Bao., Zhang, B., and Zhou, Z. (2021). An Update of Genetics, Co-morbidities and Management of Hyperuricemia. *Clin. Exp. Pharmacol. Physiol.*

Zhu, Y., Pandya, B. J., and Choi, H. K. (2011). Prevalence of Gout and Hyperuricemia in the US General Population: the National Health and Nutrition Examination Survey 2007-2008. *Arthritis Rheum.* 63, 3136–3141. doi:10.1002/art.30520

# Modified Huangqi Chifeng Decoction Attenuates Proteinuria by Reducing Podocyte Injury in a Rat Model of Immunoglobulin a Nephropathy

Meiying Chang[1†], Bin Yang[2†], Liusheng Li[1], Yuan Si[1], Mingming Zhao[1], Wei Hao[3], Jinning Zhao[3] and Yu Zhang[1]*

[1]Department of Nephrology, Xiyuan Hospital, China Academy of Chinese Medical Sciences, Beijing, China, [2]Department of Pathology, Xiyuan Hospital, China Academy of Chinese Medical Sciences, Beijing, China, [3]Medical Animal Experimental Center, Xiyuan Hospital, China Academy of Chinese Medical Sciences, Beijing, China

Modified Huangqi Chifeng decoction (MHCD) has been used to reduce proteinuria in immunoglobulin A nephropathy (IgAN) for many years. Previously, we have demonstrated its protective role in glomerular mesangial cells. Podocyte injury, another key factor associated with proteinuria in IgAN, has also attracted increasing attention. However, whether MHCD can reduce proteinuria by protecting podocytes remains unclear. The present study aimed to investigate the protective effects of MHCD against podocyte injury in a rat model of IgAN. To establish the IgAN model, rats were administered bovine serum albumin, carbon tetrachloride, and lipopolysaccharide. MHCD in three doses or telmisartan was administered once daily for 8 weeks ($n$ = 10 rats/group). Rats with IgAN developed proteinuria at week 6, which worsened over time until drug intervention. After drug intervention, MHCD reduced proteinuria and had no effect on liver and kidney function. Furthermore, MHCD alleviated renal pathological lesions, hyperplasia of mesangial cells, mesangial matrix expansion, and podocyte foot process fusion. Western blot analysis revealed that MHCD increased the expression of the podocyte-associated proteins nephrin and podocalyxin. Additionally, we stained podocyte nuclei with an antibody for Wilms' tumor protein one and found that MHCD increased the podocyte number in rats with IgAN. In conclusion, these results demonstrate that MHCD attenuates proteinuria by reducing podocyte injury.

Keywords: modified huangqi chifeng decoction, IgA nephropathy, podocyte injury, nephrin, podocalyxin

## INTRODUCTION

Immunoglobulin A (IgA) nephropathy (IgAN) is a glomerular disease characterized by IgA deposition in the mesangial region. Its clinical manifestations include proteinuria, hematuria, acute kidney injury, hypertriglyceridemia, and hypertension. IgAN is the main cause of end-stage renal disease in patients with primary glomerular disease in China (Yang et al., 2020). Although clinical manifestations vary, the majority of patients with IgAN exhibit progressive symptoms, with progression to end-stage renal disease within 10 years after diagnosis in 10–30% of cases (Liu et al., 2018). While progression is driven by podocyte injury and depletion (Hishiki et al., 2001; Lemley et al., 2002; Tomino, 2007; Xu et al., 2010), podocyte injury alone is the dominant cause (Menon et al.,

2013; Liu et al., 2018). Therefore, the mechanism by which podocyte injury contributes to IgAN warrants investigation and might provide a basis for therapeutic strategies to delay progression.

Glomerular podocytes, highly specialized epithelial cells, together with the glomerular basement membrane, play an important role in glomerular filtration (Asao et al., 2012). Podocytes stabilize the glomerular architecture against the distention of the glomerular basement membrane by providing a large filtration surface through the slit diaphragm structure. In addition to the crucial interaction between podocyte foot extensions controlling glomerular filtration, certain proteins (i.e., nephrin, podocin, and podocalyxin) involved in the maintenance of the structural and functional integrity of the filtration barrier in the kidney have been identified (Mundel and Shankland, 2002; Asao et al., 2012; Akankwasa et al., 2018). Podocalyxin is present on the apical aspects of podocytes and offers structural support to the capillary loop, and nephrin is expressed on the lateral aspect extending into the slit diaphragm and impedes the filtration of large molecules into the urinary space (Akankwasa et al., 2018). Changes in the expression and distribution of nephrin precede and can cause foot process fusion and proteinuria (Lu et al., 2013). The role of podocytes in IgAN requires further investigation.

Several traditional Chinese medicines have been used for the treatment of IgAN, and their effects have been ascertained by clinical and animal experiments (Yang et al., 2018; Bai et al., 2019a; Deng et al., 2019; Li et al., 2020a; Li et al., 2020b). Modified Huangqi Chifeng decoction (MHCD), a compound formula in traditional Chinese medicine, comprises seven herbs: *Astragalus membranaceus* Bge, *Euryale ferox* Salish, *Rosae Laevigatae* Fructus, *Radix Paeoniae* Rubra, *Saposhnikoviae* Radix, *Rhizoma Dioscoreae* Nipponicae, *Hedyotis Diffusae* Herba. MHCD has been shown to alleviate proteinuria in patients with IgAN in single-case-control and real-world studies (Jiao and Zhang, 2018; Yu and Zhang, 2018). Furthermore, MHCD protects against renal fibrosis and podocyte injury in a rat model induced by doxorubicin or in mesangial cells induced by lipopolysaccharide (LPS) (Gao et al., 2016; Jiao and Li, 2016; Liu and Li, 2016; Yu et al., 2018). However, only a few studies have focused on podocyte protection using traditional Chinese medicine in rats with IgAN. In this study, we investigated the protective effects of MHCD on podocytes in rats with IgAN, and analyzed the molecular and cellular mechanisms underlying these effects.

## MATERIALS AND METHODS

### Chemicals and Reagents

MHCD comprises seven herbs: 30 g Sheng Huangqi (Astragalus membranaceus Bge), 20 g Qian Shi (Euryale ferox Salish), 10 g Jin Ying-zi (Rosae Laevigatae Fructus), 10 g Chi Shao (Radix Paeoniae Rubra), 10 g Fang Feng (Saposhnikoviae Radix), 20 g Chuan Shan-long (Rhizoma Dioscoreae Nipponicae), and 20 g Bai Hua-she-she-cao (Hedyotis Diffusae Herba). The herbs were purchased from the Xiyuan Hospital of the China Academy of
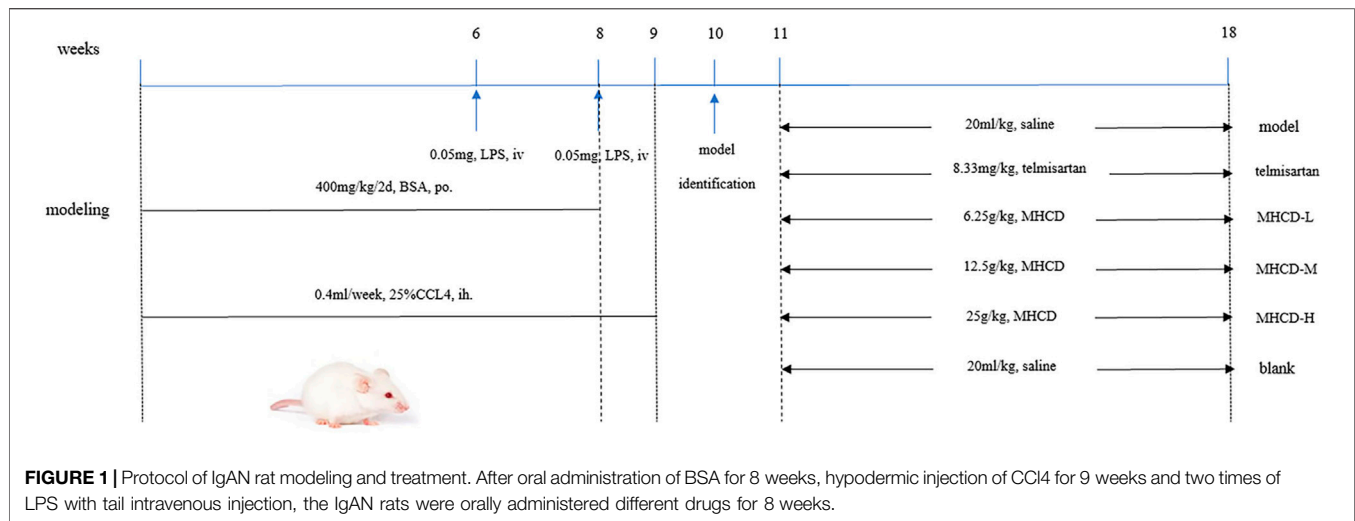
Chinese Medical Sciences. The herbs were initially soaked in water for 1 h and then boiled twice for 30 min each time. The liquid was sealed, vacuum dried, and stored in a glass bottle in a refrigerator at 4°C until use. Telmisartan (Micardis; 80 mg/pill) was purchased from Boehringer Ingelheim International GmbH (Ingelheim am Rhein, Germany). Bovine serum albumin (BSA), LPS, and carbon tetrachloride (CCl4) were purchased from Sigma-Aldrich (St. Louis, MO, United States).

The primary antibodies and Alexa Fluor 488-labeled goat anti-rabbit IgG secondary antibodies (No. ZA-0446 and ZF-0511, respectively) for immunofluorescence assays were purchased from ZSGB Biotechnology Co., Ltd. (Beijing, China). The periodic acid Schiff (PAS) Stain Kit was purchased from X-Y Biotechnology (No. XY7640; Shanghai, China). The Masson's Trichrome Stain Kit was purchased from Solarbio (Beijing, China). The primary antibody for Wilms' tumor protein 1 (WT1) was purchased from Novus (No. NBP2-44606; St. Charles, MO, United States). The anti-mouse/rabbit IgG secondary antibodies were purchased from ZSGB-BIO (No. PV-6000; Beijing, China). The primary antibodies for nephrin and podocalyxin (No. A3048 and A10200, respectively) for western blot analysis were obtained from Abclonal Technology (Wuhan, China). Goat anti-rabbit IgG-HRP was obtained from Jackson ImmunoResearch (No. 111-035-003; West Grove, PA, United States). RIPA lysis buffer and the BCA Assay Kit (No. R0010 and PC0020, respectively) were purchased from Solarbio.

### Animal Groups and Treatments

Sixty-six 3–5-week-old male Sprague–Dawley rats, weighing 150 ± 10 g, were purchased from Beijing Vital River Laboratory Animal Technology Co., Ltd. (Beijing, China). Animal welfare and experimental procedures were performed in strict accordance with the guidelines of the Animal Ethics Committee of Xiyuan Hospital of China Academy of Chinese Medical Sciences. Animals were housed in humidity-controlled rooms (60 ± 10%) at 24 ± 1°C with a 12 h light/dark cycle and free access to standard food and tap water. All rats were housed in metabolic cages and acclimated to laboratory conditions for 7 days, after which they were randomly divided into either the blank (n = 13) or model (n = 53) group.

The rat IgAN model was established by administering BSA, LPS, and CCl4 according to previously described methods (Peng et al., 2013; Zhang et al., 2014; Liu et al., 2018), with slight modifications (**Figure 1**). In brief, the immunogen BSA was intragastrically administered at 400 mg/kg once every 2 days for eight consecutive weeks, and 0.1 ml CCl4 dissolved in 0.3 ml castor oil was subcutaneously administered weekly for 9 weeks. During weeks 6 and 8, LPS (0.05 mg) was injected through the tail vein. Rats in the blank group were intragastrically administered an equal volume of distilled water and were administered equal amounts of physiological saline through tail vein injection (to match the LPS injection) and via the subcutaneous route (CCl₄). The methods for administration were the same as those used in the model group. At week 10, three rats from both the blank and model groups were used for model validation. After verifying successful model establishment, the blank group was maintained (n = 10), and rats in the model group

**FIGURE 1 |** Protocol of IgAN rat modeling and treatment. After oral administration of BSA for 8 weeks, hypodermic injection of CCl4 for 9 weeks and two times of LPS with tail intravenous injection, the IgAN rats were orally administered different drugs for 8 weeks.

**TABLE 1 |** Semiquantitative standard for IgA deposition.

| Immunofluorescence deposition under light microscope | Immunofluorescence intensity of IgA |
|---|---|
| No fluorescence under low-power lens but seemingly visible under high-power lens | − |
| Fluorescence appears to be visible under low-power lens and can be seen with high-power lens | + |
| Fluorescence can be seen under low-power lens and can be clearly seen under high-power lens | + + |
| Fluorescence can be clearly seen under low-power lens and is strong under high-power lens | + + + |
| Fluorescence is strong under low-power lens and very strong under high-power lens | + + + + |

($n$ = 50) were randomly divided into the following five groups: model group, telmisartan group, MHCD-H group, MHCD-M group, and MHCD-L group ($n$ = 10 rats/group). The corresponding drug intervention for each group was initiated at week 11. Rats in the telmisartan group were intragastrically administered telmisartan at a dose of 8.33 mg/kg/d. Rats in the MHCD-H, MHCD-M, and MHCD-L groups were intragastrically administered MHCD at 25, 12.5, and 6.25 g/kg/d, respectively, for 8 weeks until the end of week 18. The blank and model groups received equal volumes of normal saline. All drugs were diluted with distilled water, and the dosages were evaluated by body surface coefficient conversion between humans and rats.

## Sample Collection and Preparation

Urine was collected from rats in metabolic cages to determine 24 h proteinuria levels. Urine was collected once every 2 weeks. After the last intragastric administration at week 18, the rats were anesthetized with 3% chloral hydrate and the blood was obtained from the abdominal aorta to determine the levels of albumin, serum creatinine, blood urea nitrogen, alanine transaminase, and aspartate transaminase, using an automatic biochemical analyzer. After blood was drawn from the abdominal aorta, the kidney was rapidly harvested. A part of the renal cortex was placed in 10% formalin fixative solution for optical microscopy and immunohistochemical detection, a portion was fixed in 20% glutaraldehyde solution for electron microscopy and

subsequent immunofluorescence detection, and a portion was stored at −70°C for western blot analysis.

## Immunofluorescence Intensity of Immunoglobulin A

As demonstrated in **Table 1**, immunofluorescence intensity was determined using the standard five-point semi-quantitative method. At least ten glomeruli (magnification, ×400) were observed in each section. They were scored according to the intensity of microscopic expression in each glomerulus.

## Histopathological Analysis

Sections of cortical tissues were fixed in 10% buffered formalin at room temperature for 48 h, embedded in paraffin, and sliced to 4 μm-thick sections. The sections were stained at room temperature with hematoxylin-eosin (HE) for 3 min, followed by hydrochloric acid and alcohol for differentiation, and a graded series of alcohol and xylene dehydration. Sections were sealed, and PAS and Masson's trichrome staining were performed according to the kit instructions. Photomicrographs of HE-, PAS-, and Masson's trichrome-stained sections were obtained under a light microscope (magnification, ×200).

## Immunohistochemistry Assay

Podocyte counts can be obtained based on the expression of WT1 in glomeruli. The paraffin sections were first dewaxed with xylene
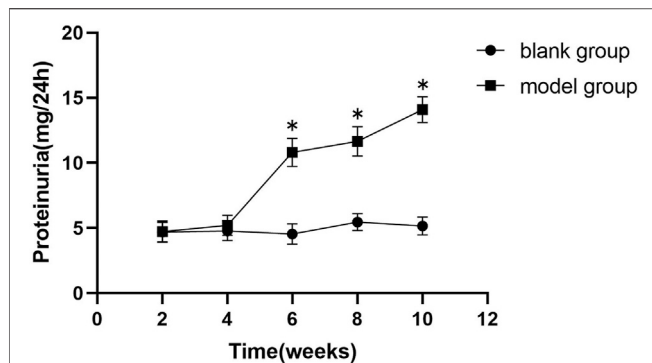
**FIGURE 2 |** The 24 h proteinuria of the model group rats increases significantly from the week 6 of the experiment. Data are expressed as means ± standard deviation (SD). *$p < 0.01$ vs. blank group.

and a graded series of alcohol. After using sodium citrate for antigen retrieval, endogenous peroxidase was quenched with 3% hydrogen peroxide, and the sections were incubated with the WT1 antibody (1:100) overnight at 4°C. The sections were incubated with PV-6000 for 30 min at room temperature, followed by hematoxylin redyeing, gradient alcohol dehydration, and neutral gum sealing. Finally, under a light microscope, brown-yellow particles in the nucleus indicated positive expression. Five non-overlapping fields were randomly observed under a microscope (magnification, ×400); positive cells in each field were counted with Image-Pro Plus 6.0 analysis software, and the average value was obtained.

## Electron Microscopy

Renal cortical tissue was fixed in 2.5% glutaraldehyde at 4°C for 24 h, washed with phosphate-buffered saline, and sliced to a thickness of 70–90 nm. After staining with osmium tetroxide and lead citrate at room temperature for 5–10 min, changes in the podocyte foot process and its fine structure were observed under a Hitachi H-600 transmission electron microscope (magnification, ×8,200 and ×16,500; Hitachi, Ltd., Tokyo, Japan).

## Western Blot Analysis

Total protein was extracted from approximately 30 g of kidney tissue with RIPA buffer containing PMSF. The protein concentration was measured using a BCA kit. Proteins were separated using 8–10% gradient SDS-PAGE and then transferred to a PVDF membrane. The membrane was then incubated with primary antibodies against nephrin (1:2000) and podocalyxin (1:2000) overnight at 4°C after blocking with TBST containing 5% skim milk. After incubation with secondary antibodies for 1 h, membranes were treated with ECL chemiluminescence reagents. ImageJ 4.0 was used to analyze the grayscale values for each group, and β-actin was used as the internal reference protein.

## Statistical Analysis

All values are expressed as means ± standard deviation (SD). One-way ANOVA for multiple comparisons was used to analyze

differences among groups. The Kruskal–Wallis test was used for comparisons of fluorescence intensity data. Statistical analyses were performed using GraphPad Prism (version 8.0) and SPSS (version 20.0). The threshold for statistical significance was set at $p < 0.05$.

## RESULTS

### General Condition of Rats in Each Group

After each subcutaneous injection of $CCl_4$, rats in the model group exhibited reduced activity and listlessness, with gradual recovery beginning the next day. After the injection of LPS during week 6, rats in the model group exhibited a reduction in food intake, messy hair, and listlessness, which typically returned to normal in approximately 6 days. Rats in the blank group exhibited free movement, a normal diet, and smooth body hair.

### Modified Huangqi Chifeng Decoction Ameliorates Proteinuria

As demonstrated in **Figure 2** and **Figure 3**, proteinuria in the model group began to increase at week six and worsened over time until drug intervention. After drug intervention, 24 h proteinuria was lower in rats in the telmisartan and MHCD groups than in those in the model group (both $p < 0.01$). Compared to the telmisartan group, all MHCD groups showed reduced 24 h proteinuria (all $p < 0.01$). Rats in the MHCD-H group showed significantly lower 24 h proteinuria than those in the MHCD-L group ($p < 0.05$), indicating that MHCD ameliorates proteinuria in rats with IgAN.

### Modified Huangqi Chifeng Decoction Does Not Alter Certain Biochemical Measurements of Liver and Kidney Function

Besides efficacy, we evaluated the safety indexes in rats. The results showed no significant differences in five biochemical
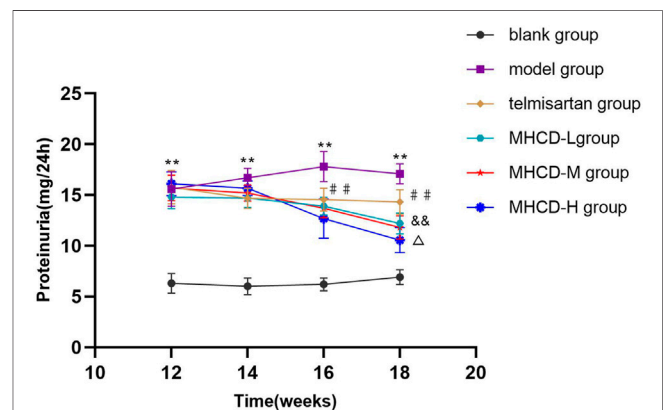


**FIGURE 3 |** MHCD ameliorates proteinuria over time. Data are expressed as means ± SD ($n = 10$). **$p < 0.01$ vs. blank group; # #$p < 0.01$ vs. model group; &&$p < 0.01$ vs. Telmisartan group;△$p < 0.05$ vs. MHCD-L group. MHCD, modified Huangqi Chifeng decoction.
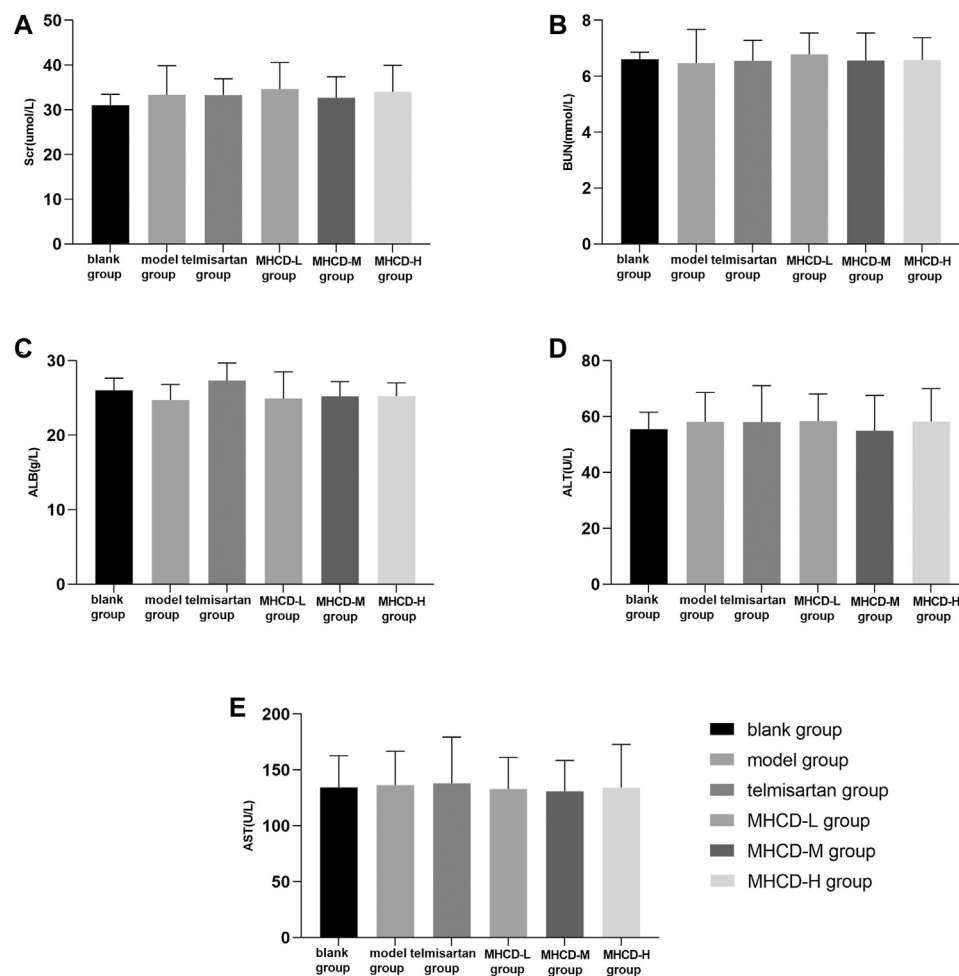
**FIGURE 4 |** MHCD does not alter certain biochemical measurements of liver and kidney function while ameliorating proteinuria. Data are expressed as means ± SD (*n* = 10). Scr, serum creatinine; BUN, blood urea nitrogen; ALB, albumin; ALT, alanine transaminase; AST, aspartate transaminase.

parameters between rats in the blank group and those in the other groups (all *p* > 0.05; **Figure 4**). These results further support the application of MHCD.

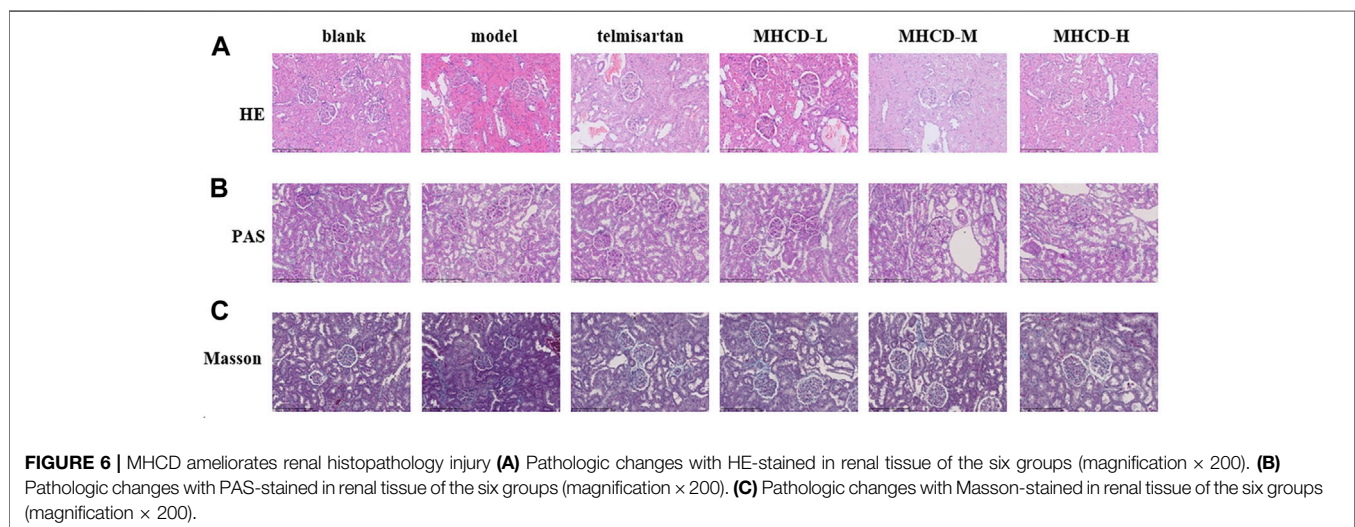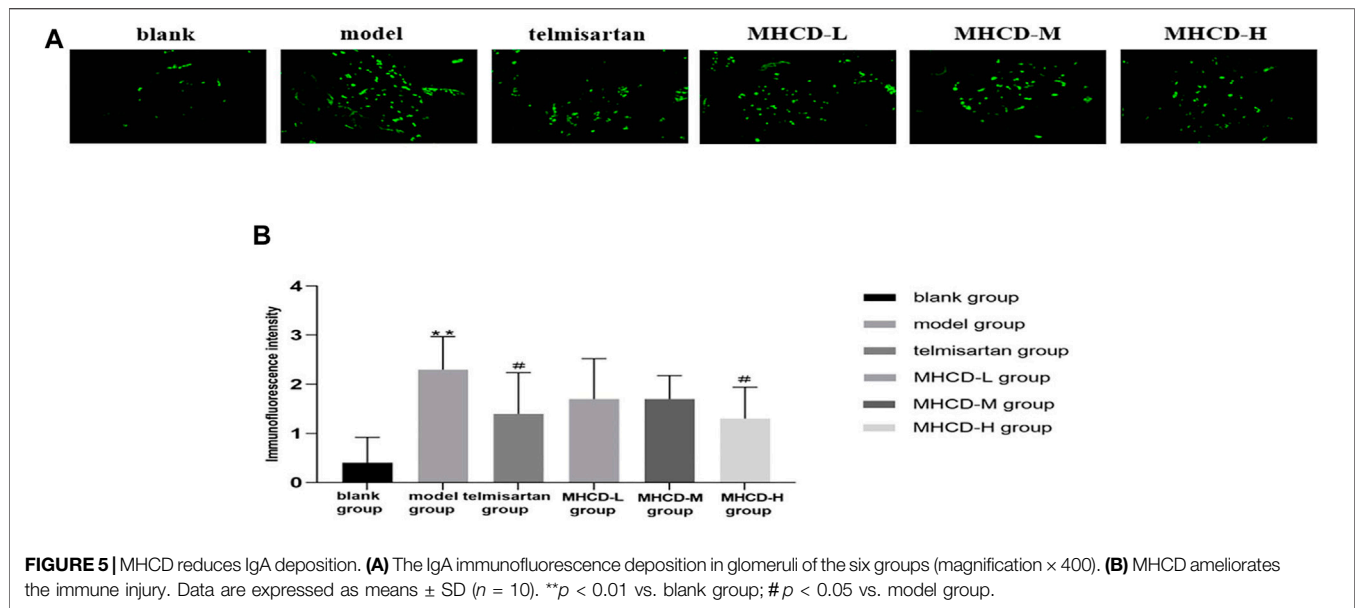## Modified Huangqi Chifeng Decoction Reduces Immunoglobulin A Deposition

IgA immunofluorescence was nearly undetectable in the glomeruli of rats in the blank group. In the model rats, IgA was strongly expressed in the glomerular mesangium. Rats in the telmisartan group showed lower IgA immunofluorescence than those in the model group (**Figure 5A**). After drug intervention, IgA deposition was significantly lower in rats in the telmisartan and MHCD-H groups than in those in the model group (both *p* < 0.05; **Figure 5B**). These results suggest that MHCD alleviates immune injury in rats with IgAN.

## Modified Huangqi Chifeng Decoction Ameliorates Renal Histopathology Injury

Renal pathological changes were examined by HE, PAS, and Masson's trichrome staining (**Figure 6**). Compared to the blank group, the model group had a greater number of proliferative mesangial cells, increased extracellular matrix deposition, a thickened glomerular basement membrane, and disordered tubular cells. Telmisartan and MHCD treatments ameliorated the renal pathological lesions in rats with IgAN. These results demonstrate the protective effect of MHCD on the kidneys of rats with IgAN.

As determined by electron microscopy (**Figure 7A**, ×8,200), the foot process and basement membrane of rats in the blank group exhibited a normal morphology; the podocyte foot processes were arranged in an orderly manner and were uniform in size. Podocytes in model group rats were flattened or fused, along with a thickened basement membrane and an increased number of proliferating

FIGURE 5 | MHCD reduces IgA deposition. (A) The IgA immunofluorescence deposition in glomeruli of the six groups (magnification × 400). (B) MHCD ameliorates the immune injury. Data are expressed as means ± SD ($n = 10$). **$p < 0.01$ vs. blank group; # $p < 0.05$ vs. model group.



FIGURE 6 | MHCD ameliorates renal histopathology injury (A) Pathologic changes with HE-stained in renal tissue of the six groups (magnification × 200). (B) Pathologic changes with PAS-stained in renal tissue of the six groups (magnification × 200). (C) Pathologic changes with Masson-stained in renal tissue of the six groups (magnification × 200).

mesangial cells. The degree of fusion of podocyte foot processes in rats in all MHCD groups was lower than that in those in the model group, to various extents.

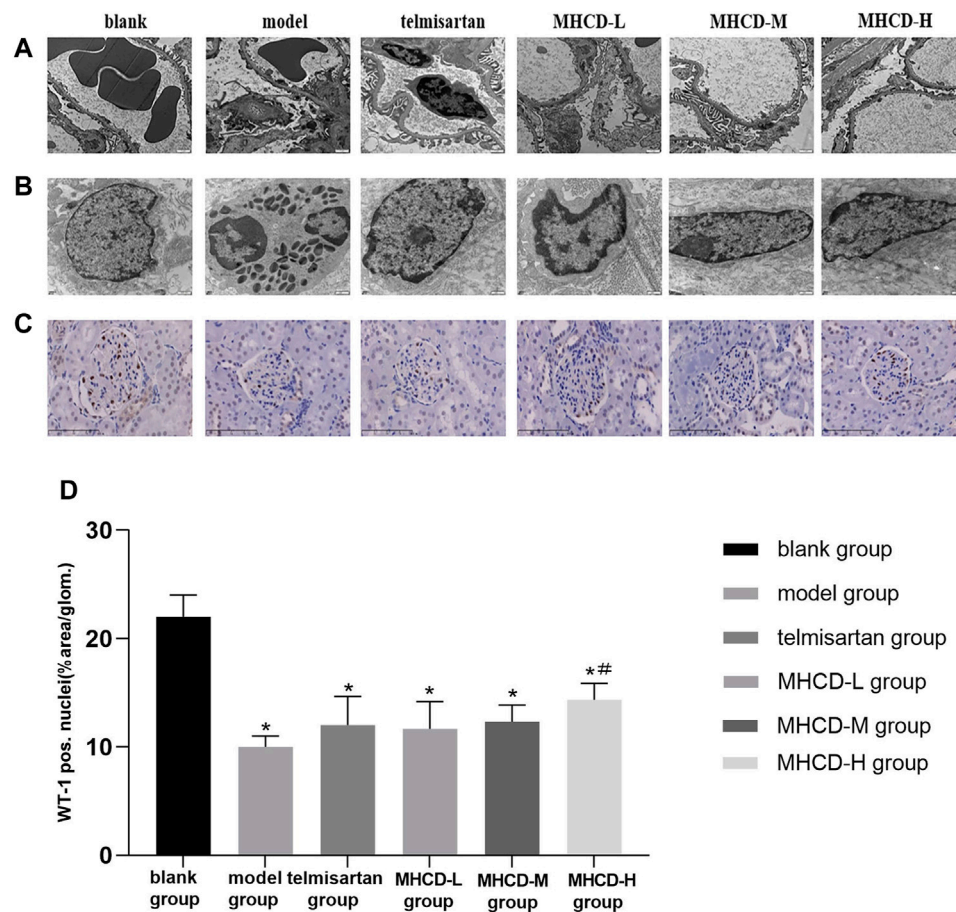## Modified Huangqi Chifeng Decoction Protects Against Podocyte Injury

Changes in the fine structure of the foot process were observed via electron microscopy (**Figure 7B**; ×16,500). The podocyte cell body in rats in the blank group was typical, with a high number of organelles, clear nucleoli, smooth and complete nuclear membrane edges, fine chromatin, and a uniform distribution in the nuclei. In model group rats, podocytes shrank substantially, intracytoplasmic organelles decreased, and chromatin agglomeration and nuclear fragmentation were detected. Atrophy of podocytes was reduced, and the number of

intracytoplasmic organelles was higher in rats in the MHCD groups than in those in the model group.

WT1 immunohistochemistry was used to evaluate the morphological state of podocytes and to stain nuclei (**Figure 7C**). After drug intervention, the number of WT1-positive podocytes was significantly higher in rats in MHCD-H than in those in the model group ($p < 0.05$; **Figure 7D**). These results further support the protective effect of MHCD on the podocytes of rats with IgAN.

## Modified Huangqi Chifeng Decoction Increases the Expression of Podocyte-Associated Proteins

To further investigate the molecular mechanism by which MHCD affects podocytes in rats with IgAN, the levels of the podocyte-associated proteins nephrin and podocalyxin were evaluated.

**FIGURE 7 |** MHCD protects against podocyte injury. **(A)** The foot process and basement membrane were observed under electron microscopy (magnification × 8,200). **(B)** Changes in the fine structure of the foot process were observed under electron microscopy (magnification × 16,500). **(C)** WT1 immunohistochemistry of the six groups (magnification × 400). **(D)** Average percent staining area and WT1-positive podocytes per glomerulum in the IgAN rat model obtained using Image-Pro Plus 6.0 analysis software. Data are expressed as means ± SD ($n = 3$). *$p < 0.05$ vs. blank group; #$p < 0.05$ vs. model group. **(E–G)** Protein levels of nephrin and podocalyxin in the six groups. For relative quantification of proteins, β-actin was used as an internal control. The relative expression of proteins was calculated using Image J. Data are expressed as means ± SD ($n = 3$). ***$p < 0.01$ vs. blank group; # #$p < 0.01$ vs. model group; &&$p < 0.01$ vs. Telmisartan group; ▲▲$p < 0.01$ vs. MHCD-L group; ※$p < 0.05$ vs. MHCD-M group; *$p < 0.05$ vs. telmisartan group.

Nephrin levels were significantly lower in rats in the model group than in those in the blank group ($p < 0.01$), but were higher in rats in the MHCD-H group than in those in the model group ($p < 0.01$; **Figures 7E, F**). Furthermore, nephrin levels were significantly higher in rats in the MHCD-H group than in those in all other groups (all $p < 0.05$). Podocalyxin levels were also significantly lower in rats in the model group than in those in the blank group ($p < 0.01$), but were higher in rats in the MHCD-H group than in those in the model group ($p < 0.01$; **Figures 7E, G**). Podocalyxin levels were significantly higher in rats in the MHCD-H group than in those in all other groups (all $p < 0.05$).

## DISCUSSION

IgA nephropathy is the most common glomerulonephritis worldwide. According to the 2012 KDIGO clinical practice

guideline, we recommend long-term angiotensin-converting enzyme inhibitor (ACE-I) or angiotensin receptor blocker (ARB) treatment when proteinuria is > 1 g/d, with up-titration of the drug depending on blood pressure (Beck et al., 2013). It has been reported that angiotensin II (AngII) plays an important role in the injury of podocytes. AngII can lead to the reorganization of actin cytoskeleton and induction of podocyte apoptosis (Ren et al., 2012; Wang et al., 2016). In addition, some studies have confirmed the protective effect of telmisartan on podocytes (Villa et al., 2011; Fukami et al., 2013). Therefore, telmisartan, as a commonly used drug ARB, was selected as the positive control in this study. For patients with persistent proteinuria of ≥1 g/d, despite 3–6 months of optimized supportive care (including ACE-I or ARBs and blood pressure control), and GFR of >50 ml/min per 1.73 m$^2$, according to the 2012 KDIGO clinical practice guideline, we recommend a 6-months course of corticosteroid therapy (Beck et al., 2013).
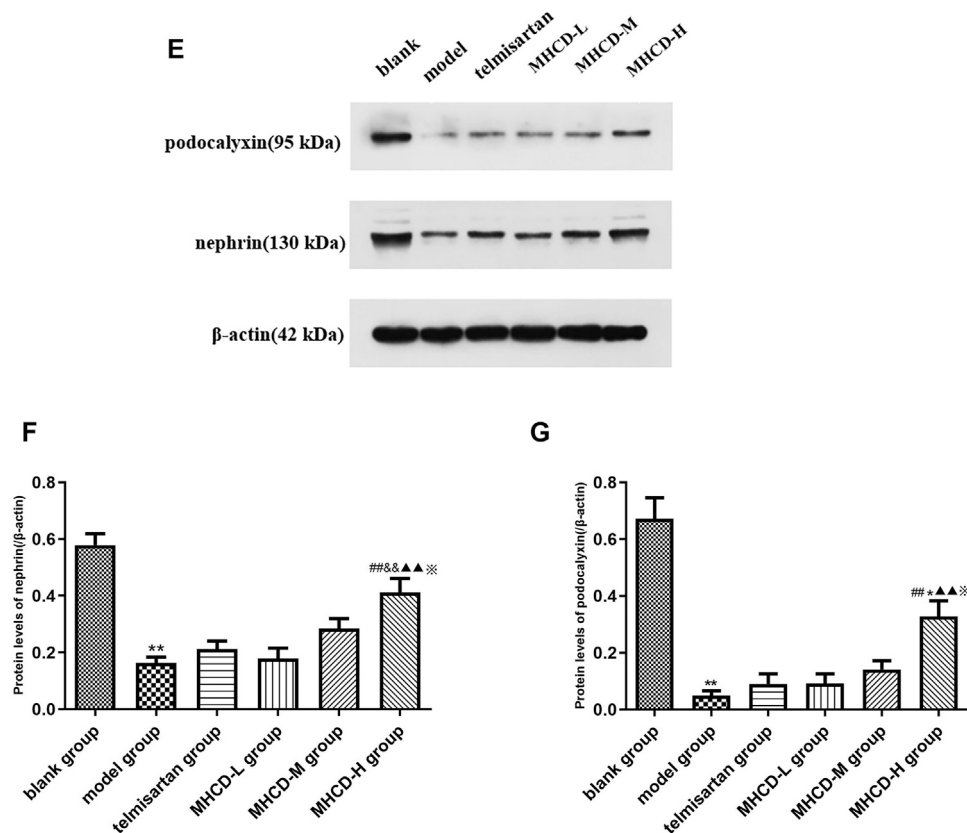
FIGURE 7 | (Continued).

However, the role of immunosuppression in the management of IgA nephropathy remains highly controversial. The STOP-IgAN and TESTING trials were terminated due to adverse events (Lv et al., 2017; O'Shaughnessy and Lafayette, 2017). Therefore, it is of social significance and scientific value to seek new treatment methods.

In China, traditional Chinese medicines (TCMs) have an extensive history of application, and there is substantial literature on the treatment of IgAN with TCM. Furthermore, various TCM extracts or formulae have been demonstrated to have renal-protective effect (Li et al., 2017; Yang et al., 2018; Bai et al., 2019a; Bai et al., 2019b; Li et al., 2020a; Li et al., 2020b; Li et al., 2020c; Li and Li, 2020). Modified Huangqi Chifeng decoction, a compound formula in TCM, has been used to treat IgAN for several years. The results of this study clearly demonstrate the protective effect of MHCD on glomerular podocytes.

Proteinuria is one of the main clinical symptoms of IgAN. As expected, rats in the model group exhibited a marked increase in proteinuria at the start of week 6, which gradually increased thereafter. Proteinuria in rats in the MHCD and telmisartan groups started to decline from week 14. Modified Huangqi Chifeng decoction, especially at a high dose, attenuated proteinuria and did not alter biochemical parameters of liver and kidney functions in rats.

Histological changes, including mesangial cell proliferation, increased mesangial matrix, tubulointerstitial inflammation, fibrosis, and podocyte fusion, were also observed in the present study, which is consistent with previous findings (Coppo, 2017; Coppo, 2019). After MHCD intervention, pathological damage to kidney tissues was relieved to various degrees, as evidenced by light microscopy, and the IgA deposition in MHCD-H-treated rats in the mesangial region of the glomeruli was also reduced, as evidenced by immunofluorescence microscopy. Under electron microscopy, compared to that in rats in the model group, the extent of podocyte foot process fusion in rats in all MHCD groups was reduced to various degrees, podocyte atrophy was alleviated, and the number of intracytoplasmic organelles was increased. In addition, MHCD increased the expression of the podocyte-associated proteins nephrin and podocalyxin and increased the number of podocytes in rats with IgAN.

Proteinuria is an early consequence of podocyte injury and a typical sign of kidney disease (Nagata, 2016). Endothelial cells of glomerular capillaries, the surrounding podocytes, and the fused extracellular matrix form the glomerular filtration barrier (Scott and Quaggin, 2015). Structurally, podocytes serve as the last gatekeepers in the glomerular filtration barrier. The foot processes of podocytes contain an actin-based cytoskeleton linked to the glomerular basement

membrane (Reiser et al., 2000). The foot processes of podocytes form a highly-branched interdigitating network with the foot processes of neighboring podocytes. Slit diaphragm bridges the filtration slits between opposing podocyte foot processes, thereby forming the final barrier to urinary protein loss (Leung et al., 2018). Haraldsson *et al.* also pointed out that highly differentiated and specialized podocytes are of utmost importance for an intact barrier (Haraldsson et al., 2008). Podocyte foot processes are maintained by the actin cytoskeletal system, and nephrin and podocalyxin lead to loss of the foot process, which is closely associated with proteinuria (Nagata, 2016; Akankwasa et al., 2018).

Podocyte stress and adaptation observed in podocytopathies manifest as alterations in the podocyte charge or shape, an active process resulting from the rearrangement of the actin cytoskeleton preceding podocyturia (i.e., the shedding of viable podocytes in urine) (Carney, 2013; Kriz et al., 2013; Nagata, 2016). Podocyte injury is used as a clinical prognostic index for glomerular diseases (Asanuma and Mundel, 2003; Xu et al., 2010; Jiang et al., 2012; Chen et al., 2017). Lu *et al.* found that the expression of nephrin in rats with IgAN increases at an early timepoint and decreases thereafter, suggesting this increase to be a compensatory change and that the decrease in nephrin levels could be related to podocyte injury (Lu et al., 2013). Jiang *et al.* reported that the number of urinary podocytes reflects the loss of podocytes in renal tissues, which might be a marker of IgAN progression (Jiang et al., 2012). Indeed, podocyte injury precedes the increase in proteinuria; therefore, podocytes are primary therapeutic targets for IgAN (Xu et al., 2010).

In the present study, the levels of the podocyte-associated proteins podocalyxin and nephrin were reduced in rats with IgAN. MHCD augmented the levels of these proteins as well as the number of podocytes, as determined by WT1 staining. After drug intervention, the numbers of WT1-positive podocytes in rats in MHCD-H group increased significantly ($p < 0.05$). MHCD reduced podocyte foot process fusion, suggesting that it has an obvious protective effect on podocytes.

In conclusion, the results of the present study suggest that MHCD ameliorates proteinuria in rats with IgAN. Additionally, light microscopy, electron microscopy, and western blot analysis demonstrated that MHCD exerts a therapeutic effect on IgAN *in vivo* by maintaining podocyte function. Thus, MHCD could serve as an effective drug for the treatment of IgAN. Although the

general mechanism underlying the effects of MHCD was revealed, detailed analyses of the precise mechanism will be an important focus of our future research. Specifically, our future work will focus on studying the signaling pathways related to podocyte-associated proteins and the target molecules of MHCD.

## DATA AVAILABILITY STATEMENT

The raw data supporting the conclusion of this article will be made available by the authors, without undue reservation.

## ETHICS STATEMENT

The animal study was reviewed and approved by the Medical Ethics Committee, Xiyuan Hospital, China Academy of Chinese Medical Sciences.

## AUTHOR CONTRIBUTIONS

MC and YZ conceived of and proposed the idea, designed the study. MC, BY, LL, WH, and JZ preformed the experiment. MZ and YS participated in data analysis. MC, BY and YZ contributed to writing assistance and reading the manuscript. All authors contributed to the article and approved the submitted version.

## FUNDING

## ACKNOWLEDGMENTS

## REFERENCES

Akankwasa, G., Jianhua, L., Guixue, C., Changjuan, A., and Xiaosong, Q. (2018). Urine Markers of Podocyte Dysfunction: a Review of Podocalyxin and Nephrin in Selected Glomerular Diseases. *Biomarkers Med.* 12, 927–935. doi:10.2217/bmm-2018-0152

Asanuma, K., and Mundel, P. (2003). The Role of Podocytes in Glomerular Pathobiology. *Clin. Exp. Nephrol.* 7, 255–259. doi:10.1007/s10157-003-0259-6

Asao, R., Asanuma, K., Kodama, F., Akiba-Takagi, M., Nagai-Hosoe, Y., Seki, T., et al. (2012). Relationships between Levels of Urinary Podocalyxin, Number of Urinary Podocytes, and Histologic Injury in Adult Patients with IgA Nephropathy. *Clin. J. Am. Soc. Nephrol.* 7, 1385–1393. doi:10.2215/CJN.08110811

Bai, L., Li, H., Li, J., Song, J., Zhou, Y., Liu, B., et al. (2019a). Immunosuppressive Effect of Artemisinin and Hydroxychloroquine Combination Therapy on IgA Nephropathy via Regulating the Differentiation of CD4+ T Cell Subsets in Rats. *Int. Immunopharmacol.* 70, 313–323. doi:10.1016/j.intimp.2019.02.056

Bai, L., Li, J., Li, H., Song, J., Zhou, Y., Lu, R., et al. (2019b). Renoprotective Effects of Artemisinin and Hydroxychloroquine Combination Therapy on IgA Nephropathy via Suppressing NF-κB Signaling and NLRP3 Inflammasome Activation by Exosomes in Rats. *Biochem. Pharmacol.* 169, 113619. doi:10.1016/j.bcp.2019.08.021

Beck, L., Bomback, A. S., Choi, M. J., Holzman, L. B., Langford, C., Mariani, L. H., et al. (2013). KDOQI US Commentary on the 2012 KDIGO Clinical Practice Guideline for Glomerulonephritis. *Am. J. Kidney Dis.* 62, 403–441. doi:10.1053/j.ajkd.2013.06.002

Carney, E. F. (2013). Podocyturia Predicts Pre-eclampsia. *Nat. Rev. Nephrol.* 9, 310. doi:10.1038/nrneph.2013.72

Chen, L., Chen, D.-Q., Wang, M., Liu, D., Chen, H., Dou, F., et al. (2017). Role of RAS/Wnt/β-catenin axis Activation in the Pathogenesis of Podocyte Injury and Tubulo-Interstitial Nephropathy. *Chem. Biol. Interact.* 273, 56–72. doi:10.1016/j.cbi.2017.05.025

Coppo, R. (2017). Clinical and Histological Risk Factors for Progression of IgA Nephropathy: an Update in Children, Young and Adult Patients. *J. Nephrol.* 30, 339–346. doi:10.1007/s40620-016-0360-z

Coppo, R. (2019). Towards a Personalized Treatment for IgA Nephropathy Considering Pathology and Pathogenesis. *Nephrol. Dial. Transpl.* 34, 1832–1838. doi:10.1093/ndt/gfy338

Deng, F., Zhang, J., Li, Y., Wang, W., Hong, D., Li, G., et al. (2019). Hirudin Ameliorates Immunoglobulin A Nephropathy by Inhibition of Fibrosis and Inflammatory Response. *Ren. Fail.* 41, 104–112. doi:10.1080/0886022x.2019.1583113

Fukami, K., Yamagishi, S.-i., Kaifu, K., Matsui, T., Kaida, Y., Ueda, S., et al. (2013). Telmisartan Inhibits AGE-Induced Podocyte Damage and Detachment. *Microvasc. Res.* 88, 79–83. doi:10.1016/j.mvr.2013.04.006

Gao, Y. H., Zhang, Y., Li, P., Liu, H. X., Li, S., and Yu, Z. K. (2016). Anti-renal Fibrosis Mechanism of Modified Huangqi Chifeng Decoction Based on TGF-p1/Smad Signal Pathway. *Zhongguo Zhong Xi Yi Jie He Za Zhi* 36, 1486–1490. doi:10.7661/CJIM.2016.12.1486

Haraldsson, B., Nyström, J., and Deen, W. M. (2008). Properties of the Glomerular Barrier and Mechanisms of Proteinuria. *Physiol. Rev.* 88, 451–487. doi:10.1152/physrev.00055.2006

Hishiki, T., Shirato, I., Takahashi, Y., Funabiki, K., Horikoshi, S., and Tomino, Y. (2001). Podocyte Injury Predicts Prognosis in Patients with Iga Nephropathy Using a Small Amount of Renal Biopsy Tissue. *Kidney Blood Press. Res.* 24, 99–104. doi:10.1159/000054214

Jiang, W.-l., Peng, Y.-m., Liu, Y.-h., Liu, H., Chen, G.-c., Xu, X.-q., et al. (2012). Evaluation of Renal Clinicopathological Changes in IgA Nephropathy by Urinary Podocytes Excretion and Podocalyxin Expression. *Ren. Fail.* 34, 821–826. doi:10.3109/0886022X.2011.643352

Jiao, Z. N., Zhao, M. M., Zhang, Y., Li, S., Si Y., et al. (2018). Single Case Randomized Controlled Research of Modified Huangqi Chifeng Decoction in the Treatment of Proteinuria Due to IgA Nephropathy. *China Med. Herald* 01, 95–98.

Jiao, Z. N., Zhang, Y., Li, P., Wang, Y. J., Liu, H. X., Gao, Y. H., et al. (2016). Impacts of the Modified Huangqi Chifeng Decoction on the Proliferation of Glomerular Mesangial Cell and the Secretion of Extracellular Matrix in Mice. *World J. Integrated Traditional West. Med.* 11, 941–944. doi:10.13935/j.cnki.sjzx.160715

Kriz, W., Shirato, I., Nagata, M., LeHir, M., and Lemley, K. V. (2013). The Podocyte's Response to Stress: the enigma of Foot Process Effacement. *Am. J. Physiol. Renal Physiol.* 304, F333–F347. doi:10.1152/ajprenal.00478.2012

Lemley, K. V., Lafayette, R. A., Safai, M., Derby, G., Blouch, K., Squarer, A., et al. (2002). Podocytopenia and Disease Severity in IgA Nephropathy. *Kidney Int.* 61, 1475–1485. doi:10.1046/j.1523-1755.2002.00269.x

Leung, J. C. K., Lai, K. N., and Tang, S. C. W. (2018). Role of Mesangial-Podocytic-Tubular Cross-Talk in IgA Nephropathy. *Semin. Nephrol.* 38, 485–495. doi:10.1016/j.semnephrol.2018.05.018

Li, H., Lu, R., Pang, Y., Li, J., Cao, Y., Fu, H., et al. (2020a). Zhen-Wu-Tang Protects IgA Nephropathy in Rats by Regulating Exosomes to Inhibit NF-κB/NLRP3 Pathway. *Front. Pharmacol.* 11, 1080. doi:10.3389/fphar.2020.01080

Li, L., Gong, Z., Xue, P., Wang, D., Xu, M., Sui, S., et al. (2020b). Expression of miRNA-223 and NLRP3 Gene in IgA Patients and Intervention of Traditional

Chinese Medicine. *Saudi J. Biol. Sci.* 27, 1521–1526. doi:10.1016/j.sjbs.2020.04.034

Li, P., Chen, Y.-z., Lin, H.-l., Ni, Z.-h., Zhan, Y.-l., Wang, R., et al. (2017). Abelmoschus Manihot - a Traditional Chinese Medicine versus Losartan Potassium for Treating IgA Nephropathy: Study Protocol for a Randomized Controlled Trial. *Trials* 18, 170. doi:10.1186/s13063-016-1774-6

Li, P., Lin, H., Ni, Z., Zhan, Y., He, Y., Yang, H., et al. (2020c). Efficacy and Safety of Abelmoschus Manihot for IgA Nephropathy: A Multicenter Randomized Clinical Trial. *Phytomedicine* 76, 153231. doi:10.1016/j.phymed.2020.153231

Li, S., and Li, J.-p. (2020). Treatment Effects of Chinese Medicine (Yi-Qi-Qing-Jie Herbal Compound) Combined with Immunosuppression Therapies in IgA Nephropathy Patients with High-Risk of End-Stage Renal Disease (TCM-WINE): Study Protocol for a Randomized Controlled Trial. *Trials* 21, 31. doi:10.1186/s13063-019-3989-9

Liu, B., He, Y., Lu, R., Zhou, J., Bai, L., Zhang, P., et al. (2018). Zhen-Wu-tang Protects against Podocyte Injury in Rats with IgA Nephropathy via PPARγ/NF-κB Pathway. *Biomed. Pharmacother.* 101, 635–647. doi:10.1016/j.biopha.2018.02.127

Liu, H. X., Zhang, Y., Li, P., Gao, Y. H., Li, S., and Yu, Z. K. (2016). Effect of Modified Hangqi Chifeng Decoction Containing Serum on the Expression of Col IV, MMP-2, and TIMP-2 in Glomerular Mesangial Cells Induced by LPS. *Zhongguo Zhong Xi Yi Jie He Za Zhi* 36, 592–596. doi:10.7661/CJIM.2016.05.0592

Lu, H.-Y., Chen, L.-Z., Jiang, X.-Y., Mo, Y., Ling, Y.-H., and Sun, L.-Z. (2013). Temporal and Spatial Expression of Podocyte-Associated Molecules Are Accompanied by Proteinuria in IgA Nephropathy Rat Model. *Physiol. Res.* 62, 35–45. doi:10.33549/physiolres.932380

Lv, J., Zhang, H., Wong, M. G., Jardine, M. J., Hladunewich, M., Jha, V., et al. (2017). Effect of Oral Methylprednisolone on Clinical Outcomes in Patients with IgA Nephropathy. *JAMA* 318, 432–442. doi:10.1001/jama.2017.9362

Menon, M. C., Chuang, P. Y., and He, J. C. (2013). Role of Podocyte Injury in IgA Nephropathy. *Contrib. Nephrol.* 181, 41–51. doi:10.1159/000348461

Mundel, P., and Shankland, S. J. (2002). Podocyte Biology and Response to Injury. *J. Am. Soc. Nephrol.* 13, 3005–3015. doi:10.1097/01.asn.0000039661.06947.fd

Nagata, M. (2016). Podocyte Injury and its Consequences. *Kidney Int.* 89, 1221–1230. doi:10.1016/j.kint.2016.01.012

O'Shaughnessy, M. M., and Lafayette, R. A. (2017). Corticosteroids for IgA Nephropathy: TESTING for Benefit, Discovering Harm. *JAMA* 318, 429–431. doi:10.1001/jama.2017.9359

Peng, S.-N., Zeng, H. H., Fu, A. X., Chen, X. W., and Zhu, Q. X. (2013). Effects of Rhein on Intestinal Epithelial Tight junction in IgA Nephropathy. *World J. Gastroenterol.* 19, 4137–4145. doi:10.3748/wjg.v19.i26.4137

Reiser, J., Kriz, W., Kretzler, M., and Mundel, P. (2000). The Glomerular Slit Diaphragm Is a Modified Adherens junction. *J. Am. Soc. Nephrol.* 11, 1–8. doi:10.1681/asn.v1111

Ren, Z., Liang, W., Chen, C., Yang, H., Singhal, P. C., and Ding, G. (2012). Angiotensin II Induces Nephrin Dephosphorylation and Podocyte Injury: Role of Caveolin-1. *Cell Signal.* 24, 443–450. doi:10.1016/j.cellsig.2011.09.022

Scott, R. P., and Quaggin, S. E. (2015). The Cell Biology of Renal Filtration. *J. Cel Biol* 209, 199–210. doi:10.1083/jcb.201410017

Tomino, Y. (2007). Pathogenesis of IgA Nephropathy. *Contrib. Nephrol.* 157, 1–7. doi:10.1159/000102280

Villa, L., Boor, P., Konieczny, A., Kunter, U., van Roeyen, C. R. C., Denecke, B., et al. (2011). Effects and Mechanisms of Angiotensin II Receptor Blockade with Telmisartan in a Normotensive Model of Mesangioproliferative Nephritis. *Nephrol. Dial. Transpl.* 26, 3131–3143. doi:10.1093/ndt/gfr096

Wang, S., Chen, C., Su, K., Zha, D., Liang, W., Hillebrands, J., et al. (2016). Angiotensin II Induces Reorganization of the Actin Cytoskeleton and Myosin Light-Chain Phosphorylation in Podocytes through rho/ROCK-Signaling Pathway. *Ren. Fail.* 38, 268–275. doi:10.3109/0886022x.2015.1117896

Xu, L., Yang, H.-C., Hao, C.-M., Lin, S.-T., Gu, Y., and Ma, J. (2010). Podocyte Number Predicts Progression of Proteinuria in IgA Nephropathy. *Mod. Pathol.* 23, 1241–1250. doi:10.1038/modpathol.2010.110

Yang, L., Wang, Y., Nuerbiye, A., Cheng, P., Wang, J.-H., Kasimu, R., et al. (2018). Effects of Periostracum Cicadae on Cytokines and Apoptosis Regulatory

Proteins in an IgA Nephropathy Rat Model. *Int. J. Mol. Sci.* 19, 1599. doi:10.3390/ijms19061599

Yang, X., Zhu, A., and Meng, H. (2020). Tonsillar Immunology in IgA Nephropathy. *Pathol. Res. Pract.* 216, 153007. doi:10.1016/j.prp.2020.153007

Yu, Z. K., Li, L. S., Zhang, Y., Zhao, M. M., Si, Y., Zhang, L. M., et al. (2018). Efficacy Study on Modified Huangqi Chifeng Decoction in Treatment of IgA Based on Real World Study. *World Chin. Med.* 11, 2819–2822. doi:10.3969/j.issn.1673-7202.2018.11.039

Yu, Z. K., Yang, B., Zhang, Y., Li, L. S., Zhao, J. N., and Hao, W. (2018). Modified Huangqi Chifeng Decoction Inhibits Excessive Autophagy to Protect against Doxorubicin-induced N-ephrotic S-yndrome in R-ats via the PI3K/mTOR S-ignaling P-athway. *Exp. Ther. Med.* 16, 2490–2498. doi:10.3892/etm.2018.6492

Zhang, X., Wu, X., Xiong, L., Yi, Z., He, Q., He, X., et al. (2014). Role of Vitamin D3 in Regulation of T Helper Cell 17 and Regulatory T-Cell Balance in Rats with Immunoglobulin a Nephropathy. *Iran J. Kidney Dis.* 8, 363–370.

# Glomerular Damage in Trichloroethylene-Sensitized Mice: Targeting Cathepsin L-Induced Hyperactive mTOR Signaling

Feng Wang[1,2†], Yuying Dai[3†], Meng Huang[3†], Chenchen Zhang[1†], Liping Huang[3], Hui Wang[2,4], Liangping Ye[2,4], Qifeng Wu[5], Xuejun Zhang[2,4*] and Qixing Zhu[2,4*]

[1]Department of Dermatology, The Second Hospital of Anhui Medical University, Hefei, China, [2]Key Laboratory of Dermatology, Ministry of Education, The First Affiliated Hospital of Anhui Medical University, Hefei, China, [3]Department of Occupational Health and Environmental Health, School of Public Health, Anhui Medical University, Hefei, China, [4]Department of Dermatology, The First Affiliated Hospital of Anhui Medical University, Hefei, China, [5]Poison Control Center, Guangdong Province Hospital for Occupational Disease Prevention and Treatment, Guangzhou, China

Trichloroethylene (TCE) is a serious health hazard for workers with daily exposure, causing occupational medicamentosa-like dermatitis due to TCE (OMDT) and glomerular damage. Recent studies suggest that mTORC1 signaling is activated in various glomerular disorders; however, the role of mTORC1 signaling in TCE-induced glomerular damage remains to be explored. In the present study, 6 OMDT patients were enrolled and a TCE-sensitized mouse model was established to investigate molecular mechanisms underlying the glomerular damage associated with OMDT. Glomerular damage was assessed by levels of urine nephrin, H&E staining, and renal function test. Ultrastructural change of podocyte was investigated by transmission electron microscopy. The podocyte-related molecules including nephrin, α-actinin-4, and integrin β1 were visualized by immunofluorescence. The activation of mTORC1 signaling was confirmed by Western blot. Glomerular apoptosis was examined by the TUNEL test and Western blotting. Expression and location of cathepsin L (CTSL) were assessed by RT-PCR and immunofluorescence. Our results showed that TCE sensitization caused damage to glomerular structural integrity and also increased the activation of mTORC1 signaling, which was accompanied by podocyte loss, hypertrophy, and glomerular apoptosis. Importantly, we also found that over-expressed CTSL was mainly located in podocyte and CTSL inhibition could partially block the activation of mTORC1 signaling. Thus, our findings suggested a novel mechanism whereby hyperactive mTOR signaling contributes to TCE sensitization–induced and immune-mediated glomerular damage via CTSL activation.

**Keywords: trichloroethylene, podocyte, apoptosis, mTOR, cathepsin L**

# INTRODUCTION

Trichloroethylene (TCE) is a volatile and chlorinated organic solvent widely used in industrial settings such as metal degreasing, parts cleaning, and refrigerants manufacturing (Byrum et al., 2019; Pan et al., 2019). Over the past decades, the extensive use of TCE has caused more than 50 million pounds annually released into the environment in the United States and even heavier in China (Huang et al., 2014). There are more than 20,000 workers that are exposed to TCE every year and TCE has become an intractable environment concern, and a serious health hazard to the public in China (Huang et al., 2014). The International Agency for Research on Cancer (IARC) has determined TCE as Group 1 carcinogen to humans (IARC, 2014). Recent epidemiological studies show that TCE exposure was closely linked to cancers such as renal cancer and non-Hodgkin lymphoma (Guha et al., 2012; Lee et al., 2019), and trichloroethylene hypersensitivity syndrome (THS) (Li et al., 2019).

THS, also called occupational medicamentosa-like dermatitis due to trichloroethylene (OMDT) in China, is a severe hypersensitivity reaction, after TCE skin contact or inhalation in occupational environment (Ministry of Health, 2006). OMDT is a T-cell–mediated type IV hypersensitivity reaction, presented with erythema, rash, blisters, and systems damage (Lin et al., 2019). However, the allergy theory alone could not fully explain the complicated pathogenesis of OMDT, including the severe hepatitis and renal complications. Studies in humans and experimental animals confirmed that a mixed-type allergic response involving cellular and humoral immunity (Huang et al., 2015) contributes to the multiple organ injuries in OMDT. Glomerulus is responsible for filtering blood under physiological conditions and is a primary target of various physical and chemical factors in kidney disorders. Our previous studies reported pathological changes of glomerulus with impaired filtration function in TCE-induced immune kidney disorder with unknown mechanisms (Wang et al., 2019b).

Podocytes are terminally differentiated epithelial cells, covering the surface of glomerular basement membrane (GBM) via foot process extensions (Sakhi et al., 2019). The special foot processes form the slit diaphragm (SD), which is the ultimate filtration barrier of glomerulus (Maeda et al., 2018). In addition, to accomplish the normal filtering task, various molecules such as nephrin and podocin, integrin β1, and α-actinin-4 work together as an interacting network and ensure the normal podocyte's cytoskeleton and glomerular integrity (Sawada et al., 2016; Rinschen et al., 2017). However, this dynamic balance of the molecular network is easily broken and the imbalance leads to renal dysfunction and even proteinuria (Kriz and Lemley, 2015).

In general, mammalian target of rapamycin (mTOR) is a highly conserved serine/threonine kinase that plays an important role for cell proliferation, autophagy, and apoptosis (Fantus et al., 2016; Cui et al., 2020). mTOR contains two catalytic subunits such as mTOR complex 1 (mTORC1) and mTOR complex 2, and mTORC1 signaling is

capable to regulate the podocyte size, implicated in a variety of kidney disorders (Zschiedrich et al., 2017; Puelles et al., 2019). However, whether the activation of mTORC1 signaling is involved in the podocyte damage in TCE sensitization or not is still unknown. Here, we employed a mouse model of TCE skin sensitization to uncover the detailed role of mTORC1 signaling in TCE-induced glomerular damage.

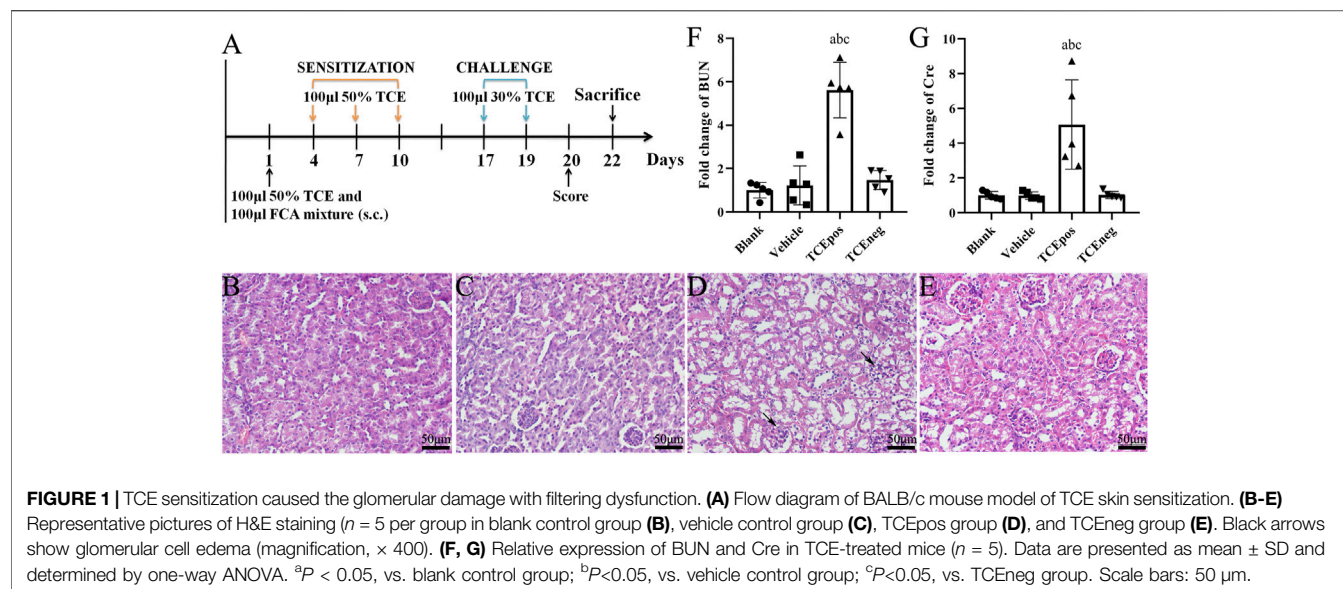# MATERIALS AND METHODS

## Reagents

TCE (99.9% purity), Freund's complete adjuvant (FCA, composition: 85% Drakeol 6 VR (mineral oil); 15% mannide monooleate (Arlacel A); 20 mg *Mycobacterium*), and *In Situ* Cell Death Detection Kit were purchased from Sigma-Aldrich (St. Louis, Missouri, United States). Acetone and olive oil were purchased from Shanghai Chemical Reagent Company (Shanghai, China). The human nephrin DuoSet ELISA kit was obtained from R&D System (Minneapolis, United States). TRIzol and RevertAid First Strand cDNA Synthesis Kit were obtained from ThermoFisher Scientific (MA, United States). The antibodies against nephrin, α-actinin-4, cathepsin L, IgG H&L AlexaFluor[®] 488, and AlexaFluor[®] 594 were purchased from Abcam (Cambridge, United Kingdom). The antibody against podocin was purchased from Santa Cruz Biotechnology (Dallas, TX, United States). The antibody against integrin β1 was purchased from Affinity Biosciences (OH, United States). Antibodies against mTOR, p-mTOR, 4EBP1, p-4EBP1, p70S6K, p-p70S6K, Bax, Bcl-2, caspase-3, and GAPDH were purchased from Cell Signaling Technology (Beverly, MA, United States). 4′, 6-diamidino-phenylindole dihydrochloride (DAPI) was purchased from Solarbio Life Sciences (Beijing, China). Rapamycin and Z-Phe-Tyr-CHO were supplied by Selleck and Santa Cruz Biotechnology, respectively.

## Ethics

The experimental design and all protocols were approved by the Biomedical Ethics Committee of Anhui Medical University (No. 20160216) and Experimental Animal Ethics Committee of Anhui Medical University (No. LLSC20160312) and followed the Declaration of Helsinki principles. All participants were informed about the objective and methods of this study before signing the informed consent. The mouse experiments were performed in accordance with NIH guidelines for care and use of laboratory animals.

## Study Participants

Newly diagnosed OMDT patients and healthy controls were recruited from January 2017 to December 2019 at Poison Control Center of Guangdong Province Hospital for Occupational Disease Prevention and Treatment. The OMDT was diagnosed based on the history of TCE exposure, fever, skin lesions, and multisystem damage according to the Chinese National Diagnostic Criteria (GBZ 185-2006). Urine was collected before and after clinical treatment for nephrin

**FIGURE 1 |** TCE sensitization caused the glomerular damage with filtering dysfunction. **(A)** Flow diagram of BALB/c mouse model of TCE skin sensitization. **(B-E)** Representative pictures of H&E staining ($n$ = 5 per group in blank control group **(B)**, vehicle control group **(C)**, TCEpos group **(D)**, and TCEneg group **(E)**. Black arrows show glomerular cell edema (magnification, × 400). **(F, G)** Relative expression of BUN and Cre in TCE-treated mice ($n$ = 5). Data are presented as mean ± SD and determined by one-way ANOVA. [a]$P$ < 0.05, vs. blank control group; [b]$P$<0.05, vs. vehicle control group; [c]$P$<0.05, vs. TCEneg group. Scale bars: 50 µm.

**TABLE 1 |** Sensitization rate and kidney impairment incidence in mice.

| Groups | Mice (n) | Score | | | | Rate (%) | |
|---|---|---|---|---|---|---|---|
| | | 0 | 1 | 2 | 3 | Sensitization | Kidney impairment |
| Blank control | 10 | 0 | 0 | 0 | 0 | 0.0 | 0 |
| Vehicle control | 10 | 0 | 0 | 0 | 0 | 0.0 | 0 |
| TCE treatment | 40 | 25 | 9 | 4 | 2 | 37.5 (15/40) | 35.0 (14/40) |
| TCEpos | 15 | | 9 | 4 | 2 | | |
| TCEneg | 25 | 25 | | | | | |
| RAPA + TCE treatment | 40 | 26 | 11 | 3 | 0 | 35.0 (14/40) | 15.0 (6/40) |
| RAPA + TCEpos | 14 | | 11 | 3 | 0 | | |
| RAPA + TCEneg | 26 | 26 | | | | | |
| CTSLinh + TCE treatment | 40 | 27 | 9 | 4 | 0 | 32.5 (13/40) | 12.5 (5/40) |
| CTSLinh + TCEpos | 13 | | 9 | 4 | 0 | | |
| CTSLinh + TCEneg | 27 | 27 | | | | | |

*CTSL, cathepsin L; inh, inhibitor; TCE, trichloroethylene; pos, positive; neg, negative; RAPA, rapamycin.*

examination. The baseline data of OMDT patients in the present study is summarized in **Table 2**.

## Mice and TCE Exposure

A total of 140 female BALB/c mice (6–8 weeks-old and 18–20 g of weight) were obtained from the Experimental Animal Center of Anhui Medical University. Mice were housed in specific pathogen free environment with food and water *ad libitum*. The feeding conditions were manually set as follows: 22.5 ± 0.5°C temperature, 50 ± 5% humidity, and 12 h light/dark cycle. Mice were acclimated for 7 days before experimental initiation. The mouse model of TCE skin sensitization was established according to previous studies (Wang et al., 2015; Wang et al., 2019a; Wang et al., 2019b). Briefly, sensitization phase and challenge phase were conducted sequentially after the initial administration of 100 µL 50% TCE mixture and equal FCA on the 1st day. The sensitization phase was carried out by spread of 100 µL 50% TCE mixture (TCE: olive oil: acetone = 5: 2: 3, v/v/v)

on the back skin every 3 days for three times until the 10th day. Then, the challenge phase was performed 2 times by topical application of 100 µL 30% TCE mixture (TCE: olive oil: acetone = 3: 2: 5, v/v/v) on the same area on the 17th day and 19th day (**Figure 1A**). Mice with physiological saline or vehicle (the same proportions of olive oil and acetone without TCE) treatment were considered as controls. Additionally, to explore the mTOR signaling, rapamycin and Z-Phe-Tyr-CHO were applied by intraperitoneal injection at a dose of 4 mg/kg and 10 mg/kg, respectively. The details of the group design are listed in **Table 1**.

Twenty four hours after the last challenge, the cutaneous allergic reactions were scored by the severity of erythema and edema: 0, absolutely normal; 1, scattered or mild erythema; 2, moderate and diffuse erythema; 3, intensive erythema and swelling. Score ≥ 1 is identified as positive sensitization and score = 0 means negative sensitization. Mice were euthanized by $CO_2$ and sacrificed, 72 h after the last challenge. Blood was taken from ophthalmic venous plexus and centrifuged to separate

serum from blood cells at 4°C, 1000 × g for 30 min. The collected kidneys were embedded in paraffin for histological examination, or embedded in the optimal freezing medium (OCT) for immunofluorescence and glomeruli were isolated from fresh kidney tissues.

## ELISA

Levels of nephrin in the urine of OMDT patients were analyzed by ELISA following the manufacturer's instructions. In brief, the plate was coated with the capture antibody and was blocked by reagent diluent. The urine samples and prepared standards were added into well plates for two hours incubation. Then, diluted detection antibody, streptavidin-HRP working dilution, substrate solution, and stop solution were added to each well sequentially. Finally, the optical density was determined by a microplate reader (Bio-Tek, μQuant) and the concentration of urine nephrin was calculated by the standard curve.

## Histological Examination

Fresh kidneys were removed and fixed with 10% formaldehyde for about 48 h. Then, the kidneys were embedded in paraffin and sectioned at 5 μm thickness. After standard dewaxing and hydration, sections were stained by hematoxylin/eosin staining (H&E staining) to analyze the morphological changes in glomerulus.

## Transmission Electron Microscope Detection

To assess the ultrastructural changes of podocyte, the fresh kidney cortex was cut into 1 mm$^3$ and fixed in 2.5% glutaraldehyde for 6–12 h. After postfixation in 2% osmic acid solution for 2 h, the samples were dehydrated by graded ethanol (50% ethanol, 70% ethanol, and 90% ethanol) and propylene oxide, and embedded in Epon 812. Then, the samples were sectioned at 60 nm thickness and scanned in a transmission electron microscope (JEM-1230, Japan).

## Renal Function Assessment

Blood urea nitrogen (BUN) and serum creatinine (Cre) are classical and conventional indicators to reflect the renal function in clinical practice. In this study, BUN and Cre were measured by commercial assay kits (Nanjing Jiancheng Bioengineering Institute, China). The optical density of BUN and Cre was recorded at 640 and 546 nm respectively in a microplate reader (Bio-Tek, μQuant). Then, the levels of BUN and Cre were calculated according to the standard curve handled simultaneously with the samples.

## TUNEL Assays

TUNEL assays were performed by *In Situ* Cell Death Detection Kit, POD (Roche). Briefly, the sections were covered with proteinase K working fluid for 30 min after routine dewaxing and hydration. Then, the prepared TUNEL reaction mixture was added to the sections in a dark humid chamber for 60 min. After PBS rinse for 3 times, a drop of PBS was added onto the sections to count the apoptotic cells under fluorescence microscope. Next,

50 μL converter-POD was covered on the sections in a dark humid chamber at 37°C for 30 min. DAB working fluid was used to stain the apoptotic cells counterstained with hematoxylin. The counting and analysis were performed under an optical microscope and the representative fields were collected simultaneously.

## Immunohistochemistry and Immunofluorescence Examination

Fresh kidney tissues were embedded in OCT compound. The tissues were cut into of 5 μm thickness frozen sections in a Leica CM1850 cryostat (Wetzlar, Germany) and the sections were fixed with precooled acetone for 5 min. Next, 0.3% Triton X-100 was covered on the sections for 30 min, followed by blocking with goat serum working fluid for 2 h at room temperature. The primary antibodies including anti-CTSL, anti-podocin (Diluted at 1:1000), anti-nephrin, anti-integrin β1 (Diluted at 1:200), and anti–α-actinin-4 were then incubated with the sections overnight at 4°C. Then, the sections were taken out and rewarmed to 37°C for 30 min, before linking to fluorescein labeled secondary antibodies: goat anti-rabbit IgG H&L (Diluted at 1:200) or goat anti-mouse IgG H&L (Diluted at 1:400). Two hours later, the sections were washed with PBS and the nuclei were counterstained with DAPI for 15 min. The localization and expression of marker proteins were observed under an inverted fluorescence microscope (Olympus, IX73, Japan) with appropriate excitation and emission filters.

## Glomeruli Isolation

After skin sterilization via 75% alcohol and ligation of superior mesenteric artery, thoracic aorta, the distal abdominal aorta, and distal inferior vena cava were dissected. A capillary was inserted into the middle of the abdominal aorta and precooled sterile PBS was pumped into kidney. After the residual blood in kidney was removed, 4 × 10$^7$ magnetic beads in 20 ml normal saline were slowly pumped into kidney via the inserted capillary. Kidney was removed and cut into 1 mm$^3$ small pieces for digestion using 1 mg/ml collagenase A. Then, the fluid was filtrated by a 100-μm cell strainer for 2 times. The collected suspension was centrifuged at 200 × g for 5 min and the sedimentation was resuspended with PBS. Finally, glomeruli were collected by a magnetic particle concentrator to extract total proteins.

## RT-PCR

The total RNA was extracted from glomerulus by TRIzol and cDNA was synthesized by RevertAid First Strand cDNA Synthesis Kit. The process of PCR was accomplished with SYBR Green I Master under LightCycler 480 system. The primer sequences of *cathepsin L* and *GAPDH* mRNA used here are listed as follows: *cathepsin L*, forward, 5'-CCC TAT GAA GCG AAG GAC GG-3', reverse, 5'-CTG GAG AGA CGG ATG GCT TG-3'; *GAPDH*, forward, 5'-CCC TTA AGA GGG ATG CTG CC-3', reverse, 5'-TAC GGC CAA ATC CGT TCA CA-3'.

## Western Blot Analysis

Total proteins were extracted from glomerulus by lysis buffer and the protein concentration was detected by using the BCA assay.

The final concentration of protein samples was diluted to 10 mg/ml mixed with loading buffer. A total of 10 μL protein sample was added to the prepared gels and separated by SDS-PAGE. The proteins were then transferred to a PVDF membrane (0.45 μm, Millipore, United States), followed by blocking in 5% skim milk powder for 2 h at room temperature. The membranes were incubated at 4°C overnight with the primary antibodies against mTOR, phospho-mTOR, Akt, phospho-Akt, Bax, Bcl-2, caspase-3, β-actin, and GAPDH (diluted at 1:1000). Next, the membrane was washed by PBST and incubated with goat anti-rabbit IgG antibody (Diluted at 1:100000) or goat anti-mouse IgG antibody (Diluted at 1:10000) for 2 h at room temperature. Proteins were assessed by WesternBright ECL HRP substrate kit (Advansta, 171005-80, United States) in a chemiluminescence system (CLiNX ChemiScope 6000 Touch, Shanghai, China).

## Statistical Analysis

Statistical analysis was performed using GraphPad Prism software (version 6, San Diego, CA). Data were presented as mean ± SD. The paired $t$-test was carried out to compare the difference of nephrin in urine before and after clinical treatment. The $\chi^2$ test was used to compare the difference of mice sensitization rate and the incidence of kidney impairment. One-way ANOVA followed by Tukey's or Bonferroni's test was applied to compare statistical differences between multiple groups. $P$-value < 0.05 was considered statistically significant and $P$-value < 0.01 was also displayed in the results.

## RESULTS

## Sensitization Rate and Occurrence of Kidney Impairment in Mice

As shown in **Table 1**, a total of 42 mice with mild or severe skin erythema and/or edema displayed a positive sensitization and the overall sensitization rate (excluding blank control and vehicle control group) was 35.0%. No visible skin lesions were found in mice from blank control group and vehicle control group. According to the cutaneous reaction and pharmacologic pretreatment, mice were grouped as follows: blank control group ($n$ = 10), vehicle control group ($n$ = 10), TCE sensitization positive subgroup (TCEpos, $n$ = 15) and TCE sensitization negative subgroup (TCEneg, $n$ = 25), TCE sensitization positive subgroup with rapamycin (mTOR inhibitor) pretreatment (RAPA + TCEpos, $n$ = 14), TCE sensitization negative subgroup with rapamycin pretreatment (RAPA + TCEneg, $n$ = 26), TCE sensitization positive subgroup with Z-Phe-Tyr-CHO (cathepsin L inhibitor) pretreatment (CTSLinh + TCEpos, $n$ = 13), and TCE sensitization negative subgroup with Z-Phe-Tyr-CHO pretreatment (CTSLinh + TCEneg, $n$ = 27).

H&E staining showed that 14 sensitization positive mice with renal structural changes were found in TCE treatment group whereas the number were dropped to 6 and 5 in RAPA + TCE treatment group and CTSLinh + TCE treatment group, respectively. The incidence of kidney damage in TCE treatment group was significantly higher than RAPA + TCE

treatment group (15.0%) and CTSLinh + TCE treatment group (12.5%). These results showed that inhibition of mTOR and CTSL reduced TCE-induced sensitization, and suggest that mTOR and CTSL are involved in TCE-induced skin sensitization.

## TCE Sensitization Caused the Glomerular Damage With Filtration Dysfunction

OMDT is a rare but severe disorder with a prevalence of less than 1% among TCE-exposed workers (Lin et al., 2019). Six OMDT patients, including 2 females and 4 males, and 10 health controls were recruited in our study. Increased levels of serum BUN, urine albumin, and urine erythrocyte were found in several participants. The baseline data and kidney damage–related index was listed in **Table 2**.

In mice, H&E staining showed glomerular cell edema with or without inflammatory cell infiltration in TCEpos group. In contrast, no detectable structural changes were found in blank control group, vehicle control group, and TCEneg group (**Figures 1B–E**). Compared to vehicle control group, the levels of both BUN and Cre were increased in TCEpos group ($p$ < 0.05), whereas no significant differences were found among blank control group, vehicle control group, and TCEneg group ($p$ > 0.05) (**Figures 1F,G**). These data demonstrated TCE sensitization-specific glomerular structural and functional damage in both human and mouse model.

## Podocyte Morphological Changes Involved in TCE-Induced Glomerular Damage

To estimate the ultrastructural changes in podocytes, transmission electron microscopy for mice was performed. The observations showed a well-distributed glomerular basement membrane and an orderly arranged foot process in blank control group, vehicle control group, and TCEneg group. However, podocyte hypertrophy with thickened glomerular basement membrane and fusion of foot processes were found in TCEpos group (**Figure 2**). In summary, these findings suggest that podocyte damage occurred in TCE-induced glomerular disorders.

## Loss of Podocytes Occurred in OMDT Patients and TCE-Sensitized Mice

To assess the loss of podocyte in OMDT, nephrin, a specific marker of podocyte, was determined in urine before and after clinical treatment. The levels of nephrin in urine were significantly decreased after clinical treatment. Compared to the healthy control, the level of nephrin in OMDT patients before clinical treatment was increased and back to normal range after clinical treatment ($p$ < 0.05, **Figure 3A**). In mice, podocytes were also lost in TCEpos group, presented as decreased levels of nephrin (**Figures 3B,E**). These data suggest that loss of podocytes contributes to the glomerular structure damage in OMDT.

Of importance, integrin β1 and α-actinin-4 are the key constitutive proteins of podocyte. Integrin β1 is a molecule for

**TABLE 2 |** The baseline data of OMLDT patients in the present study.

| | Gender | Ethnicities | Age | BMI | Pre-existing renal conditions | Comorbidities | Latent period (days) | Renal dysfunction |
|---|---|---|---|---|---|---|---|---|
| Case 1 | Female | Han | 29 | 17.9 | No | No | 38 | NO |
| Case 2 | Male | Han | 18 | 22.3 | No | No | 32 | NO |
| Case 3 | Male | Han | 21 | 24.4 | No | No | 37 | NO |
| Case 4 | Female | Han | 19 | 24.5 | No | No | 30 | YES (BUN 10.91) |
| Case 5 | Male | Han | 22 | 28.4 | No | No | 18 | YES (BUN 9.7) |
| Case 6 | Male | Han | 18 | 17.1 | No | No | 27 | YES (PRO +, BLD +) |

*BLD, urinary blood; BMI, body mass index; BUN, blood urea nitrogen (mmol/L); PRO, urinary protein.*
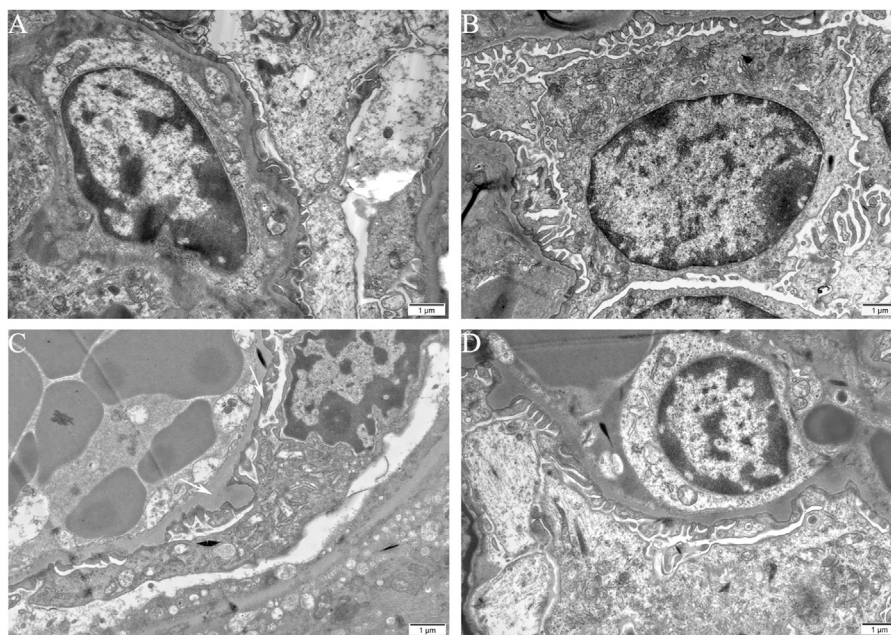


**FIGURE 2 |** Podocyte morphological changes involved in TCE-induced glomerular damage. Representative observations in transmission electron microscopy (n = 5 per group, magnification, × 15000) of mice glomerulus from blank control group **(A)**, vehicle control group **(B)**, TCEpos group **(C)**, TCEneg group **(D)**. White arrows show podocyte hypertrophy with thickened glomerular basement membrane, fusion of foot processes in TCEpos group. Scale bars: 1 μm.

adhesion of podocytes to glomerular basement membrane and α-actinin-4 is crucial to sustain the normal cytoskeleton of podocyte. Therefore, we also measured the levels of integrin β1 and α-actinin-4 in mice glomerulus by immunofluorescence test with recorded fluorescence intensity in ImageJ software. Our results revealed that the expression of both α-actinin-4 and integrin β1 was decreased in glomerulus from TCEpos group than vehicle control group ($p < 0.05$). No statistical differences were found among blank control group, vehicle control group, and TCEneg group ($p > 0.05$) (**Figures 3C,D,F,G**).

## Glomerular Apoptosis Participated in TCE-Induced Kidney Disorder

Considering that cell apoptosis was one of the common reasons of podocyte hypertrophy and glomerular integrity damage (Priante

et al., 2019), we assessed the glomerular apoptosis by TUNEL staining. The proportion of glomerular dead cells in TCEpos group was significantly elevated compared with TCEneg group, vehicle control group, and blank control group (both $p < 0.05$) (**Figure 4**), suggesting increased cell death via apoptosis by TCE sensitization.

To further evaluate the participation of glomerular apoptosis, we tested the expression of Bax/Bcl-2/caspase-3, which is widely recognized as an apoptosis pathway (Ma et al., 2020). We showed that the pro-apoptotic molecules Bax and caspase-3 were elevated whereas the anti-apoptotic molecule Bcl-2 was decreased in TCEpos group compared with TCEneg group ($p < 0.05$). No significant differences were found among blank control, vehicle group, and TCEneg group ($p > 0.05$) (**Figure 5**).
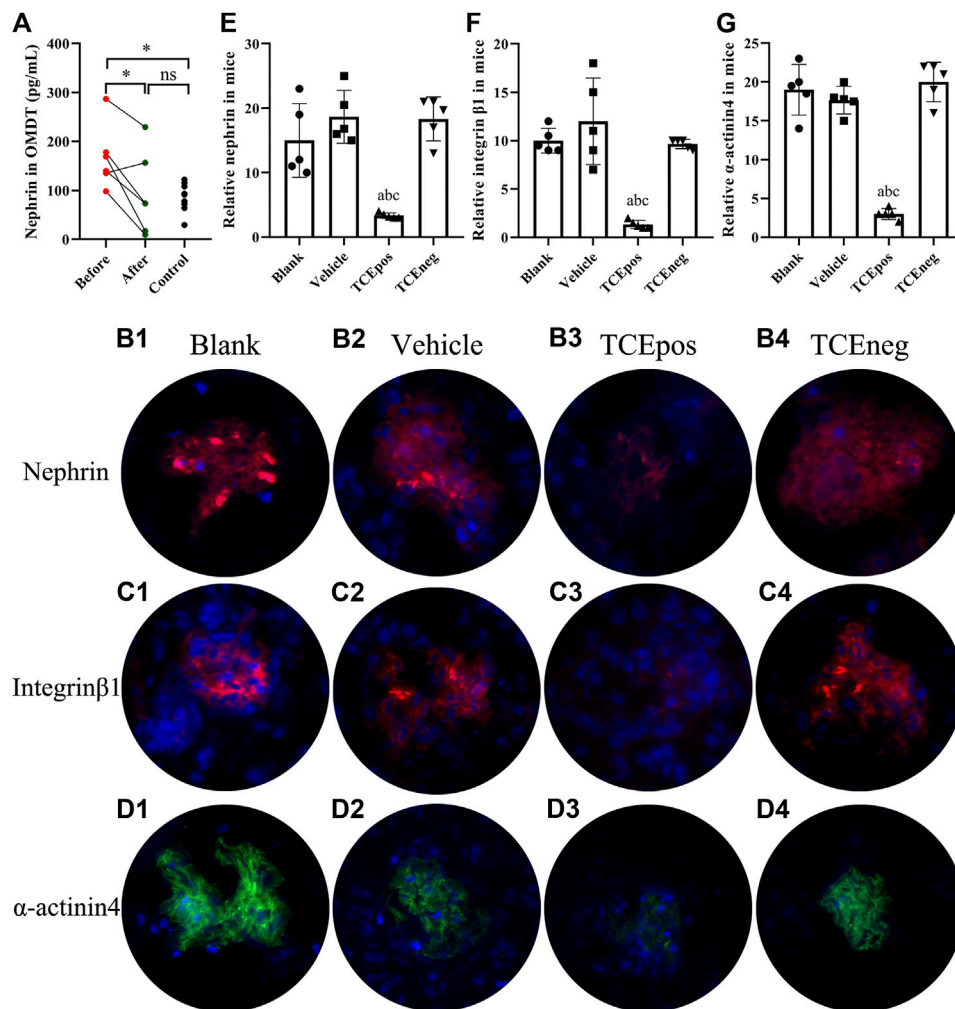
**FIGURE 3 |** Loss of podocytes occurred in OMDT patients and TCE-sensitized mice. **(A)** Expression of urine nephrin before and after clinical treatment in OMDT patients ($n$ = 6). **(B–D)** Representative results of immunofluorescence test in mice ($n$ = 5 per group). **(B1–B4)** Expression of nephrin in blank control group **(B1)**, vehicle control group **(B2)**, TCEpos group **(B3)**, and TCEneg group **(B4)**. **(C1–C4)** Expression of integrin β1 in blank control group **(C1)**, vehicle control group **(C2)**, TCEpos group **(C3)**, and TCEneg group **(C4)**. **(D1–D4)** Expression of α-actinin-4 in blank control group **(D1)**, vehicle control group **(D2)**, TCEpos group **(D3)**, and TCEneg group **(D4)**. **(E-G)** The fluorescence intensity of nephrin, integrin β1, and α-actinin-4 calculated in Image J software. Data are presented as mean ± SD and determined by paired $t$-test or one-way ANOVA, $*p < 0.05$, $^{ns}P>0.05$; $^aP < 0.05$, $vs.$ blank control group; $^bP<0.05$, $vs.$ vehicle control group; $^cP<0.05$, $vs.$ TCEneg group.

## Hyperactive mTORC1 Pathway Was Involved in TCE-Induced Glomerular Damage

The mouse glomeruli were isolated to evaluate the levels of key phosphorylated (p-) proteins involved in the mTORC1 signaling activation. Compared to TCEneg group, the relative expression of mTORC1 signaling molecules including p-mTORC1 and downstream molecules p-4EBP1 and p-p70S6K were increased in TCEpos group ($p < 0.05$). No significant differences were observed among the blank control group, vehicle control group, and TCEneg group ($p > 0.05$) (**Figure 6**). These data suggest that mTORC1 pathway was involved in TCE-induced glomerular damage.

## mTORC1 Pathway Inhibition Alleviated the Glomerular Damage in TCE Sensitization

To explore the role of hyperactive mTOR signaling in mice, rapamycin was applied by intraperitoneal injection (**Figure 7A**). As shown in **Figure 7**, the process of mTORC1 phosphorylation was completely blocked after rapamycin injection. The relative expressions of downstream p-4EBP1 and p-p70S6K were also decreased, confirmed by Western blot (**Figure 7B**). After pharmacological inhibition of mTOR signaling, we found that glomerular damage was improved dramatically in mice (**Figure 7C**). The proportion of apoptotic glomerular cells and the pro-apoptotic Bax and caspase-3 were decreased in RAPA + TCEpos group compared with TCEpos group ($p < 0.05$) (**Figures 7B,D**). Collectively, these results suggest that hyperactive mTOR
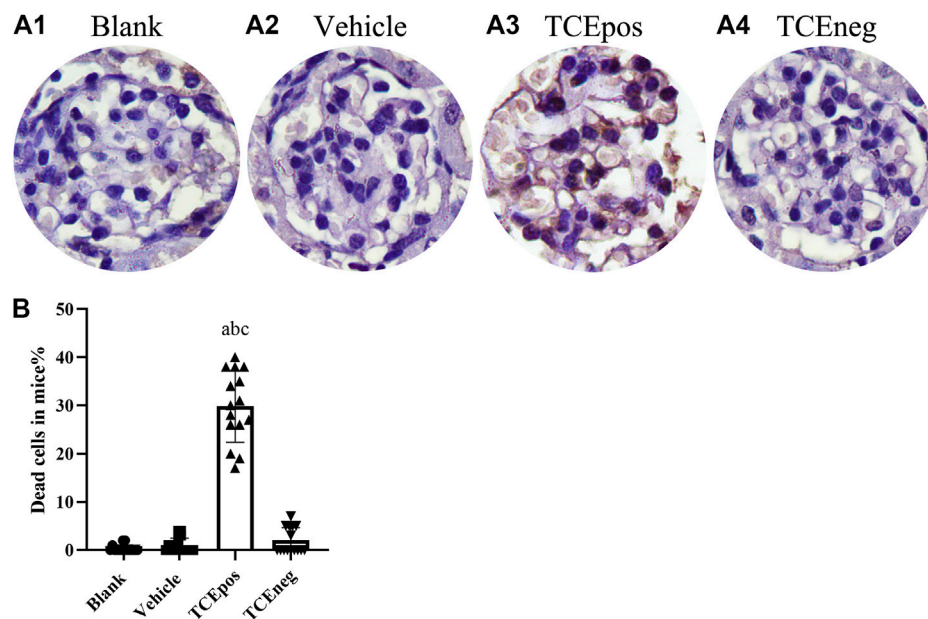
**FIGURE 4** | An increase proportion of dead cells in TCE-induced kidney glomerular damage **(A)** Representative photographs of TUNEL staining in blank control group **(A1)**, vehicle control group **(A2)**, TCEpos group **(A3)**, and TCEneg **(A4)**. **(B)** The proportion of TUNEL staining positive cells in TCE-treated mice. Note: the brown of nuclei indicates the positive staining. Data are presented as mean ± SD and determined by one-way ANOVA, [a]$P < 0.05$, vs. blank control group; [b]$P<0.05$, vs. vehicle control group; [c]$P<0.05$, vs. TCEneg group.

signaling contributes to glomerular cell death due to apoptosis caused by TCE sensitization.

## Cathepsin L–Mediated Hyperactive mTORC1 Signaling in TCE-Induced Glomerular Injury

To further investigate the possible regulator of mTOR signaling, we focused on the lysosomal cysteine protease cathepsin L (CTSL), which is a powerful proteolytic enzyme to regulate cell fate, including apoptosis, autophagy, proliferation, and plays a key role in metastasis (Cocchiaro et al., 2017). In line with our previous studies, we found an increase of CTSL expression in TCEpos group compared to vehicle control group ($p < 0.05$), and the expression of CTSL was mainly blocked in CTSLinh + TCEpos group (**Figures 8A–D**).

We located the CTSL expression in glomeruli via immunofluorescence analysis with colocalization experiment. Using podocin as a hallmark of podocyte, we identified that CTSL was mainly expressed in podocyte (**Figure 8C**). Moreover, we additionally applied CTSL inhibitor to mice and examined the effect on mTOR activation (**Figure 8A**). We showed that p-mTOR was downregulated in CTSLinh + TCEpos group compared with TCEpos group (**Figures 8E,F**). These consistent results suggest that CTSL acts as a key driver for hyperactive mTOR signaling in TCE-induced glomerular damage.

## DISCUSSION

TCE-induced immune kidney disorder is one of the most common complications of OMDT. Although the fatality rate

of which is not more than hepatitis, it is closely related to the severity of disease and associated with a poor prognosis (Wei et al., 2008; Liu, 2009). Diffuse inflammation, renal dysfunction, and positive urinary proteins are often manifested in the process of TCE-induced renal damage (Liu, 2009; Xu et al., 2009). Liu (2009) reported a case after exposure to TCE for about one month with quick deterioration of renal function, displaying with a high level of BUN 23.2 mmol/L, Cre 426.4 μmol/L, and uric acid 660.2 mmol/L. Furthermore, limb edema and oliguria are also involved in some patients (Zhang et al., 2011). Consistently, our previous studies also found an increase of various proinflammatory cytokines, including TNF-α, IL-1β, IL-17, and IL-6, in TCE-hypersensitivity induced kidney damage (Wang et al., 2020; Yang et al., 2020). In this study, we focused on mTOR signaling pathway in TCE-induced inflammatory renal diseases. We measured the levels of urine nephrin to assess the damage of glomerular structure integrity. As expected, the levels of urine nephrin before clinical treatment were higher than that of after clinical treatment, which suggests a loss of nephrin from glomerulus and hence a damage of glomerular structure integrity. Consistent with findings in human cases, we also found glomerular proliferation and swelling in morphology with increased serum levels of BUN and Cre in TCE sensitization positive mice. Therefore, the above observations both in patients and mice pointed out that the normal structure and function of glomerulus are damaged to a certain degree in the process of TCE sensitization.

Acting as the special type of glomerular components, podocyte is a highly polarized epithelial cell with limited capacity to proliferate (Nagata, 2016). The structural integrity of podocyte
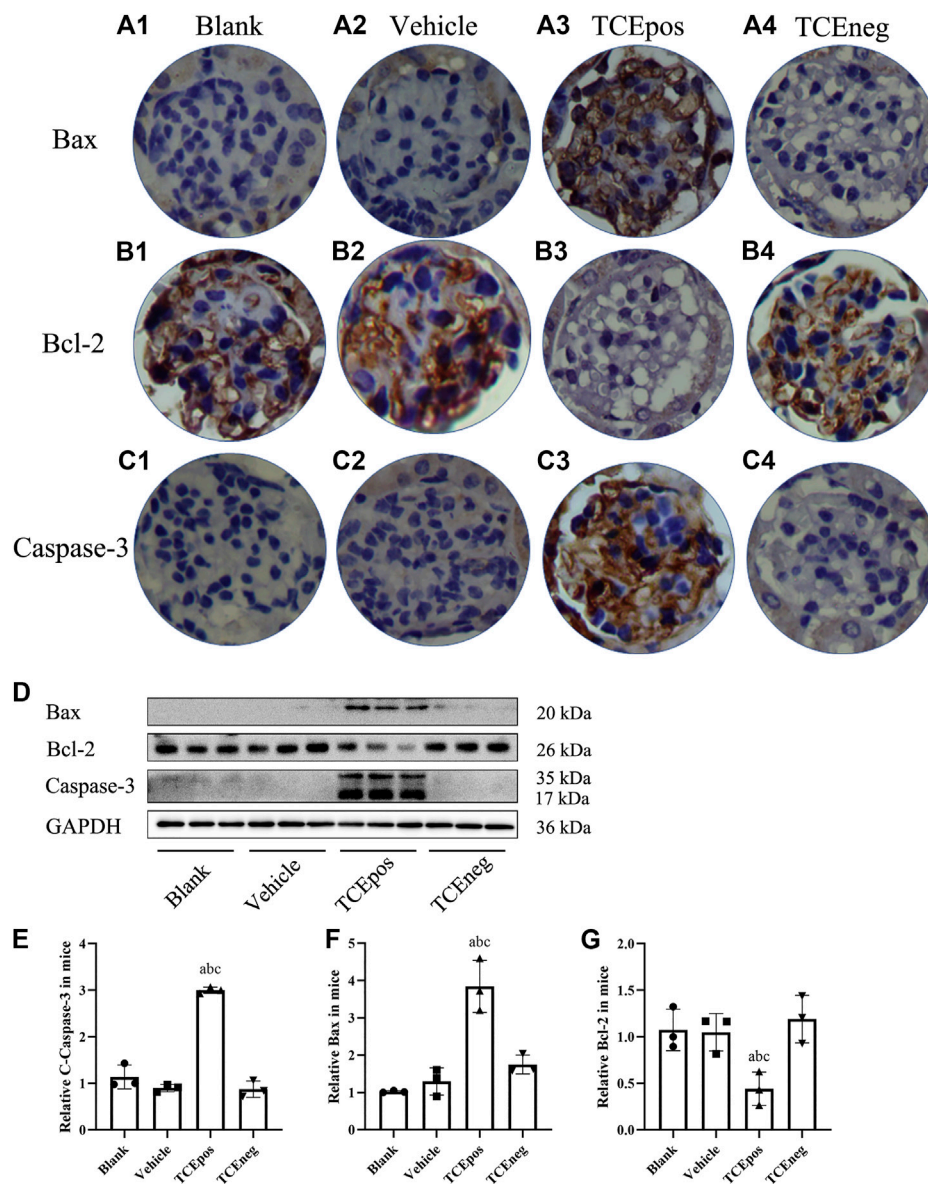
**FIGURE 5 |** Activation of Bax/Bcl-2/caspase-3 pathway in TCE-induced glomerular damage. **(A1–A4)** Expression of proapoptotic molecule Bax; **(B1–B4)** expression of anti-apoptotic molecule Bcl-2; **(C1–C4)** expression of proapoptotic molecule caspase-3 in blank control group, vehicle control group, TCEpos group, and TCEneg group ($n = 5$ per group). **(D)** Western blot bands of Bax, Bcl-2, and caspase-3 in blank control group, vehicle control group, TCEpos group, and TCEneg group ($n = 3$ per group). **(E–G)** Relative expression of Bax, Bcl-2, and caspase-3 calculated by gray values in image J software in above groups. Data are presented as mean ± SD and determined by one-way ANOVA, [a]$P < 0.05$, vs. blank control group; [b]$P<0.05$, vs. vehicle control group; [c]$P<0.05$, vs. TCEneg group.

is essential in the formation of glomerular filtration barrier and the healthy podocytes are required for the normal filtration function (Torban et al., 2019). Loss of podocytes from glomerular basement membrane presented as filtration dysfunction and even proteinuria in various kidney disorders, including diabetic nephropathy, lupus nephropathy, membranous glomerulonephritis, glomerulosclerosis, and so on (Sakhi et al., 2019). In TCE-induced glomerular disorders, podocyte hypertrophy with thickened GBM, fusion of foot processes was found under a transmission electron microscope. Furthermore, we also found that a decline of

integrin β1 which is the transmembrane anchoring molecule for podocyte adhesion to GBM (Perico et al., 2016; Sawada et al., 2016) can likely be a reason for the loss of podocyte. A decrease of α-actinin-4 which is a key molecule for maintain the healthy cytoskeleton may explain the foot process fusion and effacement. Collectively, decline of nephrin, α-actinin-4, and integrin β1 may indicate that podocyte damage participates in the renal dysfunction caused by TCE sensitization.

Furthermore, we also assessed apoptosis of glomerular cells in TCE-induced glomerular damage. Bax and caspase-3 are known to promote the apoptotic progression, whereas Bcl-2 works
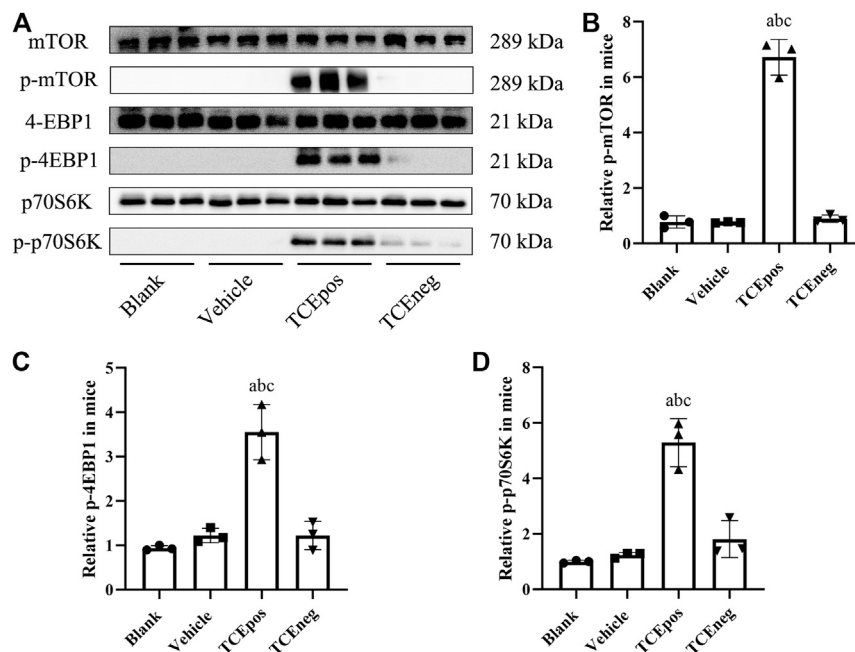
**FIGURE 6 |** Hyperactive mTORC1 pathway was involved in TCE-induced glomerular damage. **(A)** Western blot bands of mTORC1 signaling molecules, mTORC1, p-mTORC1, 4EBP1, p-4EBP1, p70S6K, and p-p70S6K, in blank control group, vehicle control group, TCEpos group, and TCEneg group ($n = 3$ per group) **(B–D)** The relative expression of p-mTOR **(B)**, p-4EBP1 **(C)**, and p-p70S6K **(D)** calculated by gray values in ImageJ software in above groups. Data are presented as mean ± SD and determined by one-way ANOVA, [a]$P < 0.05$, vs. blank control group; [b]$P<0.05$, vs. vehicle control group; [c]$P<0.05$, vs. TCEneg group.
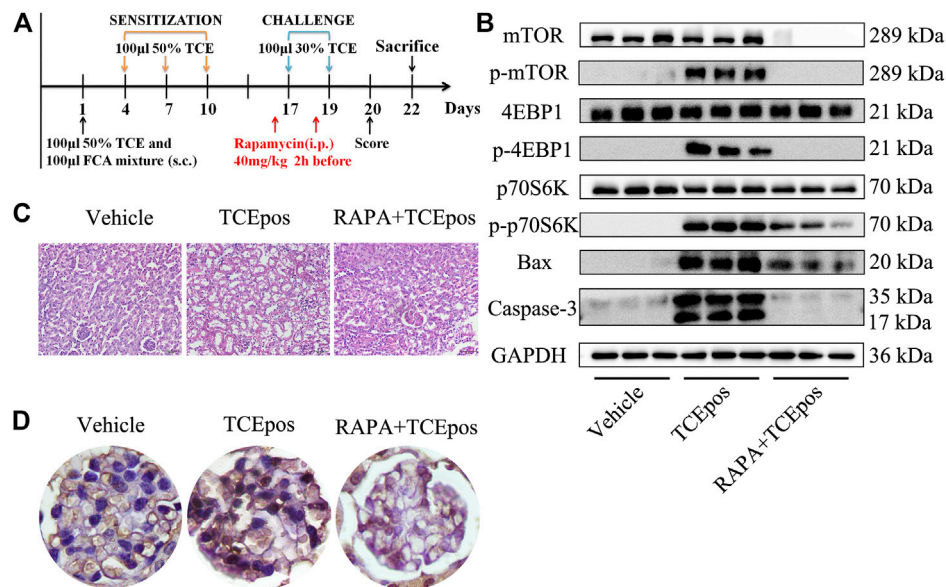


**FIGURE 7 |** mTORC1 pathway inhibition alleviated the glomerular damage in TCE sensitization. **(A)** mTORC1 inhibitor (rapamycin, RAPA) was applied to mice by intraperitoneal injection at 40 mg/kg 2 h before each challenge. **(B)** Phosphorylation process of mTOR signaling molecules were almost blocked and the proapoptotic molecules Bax and caspase-3 were also declined in RAPA + TCEpos group according to western blot bands ($n = 3$ per group). **(C)** The pathological changes of glomeruli were improved dramatically in mice from RAPA + TCEpos group. **(D)** The representative photograph of TUNEL staining showed less dead glomerular cells in RAPA + TCEpos group.
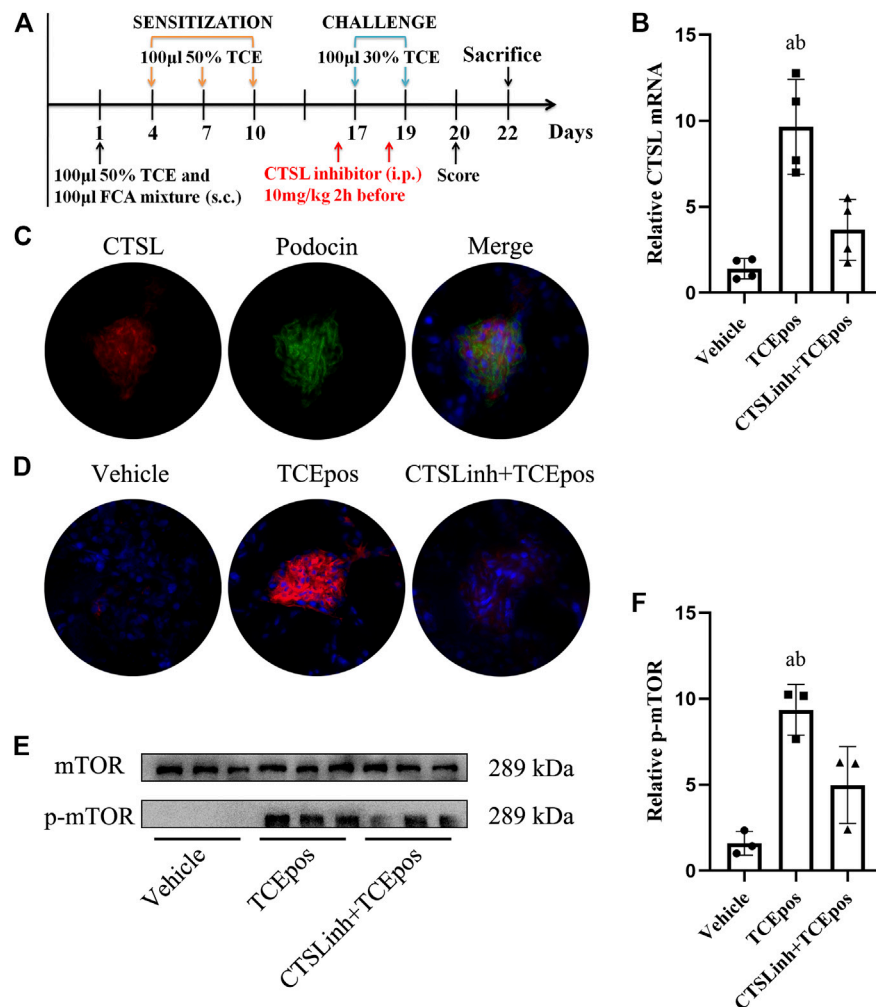
**FIGURE 8** | Cathepsin L (CTSL) mediated hyperactive mTORC1 signaling in TCE-induced glomerular injury. **(A)** CTSL inhibitor (CTSLinh) was applied to mice by intraperitoneal injection at 10 mg/kg 2 h before each challenge. **(B)** The relative expression of *CTSL mRNA* in vehicle group, TCEpos group, and CTSLinh + TCEpos group according to RT-PCR analysis (*n* = 4 per group). **(C)** The co-location of CTSL and podocin (a podocyte marker) in glomerulus of TCEpos group. **(D)** The expression of CTSL confirmed by immunofluorescence test (*n* = 5 per group). **(E)** Western blot bands of mTORC1 and p-mTORC1 in vehicle control group, TCEpos group, and CTSLinh + TCEpos group (*n* = 3 per group). **(F)** The relative expression of p-mTOR calculated by gray values in ImageJ software. Data are presented as mean ± SD and determined by one-way ANOVA, *$p$ < 0.05.

conversely (Ma et al., 2020). The balance between the pro-apoptotic Bax, caspase-3 and anti-apoptotic Bcl-2 determines cell survival or death (Pal et al., 2016). We showed that the proportion of both apoptotic glomerular cells and the pro-apoptotic Bax and caspase-3 were increased in TCE positive sensitized mice. Thus, these coherent data suggest that glomerular apoptosis also contribute to the TCE-induced kidney damage.

To uncover the molecular mechanism of podocyte damage and glomerular apoptosis, we focused on mTORC1 signaling which has proven to be critical in glomerular diseases via promoting cellular growth and metabolism (Zschiedrich et al., 2017; Lei et al., 2018). However, hyperactivated mTORC1 signaling was considered to be the main causes of podocyte hypertrophy, foot process fusion, and ultimately cell death (Puelles et al.,

2019). During activation of mTORC1 signaling, two downstream molecules, p70S6K and 4EBP1, are phosphorylated (Hall et al., 2018). In this study, the over-activation of mTORC1 signaling was evidenced by increased expression of p-mTOR, p-p70S6K, and p-4EBP1. To further elucidate the role of mTORC1 signaling in TCE-induced glomerular damage, we applied rapamycin by intraperitoneal injection to TCE positive sensitized mice. After rapamycin pretreatment, the hyperactive mTORC1 signaling was effectively minimized in mice glomerulus. Furthermore, we found that glomerular apoptosis and structural destruction were also ameliorated after pharmacological inhibition of hyperactive mTORC1 signaling. Collectively, we identified that hyperactive mTORC1 signaling caused glomerular damage and rapamycin reversed cell injuries in TCE-induced glomerular damage.

Furthermore, we explored the possible upstream driver of mTORC1 signaling in TCE-induced glomerular damage. Studies have shown that CTSL could cleave the key elements of normal podocyte architecture and cause podocyte reorganization, foot process effacement, and even proteinuria (Reiser et al., 2010). In addition, a role of CTSL in regulation of mTORC1 signaling activation via cleaving intracellular complement 3 has been reported (Satyam et al., 2017). Our previous studies have also found that over-expressed CTSL could aggravate kidney damage via activating intracellular complement system and inducing endothelin-1 signaling to promote the release of inflammatory cytokines (Wang et al., 2020; Yang et al., 2020). In this study, we further located CTSL to podocyte and investigated whether over-expressed CTSL played a role in mTORC1-mediated glomerular damage. We found that a downregulation of mTOR phosphorylation after CTSL inhibitor pretreatment. Therefore, these results suggest that CTSL could be a driver for hyperactive mTORC1 signaling in TCE-induced glomerular damage.

However, there are some limitations in the present study. First, only 6 OMDT cases were enrolled in the present study due to the fact that OMDT is a rare but life-threatening disorder with a prevalence of less than 1% among TCE-exposed workers and the overall incidence was less than 1 case/million adults/year (Lin et al., 2019). Second, only female mice were used to establish the mouse model of TCE skin sensitization. Two main reasons were considered. On the one hand, there is no evidence of sex-based differences in TCE-sensitized workers, and both male and female exposure workers are susceptible to TCE sensitization. On the other hand, female mice have been shown to exhibit more consistent pronounced inflammatory response than male mice with elevated levels of CD4^{+} T-cells and relevant proinflammatory cytokine, and thereby are more widely used in animal models of allergic diseases, like asthma, atopic dermatitis, and allergic rhinitis (Melgert et al., 2005). Third, no *in vitro* sensitization experiment was performed, as how to maintain the *in situ* environment of TCE sensitization *in vitro* is unresolved. Finally, the mouse model of TCE sensitization is an appropriate substitute of guinea pig maximization test (GPMT), which is a classical method for evaluating skin sensitization by various chemicals including TCE, but it's not widely used due to lack of relevant antibodies and reagents for guinea pigs.

In conclusion, our results highlight that glomerular damage involved in TCE-induced immune kidney disorder in which hyperactive mTORC1 signaling contributed to podocyte loss, hypertrophy, and glomerular apoptosis in TCE-induced glomerular injuries. Furthermore, our data identify a role of CTSL in the regulation of over-activated mTORC1 signaling in TCE sensitization positive mice and the associate glomerular damage.

## DATA AVAILABILITY STATEMENT

The original contributions presented in the study are included in the article/Supplementary Material; further inquiries can be directed to the corresponding authors.

## ETHICS STATEMENT

The studies involving human participants were reviewed and approved by the Biomedical Ethics Committee of Anhui Medical University. The patients/participants provided their written informed consent to participate in this study. The animal study was reviewed and approved by Experimental Animal Ethics Committee of Anhui Medical University.

## AUTHOR CONTRIBUTIONS

FW, XZ, and QZ assisted with experimental design, data analysis, and manuscript writing; YD, MH, and CZ contributed by conducting the mice experiment; LH, HW, LY, and QW conducted the recruitment of study participants.

## FUNDING

## REFERENCES

Byrum, S. D., Washam, C. L., Patterson, J. D., Vyas, K. K., Gilbert, K. M., and Blossom, S. J. (2019). Continuous Developmental and Early Life Trichloroethylene Exposure Promoted DNA Methylation Alterations in Polycomb Protein Binding Sites in Effector/Memory CD4(+) T Cells. *Front. Immunol.* 10, 2016. doi:10.3389/fimmu.2019.02016

Cocchiaro, P., De Pasquale, V., Della Morte, R., Tafuri, S., Avallone, L., Pizard, A., et al. (2017). The Multifaceted Role of the Lysosomal Protease Cathepsins in Kidney Disease. *Front Cel Dev Biol* 5, 114. doi:10.3389/fcell.2017.00114

Cui, Z., Liu, L., Kwame Amevor, F., Zhu, Q., Wang, Y., Li, D., et al. (2020). High Expression of miR-204 in Chicken Atrophic Ovaries Promotes Granulosa Cell Apoptosis and Inhibits Autophagy. *Front. Cel Dev Biol* 8, 580072. doi:10.3389/fcell.2020.580072

Fantus, D., Rogers, N. M., Grahammer, F., Huber, T. B., and Thomson, A. W. (2016). Roles of mTOR Complexes in the Kidney: Implications for Renal Disease and Transplantation. *Nat. Rev. Nephrol.* 12, 587–609. doi:10.1038/nrneph.2016.108

Guha, N., Loomis, D., Grosse, Y., Lauby-Secretan, B., Ghissassi, F. E., Bouvard, V., et al. (2012). Carcinogenicity of Trichloroethylene, Tetrachloroethylene, Some Other Chlorinated Solvents, and Their Metabolites. *Lancet. Oncol.* 13, 1192-1193. doi:10.1016/s1470-2045(12)70485-0

Hall, G., Lane, B. M., Khan, K., Pediaditakis, I., Xiao, J., Wu, G., et al. (2018). The Human FSGS-Causing ANLN R431C Mutation Induces Dysregulated PI3K/AKT/mTOR/Rac1 Signaling in Podocytes. *Jasn* 29, 2110–2122. doi:10.1681/asn.2017121338

Huang, P., Ren, X., Huang, Z., Yang, X., Hong, W., Zhang, Y., et al. (2014). Serum Proteomic Analysis Reveals Potential Serum Biomarkers for Occupational Medicamentosa-like Dermatitis Caused by Trichloroethylene. *Toxicol. Lett.* 229, 101–110. doi:10.1016/j.toxlet.2014.05.024

Huang, Y., Xia, L., Wu, Q., Zeng, Z., Huang, Z., Zhou, S., et al. (2015). Trichloroethylene Hypersensitivity Syndrome Is Potentially Mediated through its Metabolite Chloral Hydrate. *PLoS One* 10, e0127101. doi:10.1371/journal.pone.0127101

Iarc (2014). *Agents Classified by the IARC Monographs*, Lyon, France: International Agency for Research on Cancer.

Kriz, W., and Lemley, K. V. (2015). A Potential Role for Mechanical Forces in the Detachment of Podocytes and the Progression of CKD. *Jasn* 26, 258–269. doi:10.1681/asn.2014030278

Lee, K.-M., Zhang, L., Vermeulen, R., Hu, W., Bassig, B. A., Wong, J. J., et al. (2019). Alterations in Immune and Renal Biomarkers Among Workers Occupationally Exposed to Low Levels of Trichloroethylene below Current Regulatory Standards. *Occup. Environ. Med.* 76, 376–381. doi:10.1136/oemed-2018-105583

Lei, J., Zhao, L., Zhang, Y., Wu, Y., and Liu, Y. (2018). High Glucose-Induced Podocyte Injury Involves Activation of Mammalian Target of Rapamycin (mTOR)-Induced Endoplasmic Reticulum (ER) Stress. *Cell Physiol Biochem* 45, 2431–2443. doi:10.1159/000488231

Li, W., Liu, X., Yang, X., Chen, Y., Pang, Y., Qi, G., et al. (2019). Effect of Trichloroacetaldehyde on the Activation of CD4+T Cells in Occupational Medicamentosa-like Dermatitis: An In Vivo and In Vitro Study. *Toxicology* 423, 95–104. doi:10.1016/j.tox.2019.05.014

Lin, D., Wang, D., Li, P., Yang, Y., Liu, W., Zhang, L., et al. (2019). A Pilot Study to Assess Peripheral Blood TCR β-chain CDR3 Repertoire in Occupational Medicamentosa-like Dermatitis Due to Trichloroethylene Using High-Throughput Sequencing. *Environ. Toxicol. Pharmacol.* 71, 103211. doi:10.1016/j.etap.2019.103211

Liu, J. (2009). Clinical Analysis of Seven Cases of Trichloroethylene Medicamentose-like Dermatitis. *Ind. Health* 47, 685–688. doi:10.2486/indhealth.47.685

Ma, M., Wang, X., Liu, N., Shan, F., and Feng, Y. (2020). Low-dose Naltrexone Inhibits Colorectal Cancer Progression and Promotes Apoptosis by Increasing M1-type Macrophages and Activating the Bax/Bcl-2/caspase-3/PARP Pathway. *Int. Immunopharmacology* 83, 106388. doi:10.1016/j.intimp.2020.106388

Maeda, K., Otomo, K., Yoshida, N., Abu-Asab, M. S., Ichinose, K., Nishino, T., et al. (2018). CaMK4 Compromises Podocyte Function in Autoimmune and Nonautoimmune Kidney Disease. *J. Clin. Invest.* 128, 3445–3459. doi:10.1172/jci99507

Melgert, B. N., Postma, D. S., Kuipers, I., Geerlings, M., Luinge, M. A., Strate, B. W. A., et al. (2005). Female Mice Are More Susceptible to the Development of Allergic Airway Inflammation Than Male Mice. *Clin. Exp. Allergy* 35, 1496–1503. doi:10.1111/j.1365-2222.2005.02362.x

Ministry of Health (2006). *Diagnostic Criteria of Occupational Medicamentosa-like Dermatitis Due to Trichloroethylene*. Beijing: People's Medical Publishing House.

Nagata, M. (2016). Podocyte Injury and its Consequences. *Kidney Int.* 89, 1221–1230. doi:10.1016/j.kint.2016.01.012

Pal, M. K., Jaiswar, S. P., Srivastav, A. K., Goyal, S., Dwivedi, A., Verma, A., et al. (2016). Synergistic Effect of Piperine and Paclitaxel on Cell Fate via Cyt-C, Bax/Bcl-2-Caspase-3 Pathway in Ovarian Adenocarcinomas SKOV-3 Cells. *Eur. J. Pharmacol.* 791, 751–762. doi:10.1016/j.ejphar.2016.10.019

Pan, Y., Hou, X., Meng, Q., Yang, X., Shang, L., Wei, X., et al. (2019). The Critical Role for TAK1 in Trichloroethylene-Induced Contact Hypersensitivity In Vivo and in CD4+ T Cell Function Alteration by Trichloroethylene and its Metabolites In Vitro. *Toxicol. Appl. Pharmacol.* 380, 114705. doi:10.1016/j.taap.2019.114705

Perico, L., Conti, S., Benigni, A., and Remuzzi, G. (2016). Podocyte-actin Dynamics in Health and Disease. *Nat. Rev. Nephrol.* 12, 692–710. doi:10.1038/nrneph.2016.127

Priante, G., Gianesello, L., Ceol, M., Del Prete, D., and Anglani, F. (2019). Cell Death in the Kidney. *Int. J. Mol. Sci.* 20. doi:10.3390/ijms20143598

Puelles, V. G., Van Der Wolde, J. W., Wanner, N., Scheppach, M. W., Cullen-Mcewen, L. A., Bork, T., et al. (2019). mTOR-mediated Podocyte Hypertrophy Regulates Glomerular Integrity in Mice and Humans. *JCI Insight* 4. doi:10.1172/jci.insight.99271

Reiser, J., Adair, B., and Reinheckel, T. (2010). Specialized Roles for Cysteine Cathepsins in Health and Disease. *J. Clin. Invest.* 120, 3421–3431. doi:10.1172/jci42918

Rinschen, M. M., Hoppe, A.-K., Grahammer, F., Kann, M., Völker, L. A., Schurek, E.-M., et al. (2017). N-degradomic Analysis Reveals a Proteolytic Network Processing the Podocyte Cytoskeleton. *Jasn* 28, 2867–2878. doi:10.1681/asn.2016101119

Sakhi, H., Moktefi, A., Bouachi, K., Audard, V., Henique, C., Remy, P., et al. (2019). Podocyte Injury in Lupus Nephritis. *J. Clin. Med.* 8. doi:10.3390/jcm8091340

Satyam, A., Kannan, L., Matsumoto, N., Geha, M., Lapchak, P. H., Bosse, R., et al. (2017). Intracellular Activation of Complement 3 Is Responsible for Intestinal Tissue Damage during Mesenteric Ischemia. *J.I.* 198, 788–797. doi:10.4049/jimmunol.1502287

Sawada, K., Toyoda, M., Kaneyama, N., Shiraiwa, S., Moriya, H., Miyatake, H., et al. (2016). Upregulation of Alpha3beta1-Integrin in Podocytes in Early-Stage Diabetic Nephropathy. *J. Diabetes Res.* 2016, 9265074. doi:10.1155/2016/9265074

Torban, E., Braun, F., Wanner, N., Takano, T., Goodyer, P. R., Lennon, R., et al. (2019). From Podocyte Biology to Novel Cures for Glomerular Disease. *Kidney Int.* 96, 850–861. doi:10.1016/j.kint.2019.05.015

Wang, F., Huang, L.-p., Dai, Y.-y., Huang, M., Jiang, W., Ye, L.-p., et al. (2019a). Terminal Complement Complex C5b-9 Reduced Megalin and Cubilin-Mediated Tubule Proteins Uptake in a Mouse Model of Trichloroethylene Hypersensitivity Syndrome. *Toxicol. Lett.* 317, 110–119. doi:10.1016/j.toxlet.2019.10.002

Wang, F., Huang, L.-p., Yang, P., Ye, L.-p., Wu, C., and Zhu, Q.-x. (2019b). Inflammatory Kidney Injury in Trichloroethylene Hypersensitivity Syndrome Mice: Possible Role of C3a Receptor in the Accumulation of Th17 Phenotype. *Ecotoxicology Environ. Saf.* 186, 109772. doi:10.1016/j.ecoenv.2019.109772

Wang, G., Zhang, J., Dai, Y., Xu, Q., and Zhu, Q. (2020). Local Renal Complement Activation Mediates Immune Kidney Injury by Inducing Endothelin-1 Signalling and Inflammation in Trichloroethylene-Sensitised Mice. *Toxicol. Lett.* 333, 130–139. doi:10.1016/j.toxlet.2020.07.036

Wang, H., Zhang, J.-x., Li, S.-l., Wang, F., Zha, W.-s., Shen, T., et al. (2015). An Animal Model of Trichloroethylene-Induced Skin Sensitization in BALB/c Mice. *Int. J. Toxicol.* 34, 442–453. doi:10.1177/1091581815591222

Wei, J. H., Xian-Min, G. E., Su-Hua, S. U., Liang, Q. R., Chen, J., and Hang-Tian, L. I. (2008). *Clinical Observation on 6 Cases of Occupational Medicamentose-like Dermatitis Induced by Trichloroethylene*. China Occupational Medicine.

Xu, X., Yang, R., Wu, N., Zhong, P., Ke, Y., Yuan, L. J., et al. (2009). Severe Hypersensitivity Dermatitis and Liver Dysfunction Induced by Occupational Exposure to Trichloroethylene. *Ind. Health* 47, 107–112. doi:10.2486/indhealth.47.107

Yang, X., Jiang, W., Huang, M., Dai, Y., Li, B., Wang, X., et al. (2020). Intracellular Complement Activation in Podocytes Aggravates Immune Kidney Injury in Trichloroethylene-Sensitized Mice. *J. Toxicol. Sci.* 45, 681–693. doi:10.2131/jts.45.681

Zhang, L. H., She, X. J., Min, L. I., Huang, L. R., and Liu, J. H. (2011). Dynamic Observation on Kidneys,livers and Spleens by Brightness Mode Ultrasonic Imaging in Patients of Occupational Medicamentosa-like Dermatitis Induced by Trichloroethylene. *Chin. J. Ind. Med.* 24, 185–187.

Zschiedrich, S., Bork, T., Liang, W., Wanner, N., Eulenbruch, K., Munder, S., et al. (2017). Targeting mTOR Signaling Can Prevent the Progression of FSGS. *Jasn* 28, 2144–2157. doi:10.1681/asn.2016050519

**Conflict of Interest:** The authors declare that the research was conducted in the absence of any commercial or financial relationships that could be construed as a potential conflict of interest.

**Publisher's Note:** All claims expressed in this article are solely those of the authors and do not necessarily represent those of their affiliated organizations, or those of the publisher, the editors and the reviewers. Any product that may be evaluated in this article, or claim that may be made by its manufacturer, is not guaranteed or endorsed by the publisher.

# Dual sEH/COX-2 Inhibition Using PTUPB—A Promising Approach to Antiangiogenesis-Induced Nephrotoxicity

Wojciech K. Jankiewicz[1]*[†], Scott D. Barnett[1†], Anna Stavniichuk[1†], Sung Hee Hwang[2†], Bruce D. Hammock[2†], Jawad B. Belayet[3†], A. H. Khan[1] and John D. Imig[1†]*

[1]Drug Discovery Center and Cardiovascular Center, Medical College of Wisconsin, Milwaukee, WI, United States, [2]Department of Entomology and Nematology and Comprehensive Cancer Center, University of California, Davis, Davis, CA, United States, [3]Department of Chemistry and Biochemistry, University of Wisconsin Milwaukee, Milwaukee, WI, United States

Kidney injury from antiangiogenic chemotherapy is a significant clinical challenge, and we currently lack the ability to effectively treat it with pharmacological agents. Thus, we set out to investigate whether simultaneous soluble epoxide hydrolase (sEH) and cyclooxygenase-2 (COX-2) inhibition using a dual sEH/COX-2 inhibitor PTUPB could be an effective strategy for treating antiangiogenic therapy-induced kidney damage. We used a multikinase inhibitor, sorafenib, which is known to cause serious renal side effects. The drug was administered to male Sprague–Dawley rats that were on a high-salt diet. Sorafenib was administered over the course of 56 days. The study included three experimental groups; 1) control group (naïve rats), 2) sorafenib group [rats treated with sorafenib only (20 mg/kg/day p.o.)], and 3) sorafenib + PTUPB group (rats treated with sorafenib only for the initial 28 days and subsequently coadministered PTUPB (10 mg/kg/day i.p.) from days 28 through 56). Blood pressure was measured every 2 weeks. After 28 days, sorafenib-treated rats developed hypertension (161 ± 4 mmHg). Over the remainder of the study, sorafenib treatment resulted in a further elevation in blood pressure through day 56 (200 ± 7 mmHg). PTUPB treatment attenuated the sorafenib-induced blood pressure elevation and by day 56, blood pressure was 159 ± 4 mmHg. Urine was collected every 2 weeks for biochemical analysis. After 28 days, sorafenib rats developed pronounced proteinuria (9.7 ± 0.2 P/C), which intensified significantly (35.8 ± 3.5 P/C) by the end of day 56 compared with control (2.6 ± 0.4 P/C). PTUPB mitigated sorafenib-induced proteinuria, and by day 56, it reduced proteinuria by 73%. Plasma and kidney tissues were collected on day 56. Kidney histopathology revealed intratubular cast formation, interstitial fibrosis, glomerular injury, and glomerular nephrin loss at day 56 in sorafenib-treated rats. PTUPB treatment reduced histological features by 30%–70% compared with the sorafenib-treated group and restored glomerular nephrin levels. Furthermore, PTUPB also acted on the glomerular permeability barrier by decreasing angiotensin-II-induced glomerular permeability to albumin. Finally, PTUPB improved *in vitro* the viability of human mesangial cells. Collectively, our data demonstrate the potential of using PTUPB or dual sEH/COX-2 inhibition as a therapeutic strategy against sorafenib-induced glomerular nephrotoxicity.

Keywords: cyclooxygenase (COX), soluble epoxide hydrolase (sEH), vascular endothelial growth factor, nephrotoxicity, kidney injury, glomerular injury, eicosanoids, multitarget drugs

# INTRODUCTION

Antiangiogenic drugs are widely used in cancer treatment. They block neovascularization of tumors and, thus, prevent tumor growth. Vascular endothelial growth factor (VEGF) tyrosine kinase inhibitors (TKIs) are a major class of these drugs. They are used to treat malignant neoplasms and, more recently, age-related neovascular macular degeneration, which is an irreversible eye disease leading to blindness (Apte et al., 2019). VEGF TKIs comprise a wide class of compounds: sorafenib, regorafenib, axitinib, cabozantinib, lenvatinib, nintedanib, pazopanib, sunitinib, and vandetanib. To date, the FDA has approved sorafenib for three indications: treatment of advanced renal cell carcinoma (approved in 2005), treatment of inoperable hepatocellular carcinoma (approved in 2007), and treatment of metastatic differentiated thyroid cancer (approved in 2013) (White and Cohen, 2015). Sorafenib inhibits angiogenesis by targeting c-Kit, FLT-3, VEGFR-2, VEGFR-3, and PDGFR-β, and inhibits proliferation through targeting Raf-1, B-Raf, and Ras/Raf/MEK/ERK (Zhu et al., 2017). VEGF TKIs are used alone or in combination therapy with immune checkpoint inhibitors (Rassy et al., 2020). With around 400,000 cases of renal cell carcinoma, 500,000 cases of hepatocellular carcinoma, and 500,000 cases of thyroid cancer diagnosed each year, to date, sorafenib has potentially saved thousands of lives (Bray et al., 2018).

Unfortunately, VEGF TKIs come with severe limitations in the form of hypertension, proteinuria, and renal injury (Humphreys and Atkins, 2009; Jhaveri et al., 2011; Estrada et al., 2019; Versmissen et al., 2019; Neves et al., 2020). Current guidelines involve monitoring and management of the side effects including blood pressure medications to lower hypertension (Versmissen et al., 2019). Renal injury from VEGF TKIs includes glomerular barrier breakdown, mesangiolysis, and thrombotic microangiography (Kelly et al., 2009; Overkleeft et al., 2009; Estrada et al., 2019). These are serious problems because kidney damage can force discontinuation of an otherwise effective anticancer therapy as glomerular injury can progress to chronic kidney disease or life-threatening end-stage renal disease (Venkatachalam et al., 2010). Importantly, there are no pharmacological means that could help protect the kidneys from the injury. A strong need exists for a pharmacological agent that could diminish kidney injury that is caused by VEGF TKIs. We propose that dual soluble epoxide hydrolase (sEH)/cyclooxygenase-2 (COX-2) inhibition can protect the kidneys from VEGF-TKI-induced damage by decreasing glomerular damage.

PTUPB is a dual sEH/COX-2 inhibitor, which acts to increase epoxyeicosatrienoic acids and decrease COX-2 inflammatory prostanoids (Cheng et al., 2002; Hye Khan et al., 2016; Sun et al., 2020). sEH inhibition lowers blood pressure, decreases inflammation, and can combat glomerular and kidney injury (Yu et al., 2000; Imig, 2012; Kim et al., 2014; Liu, 2019; Jiang et al., 2020). COX-2 is involved in the production of inflammatory prostanoids, and its inhibition is known to decrease kidney injury (Cheng et al., 2002; Fujihara et al., 2003; Harris, 2013). Earlier studies have shown PTUPB to highly selectively inhibit COX-2 over COX-1 (Hwang et al., 2011).

Our lab has previously shown that PTUPB can mitigate kidney injury in a rat model of diabetic nephropathy (Hye Khan et al., 2016). Other studies have shown that PTUPB can reduce inflammation, oxidative stress, and cell senescence (Dileepan et al., 2019; Sun et al., 2020; Zhang et al., 2020). PTUPB has also been reported to improve nonalcoholic fatty liver disease, at least in part, through inhibiting inflammation (Sun et al., 2020). Previous work also indicates that PTUPB can prevent cisplatin-, carboplatin-, and paclitaxel-induced cytokine and eicosanoid storm and suppress debris-stimulated ovarian tumor growth (Zhang et al., 2020). Emerging evidence also suggests that PTUPB has antitumor activity and can potentiate tumor cytotoxicity of other drugs (Li et al., 2017; Wang et al., 2018). In the current study, we demonstrate that interventional PTUPB treatment can protect the kidney from sorafenib-induced nephrotoxicity.

# MATERIALS AND METHODS

## Chemicals

The chemistry and synthesis process of dual COX-2/sEH inhibitor, 4-(5-phenyl-3-{3-[3-(4-trifluoromethylphenyl)-ureido]-propyl}-pyrazol-1-yl)-benzenesulfonamide (PTUPB) was described earlier (Hwang et al., 2011). Sorafenib was obtained from LC Laboratories (Woburn, MA, USA). Unless otherwise stated, all chemicals used in this study were obtained from Sigma Aldrich (St. Louis, MO, USA).

## Animal study

This study was approved and carried out according to the guidelines of the Medical College of Wisconsin Institutional Animal Care and Use Committee. The Biomedical Resource Center at the Medical College of Wisconsin housed animals with free access to water and food under a 12/12 h light–dark cycle. Male Sprague–Dawley rats (8–10 weeks old) were purchased from Charles River Laboratories, Spokane, IL, USA. The study comprised three treatment groups: control group, sorafenib group, and sorafenib + PTUPB group (**Figure 1A**, $n = 8$ rats/group). Rats were acclimated to blood pressure measurements over the course of 7 days prior to the commencement of the study. The animals were placed on a high-salt diet (8% NaCl) (TD.92012, Envigo, Madison, WI, USA). Systolic blood pressure was measured on days 0, 14, 28, 42, and 56 using a tail cuff system (IITC Life Science, Woodland Hills, CA, USA). Sorafenib was orally administered to the sorafenib and sorafenib + PTUPB groups at a dose of 20 mg/kg/day. PTUPB was coadministered in the sorafenib + PTUPB group at a dose of 10 mg/kg/day from day 28 through 56 through an intraperitoneal osmotic pump (ALZET® osmotic pump, DURECT Corporation, Cupertino, CA, USA). Urine samples were collected using metabolic cages on days 0, 28, and 56. On day 56, animals were euthanized; blood and kidney samples were obtained. Kidney samples for histological and immunohistochemical studies were fixed in 10% buffered formalin and stored at room temperature. Kidney tissue samples for gene expression analysis were snap frozen in liquid nitrogen and stored at −80°C.
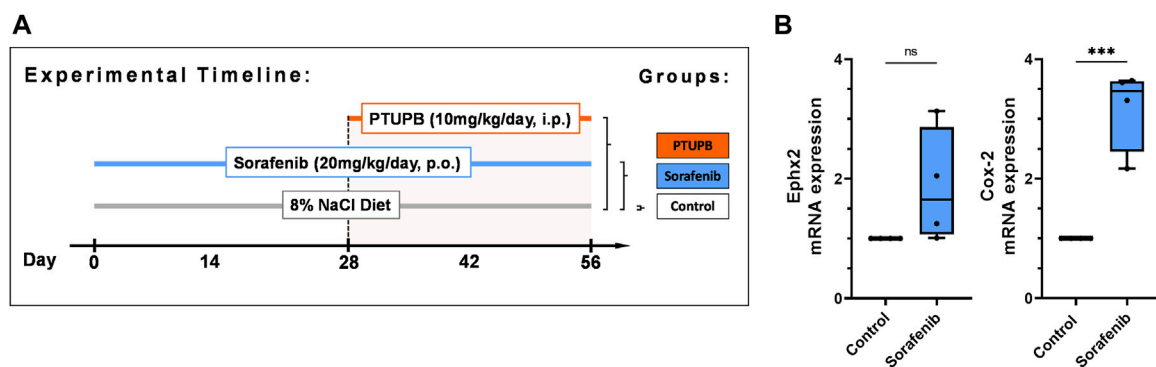
**FIGURE 1 |** Overview. Timeline showing the experimental design **(A)**. Expression of soluble epoxide hydrolase enzyme (Ephx2) and cycolooxygenase-2 (COX-2) sorafenib treatment **(B)**. ($n$ = 4–6 rats/group, Dots represent the average of duplicate measures for each individual rat. ns $p > 0.05$, ***$p \leq 0.001$ determined by Student's t-test. Data are reported as box and whisker plots with median, minimum to maximum, and 10 to 90 percentiles.

## Real-time polymerase chain reaction

MRNA expression of Ephx2, Cox-2, ZEB1, TWIST, and α-SMA was determined by real-time polymerase chain reaction (RT-PCR). Samples were homogenized using TissueLyser II (Qiagen, Redwood City, CA, USA). RNA was extracted from sample homogenates using the RNeasy Mini Kit (Qiagen, Redwood City, CA, USA) according to the protocol of the manufacturer. The RNA samples were quantified spectrophotometrically with a NanoDrop, and 1 µg of total RNA was reverse transcribed to cDNA using iScript™ Select cDNA Synthesis Kit (Bio-Rad, Hercules, CA, USA). Gene expression was quantified by iScript One-Step RT-PCR Kit with SYBR green using the MyiQ™ Single Color RT-PCR Detection System (Bio-Rad Laboratories, Hercules, CA, USA). Dissociation curve analysis was performed with iQ5 Optical System Software, Version 2.1 (Bio-Rad Laboratories, Hercules, CA, USA). Each amplified sample was analyzed for homogeneity. Samples were denatured at 95°C for 2 min. Next, the PCR was performed using a protocol of 40 cycles at 95°C for 10 s and at 60°C for 30 s. Samples were run in triplicate. Gene expression fold changes were compared with controls determined by the comparative threshold cycle (Ct) method. Target gene expression levels were determined by normalizing Ct values to housekeeping genes. Statistical analyses were carried out using six samples from each experimental group and comparing with the control group.

## Histology

Renal tissues were fixed in 10% formalin, sectioned at 5-µm thickness, mounted on slides, and stained with periodic acid-Schiff (PAS) (Acros Organics, Fairlawn, NJ, USA) or picrosirius red (PSR) (Alfa Aesar, Tewksbury, MA, USA). PAS-stained renal sections were evaluated for the presence of tubular casts. PSR-stained renal sections were evaluated for collagen-positive renal interstitial fibrotic changes and expressed as percent area relative to the total area analyzed. Glomerular injury was blindly scored on kidney sections stained with PAS staining using the following numeric scale: 0 = no damage; +1 = very mild; +2 = mild; +3 = moderate and +4 = severe. All analyses were conducted by two

observers in a blinded fashion for histological examination at ×200 magnification using NIS Elements AR version 3.0 imaging software (Nikon Instruments Inc., Melville, NY, USA).

## Immunofluorescence

Kidney slides were deparaffinized and rehydrated followed by overnight incubation with an anti-nephrin antibody (1:100; Santa Cruz Biotechnology, Inc., Dallas, TX, USA) to determine renal expression of nephrin. Donkey anti-rabbit IgG H&L (Alexa Fluor® 488) secondary antibody (1:200; Abcam, Cambridge, MA, USA) was used for development with fluorescence quenching liquid (Vector Laboratories, Burlingame, CA, USA). Stained histological sections were examined with a Nikon 55i microscope at ×200 magnification with fluorescent excitation, and images were analyzed using Nikon NIS Elements Software (Nikon Instruments Inc., Melville, NY, USA). Positively stained areas specific for the target protein used were expressed as percent area relative to total area analyzed. Analyses were carried out by two observers blinded to sample identity.

## Glomerular permeability

Glomeruli were isolated from adult male Sprague–Dawley rats, and the experiment was performed following a previously described protocol (Ilatovskaya et al., 2017). First, to label the inside of the glomeruli, kidneys were perfused through the femoral vein with an FTIC–dextran solution (150-kDa FTIC–dextran in 0.9% NaCl) (TdB Consultancy AB, Uppsala, Sweden) and isolated. The following steps were performed on ice: The kidney cortex was separated from the medulla and cut into 1-mm³ cubes. Next, the glomeruli were separated by differential sieving (sieve nos. 100, 150, and 200). Sieve no. 200 was used to capture the glomeruli. The isolated glomeruli were stored in a 5% BSA–TRITC–dextran solution (150-kDa TRITC–dextran and 5% BSA in RMPI) (TdB Consultancy AB, Uppsala, Sweden) and stored on ice for immediate use in experiments. The isolated glomeruli were incubated with angiotensin II (002-12, Phoenix Pharmaceuticals) for 30 min, and co-incubated with angiotensin II and PTUPB for 30 min. Under experimental conditions, the 5%

BSA bath solution was exchanged for a 1% BSA solution, and a change in glomerular volume occurred due to the oncotic gradient. Glomerular volume changes were monitored using the Nikon A1R+ (Nikon Instruments Inc., Melville, NY, USA) and calculated from z-stack reconstructions using the Fiji image analysis software (ImageJ 1.52s, National Institute of Health, MD, USA) (Schindelin et al., 2012). The relative change in volume, $\{\Delta V = [(V_{final} - V_{initial})/V_{initial}] * 100\}$, can be compared with control values to obtain the ratio of the oncotic force exerted by that solute to its theoretical oncotic force, which is called the reflection coefficient ($\sigma alb = \Delta V_{experimental}/\Delta V_{control}$). From here a conventional permeability value is obtained ($Palb = 1 - \sigma alb$) for which a value of "1" denotes complete permeability of albumin, and a value of "0" signifies no permeability of albumin relative to the control.

## Cell culture

Human renal mesangial cells (4200, ScienCell, Carlsbad, CA, USA) were cultured at 37°C (in 5% $CO_2$) in RPMI 1640 medium (Gibco™, LS11875093) containing 10% FBS, 100 U/ml of penicillin, and 0.1 mg/ml of streptomycin. The cells were subcultured following the protocol of the manufacturer. Human prostate cancer cells (DU145) (HTB-81, ATCC, Manassas, VA, USA) were cultured at 37°C (in 5% $CO_2$) in Eagle's minimum essential medium (EMEM) (0-2003, ATCC, Manassas, VA, USA) containing 100 U/ml of penicillin and 0.1 mg/ml of streptomycin. The cells were subcultured per the protocol of the manufacturer.

## Cell viability

Human renal mesangial cells or human prostate cancer cells were plated in a 96-well TPP plate and allowed to adhere. Mesangial cells were serum starved for 24 h prior to treatment. The cells were pretreated with PTUPB and incubated for 1 h. Next, sorafenib was added, and the cells were incubated for 48 h. At the end, cell viability was determined using an MTT assay (ab211091, Abcam, Cambridge, MA, USA). The experimental media were aspirated, and the cells were incubated in an MTT reagent solution for 3 h (50 μl of the MTT reagent in 50 μl of FBS-free culture media per well). Next, the MTT reagent solution was aspirated, and the cells were solubilized. The plate was placed on an orbital shaker and mixed at a high setting for 30 min. Absorbance was read using the FLUOstar Omega spectrometer (BMG Labtech Inc., Cary, NC, USA) at 590 nm.

## Proliferation

Mesangial cell proliferation was determined by live cell imaging. Mesangial cells were seeded at 7,500 cells per well in a 96-well TPP plate, allowed to adhere, treated with sorafenib, and imaged over 48 h using an Incucyte system (Sartorius, Göttingen, Germany) configured with a ×4 objective. Cell confluency was calculated as percent area and expressed as fold change relative to the initial confluency at hour 0 using the Fiji image analysis software (ImageJ 1.52s, National Institute of Health, MD, USA).

## Apoptosis

Mesangial cells were seeded on glass coverslips in a 24-well plate and grown to 80%–90% confluency and subsequently treated with sorafenib and/or PTUPB and incubated over 24 h. Apoptosis was measured using the TUNEL assay (C10245, Thermofisher, Waltham, MA, USA) per the instructions of the manufacturer. Cell nuclei were stained using the Hoechst 33342 nuclear dye (1: 5,000) provided with the kit. Stained coverslips were visualized at a ×200 magnification with a fluorescence microscope. The analysis was carried out using the Fiji image analysis software (ImageJ 1.52s, National Institute of Health, MD, USA). Total fluorescent signal was measured relative to the number of cells in a field of vision. Analysis was carried out by two observers blinded to the sample identity.

## Statistical analysis

All data are expressed as mean values. GraphPad Prism® Version 4.0 software was utilized to conduct a one-way ANOVA followed by Tukey's *post-hoc* test to establish statistical significance between the groups (GraphPad Software Inc., La Jolla, CA, USA). Two-tailed unpaired Student's *t*-test was applied to determine statistical significance between groups. Value of $p \leq 0.05$ were considered significant.

# RESULTS

## Sorafenib treatment upregulated soluble epoxide hydrolase and cyclooxygenase-2 expression in the kidneys

After 56 days of treatment, sorafenib resulted in an upregulation of mRNA expression of two enzymes metabolizing arachidonic acid metabolites in the kidneys: the soluble epoxide hydrolase enzyme (Ephx2) was upregulated 1.9-fold, and the cycolooxygenase-2 enzyme (COX-2) was upregulated 3.2-fold. (**Figure 1B**).

## PTUPB mitigated the blood pressure elevation and progression of proteinuria

To monitor the overall disease progression and impact on kidney and cardiovascular health, we collected urine samples and measured the blood pressure at designated time points throughout the study. At the outset, the average blood pressure in all three groups was 114 ± 4 mmHg. After the sorafenib treatment started, the blood pressure in the sorafenib-treated and control animals begun to diverge. Halfway into the study (day 28), the blood pressures in the animals that received sorafenib increased by 48 mmHg compared with those of the control group (**Figure 2A**). PTUPB treatment began on day 28 (**Figure 1A**). Throughout the remainder of the study, the blood pressure of the animals that were being treated with sorafenib alone continued to increase and ultimately rose by an additional 39 mmHg (day 56). In contrast, blood pressure in the animals of the sorafenib + PTUPB group was decreased by 7 mmHg (**Figure 2A**).

Urinary protein excretion followed a similar trend. At the beginning protein excretion was low in all animals. Over the course of the study, protein excretion in the control group
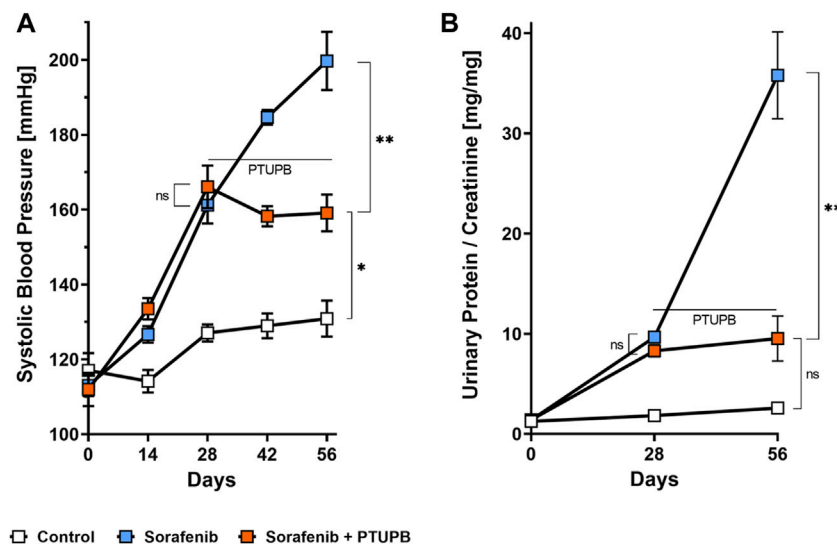
**FIGURE 2 |** Blood pressure and proteinuria. Hypertension developed in the sorafenib-treated animals (blue trace); the rise in blood pressure was mitigated by 4-(5-phenyl-3-{3-[3-(4-trifluoromethylphenyl)-ureido]-propyl}-pyrazol-1-yl)-benzenesulfonamide (PTUPB) coadministration (orange trace) **(A)**. Proteinuria developed in the sorafenib group (blue trace), which was mitigated by PTUPB (orange trace) **(B)**. The horizontal line marks when PTUPB started being coadministered alongside sorafenib in the PTUPB group (n = 4–8 rats/group, average at each time point represents duplicate measures for each individual rat, ns $p > 0.05$, *$p \le 0.05$, **$p \le 0.01$ determined by ANOVA followed by the Tukey *post-hoc* test). Data are reported as connected scatterplots with SEM.

remained relatively steady. However, the sorafenib-treated animals showed a different trend. On day 28, their urinary protein levels were 4.9-fold higher than the control group. On day 56, animals that received sorafenib alone showed pronounced proteinuria, with urinary protein levels that are 13.9-fold higher than the control group. In contrast, the urinary protein levels in animals that had been cotreated with PTUPB were 73% lower. The data show that the intervention with PTUPB could reverse the progression of sorafenib-induced proteinuria (**Figure 2B**).

## PTUPB mitigated the progression of renal fibrosis and tubular injury

Tubulopathies appear with kidney injury and indicate disease progression. We assessed the extent of tubular cast formation in the renal cortex and medulla. In general, we found significant amounts of tubular casts after 56 days of sorafenib administration. However, tubular casts covered a significantly lower percent area in the sections of PTUPB-treated animals. We have assessed these changes separately in the cortex and medulla portions of the sections. Although cortical casts were not yet fully evident by day 28 of sorafenib treatment, the beginnings of their formation were visible. After 56 days of sorafenib administration, cortical casts were increased by 21.7-fold compared with the control group. This increase was successfully mitigated by cotreatment with PTUPB, which reduced the cortical casts by 62% compared with the sorafenib group (**Figure 3A**). Similarly, medullary casts were increased by 6.2-fold after 28 days of sorafenib administration, and by 10.5-fold after 56 days. PTUPB cotreatment lowered the cortical and medullary cast areas by 39% and 64%, respectively (**Figure 3B**).

We next studied the impact of sorafenib and PTUPB on renal fibrosis. Kidney sections were stained with picrosirius red (PSR) to visualize collagen-positive areas. Kidney fibrotic changes were increased by 9.7-fold after 28 days, and 25.5-fold after 56 days of sorafenib administration. Cotreatment with PTUPB decreased fibrosis by 69% with respect to day 28, and by 88% with respect to day 56; this suggests that PTUPB stopped, or may have even reversed, fibrosis progression (**Figure 4B**). These fibrotic changes were reflected in epithelial-to-mesenchymal transition (EMT) marker mRNA expression levels. Sorafenib increased ZEB1 expression by 44.1-fold, TWIST expression by 4.6-fold, and α-SMA by 2.1-fold over the control. In contrast, PTUPB treatment reduced ZEB1 expression by 63%, TWIST expression by 93%, and α-SMA expression by 48% compared with the sorafenib group (on day 56). (**Figure 4A**).

## PTUPB mitigated glomerular injury

The extent of glomerular injury was histologically assessed and scored on a 1–4 scale, where a higher number denotes a greater extent of renal injury. After 56 days, the glomerular injury in the sorafenib group was increased by 5.7-fold, which was decreased by cotreatment with PTUPB by 33% (**Figures 5A, B**). We next determined whether our treatments affected nephrin level changes, as nephrin is a key protein necessary for glomerular health. On day 56, nephrin levels were decreased in the sorafenib group by 73%, and PTUPB cotreatment resulted in a 2.8-fold improvement (**Figures 5C, D**).

To see if PTUPB can protect the glomerular filtration barrier itself, we tested its impact on the permeability of isolated glomeruli to albumin *in vitro*. Glomeruli were preincubated with PTUPB, and glomerular permeability was increased with
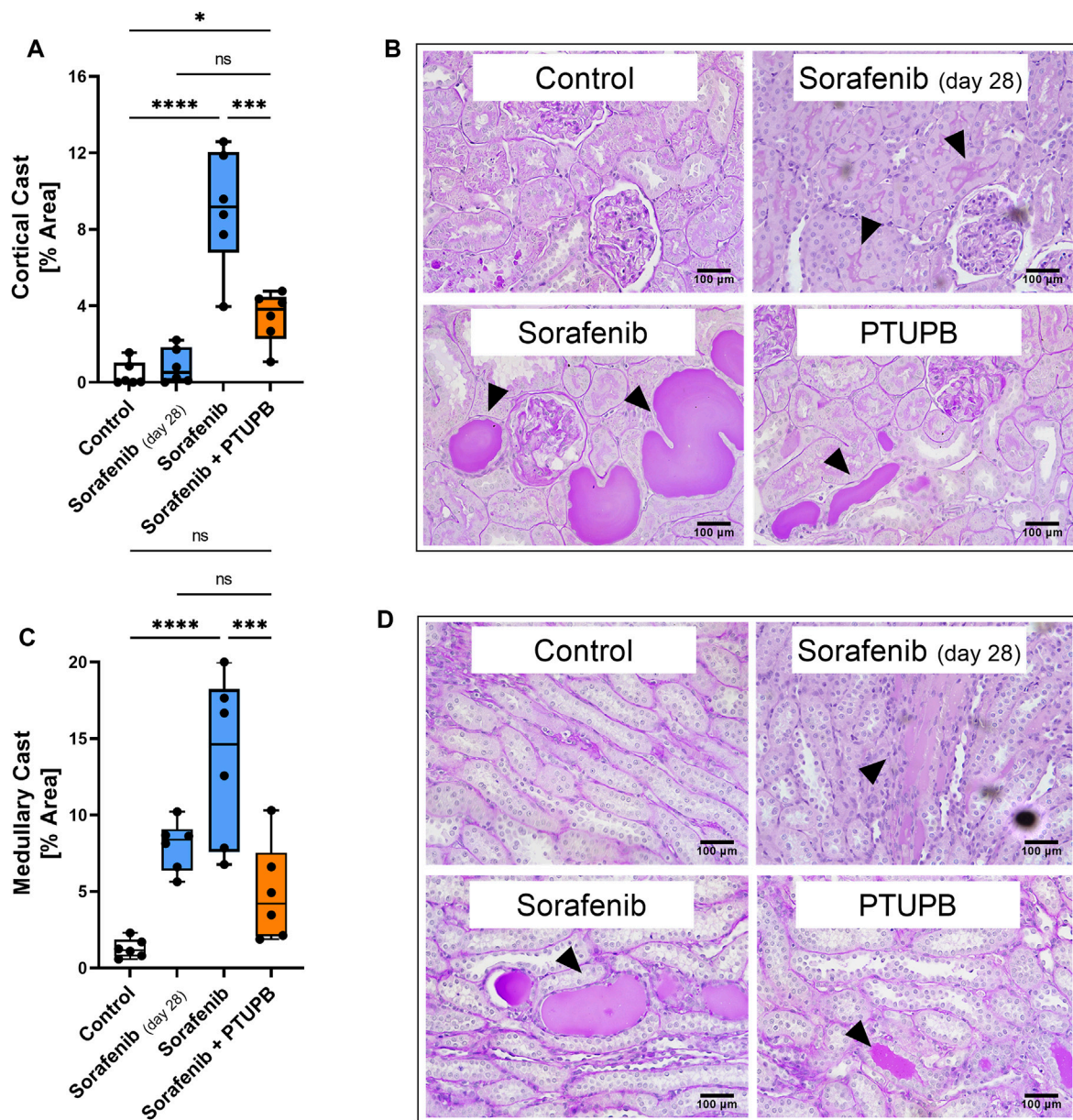
**FIGURE 3 |** Tubular injury. Sorafenib induced and PTUPB mitigated intratubular cast formation in the cortex **(A)**. Representative images of cortical casts [periodic acid-Schiff (PAS) staining]. Arrowheads point to cast areas. **(B)** Sorafenib induced and PTUPB mitigated intratubular cast formation in the medulla **(C)**. Representative images of cortical casts (PAS staining). Arrowheads point to cast areas. **(D)** ($n$ = 6 rats/group. Dots represent the average of duplicate measures for each individual rat., ns $p > 0.05$, *$p \leq 0.05$, **$p \leq 0.01$, ***$p \leq 0.001$, ****$p \leq 0.0001$ determined by ANOVA followed by the Tukey *post-hoc* test. Data are reported as box and whisker plots with median, minimum to maximum, and 10 to 90 percentiles.

angiotensin II. PTUPB reduced the angiotensin-II-induced glomerular permeability by 51%, which shows that PTUPB can protect the glomerular filtration barrier (**Figure 5E**). Next, we studied whether PTUPB can impact mesangial cell viability since mesangial cell death, mesangiolysis, is a common feature seen with sorafenib nephrotoxicity. We wanted to test if PTUPB could protect against sorafenib-induced mesangial cytotoxicity. We found that after 48 h, sorafenib decreased mesangial viability by 24% compared with the control, and coincubation with

PTUPB increased their viability by 1.4-fold, restoring it back to control levels (**Figure 5F**). Finally, we evaluated the contribution of apoptosis to sorafenib-induced mesangial cytotoxicity. We confirmed that sorafenib is cytotoxic to cultured mesangial cells (**Figure 6A**) and determined that sorafenib induced apoptosis in mesangial cells, with the highest dose, 10 µM, increasing apoptotic signal by 3.9-fold (**Figure 6B**). PTUPB lowered sorafenib-induced mesangial cell apoptosis by 69% (**Figures 7A, B**). These findings demonstrate
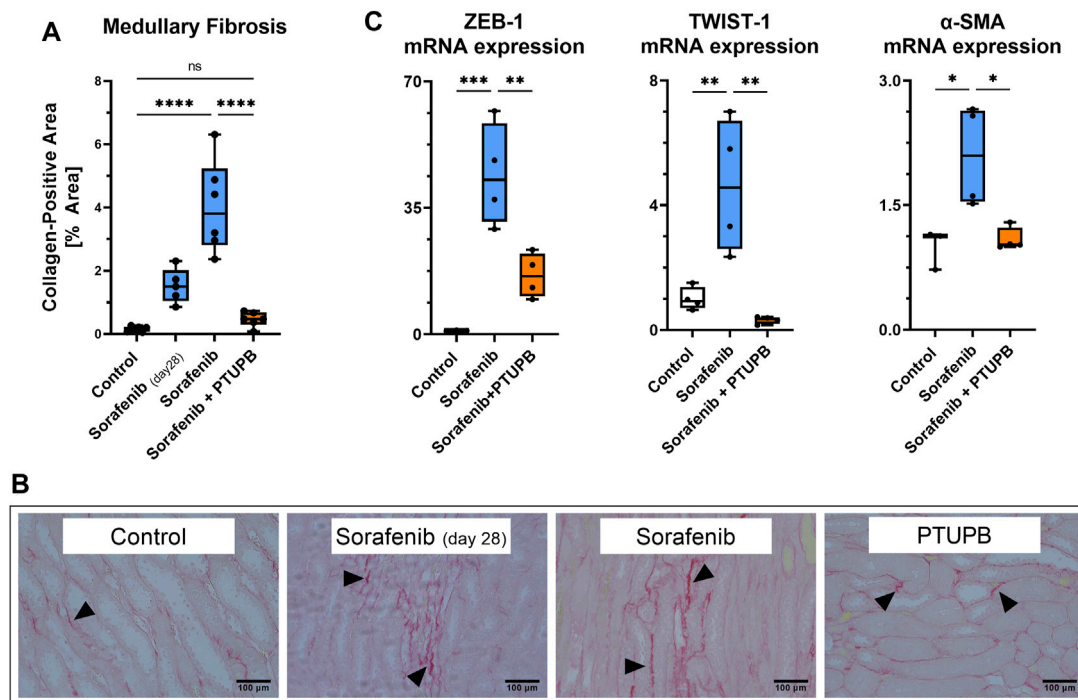
**FIGURE 4 |** Fibrosis. Fibrotic changes developed in the medulla of sorafenib-treated animals. PTUPB reversed fibrosis progression **(A)**. Representative images of fibrotic changes [picrosirius red (PSR) staining]. Arrowheads point to fibrotic areas. **(B)** Sorafenib treatment elevated ZEB-1 and TWIST-1 (EMT markers) as well as α-SMA (myofibroblast marker). PTUPB mitigated the increase in those markers **(C)**. $n$ = 4–6 rats/group. Dots represent the average of duplicate measures for each individual rat. ns $p$ > 0.05, *$p$ ≤ 0.05, **$p$ ≤ 0.01, ***$p$ ≤ 0.001, ****$p$ ≤ 0.0001 determined by ANOVA followed by the Tukey *post-hoc* test. Data are reported as box and whisker plots with median, minimum to maximum, and 10 to 90 percentiles.

direct PTUPB actions at the level of the glomerulus and the mesangial cell to combat sorafenib-induced nephrotoxicity.

## PTUPB does not impair the antitumor activity of sorafenib

Finally, we tested whether in combination, PTUPB would interfere with the antitumor activity of sorafenib. To answer this question, human prostate cancer cells were cotreated with sorafenib and PTUPB together. We found that in the 1- to 10-μM range, PTUPB did not adversely affect the antitumor activity of sorafenib (**Figure 8B**).

## DISCUSSION

Antiangiogenic chemotherapeutics have become a major class of drugs deployed for the treatment of solid tumors (neoplasms). They inhibit the VEGF signaling pathway and neovascularization of tumors, which prevents the blood supply to a tumor, thus, limiting tumor growth (Grothey and Galanis, 2009). Despite their effectiveness as tumor-combating agents, VEGF TKIs can exert a range of adverse effects on cardiovascular and kidney health (Kappers et al., 2009; Perazella, 2012; Estrada et al., 2019; Neves et al., 2020; Dobbin et al., 2021). In the present study, sorafenib caused elevation of kidney sEH and COX-2 enzymes. Previous

findings have demonstrated that sEH and COX-2 induction has been linked to inflammation and kidney injury (Imig, 2006). Thus, dual inhibition of sEH and COX-2 enzymes with PTUPB could offer a successful treatment approach. Our findings affirmed it. We found that PTUPB mitigates hypertension in sorafenib-treated animals. The present finding fits the current understanding that sEH inhibition can lower blood pressure (Zhang et al., 2020). This is important as the overall hypertension incidence in patients who receive sorafenib ranges from 6% to 43%, which is a significant clinical limitation for this class of drugs (Wu et al., 2008; Chang et al., 2017; Caletti et al., 2018; Plummer et al., 2019).

Kidney injury is a further complication of VEGF TKI chemotherpy (Izzedine et al., 2010). We found that sorafenib caused extensive proteinuria, and PTUPB successfully mitigated its development, keeping urinary protein levels comparable with those of the control group. Patients who receive sorafenib are at risk for developing proteinuria; a meta-analysis showed that the overall incidence of proteinuria in patients on anti-VEGF therapy is 63% including 6.3% for those treated for renal small cell carcinoma (Izzedine et al., 2010). A meta-analysis showed 12% overall incidence in all grades of proteinuria with sorafenib (Zhang et al., 2014a). Evidence suggests that sEH and COX-2 induction is intimated in inflammation and kidney injury (Imig, 2006; Liu, 2019). Consequently, a genome-wide associate study of 406 subjects found that an sEH polymorphism lowering sEH
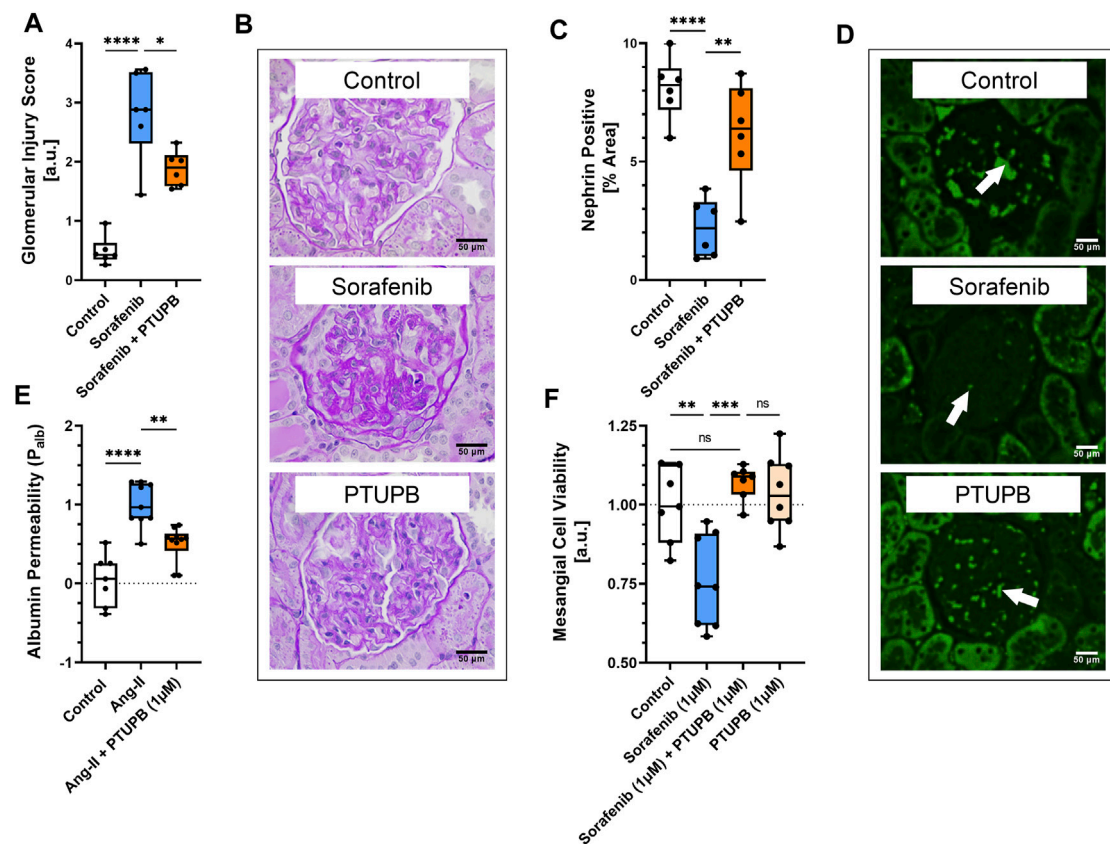
**FIGURE 5 |** Glomerular injury. Glomerular injury resulted from sorafenib-treatment (blue bar). PTUPB cotreatment improved glomerular histological features (orange bar) **(A)**. Representative images of fibrotic changes (PAS staining) **(B)**. Nephrin loss was evident in sorafenib-treated glomeruli (blue bar). PTUPB mitigated nephrin loss (orange bar) **(C)**. Representative images of nephrin changes in glomeruli (IF, nephrin stain). White arrows point to nephrin-positive areas **(D)**. PTUPB mitigated Ang-II-induced glomerular permeability (orange bar) **(E)**. PTUPB rescued mesangial cells from sorafenib cytotoxicity **(F)**. **(A–D)** $n$ = 4–6 rats/group. Dots represent the average of duplicate measures for each individual rat. **(E)** $n$ = 7–10 glomeruli from four rats. **(F)** $n$ = 7–8. Dots represent the average of duplicate measures for each well. ns $p > 0.05$, *$p \leq 0.05$, **$p \leq 0.01$, ***$p \leq 0.001$, ****$p \leq 0.0001$ determined by ANOVA followed by the Tukey *post-hoc* test. Data are reported as box and whisker plots with median, minimum to maximum, and 10 to 90 percentiles.

activity was associated with better outcomes in diabetic nephropathy (Ma et al., 2018). A similar study reported that sEH deletion has been found to mitigate kidney injury caused by streptozotocin in diabetic mice and lessen kidney injury in DOCA-salt hypertension (Manhiani et al., 2009; Elmarakby et al., 2011). At the same time, COX-2 overexpression predisposes podocytes, a major cell type of the glomerular filtration barrier, to mechanical stress injury (Cheng et al., 2007). In addition to targeting VEGF signaling, sorafenib also inhibits sEH (Hwang et al., 2013). However, sorafenib nephrotoxicity persists and is likely due to VEGF signaling actions prevailing at the level of the glomerulus in addition to the increase in kidney COX-2 expression. This suggests that further inhibition of sEH combined with COX-2 inhibition could be beneficial. Indeed, combined sEH and COX-2 inhibition with PTUPB decreased sorafenib-induced nephrotoxicity. Our present finding is consistent with the previous studies using Zucker diabetic rats, where PTUPB was also found to decrease kidney injury and proteinuria (Hye Khan et al., 2016; Khan et al., 2021).

Kidney injury can further manifest in tubular damage (tubulopathies). We found that PTUPB effectively decreased tubular injury both in the renal cortex and medulla. A common manifestation of various kinds of kidney injury is fibrosis, and VEGF inhibition has been found to exacerbate fibrosis in other organ systems such as the lungs (Partovian et al., 2000; Tuleta and Frangogiannis, 2021). We found that PTUPB halted the progression of renal fibrosis caused by sorafenib. Furthermore, the extent of fibrotic damage was less than at the outset of the treatment (day 28), which suggests that PTUPB may have reversed some of the fibrotic damage. This is also consistent with our previous work in the diabetic nephropathy model where we found that an 8-week treatment with PTUPB decreased fibrosis in Zucker diabetic rats and lowered it to control levels (Hye Khan et al., 2016). The effects of PTUPB on tissue fibrosis have been studied in the context of pulmonary fibrosis and non-alcoholic fatty liver disease. Zhang et al. (2020) found that PTUPB pretreatment decreased fibrosis in the lungs of bleomycin-treated mice. Remarkably, PTUPB was effective for treating fibrosis even when introduced at a stage

**FIGURE 6 |** Mesangial cytotoxicity. Sorafenib was cytotoxic to cultured mesangial cells. Sample time–course graph showing decrease in mesangial cell confluency with sorafenib treatment **(A)**. Sorafenib resulted in a dose-dependent increase in mesangial cell apoptosis **(B)**. $n$ = 5–10. Dots represent the average of duplicate measures for each well. *** $p \leq 0.001$, **** $p \leq 0.0001$ determined by ANOVA followed by the Tukey *post-hoc* test. Data are reported as a connected scatterplot and a box and whisker plot with median, minimum to maximum, and 10 to 90 percentiles.



**FIGURE 7 |** Apoptosis. PTUPB decreased sorafenib-induced apoptosis. Sorafenib treatment elevated apoptotic signal in mesangial cells (orange bar). PTUPB mitigated apoptotic signal in mesangial cells (blue bar) **(A)**. Representative images of TUNEL staining at ×200 (TUNEL signal in green) ($n$ = 5–10, dots represent the average of duplicate measures for each well). ns $p > 0.05$, *** $p \leq 0.001$ determined by ANOVA followed by the Tukey *post-hoc* test. Data are reported as a box and whisker plot with median, minimum to maximum, and 10 to 90 percentiles.

when fibrotic changes were mature; much like in the present study, the fibrotic changes were reversed. Zhang et al. (2020) presented evidence that these effects of PTUPB on fibrosis likely were mediated by inhibition of senescence. Sun et al. (2020) found that liver fibrosis induced by a high-fat diet was significantly diminished when mice received PTUPB over the course of 12 weeks. In the kidneys, renal tubular epithelial cells can transform into activated fibroblasts, called myofibroblasts, which highly express α-SMA. Myofibroblasts then secrete extracellular proteins such as collagens and fibronectin (Fragiadaki and Mason, 2011). This transformation process is referred to as EMT. TWIST and ZEB1 are transcription factors that promote EMT (Vandewalle et al., 2009; Fragiadaki and Mason, 2011; Wang et al., 2016; Sheng and Zhuang, 2020). Notably, we found that PTUPB lowered EMT—it downregulated 1) the transcriptional activators of EMT, TWIST and ZEB1, and 2) a myofibroblast marker, α-SMA. In the lung, Zhang et al. observed a similar decrease in α-SMA levels with PTUPB treatment (Zhang et al., 2020). The same effect of lowering α-SMA protein expression in the liver was reported by Sun et al. (2020). Furthermore, PTUPB was found to inhibit glioblastoma growth through a mechanism that involved a drastic downregulation of ZEB1 and which the authors believed was linked to PTUPB inhibiting HMMR/SOX-2 signaling (Li et al., 2017). In summary, it appears that a plausible mechanism by which PTUPB mitigates renal damage (tubular damage and fibrosis) involves blocking the transformation of renal epithelial tubular cells into myofibroblasts through EMT.
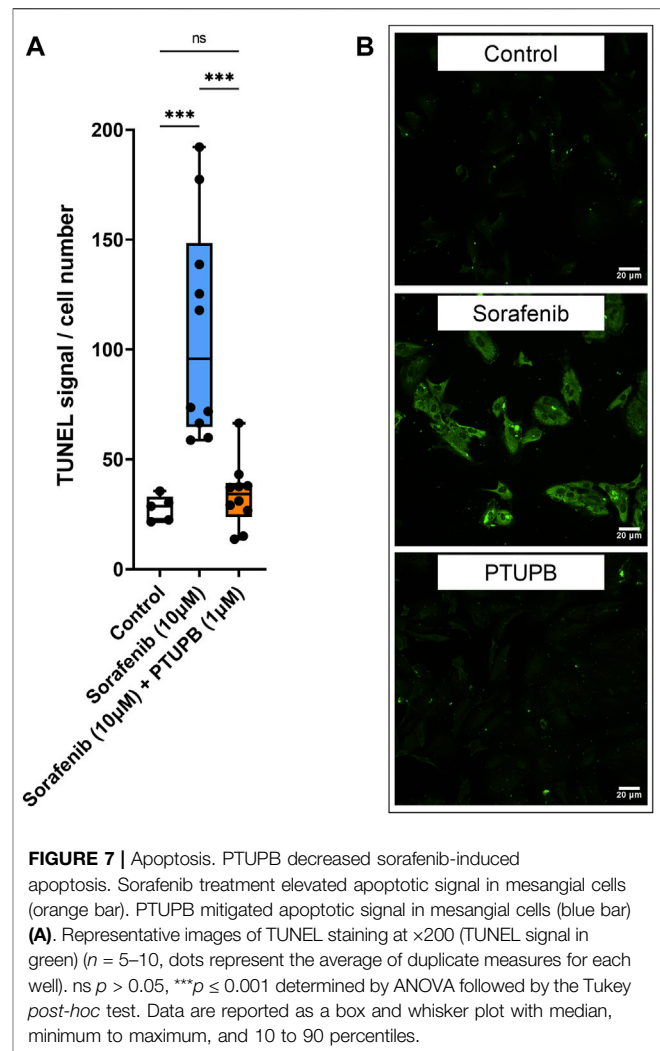
Glomerular health is vital to renal function. We found that PTUPB mitigated the otherwise extensive glomerular damage features caused by sorafenib. The glomerulus is the part of a nephron where plasma filtration takes place. This is made possible by the glomerular filtration barrier that allows for retaining elements in the plasma (and keeping them out of the filtrate). At least one likely mechanism through which PTUPB fortifies glomeruli against injury is by preventing podocyte nephrin loss. Nephrin is essential to glomerular health. Expressed by podocytes, it participates in forming the slit diaphragm, a structure that supports the glomerular filtration barrier functional integrity (Yu et al., 2018). Nephrin loss ultimately leads to podocyte effacement and proteinuria (Faul, 2014; Garg, 2018). We found that sorafenib caused significant loss of nephrin in the glomeruli. This is consistent with other reports indicating that VEGF signaling inhibition results in nephrin loss (Izzedine et al., 2010; Lankhorst et al., 2015; Terrasse, 2015). Remarkably, PTUPB treatment prevented sorafenib-induced nephrin loss and restored it to levels similar to those of the control. We further confirmed that PTUPB protected the glomerular
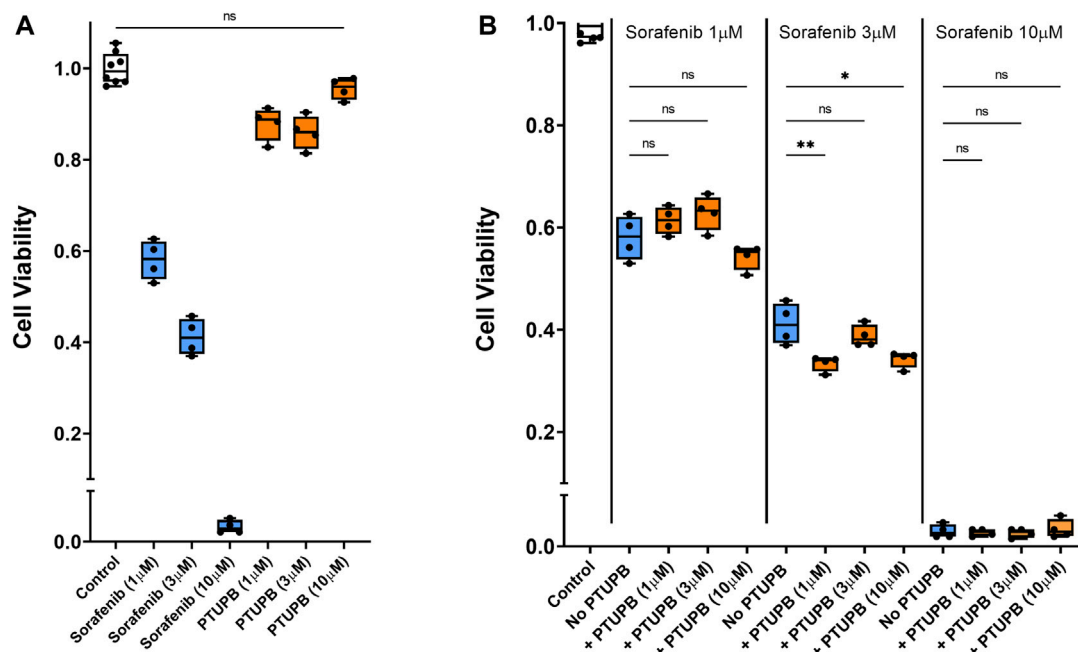
**FIGURE 8 |** Chemotherapeutic effectiveness. PTUPB did not interfere with the antitumor activity of sorafenib against the DU-145 prostate cancer cells. Sorafenib decreased viability of prostate cancer cells in a dose-dependent fashion, while PTUPB alone lacked cytotoxic effects in these cells **(A)**. In combination with sorafenib, PTUPB did not interfere with the antitumor activity in the DU-145 prostate cancer cells **(B)** (n = 4). Dots represent the average of duplicate measures for each well. ns $p$ > 0.05, *$p$ ≤ 0.05, **$p$ ≤ 0.01 determined by ANOVA followed by the Tukey *post-hoc* test. Data are reported as box and whisker plots with median, minimum to maximum, and 10 to 90 percentiles.

filtration barrier from injury in isolated glomeruli. This is an important finding for its clinical corollaries. Damage to the glomerular filtration barrier manifests in proteinuria (Yu et al., 2018), which is commonly reported in patients receiving VEGF TKI chemotherapy and has even been reported following intravitreal VEGF TKI delivery (Patel et al., 2008; Estrada et al., 2019; Hanna et al., 2019). To our knowledge, this is the first study reporting the effects of PTUPB on the glomerular filtration barrier.

While the exact mechanism through which inhibition of VEGF signaling leads to glomerular damage remains unknown, it likely involves an interplay between various effects on the cross-talk among glomerular cells (Estrada et al., 2019). Mesangial cells are an important glomerular constituent, and their death (mesangiolysis) has been a reported feature of sorafenib nephrotoxicity (Overkleeft et al., 2009; Schlöndorff and Banas, 2009). Here, we show that sorafenib treatment caused mesangial cell death. This effect has not been extensively studied elsewhere, but it is of importance since mesangial cells support the structural and functional integrity of the glomerulus (Schlöndorff and Banas, 2009). The survival of mesangial cells is dependent on VEGF singling. For example, the diminished VEGF-A secretion by podocytes can lead to mesangiolysis. In addition, mesangial cells also produce their own VEGF, which further regulates their growth through an autocrine mechanism (Tahara et al., 2011). Sorafenib targets VEGFR-2 and VEGFR-3. Human renal mesangial cells express VEGFR-1 and VEGFR-2 (Thomas et al., 2000). Thus, sorafenib likely causes mesangiolysis

by blocking singling through VEGFR-2. Importantly, PTUPB showed potency in protecting mesangial cells from this sorafenib-induced cytotoxicity. This hints at the possibility that affecting eicosanoid signaling through dual sEH/COX-2 inhibition restores some of the downstream effects of VEGFR-2 signaling or activates cellular pathways that offset the negative effects of VEGFR-2 blockage. Together, the effects on nephrin, glomerular filtration barrier, and mesangial cells suggest that the ability of PTUPB to restore glomerular health is independent of blood pressure lowering. If so, dual sEH/COX-2 inhibition by PTUPB could be a viable treatment strategy for VEGF-TKI-induced renal damage.

Intriguingly, PTUPB has been found to inhibit tumor growth and combat cancer (Li et al., 2017; Wang et al., 2018). These studies have evaluated ovarian tumor growth, glioblastoma growth, and Lewis lung carcinoma growth and metastasis (Zhang et al., 2014b; Li et al., 2017; Gartung et al., 2019). In addition, PTUPB has been found to potentiate the cisplatin anticancer activity in a mouse xenograft model of bladder cancer (Wang et al., 2018). We tested PTUPB alone and in combination with sorafenib on prostate tumor cells. Our data demonstrate that PTUPB did not lead to prostate tumor cell death or significantly enhance the ability of sorafenib to cause tumor cell death. Importantly, PTUPB did not interfere with the ability of sorafenib to cause prostate tumor cell death. These findings provide evidence that PTUPB can prevent sorafenib-induced nephrotoxicity without interfering with sorafenib-mediated anticancer actions.

# CONCLUSION

Since their inception in 1990, VEGF TKIs have been proven effective against several cancers. Our ability to harness their potential in killing neoplasm cells, however, is limited by their serious adverse effects on cardiovascular and kidney health, which sometimes may force discontinuation of an otherwise effective therapy (Venkatachalam et al., 2010; Grenon, 2013; Porta et al., 2015; Neves et al., 2020). Kidney damage is especially problematic because it can progress to end-stage renal disease if not treated. This provides a strong rationale for developing a combination approach that can protect from the progressive VEGF-TKI-induced kidney damage. Data presented in this study suggest that dual sEH/COX-2 inhibition with PTUPB could be effective as such strategy because it successfully mitigated the nephrotoxic effects of a VEGF TKI, sorafenib. We show that PUTPB reduced hypertension and proteinuria, mitigated tubular and fibrotic injury, and improved glomerular health. Our *in vitro* glomerular and cultured mesangial cell data further support our understanding of VEGF signaling and glomerular biology, and the interplay between VEGF and eicosanoid signaling pathways. Additionally, PTUPB does not interfere with the anticancer actions of sorafenib. Together, the results show that PTUPB could be an effective therapeutic agent against VEGF TKI nephrotoxicity and perhaps also other conditions resulting in glomerular injury. Further investigation is warranted.

# DATA AVAILABILITY STATEMENT

The raw data supporting the conclusion of this article will be made available by the authors, without undue reservation.

# ETHICS STATEMENT

The animal study was reviewed and approved by the Medical College of Wisconsin Institutional Animal Care and Use Committee.

# AUTHOR CONTRIBUTIONS

JI and WJ conceived the study, interpreted the data, and wrote the manuscript. WJ, SB, MK, and AS performed the experiments. BH and SH synthesized PTUPB. All authors edited the manuscript. All authors have read and agreed to the published version of the manuscript.

# FUNDING

# REFERENCES

Apte, R. S., Chen, D. S., and Ferrara, N. (2019). VEGF in Signaling and Disease: Beyond Discovery and Development. *Cell* 176, 1248–1264. doi:10.1016/j.cell.2019.01.021

Bray, F., Ferlay, J., Soerjomataram, I., Siegel, R. L., Torre, L. A., and Jemal, A. (2018). Global Cancer Statistics 2018: GLOBOCAN Estimates of Incidence and Mortality Worldwide for 36 Cancers in 185 Countries. *CA. Cancer J. Clin.* 68, 394–424. doi:10.3322/caac.21492

Caletti, S., Paini, A., Coschignano, M. A., De Ciuceis, C., Nardin, M., Zulli, R., et al. (2018). Management of VEGF-Targeted Therapy-Induced Hypertension. *Curr. Hypertens. Rep.* 20, 68. doi:10.1007/s11906-018-0871-1

Chang, H. M., Moudgil, R., Scarabelli, T., Okwuosa, T. M., and Yeh, E. T. H. (2017). Cardiovascular Complications of Cancer Therapy: Best Practices in Diagnosis, Prevention, and Management: Part 1. *J. Am. Coll. Cardiol.* 70, 2536–2551. doi:10.1016/j.jacc.2017.09.1096

Cheng, H., Wang, S., Jo, Y. I., Hao, C. M., Zhang, M., Fan, X., et al. (2007). Overexpression of Cyclooxygenase-2 Predisposes to Podocyte Injury. *J. Am. Soc. Nephrol.* 18, 551–559. doi:10.1681/ASN.2006090990

Cheng, H. F., Wang, C. J., Moeckel, G. W., Zhang, M. Z., McKanna, J. A., and Harris, R. C. (2002). Cyclooxygenase-2 Inhibitor Blocks Expression of Mediators of Renal Injury in a Model of Diabetes and Hypertension. *Kidney Int.* 62, 929–939. doi:10.1046/j.1523-1755.2002.00520.x

Dileepan, M., Rastle-Simpson, S., Greenberg, Y., Wijesinghe, D. S., Kumar, N. G., Yang, J., et al. (2019). Effect of Dual SEH/COX-2 Inhibition on Allergen-Induced Airway Inflammation. *Front. Pharmacol.* 10, 1118–1131. doi:10.3389/fphar.2019.01118

Dobbin, S. J. H., Petrie, M. C., Myles, R. C., Touyz, R. M., and Lang, N. N. (2021). Cardiotoxic Effects of Angiogenesis Inhibitors. *Clin. Sci.* 135, 71–100. doi:10.1042/cs20200305

Elmarakby, A. A., Faulkner, J., Al-Shabrawey, M., Wang, M. H., Maddipati, K. R., and Imig, J. D. (2011). Deletion of Soluble Epoxide Hydrolase Gene Improves Renal Endothelial Function and Reduces Renal Inflammation and Injury in Streptozotocin-Induced Type 1 Diabetes. *Am. J. Physiol. Regul. Integr. Comp. Physiol.* 301, R1307–R1317. doi:10.1152/ajpregu.00759.2010

Estrada, C. C., Maldonado, A., and Mallipattu, S. K. (2019). Therapeutic Inhibition of VEGF Signaling and Associated Nephrotoxicities. *J. Am. Soc. Nephrol.* 30, 187–200. doi:10.1681/ASN.2018080853

Faul, C. (2014). The Podocyte Cytoskeleton: Key to a Functioning Glomerulus in Health and Disease. *Podocytopathy* 183, 22–53.

Fragiadaki, M., and Mason, R. M. (2011). Epithelial-mesenchymal Transition in Renal Fibrosis - Evidence for and against. *Int. J. Exp. Pathol.* 92, 143–150. doi:10.1111/j.1365-2613.2011.00775.x

Fujihara, C. K., Antunes, G. R., Mattar, A. L., Andreoli, N., Malheiros, D. M., Noronha, I. L., et al. (2003). Cyclooxygenase-2 (COX-2) Inhibition Limits Abnormal COX-2 Expression and Progressive Injury in the Remnant Kidney. *Kidney Int.* 64, 2172–2181. doi:10.1046/j.1523-1755.2003.00319.x

Garg, P. (2018). A Review of Podocyte Biology. *Am. J. Nephrol.* 47, 3–13. doi:10.1159/000481633

Gartung, A., Yang, J., Sukhatme, V. P., Bielenberg, D. R., Fernandes, D., Chang, J., et al. (2019). Suppression of Chemotherapy-Induced Cytokine/lipid Mediator Surge and Ovarian Cancer by a Dual COX-2/sEH Inhibitor. *Proc. Natl. Acad. Sci. U. S. A.* 116, 1698–1703. doi:10.1073/pnas.1803999116

Grenon, N. N. (2013). Managing Toxicities Associated with Antiangiogenic Biologic Agents in Combination with Chemotherapy for Metastatic Colorectal Cancer. *Clin. J. Oncol. Nurs.* 17, 425–433. doi:10.1188/13.CJON.425-433

Grothey, A., and Galanis, E. (2009). Targeting Angiogenesis: Progress with Anti-VEGF Treatment with Large Molecules. *Nat. Rev. Clin. Oncol.* 6, 507–518. doi:10.1038/nrclinonc.2009.110

Hanna, R. M., Barsoum, M., Arman, F., Selamet, U., Hasnain, H., and Kurtz, I. (2019). Nephrotoxicity Induced by Intravitreal Vascular Endothelial Growth Factor Inhibitors: Emerging Evidence. *Kidney Int.* 96, 572–580. doi:10.1016/j.kint.2019.02.042

Harris, R. C. (2013). Physiologic and Pathophysiologic Roles of Cyclooxygenase-2 in the Kidney. *Trans. Am. Clin. Climatol. Assoc.* 124, 139–151.

Humphreys, B. D., and Atkins, M. B. (2009). Rapid Development of Hypertension by Sorafenib: Toxicity or Target? *Clin. Cancer Res.* 15, 5947–5949. doi:10.1158/1078-0432.CCR-09-1717

Hwang, S. H., Wagner, K. M., Morisseau, C., Liu, J. Y., Dong, H., Wecksler, A. T., et al. (2011). Synthesis and Structure-Activity Relationship Studies of Urea-Containing Pyrazoles as Dual Inhibitors of Cyclooxygenase-2 and Soluble Epoxide Hydrolase. *J. Med. Chem.* 54, 3037–3050. doi:10.1021/jm2001376

Hwang, S. H., Wecksler, A. T., Zhang, G., Morisseau, C., Nguyen, L. V., Fu, S. H., et al. (2013). Synthesis and Biological Evaluation of Sorafenib- and Regorafenib-like sEH Inhibitors. *Bioorg. Med. Chem. Lett.* 23, 3732–3737. doi:10.1016/j.bmcl.2013.05.011

Hye Khan, M. A., Hwang, S. H., Sharma, A., Corbett, J. A., Hammock, B. D., and Imig, J. D. (2016). A Dual COX-2/sEH Inhibitor Improves the Metabolic Profile and Reduces Kidney Injury in Zucker Diabetic Fatty Rat. *Prostaglandins Other Lipid Mediat* 125, 40–47. doi:10.1016/j.prostaglandins.2016.07.003

Ilatovskaya, D. V., Palygin, O., Levchenko, V., Endres, B. T., and Staruschenko, A. (2017). The Role of Angiotensin II in Glomerular Volume Dynamics and Podocyte Calcium Handling. *Sci. Rep.* 7, 299–310. doi:10.1038/s41598-017-00406-2

Imig, J. D. (2006). Eicosanoids and Renal Vascular Function in Diseases. *Clin. Sci. (Lond)* 111, 21–34. doi:10.1042/CS20050251

Imig, J. D. (2012). Epoxides and Soluble Epoxide Hydrolase in Cardiovascular Physiology. *Physiol. Rev.* 92, 101–130. doi:10.1152/physrev.00021.2011

Izzedine, H., Massard, C., Spano, J. P., Goldwasser, F., Khayat, D., and Soria, J. C. (2010). VEGF Signalling Inhibition-Induced Proteinuria: Mechanisms, Significance and Management. *Eur. J. Cancer* 46, 439–448. doi:10.1016/j.ejca.2009.11.001

Jhaveri, K. D., Flombaum, C. D., Kroog, G., and Glezerman, I. G. (2011). Nephrotoxicities Associated with the Use of Tyrosine Kinase Inhibitors: A Single-center Experience and Review of the Literature. *Nephron Clin. Pract.* 117, c312–9. doi:10.1159/000319885

Jiang, X. S., Xiang, X. Y., Chen, X. M., He, J. L., Liu, T., Gan, H., et al. (2020). Inhibition of Soluble Epoxide Hydrolase Attenuates Renal Tubular Mitochondrial Dysfunction and ER Stress by Restoring Autophagic Flux in Diabetic Nephropathy. *Cell Death Dis* 11, 385. doi:10.1038/s41419-020-2594-x

Kappers, M. H., Van Esch, J. H., Sleijfer, S., Danser, A. H., and Van Den Meiracker, A. H. (2009). Cardiovascular and Renal Toxicity during Angiogenesis Inhibition: Clinical and Mechanistic Aspects. *J. Hypertens.* 27, 2297–2309. doi:10.1097/HJH.0b013e3283309b59

Kelly, R. J., Billemont, B., and Rixe, O. (2009). Renal Toxicity of Targeted Therapies. *Target. Oncoloncol* 4, 121–133. doi:10.1007/s11523-009-0109-x

Khan, M. A. H., Hwang, S. H., Barnett, S. D., Stavniichuk, A., Jankiewicz, W. K., Hammock, B. D., et al. (2021). Multitarget Molecule, PTUPB, to Treat Diabetic Nephropathy in Rats. *Br. J. Pharmacol.* doi:10.1111/bph.15623

Kim, J., Imig, J. D., Yang, J., Hammock, B. D., and Padanilam, B. J. (2014). Inhibition of Soluble Epoxide Hydrolase Prevents Renal Interstitial Fibrosis and Inflammation. *Am. J. Physiol. Ren. Physiol* 307, F971–F980. doi:10.1152/ajprenal.00256.2014

Lankhorst, S., Baelde, H. J., Kappers, M. H., Smedts, F. M., Hansen, A., Clahsen-van Groningen, M. C., et al. (2015). Greater Sensitivity of Blood Pressure Than Renal Toxicity to Tyrosine Kinase Receptor Inhibition with Sunitinib. *Hypertension* 66, 543–549. doi:10.1161/HYPERTENSIONAHA.115.05435

Li, J., Zhou, Y., Wang, H., Gao, Y., Li, L., Hwang, S. H., et al. (2017). COX-2/sEH Dual Inhibitor PTUPB Suppresses Glioblastoma Growth by Targeting Epidermal Growth Factor Receptor and Hyaluronan Mediated Motility Receptor. *Oncotarget* 8, 87353–87363. doi:10.18632/oncotarget.20928

Liu, J. Y. (2019). Inhibition of Soluble Epoxide Hydrolase for Renal Health. *Front. Pharmacol.* 9, 1–11. doi:10.3389/fphar.2018.01551

Ma, L., Yan, M., Kong, X., Jiang, Y., Zhao, T., Zhao, H., et al. (2018). Association of EPHX2 R287Q Polymorphism with Diabetic Nephropathy in Chinese Type 2 Diabetic Patients. *J. Diabetes Res.* 2018, 2786470. doi:10.1155/2018/2786470

Manhiani, M., Quigley, J. E., Knight, S. F., Tasoobshirazi, S., Moore, T., Brands, M. W., et al. (2009). Soluble Epoxide Hydrolase Gene Deletion Attenuates Renal Injury and Inflammation with DOCA-Salt Hypertension. *Am. J. Physiol. Ren. Physiol* 297, F740–F748. doi:10.1152/ajprenal.00098.2009

Neves, K. B., Montezano, A. C., Lang, N. N., and Touyz, R. M. (2020). Vascular Toxicity Associated with Anti-angiogenic Drugs. *Clin. Sci. (Lond)* 134, 2503–2520. doi:10.1042/CS20200308

Overkleeft, E. N., Goldschmeding, R., van Reekum, F., Voest, E. E., and Verheul, H. M. (2009). Nephrotic Syndrome Caused by the Angiogenesis Inhibitor Sorafenib. *Ann. Oncol.* 21, 184–185. doi:10.1093/annonc/mdp472

Partovian, C., Adnot, S., Raffestin, B., Louzier, V., Levame, M., Mavier, I. M., et al. (2000). Adenovirus-mediated Lung Vascular Endothelial Growth Factor Overexpression Protects against Hypoxic Pulmonary Hypertension in Rats. *Am. J. Respir. Cel Mol. Biol.* 23, 762–771. doi:10.1165/ajrcmb.23.6.4106

Patel, T. V., Morgan, J. A., Demetri, G. D., George, S., Maki, R. G., Quigley, M., et al. (2008). A Preeclampsia-like Syndrome Characterized by Reversible Hypertension and Proteinuria Induced by the Multitargeted Kinase Inhibitors Sunitinib and Sorafenib. *J. Natl. Cancer Inst.* 100, 282–284. doi:10.1093/jnci/djm311

Perazella, M. A. (2012). Onco-nephrology: Renal Toxicities of Chemotherapeutic Agents. *Clin. J. Am. Soc. Nephrol.* 7, 1713–1721. doi:10.2215/CJN.02780312

Plummer, C., Michael, A., Shaikh, G., Stewart, M., Buckley, L., Miles, T., et al. (2019). Expert Recommendations on the Management of Hypertension in Patients with Ovarian and Cervical Cancer Receiving Bevacizumab in the UK. *Br. J. Cancer* 121, 109–116. doi:10.1038/s41416-019-0481-y

Porta, C., Cosmai, L., Gallieni, M., Pedrazzoli, P., and Malberti, F. (2015). Renal Effects of Targeted Anticancer Therapies. *Nat. Rev. Nephrol.* 11, 354–370. doi:10.1038/nrneph.2015.15

Rassy, E., Flippot, R., and Albiges, L. (2020). Tyrosine Kinase Inhibitors and Immunotherapy Combinations in Renal Cell Carcinoma. *Ther. Adv. Med. Oncol.* 12, 1–13. doi:10.1177/1758835920907504

Schindelin, J., Arganda-Carreras, I., Frise, E., Kaynig, V., Longair, M., Pietzsch, T., et al. (2012). Fiji: An Open-Source Platform for Biological-Image Analysis. *Nat. Methods* 9, 676–682. doi:10.1038/nmeth.2019

Schlöndorff, D., and Banas, B. (2009). The Mesangial Cell Revisited: No Cell Is an Island. *J. Am. Soc. Nephrol.* 20, 1179–1187. doi:10.1681/ASN.2008050549

Sheng, L., and Zhuang, S. (2020). New Insights into the Role and Mechanism of Partial Epithelial-Mesenchymal Transition in Kidney Fibrosis. *Front. Physiol.* 11, 569322–569332. doi:10.3389/fphys.2020.569322

Sun, C. C., Zhang, C. Y., Duan, J. X., Guan, X. X., Yang, H. H., Jiang, H. L., et al. (2020). PTUPB Ameliorates High-Fat Diet-Induced Non-alcoholic Fatty Liver Disease via Inhibiting NLRP3 Inflammasome Activation in Mice. *Biochem. Biophys. Res. Commun.* 523, 1020–1026. doi:10.1016/j.bbrc.2019.12.131

Tahara, A., Tsukada, J., Tomura, Y., Yatsu, T., and Shibasaki, M. (2011). Vasopressin Regulates Rat Mesangial Cell Growth by Inducing Autocrine Secretion of Vascular Endothelial Growth Factor. *J. Physiol. Sci.* 61, 115–122. doi:10.1007/s12576-010-0128-5

Terrasse, M. (2015). Anti-VEGF Therapy Induces Proteinuria through Endothelial Disorganization Leading to Nephrin Decrease in Podocytes. *Int. J. Immunother. Cancer Res.* 1, 021–028. doi:10.17352/2455-8591.000006

Thomas, S., Vanuystel, J., Gruden, G., Rodríguez, V., Burt, D., Gnudi, L., et al. (2000). Vascular Endothelial Growth Factor Receptors in Human Mesangium *In Vitro* and in Glomerular Disease. *J. Am. Soc. Nephrol.* 11, 1236–1243. doi:10.1681/ASN.V1171236

Tuleta, I., and Frangogiannis, N. G. (2021). Diabetic Fibrosis. *Biochim. Biophys. Acta Mol. Basis Dis.* 1867, 166044. doi:10.1016/j.bbadis.2020.166044

Vandewalle, C., Van Roy, F., and Berx, G. (2009). The Role of the ZEB Family of Transcription Factors in Development and Disease. *Cell. Mol. Life Sci.* 66, 773–787. doi:10.1007/s00018-008-8465-8

Venkatachalam, M. A., Griffin, K. A., Lan, R., Geng, H., Saikumar, P., and Bidani, A. K. (2010). Acute Kidney Injury: A Springboard for Progression in Chronic Kidney Disease. *Am. J. Physiol. Ren. Physiol* 298, F1078–F1094. doi:10.1152/ajprenal.00017.2010

Versmissen, J., Mirabito Colafella, K. M., Koolen, S. L. W., and Danser, A. H. J. (2019). Vascular Cardio-Oncology: Vascular Endothelial Growth Factor Inhibitors and Hypertension. *Cardiovasc. Res.* 115, 904–914. doi:10.1093/cvr/cvz022

Wang, F., Zhang, H., Ma, A. H., Yu, W., Zimmermann, M., Yang, J., et al. (2018). COX-2/sEH Dual Inhibitor PTUPB Potentiates the Antitumor Efficacy of Cisplatin. *Mol. Cancer Ther.* 17, 474–483. doi:10.1158/1535-7163.MCT-16-0818

Wang, Y., Liu, J., Ying, X., Lin, P. C., and Zhou, B. P. (2016). Twist-mediated Epithelial-Mesenchymal Transition Promotes Breast Tumor Cell Invasion via Inhibition of Hippo Pathway. *Sci. Rep.* 6, 24606–24610. doi:10.1038/srep24606

White, P. T., and Cohen, M. S. (2015). The Discovery and Development of Sorafenib for the Treatment of Thyroid Cancer. *Expert Opin. Drug Discov.* 10, 427–439. doi:10.1517/17460441.2015.1006194

Wu, S., Chen, J. J., Kudelka, A., Lu, J., and Zhu, X. (2008). Incidence and Risk of Hypertension with Sorafenib in Patients with Cancer: a Systematic Review and Meta-Analysis. *Lancet Oncol.* 9, 117–123. doi:10.1016/S1470-2045(08)70003-2

Yu, S. M., Nissaisorakarn, P., Husain, I., and Jim, B. (2018). Proteinuric Kidney Diseases: A Podocyte's Slit Diaphragm and Cytoskeleton Approach. *Front. Med. (Lausanne)* 5, 221–235. doi:10.3389/fmed.2018.00221

Yu, Z., Xu, F., Huse, L. M., Morisseau, C., Draper, A. J., Newman, J. W., et al. (2000). Soluble Epoxide Hydrolase Regulates Hydrolysis of Vasoactive Epoxyeicosatrienoic Acids. *Circ. Res.* 87, 992–998. doi:10.1161/01.res.87.11.992

Zhang, C. Y., Duan, J. X., Yang, H. H., Sun, C. C., Zhong, W. J., Tao, J. H., et al. (2020). COX-2/sEH Dual Inhibitor PTUPB Alleviates Bleomycin-Induced Pulmonary Fibrosis in Mice via Inhibiting Senescence. *FEBS J.* 287, 1666–1680. doi:10.1111/febs.15105

Zhang, G., Panigrahy, D., Hwang, S. H., Yang, J., Mahakian, L. M., Wettersten, H. I., et al. (2014). Dual Inhibition of Cyclooxygenase-2 and Soluble Epoxide Hydrolase Synergistically Suppresses Primary Tumor Growth and Metastasis. *Proc. Natl. Acad. Sci. U S A.* 111, 11127–11132. doi:10.1073/pnas.1410432111

Zhang, Z. F., Wang, T., Liu, L. H., and Guo, H. Q. (2014). Risks of Proteinuria Associated with Vascular Endothelial Growth Factor Receptor Tyrosine Kinase Inhibitors in Cancer Patients: A Systematic Review and Meta-Analysis. *PLoS One* 9, e90135. doi:10.1371/journal.pone.0090135

Zhu, Y. J., Zheng, B., Wang, H. Y., and Chen, L. (2017). New Knowledge of the Mechanisms of Sorafenib Resistance in Liver Cancer. *Acta Pharmacol. Sin.* 38, 614–622. doi:10.1038/aps.2017.5

**Publisher's Note:** All claims expressed in this article are solely those of the authors and do not necessarily represent those of their affiliated organizations, or those of the publisher, the editors, and the reviewers. Any product that may be evaluated in this article, or claim that may be made by its manufacturer, is not guaranteed or endorsed by the publisher.

# Immune Characteristics of IgA Nephropathy With Minimal Change Disease

Huixian Li[1†], Wanhong Lu[1†], Haiyun Li[2], Xiaoling Liu[3], Xue Zhang[4,5], Liyi Xie[1], Ping Lan[1], Xiaoyang Yu[1], Yinjuan Dai[1], Xinfang Xie[1*] and Jicheng Lv[4,5]

[1]Department of Nephrology, The First Affiliated Hospital of Xi'an Jiaotong University, Xi'an, China, [2]MOE Key Laboratory of Environment and Genes Related to Diseases, School of Basic Medical Sciences, Xi'an Jiaotong University, Xi'an, China, [3]MOE Key Laboratory of cell Activities and Stress Adaptations, School of Life Science, Lanzhou University, Lanzhou, China, [4]Renal Division, Department of Medicine, Peking University First Hospital, Beijing, China, [5]Institute of Nephrology, Peking University, Beijing, China

**Background:** IgA nephropathy (IgAN) has a high degree of heterogeneity in clinical and pathological features. Among all subsets of IgAN, the pathogenesis of IgAN with minimal change disease (MCD-IgAN) remained controversial.

**Methods:** We analyzed the clinical and pathological characteristics of MCD-IgAN patients in a retrospective cohort. Patients diagnosed with IgAN, excluding MCD-IgAN, were randomly selected as controls. Levels of plasma galactose-deficient IgA1 (GdIgA1), IgG autoantibodies against GdIgA1, GdIgA1 deposition in the glomerulus, and inflammatory reactivity of circulating poly-IgA1 complexes to cultured mesangial cells were evaluated.

**Results:** Patients with MCD-IgAN had significantly higher levels of proteinuria and estimated glomerular filtration rate (eGFR), lower levels of albumin and urine blood cells, and milder histological lesions by a light microscope compared to IgAN patients, which bears a resemblance to MCD. Lower levels of GdIgA1 (3.41 ± 1.68 vs. 4.92 ± 2.30 μg/ml, $p = 0.009$) and IgG antiglycan autoantibodies (23.25 ± 22.59 vs. 76.58 ± 71.22 IU/ml, $p < 0.001$) were found in MCD-IgAN patients than those in IgAN controls. Meanwhile, weaker fluorescence intensities of both IgA and GdIgA1 were observed in the glomerulus of MCD-IgAN patients compared to those in IgAN patients. Furthermore, poly-IgA1 complexes from MCD-IgAN patients induced weaker inflammatory effects on cultured mesangial cells than those from IgAN patients in vitro.

**Conclusion:** The results demonstrated that MCD-IgAN cases represent a dual glomerulopathy, namely, mild IgAN with superimposed MCD, which furthermore provides substantial evidence for the corticosteroids therapy in MCD-IgAN patients as the guidelines recommended.

**Keywords: MCD-IgAN, galactose deficient IgA1, anti-glycan autoantibodies, inflammation, IgA nephropathy, minimal change disease**

# INTRODUCTION

IgA nephropathy (IgAN) is one of the most common glomerulonephritis worldwide, especially in Asia (Wyatt and Julian, 2013). Approximately 30%–40% of patients suffered a slow but relentless clinical course that could progress to end-stage kidney disease (ESKD) for 20–30 years (Lai et al., 2016; D'Amico 2004). In clinical practice, IgAN is diagnosed as dominant IgA deposition in the mesangial area by kidney biopsy. However, the clinical and pathological manifestations of IgAN are diverse (Zhang and Barratt, 2021). The clinical course of the disease ranges from isolated hematuria, subnephrotic proteinuria, nephrotic proteinuria to rapidly progressive renal failure, and kidney biopsy findings vary from mild mesangial proliferation to diffuse crescent formation, suggesting those might not be the same disease (Lai et al., 2016). Among all subsets of IgAN, cases presenting nephrotic syndrome (NS) and mild mesangial proliferation are rare, accounting for approximately 5%–10% of all IgAN patients (Barratt and Feehally, 2006; Kim et al., 2012). Therefore, this variant form of IgAN with clinical NS presentation and electron microscope (EM) features of diffuse foot process effacement resembling minimal change disease (MCD) is defined as MCD-IgAN (Floege et al., 2019).

In general, there is a reasonable correlation between clinical and pathological findings in IgAN; mounting studies indicate that heavy proteinuria at baseline is associated with more aggressive disease accompanied by severe glomerular damage or renal insufficiency (Thompson et al., 2019). While previous studies revealed the clinical features, podocytopathic variant and the good response to glucocorticoids in these MCD-IgAN patients are more consistent with MCD patients (Westhoff et al., 2006; Kim et al., 2009; Qin et al., 2013; Wang et al., 2013; Herlitz et al., 2014; Li et al., 2016). Therefore, it remained controversial whether these patients suffered from a specific podocytopathic variant type of IgAN, or the existence of MCD in mild IgAN, or even MCD with non-pathogenic IgA deposition.

Recent studies have indicated four crucial processes contributing to IgAN development (Suzuki et al., 2011). The first two established processes are the existence of higher levels of galactose-deficient IgA1 (GdIgA1) and autoantibodies against GdIgA1 in circulation (Tomana et al., 1999; Moldoveanu et al., 2007; Suzuki et al., 2009; Zhao et al., 2012). Then, poly-IgA1 complexes composed of GdIgA1(Allen et al., 2001) and its autoantibodies (Rizk et al., 2019) accumulate in the renal mesangium. The deposits finally induce mesangial proliferation, expansion of extracellular matrix, and secretion of cytokines and chemokines, resulting in renal injury (Novak et al., 2005). Until now, as a specific subset of IgAN, whether the poly-IgA1 complexes in MCD-IgAN are coincidental or playing the same pathophysiological role as in IgAN remains unclear. In this study, we examined the immune features, including levels of circulating GdIgA1, antiglycan IgG autoantibodies, renal deposits of GdIgA1, and the inflammatory effects of poly-IgA1 complexes in IgAN-MCD to elucidate it.

# MATERIALS AND METHODS

## Patients and Healthy Controls

IgAN was diagnosed by immunofluorescence showing IgA as the dominant or co-dominant immunoglobulin in the mesangial deposits and the deposition of electron-dense materials in mesangium on ultrastructural examination in the absence of secondary causes. A total of 656 patients were diagnosed as IgAN patients from January 2018 to November 2020 at the First Affiliated Hospital of Xi'an Jiaotong University, of whom 27 patients with 1) diffuse podocyte foot process effacement at electron microscopy (>50% of the capillary surface area involved); 2) mild mesangial hypercellularity; 3) without endocapillary proliferation, segmental glomerulosclerosis, interstitial fibrosis and tubular atrophy, or cellular crescents were diagnosed with MCD-IgAN (**Supplementary Figure S1**). Sixty-eight IgAN patients without nephrotic proteinuria during the same periods were randomly selected as controls at the ratio of 1:2 approximately. In the same period, age- and gender-matched healthy physical examinees were chosen randomly. Oxford Classification scores were performed for all biopsy specimens by an experienced renal pathologist. The extent of podocyte foot process effacement was evaluated under transmission electron microscopy (TEM). Clinical and pathological characteristics of all patients were collected at the time of renal biopsy. MCD-IgAN patients were followed until the remission of proteinuria. Complete remission (CR) was defined as 24-h urine protein <500 mg/day. This study was conducted in adherence to the Declaration of Helsinki and was approved by the medical ethics committee at the First Affiliated Hospital of Xi'an Jiaotong University. Plasma and urine samples from patients at the time of renal biopsy and from thirty-two age- and gender-matched healthy individuals were stored at −80°C before use.

## Plasma IgA1, Gd-IgA1, and IgG Autoantibodies Targeting the Gd-IgA1

The levels of plasma IgA1 were detected by enzyme-linked immunosorbent assay (ELISA) with a previously established protocol (Zhang et al., 2019). Plasma Gd-IgA1 levels were quantified by using the Gd-IgA1-specific monoclonal antibody KM55 ELISA Kit (IBL, Naka, Japan) according to the suggested procedure. See the detailed methods in supplementary materials.

Circulating autoantibodies of IgG against GdIgA1 were detected according to our previous protocol (Wang et al., 2021). Briefly, IgA1 F(ab)$_2$ with hinge region of its heavy chain, namely, F(ab)$_2$-HR, was used as antigen. After blocking all wells with 1% bovine serum albumin (BSA)/phosphate-buffered saline (PBS), diluted plasma (1:100) and standards were added to each well; alkaline phosphatase-conjugated goat antihuman IgG monoclonal antibody (Sigma, United States) was used for detection. Detailed methods were described in supplementary materials.

## Immunofluorescent Staining of Gd-IgA1 and IgA in Kidney

Formalin-fixed paraffin-embedded (FFPE) tissues were sectioned at 3 μm for IgA and GdIgA1 staining. Renal slides from MCD, membranous nephropathy, and healthy renal allograft were used as negative controls. Antigen retrieval was performed with 0.05% protease from *Bacillus licheniformis* (Sigma-Aldrich, St. Louis, MO, United States) at room temperature for 2 h. Then, 3% bovine serum albumin in phosphate-buffered saline was used to block the non-specific binding. Next, the slides were incubated with rat antihuman GdIgA1 antibody (Immuno-Biological Laboratories, Japan) for 1 h at 37°C followed by Alexa Fluor 555-conjugated goat antirat IgG antibody (Abcam, United States) and fluorescein isothiocyanate (FITC)-conjugated polyclonal rabbit antihuman IgA antibody (Dako, Japan) incubation at 37°C for 30 min. Immunofluorescence images were captured using a Nikon microscope 90i (Nikon Instruments Inc., Japan). Glomerular staining of IgA and Gd-IgA1 was evaluated by the Image Pro Plus analysis software version 6.0. Semiquantitative analysis of fluorescence intensity for IgA or GdIgA1 staining was described as the glomerular mean optical density (integrated option density/glomerular area). At least eight fields of glomerular vision per kidney section were randomly captured at 400× for semiquantitative assessment of immunofluorescent staining.

## Poly-IgA1 Complex Purification and Mesangial Stimulation

Ten milliliters of peripheral venous blood (EDTA anticoagulated) was collected at the renal biopsy from recruited eight patients with MCD-IgAN, seven patients with IgAN, and five patients with MCD. Poly-IgA1 complexes were separately isolated from the plasma sample of each patient by jacalin affinity chromatography and then Sephacryl S-300 gel filtration chromatography, as previously reported (Zhu et al., 2013). Primary human mesangial cells (HMCs) (ScienCellTM, Carlsbad, CA, United States) were cultured to the sixth passage with mesangial cell medium (MCM) containing mesangial cell growth supplement (MsCGS), 2.5% FBS. After overnight starvation with mesangial cell medium containing 0.05% FBS and 0% mesangial cell growth supplement, HMCs were stimulated and cultured with 100 μg/ml poly-IgA1 in MCM medium for 48 h. The supernatants were collected after being centrifuged and stored at −80°C for cytokine detection. IL-6 and MCP-1 levels in cell culture supernatants after poly-IgA1 treatment, as well as urinary MCP-1 in patients and healthy controls were detected by using ELISA kit (4A Biotech Co., Ltd., Beijing).

## Statistical Analyses

Non-normally distributed and normally distributed quantitative parameters were expressed as medians (IQRs) and means ± standard deviations, respectively. Kolmogorov–Smirnov test was performed to determine normal distributions of quantitative parameters. Categorical data were represented by frequencies or ratios. Differences in continuous variables were assessed using the non-parametric test (Mann–Whitney $U$ test) and t-test when the data were not normally distributed or normally distributed, respectively. Kaplan–Meier analysis were conducted to assess the relationship between higher and lower levels of GdIgA1, anti-GdIgA1 antibodies, and the proteinuria remission for MCD-IgAN patients. A two-sided $p$-value <0.05 was considered statistically significant. All analyses and graphs were conducted using GraphPad Prism version 8.0 for Windows (GraphPad Software, San Diego, CA, United States) and IBM-SPSS22.0 (IBM-SPSS Inc., Armonk, NY).

# RESULTS

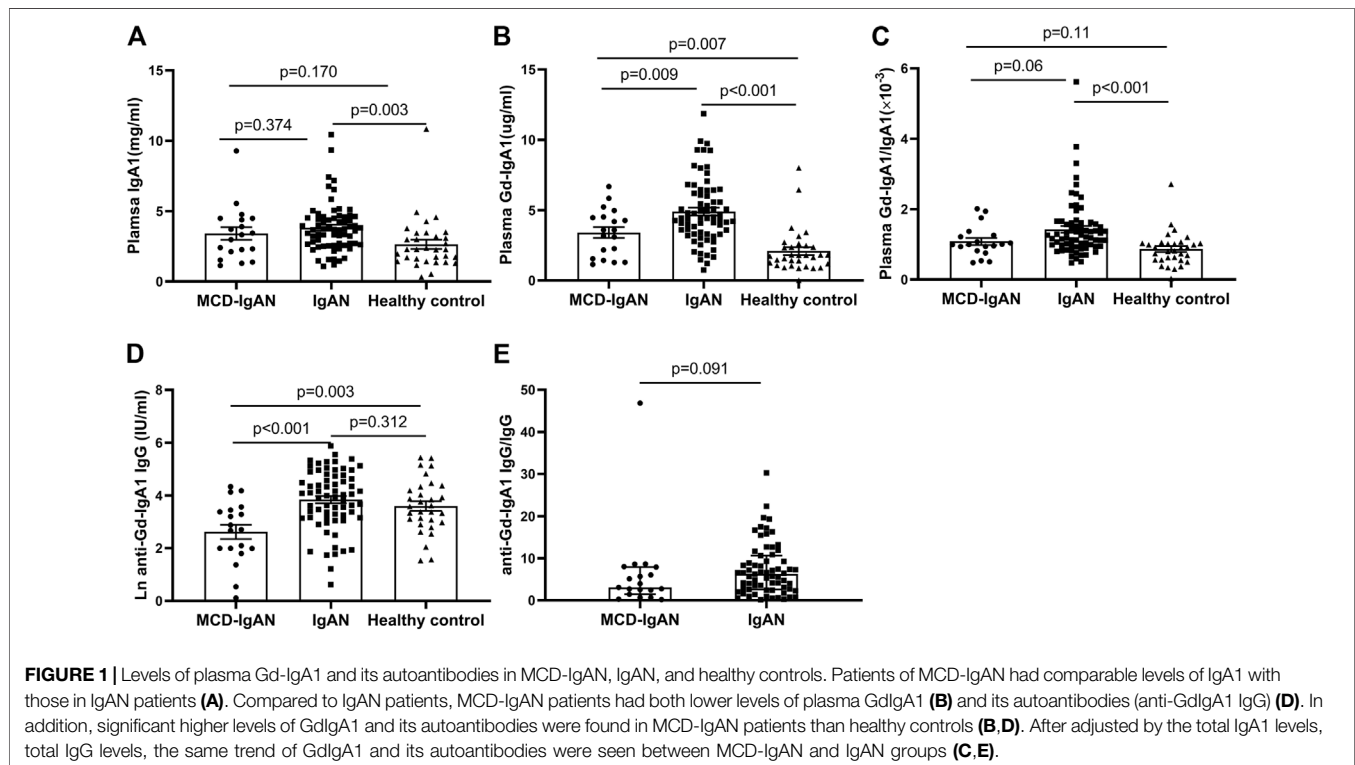## Baseline Demographic, Clinical, and Pathological Characteristics

A total of 27 MCD-IgAN patients with a mean age of 30.6 ± 12.1 years old were enrolled in this study. The mean age of MCD-IgAN patients was comparable to that in another Chinese study (Li et al., 2016) whereas lower than the median age of 46 in one study from United States (Herlitz et al., 2014). The cohort included 17 men and 10 women. The male proportion of MCD-IgAN patients was 63%, which was comparable to those in previous studies. Twenty-five patients fulfilled criteria for NS, and the remaining two patients had nephrotic range proteinuria without hypoalbuminemia (Alb 32.2 and 31.8 g/L). Compared to IgAN group, patients with MCD-IgAN had significantly higher levels of proteinuria (4.26 ± 1.81 vs. 2.12 ± 1.73 g/24 h, $p < 0.001$) and estimated glomerular filtration rate (eGFR) (120.8 ± 24.3 vs. 81.1 ± 31.5 ml/min, $p < 0.001$) while lower levels of albumin (20.0 ± 6.2 vs. 36.9 ± 6.6 g/L, $p < 0.001$), urine blood cells [10.9 (4.4, 32.4) vs. 64.2 (22.5, 194.1)/μl, $p < 0.001$], SBP (116.7 ± 16.5 vs. 131.2 ± 19.9 mmHg, $p = 0.001$) and lower percentages of C3 deposition (66.7 vs. 94.1%, $p = 0.001$), Oxford M1 (37 vs. 89.7%, $p < 0.001$), E1 (0 vs. 17.6%, $p = 0.017$), S1 (0 vs. 75%, $p < 0.001$), and T1/T2 (0 vs. 39.7%, $p < 0.001$) scores. All MCD-IgAN patients have initially received corticosteroids, of which 12 cases were treated in combination with other immunosuppressants (see **Table 1**).

## Plasma IgA1, Gd-IgA1, and IgG Antiglycan Autoantibodies

Levels of plasma IgA1, Gd-IgA1, and IgG autoantibodies against GdIgA1 were detected in 19 MCD-IgAN patients and 68 IgAN patients with blood samples available. As shown in **Figure 1A**, the levels of total IgA1 in IgAN group was significantly higher compared to those in healthy controls (3.82 ± 1.73 vs. 2.65 ± 1.87 mg/ml, $p = 0.003$), but with a comparable level in patients with MCD-IgAN patients (3.82 ± 1.73 vs. 3.41 ± 1.93 mg/ml, $p = 0.374$). However, MCD-IgAN patients had lower levels of GdIgA1 than those in IgAN patients (3.41 ± 1.68 vs. 4.92 ± 2.30 μg/ml, $p = 0.009$) and higher GdIgA1 levels than those in healthy controls (3.41 ± 1.68 vs. 2.10 ± 1.58 μg/ml, $p = 0.007$) (**Figure 1B**). After adjusting the total IgA1 concentration, there was a similar trend for Gd-IgA1/IgA1 levels with unadjusted GdIgA1 levels among the three groups (**Figure 1C**).

**TABLE 1** | The baseline clinical and pathological characteristics of MCD-IgAN and typical IgAN patients.

| Characteristics | MCD-IgAN (*n* = 27) | IgAN (*n* = 68) | *p*-value |
|---|---|---|---|
| Age (yr; mean ± SD) | 30.6 ± 12.1 | 35.7 ± 12.1 | 0.063 |
| Male sex, *n* (%) | 17 (63.0) | 39 (57.4) | 0.651 |
| Baseline SBP (mmHg; mean ± SD) | 116.7 ± 16.5 | 131.2 ± 19.9 | 0.001 |
| Baseline DBP (mmHg; mean ± SD) | 81.4 ± 10.7 | 88.1 ± 14.5 | 0.033 |
| Baseline proteinuria (g/day; mean ± SD) | 4.26 ± 1.81 | 2.12 ± 1.73 | <0.001 |
| Urine red blood cell counts (/µl) | 10.9 (4.4, 32.4) | 64.2 (22.5, 194.1) | <0.001 |
| Serum creatinine (µmol/L; mean ± SD, median, IQR) | 64.3 ± 19.0 | 95(68, 128.8) | <0.001 |
| eGFR (ml/min/1.73 m$^2$; mean ± SD) | 120.8 ± 24.3 | 81.1 ± 31.5 | <0.001 |
| CKD stage 1, *n* (%) | 25 (92.6) | 31 (45.6) | 0.001 |
| CKD stage 2, *n* (%) | 2 (7.4) | 15 (22.1) | |
| CKD stage 3, *n* (%) | 0 (0) | 16 (23.5) | |
| CKD stage 4, *n* (%) | 0 (0) | 4 (5.9) | |
| CKD stage 5, *n* (%) | 0 (0) | 2 (2.9) | |
| Serum albumin (g/L; mean ± SD) | 20.0 ± 6.2 | 36.9 ± 6.6 | <0.001 |
| Hemoglobin (g/L; mean ± SD) | 151.0 ± 18.9 | 133.7 ± 26.0 | 0.002 |
| Oxford classification of IgAN, *n* (%) | | | |
| M1 | 10 (37) | 61 (89.7) | <0.001 |
| E1 | 0 (0) | 12 (17.6) | 0.017 |
| S1 | 0 (0) | 51 (75.0) | <0.001 |
| T1/T2 | 0 (0) | 27 (39.7) | <0.001 |
| C1/2 | 0 (0) | 21 (31.3) | 0.004 |
| IgG deposition *n* (%) | 1 (3.7) | 6 (8.8) | 0.389 |
| IgM deposition *n* (%) | 17 (63) | 29 (42.6) | 0.096 |
| C3 deposition *n* (%) | 18 (66.7) | 64 (94.1) | 0.001 |
| Follow-up (mo; mean ± SD) | 11.1 ± 8.5 | 14.3 ± 7.3 | 0.080 |
| RAS blocker treatment, *n* (%) | 8 (29.6) | 46 (67.6) | 0.001 |
| Combined with corticoids and/or other immunosuppressants, *n* (%) | 27 (100) | 23 (33.8) | <0.001 |



**FIGURE 1** | Levels of plasma Gd-IgA1 and its autoantibodies in MCD-IgAN, IgAN, and healthy controls. Patients of MCD-IgAN had comparable levels of IgA1 with those in IgAN patients **(A)**. Compared to IgAN patients, MCD-IgAN patients had both lower levels of plasma GdIgA1 **(B)** and its autoantibodies (anti-GdIgA1 IgG) **(D)**. In addition, significant higher levels of GdIgA1 and its autoantibodies were found in MCD-IgAN patients than healthy controls **(B,D)**. After adjusted by the total IgA1 levels, total IgG levels, the same trend of GdIgA1 and its autoantibodies were seen between MCD-IgAN and IgAN groups **(C,E)**.

The plasma levels of IgG antiglycan autoantibodies targeting the GdIgA1 in patients with IgAN were significantly higher than those in patients with MCD-IgAN ($76.58 ± 71.22$ vs. $23.25 ± 22.59$ IU/ml, $p < 0.001$) (**Figure 1D**). In contrast, no significant difference in IgG autoantibodies levels between IgAN patients and healthy controls were found.
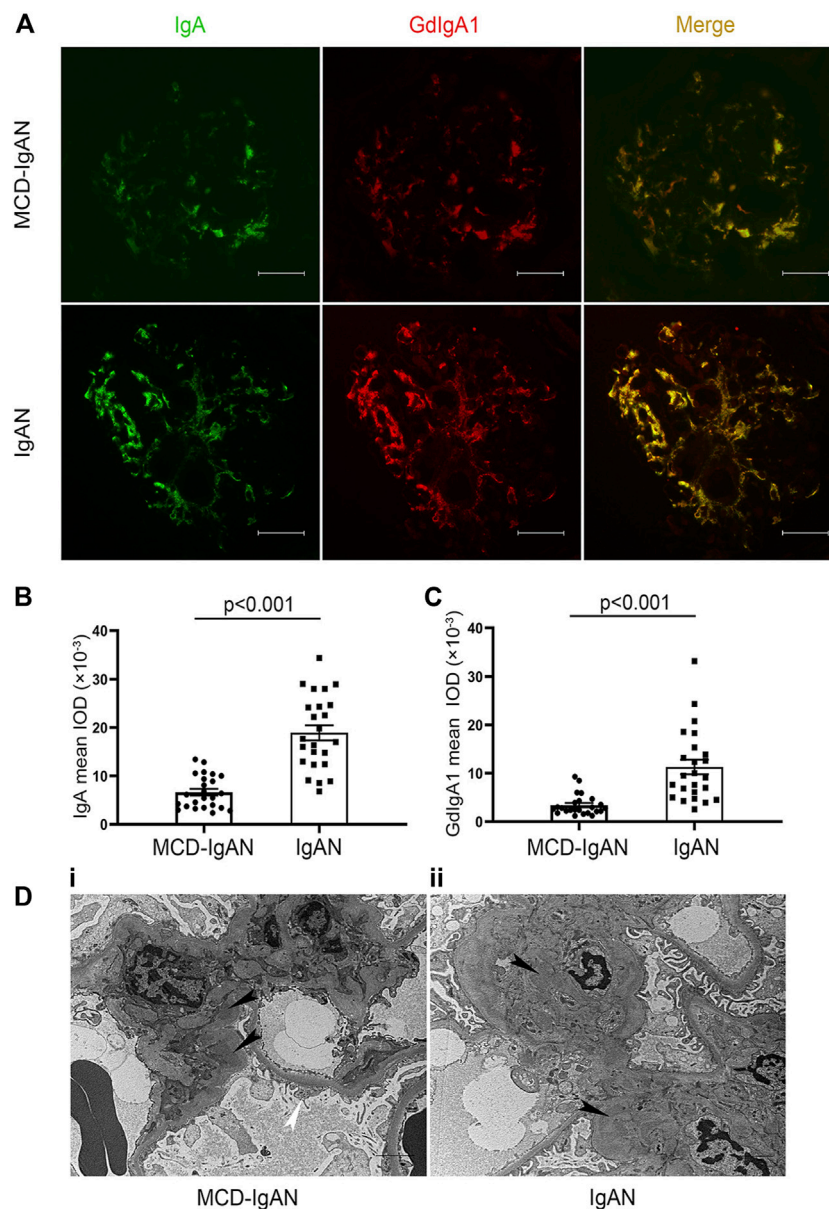
FIGURE 2 | Immunofluorescence (IF) staining of IgA and Gd-IgA1 in the glomerulus of MCD-IgAN and non-MCD-IgAN patients. **(A)** IgA (green, left panel) and GdIgA1 (red, middle panel) deposition were shown in IgAN-MCD patients **(top panel)** and IgAN patients **(bottom panel)**. IF signals of both IgA and GdIgA1were mainly concentrated in the mesangial regions of glomerulus and were co-deposited (yellow, right panel). In contrast to IgAN, weaker signals of both IgA and GdIgA1 were found in glomerulus of patients with MCD-IgAN. Significantly lower mean fluorescent optical density of IgA **(B)** and GdIgA1 **(C)** in the glomerulus were found in MCD-IgAN patients ($n = 24$) compared to IgAN patients ($n = 24$). Scale bar = 50 µm. **(D)** Typical pathological change in glomeruli under electron microscopy observation in MCD-IgAN and non-MCD-IgAN patients were shown. Examples of dense deposits in the mesangial region (black arrow) and diffuse podocyte foot process effacement were observed in the glomeruli of one MCD-IgAN patient **(i)**. Example of dense deposits was found in the mesangial region of one IgAN patient **(ii)**.
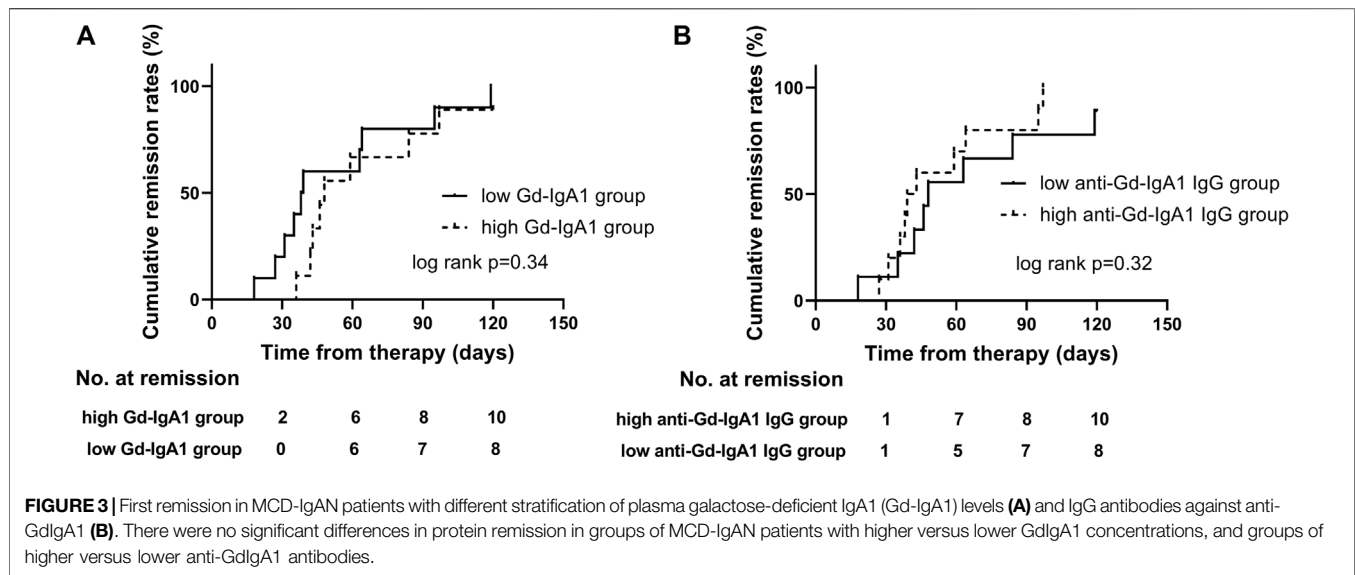
After the adjusting serum IgG level, a consistent trend for IgG autoantibodies/IgG between MCD-IgAN and IgAN group was found (**Figure 1E**).

## Glomerular Deposition of IgA and Gd-IgA1

Because of the significant difference in plasma GdIgA1 levels between MCD-IgAN and IgAN patients, available paraffin-embedded kidney tissues from 24 MCD-IgAN patients were prepared for double IF staining of IgA and Gd-IgA1. Renal tissues from 24 age- and gender-matched IgAN patients were selected as controls (**Supplementary Table S1**). Gd-IgA1 was distributed mainly in the mesangial area with co-deposits of IgA in the kidney tissue of MCD-IgAN patients, similar to those in IgAN patients (**Figure 2A**). Nevertheless, weaker fluorescence intensities of both IgA and GdIgA1 were observed in the kidney of MCD-IgAN patients compared to those in IgAN patients, as

**FIGURE 3** | First remission in MCD-IgAN patients with different stratification of plasma galactose-deficient IgA1 (Gd-IgA1) levels **(A)** and IgG antibodies against anti-GdIgA1 **(B)**. There were no significant differences in protein remission in groups of MCD-IgAN patients with higher versus lower GdIgA1 concentrations, and groups of higher versus lower anti-GdIgA1 antibodies.

shown by the analysis of mean optical density per glomerular compartment in **Figures 2B,C** (mean optical density of IgA, $18.9 \pm 7.6$ vs. $6.6 \pm 3.4 \times 10^{-3}$, $p < 0.001$, and GdIgA1, $11.5 \pm 8.0$ vs. $3.3 \pm 2.2 \times 10^{-3}$, $p < 0.001$, IgAN and MCD-IgAN, respectively). Under electron microscopy observation, dense deposits in the mesangial region (black arrow) were shown in the kidney tissue of both MCD-IgAN and IgAN patients, while diffuse podocyte foot process effacement (white arrow) was only observed in the glomeruli of MCD-IgAN patients (**Figure 2D**).
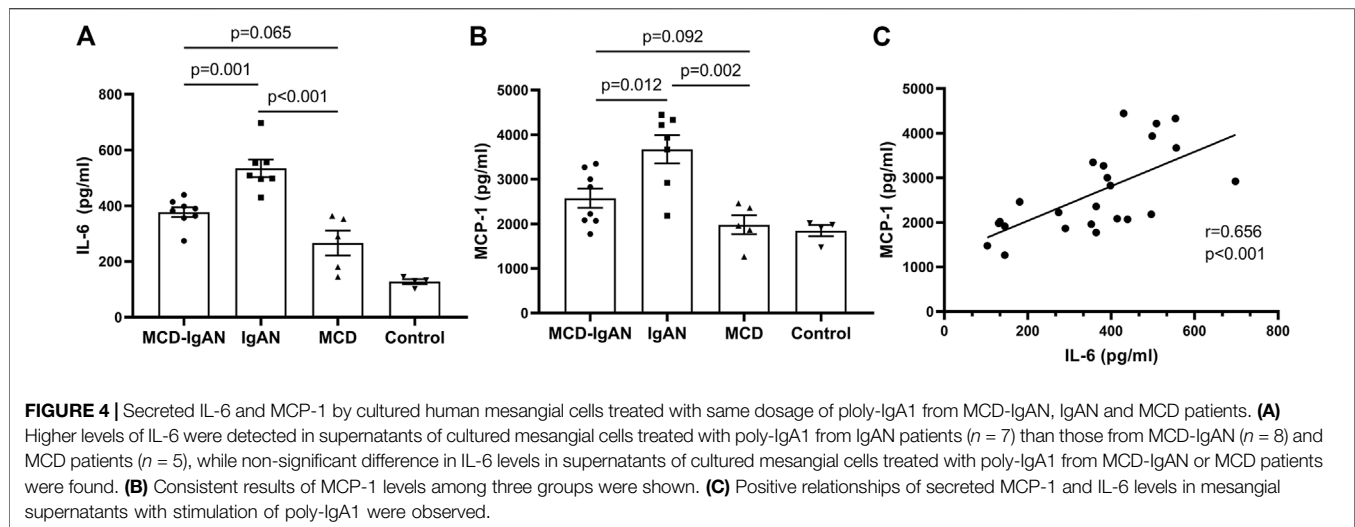
## GdIgA1 and its Autoantibodies on Proteinuria Remission

High risk of progression in IgAN is currently defined as proteinuria >1 g/24 h after therapy in the KDIGO guideline. Furthermore, higher levels of GdIgA1 and its autoantibodies are associated with poor renal outcomes in IgAN patients (Berthoux et al., 2012; Zhao et al., 2012). Here, we tried to analyze the relationship of proteinuria remission with different levels of GdIgA1 or antiglycan antibodies. Among all included patients, sixty-one cases of IgAN patients and twenty-six cases of MCD-IgAN patients were retrospectively followed for $14.3 \pm 7.3$ and $11.1 \pm 8.5$ months, respectively. Five patients (5/61, 8.2%) of the IgAN patients reached to end-stage of kidney disease or more than 30% decrease in eGFR, while none of the MCD-IgAN patients reached above kidney endpoint, and all had stable renal function at the last follow-up. Twenty-five MCD-IgAN patients achieved complete remission (CR) of proteinuria during the follow-up periods; among them, four patients experienced relapsing proteinuria. Kaplan–Meier survive analysis was conducted to estimate different levels of GdIgA1 or its autoantibodies on the effect of CR in MCD-IgAN patients. The results showed neither higher levels of GdIgA1 (log rank $p = 0.34$, **Figure 3A**) nor its antiantibodies (log rank $p = 0.32$, **Figure 3B**) were associated with the time to first CR within MCD-IgAN patients.

## Poly-IgA1 Complexes Purified From MCD-IgAN Patients Had Lower Inflammatory Effect

Plasma poly-IgA1 from eight MCD-IgAN patients, seven non-MCD-IgAN patients, and five MCD patients were purified to stimulate cultured human mesangial cells. Clinical characteristics of these patients were described in **Supplementary Table S2**. Supernatants of treated mesangial cells were collected for IL-6 and MCP-1 detection. We found that poly-IgA1 complex derived from MCD-IgAN patients, IgAN patients, and MCD patients upregulated the excretion of the mesangial cell inflammatory cytokines MCP-1 and IL-6 compared to PBS control. Poly-IgA1 complexes from MCD-IgAN patients induced lower expression of mesangial MCP-1 and IL-6 compared to those from IgAN (MCP-1: $2,574.4 \pm 607.5$ vs. $3,671.8 \pm 835.5$ pg/ml, $p = 0.012$; IL-6: $377.3 \pm 49.5$ vs. $534.3 \pm 83.6$ pg/ml, $p = 0.001$, **Figures 4A,B**) and higher levels of MCP-1 and IL-6 than those in MCD group (MCP-1: $2,574.4 \pm 607.5$ vs. $1,981.8 \pm 474.1$ pg/ml, $p = 0.092$; IL-6: $377.3 \pm 49.5$ vs. $266.3 \pm 99.5$ pg/ml, $p = 0.065$; **Figures 4A,B**). Moreover, levels of MCP-1 in supernatants were positively correlated with IL-6 (correlation coefficient = 0.656, $p < 0.001$; **Figure 4C**). The results indicated that poly-IgA1 from MCD-IgAN patients had weaker inflammatory stimulation to mesangial cells than those from IgAN patients, which was consistent with lower urinary MCP-1/creatinine levels in MCD-IgAN than IgAN patients (**Supplementary Figure S2**).

## DISCUSSION

Whether MCD-IgAN is a variant form of IgAN or simply MCD superimposed on mild underlying IgAN or even with quiescent IgA deposition coincidence of MCD has not been established yet. Although several published studies have described the clinical and pathological features of MCD-IgAN and suggested it as a

**FIGURE 4 |** Secreted IL-6 and MCP-1 by cultured human mesangial cells treated with same dosage of ploly-IgA1 from MCD-IgN, IgAN and MCD patients. **(A)** Higher levels of IL-6 were detected in supernatants of cultured mesangial cells treated with poly-IgA1 from IgAN patients ($n = 7$) than those from MCD-IgAN ($n = 8$) and MCD patients ($n = 5$), while non-significant difference in IL-6 levels in supernatants of cultured mesangial cells treated with poly-IgA1 from MCD-IgAN or MCD patients were found. **(B)** Consistent results of MCP-1 levels among three groups were shown. **(C)** Positive relationships of secreted MCP-1 and IL-6 levels in mesangial supernatants with stimulation of poly-IgA1 were observed.

dual glomerulopathy (Qin et al., 2013; Wang et al., 2013; Woo et al., 2013; Herlitz et al., 2014; Li et al., 2016; Cho et al., 2020), advanced studies on the pathogenesis of MCD-IgAN are rare. In the present study, we explored the comprehensive immune characteristics of MCD-IgAN patients. Compared to IgAN patients, MCD-IgAN patients had lower levels of plasma GdIgA1, IgG antiglycan autoantibodies, and weaker fluorescence intensities of GdIgA1 in the glomerulus than those in IgAN patients. *In vitro*, the inflammatory response of the mesangial cells (IL-6 and MCP-1 production) to poly-IgA1 complex derived from MCD-IgAN patients was significantly lower than that from IgAN participants. Our findings support MCD-IgAN as a dual glomerulopathy, namely, mild IgAN with superimposed MCD from the pathogenesis point of view.

Current studies suggested the development of IgAN as four-hit processes with aberrant glycosylation of IgA1, production of antibodies directed against galactose-deficient IgA1, formation of immune complexes, and accumulation of these complexes in the glomerular mesangium to initiate renal injury (Suzuki et al., 2011). However, with respect to MCD-IgAN, whether it shares the same immunopathogenesis of the four-hit processes as IgAN still needs to be investigated. Until now, only one published study from Cho et al. confirmed positive Gd-IgA1 deposition in the glomeruli of IgAN-MCD patients and inferred that Gd-IgA1 played a role in the pathogenesis of MCD-IgAN and IgAN (Cho et al., 2020). However, this information should be interpreted carefully. First, the frequency of mesangial Gd-IgA1 deposition in healthy donors was as high as 13%–26% (Suzuki et al., 2003; Nakazawa et al., 2019), suggesting quiescent IgA1 deposition was not uncommon (Suzuki et al., 2003; Nakazawa et al., 2019). Secondly and importantly, the glycosylation aberrancy of IgA1 alone is not sufficient to induce renal injury, the autoantibodies levels and biological effects of poly-IgA1 from MCD-IgAN are unknown in Cho's study. Therefore, in this study, we conducted the first comprehensive study and explored the multiple proposed factors that might explain the pathogenesis of MCD-IgAN, including levels of Gd-IgA1, antiglycan antibodies, deposition of Gd-IgA1, and corresponding proinflammatory effects of the

poly-IgA1complexes. We found that MCD-IgAN patients had lower circulating Gd-IgA1 and IgG glycan-specific antibodies, weaker GdIgA1 deposits than age- and gender-matched IgAN patients but higher plasma GdIgA1 than healthy controls. Moreover, purified poly-IgA1 complexes from MCD-IgAN induced weaker effects on mesangial inflammatory cytokines production than those from IgAN while higher cytokine levels than those from MCD. These findings may be related to the relatively indolent nature of IgA deposits, not as pathophysiological as IgAN patients, and mild histological lesions with lower Oxford scores in MCD-IgAN, supporting the lack of typical manifestations of IgAN. Taken together, this study provides immunological evidence supporting that MCD-IgAN represents a dual glomerulopathy, namely, mild IgAN with superimposed MCD, and should be treated in accordance with the guidelines for MCD.

In this study, we found higher Gd-IgA1 but lower anti-GdIgA1 IgG levels in plasma of MCD-IgAN patients compared to that in healthy controls (**Figures 1B,D**). These were because of the higher sensitivity and specificity of GdIgA1 than anti-GdIgA1 antibodies in IgAN. Previous studies indicated that higher levels of IgG autoantibodies were only found in IgAN patients with the highest risk for dialysis or death (Tomana et al., 1999; Moldoveanu et al., 2007; Berthoux et al., 2012), and the MCD-IgAN patients we included were at lower risk for dialysis. Furthermore, in MCD-IgAN patients, due to the loss of IgG from kidney filtration, serum total IgG (5.6 ± 3.5 g/L) was lower than that in healthy controls (7–16 g/L), as well as the IgG autoantibody levels.

Previous studies had demonstrated that the deposited IgA in the glomerulus of IgAN was galactose deficient (Allen et al., 2001; Berthelot et al., 2015; Yasutake et al., 2015), and GdIgA1 but not normal glycosylated IgA1 had high propensity to form complexes with antiglycan IgG antibodies (Suzuki et al., 2009). The contents of serum GdIgA1 play an important role in renal deposition other than total IgA. In our study, we found higher GdIgA1 levels in IgAN patients than MCD-IgAN, which was prone to deposit in kidney. Furthermore, the antibody (antihuman Ig alpha heavy

chain) we used to detect IgA deposition in the kidney can also recognize GdIgA1, so our results showed an increase in IgA deposition in IgAN patients than that in MCD-IgAN patients (**Figure 1B**) despite no difference in plasma IgA1 levels between these groups.

Although in this study we investigated the pathogenesis of MCD-IgAN, there were still several limitations. First, due to the low incidence of MCD-IgAN, this was a small single-center study with limited sample size. Second, because of the lack of appropriate animal models of IgAN and MCD-IgAN, merely *in vitro* experiments were conducted to evaluate the proinflammatory effects of IgA1 complexes from MCD-IgAN.

In conclusion, this is the first study to present a comprehensive and precise profile of immune characteristics in MCD-IgAN participants. The results strongly supported that MCD-IgAN cases represent a dual glomerulopathy, namely, mild IgAN with superimposed MCD, and provided robust evidence for the corticosteroids therapy in MCD-IgAN patients as the guidelines recommended.

## DATA AVAILABILITY STATEMENT

The raw data supporting the conclusion of this article will be made available by the authors, without undue reservation.

## ETHICS STATEMENT

The studies involving human participants were reviewed and approved by the medical ethics committee at the First Affiliated Hospital of Xi'an Jiaotong University. The patients/participants provided their written informed consent to participate in this study.

## AUTHOR CONTRIBUTIONS

XX and HL conceived of the presented idea, developed the study, and performed the experiments. XX contributed to funding acquisition. XL, HL, XZ, YD, and XY assisted the experiments. XX, HL, and WL performed the analysis, drafted the manuscript, and assembled the supplementary figures. PL, WL, and JL revised the manuscript. All authors discussed the results and commented on the manuscript.

## FUNDING

## ACKNOWLEDGMENTS

## SUPPLEMENTARY MATERIAL

The Supplementary Material for this article can be found online at: https://www.frontiersin.org/articles/10.3389/fphar.2021.793511/full#supplementary-material

## REFERENCES

Allen, A. C., Bailey, E. M., Brenchley, P. E., Buck, K. S., Barratt, J., and Feehally, J. (2001). Mesangial IgA1 in IgA Nephropathy Exhibits Aberrant O-Glycosylation: Observations in Three Patients. *Kidney Int.* 60 (3), 969–973. doi:10.1046/j.1523-1755.2001.060003969.x

Barratt, J., and Feehally, J. (2006). Treatment of IgA Nephropathy. *Kidney Int.* 69 (11), 1934–1938. doi:10.1038/sj.ki.5000419

Berthelot, L., Robert, T., Vuiblet, V., Tabary, T., Braconnier, A., Dramé, M., et al. (2015). Recurrent IgA Nephropathy is Predicted by Altered Glycosylated IgA, Autoantibodies and Soluble CD89 Complexes. *Kidney Int.* 88 (4), 815–822. doi:10.1038/ki.2015.158

Berthoux, F., Suzuki, H., Thibaudin, L., Yanagawa, H., Maillard, N., Mariat, C., et al. (2012). Autoantibodies Targeting Galactose-Deficient IgA1 Associate with Progression of IgA Nephropathy. *J. Am. Soc. Nephrol.* 23 (9), 1579–1587. doi:10.1681/ASN.2012010053

Cho, W. H., Park, S. H., Choi, S. K., Jung, S. W., Jeong, K. H., Kim, Y. G., et al. (2020). Characterization of IgA Deposition in the Kidney of Patients with IgA Nephropathy and Minimal Change. *J. Clin. Med.* 9 (8), 2619. doi:10.3390/jcm9082619

D'Amico, G. (2004). Natural History of Idiopathic IgA Nephropathy and Factors Predictive of Disease Outcome. *Semin. Nephrol.* 24 (3), 179–196. doi:10.1016/j.semnephrol.2004.01.001

Floege, J., Barbour, S. J., Cattran, D. C., Hogan, J. J., Nachman, P. H., Tang, S. C. W., et al. (2019). Management and Treatment of Glomerular Diseases (Part 1): Conclusions from a Kidney Disease: Improving Global Outcomes (KDIGO) Controversies Conference. *Kidney Int.* 95 (2), 268–280. doi:10.1016/j.kint.2018.10.018

Herlitz, L. C., Bomback, A. S., Stokes, M. B., Radhakrishnan, J., D'Agati, V. D., and Markowitz, G. S. (2014). IgA Nephropathy with Minimal Change Disease. *Clin. J. Am. Soc. Nephrol.* 9 (6), 1033–1039. doi:10.2215/CJN.11951113

Kim, J. K., Kim, J. H., Lee, S. C., Kang, E. W., Chang, T. I., Moon, S. J., et al. (2012). Clinical Features and Outcomes of IgA Nephropathy with Nephrotic Syndrome. *Clin. J. Am. Soc. Nephrol.* 7 (3), 427–436. doi:10.2215/cjn.04820511

Kim, S. M., Moon, K. C., Oh, K. H., Joo, K. W., Kim, Y. S., Ahn, C., et al. (2009). Clinicopathologic Characteristics of IgA Nephropathy with Steroid-Responsive Nephrotic Syndrome. *J. Korean Med. Sci.* 24 (Suppl. 1), S44–S49. doi:10.3346/jkms.2009.24.S1.S44

Lai, K. N., Tang, S. C., Schena, F. P., Novak, J., Tomino, Y., Fogo, A. B., et al. (2016). IgA Nephropathy. *Nat. Rev. Dis. Primers* 2, 16001. doi:10.1038/nrdp.2016.1

Li, X. W., Liang, S. S., Le, W. B., Cheng, S. Q., Zeng, C. H., Wang, J. Q., et al. (2016). Long-term Outcome of IgA Nephropathy with Minimal Change Disease: a Comparison between Patients with and without Minimal Change Disease. *J. Nephrol.* 29 (4), 567–573. doi:10.1007/s40620-015-0242-9

Moldoveanu, Z., Wyatt, R. J., Lee, J. Y., Tomana, M., Julian, B. A., Mestecky, J., et al. (2007). Patients with IgA Nephropathy Have Increased Serum Galactose-Deficient IgA1 Levels. *Kidney Int.* 71 (11), 1148–1154. doi:10.1038/sj.ki.5002185

Nakazawa, S., Imamura, R., Kawamura, M., Kato, T., Abe, T., Namba, T., et al. (2019). Difference in IgA1 O-Glycosylation between IgA Deposition Donors and IgA Nephropathy Recipients. *Biochem. Biophys. Res. Commun.* 508 (4), 1106–1112. doi:10.1016/j.bbrc.2018.12.014

Novak, J., Tomana, M., Matousovic, K., Brown, R., Hall, S., Novak, L., et al. (2005). IgA1-containing Immune Complexes in IgA Nephropathy Differentially Affect Proliferation of Mesangial Cells. *Kidney Int.* 67 (2), 504–513. doi:10.1111/j.1523-1755.2005.67107.x

Qin, J., Yang, Q., Tang, X., Chen, W., Li, Z., Mao, H., et al. (2013). Clinicopathologic Features and Treatment Response in Nephrotic IgA Nephropathy with Minimal Change Disease. *Clin. Nephrol.* 79 (1), 37–44. doi:10.5414/cn107682

Rizk, D. V., Saha, M. K., Hall, S., Novak, L., Brown, R., Huang, Z. Q., et al. (2019). Glomerular Immunodeposits of Patients with IgA Nephropathy are Enriched for IgG Autoantibodies Specific for Galactose-Deficient IgA1. *J. Am. Soc. Nephrol.* 30 (10), 2017–2026. doi:10.1681/ASN.2018111156

Suzuki, H., Fan, R., Zhang, Z., Brown, R., Hall, S., Julian, B. A., et al. (2009). Aberrantly Glycosylated IgA1 in IgA Nephropathy Patients is Recognized by IgG Antibodies with Restricted Heterogeneity. *J. Clin. Invest.* 119 (6), 1668–1677. doi:10.1172/JCI38468

Suzuki, H., Kiryluk, K., Novak, J., Moldoveanu, Z., Herr, A. B., Renfrow, M. B., et al. (2011). The Pathophysiology of IgA Nephropathy. *J. Am. Soc. Nephrol.* 22 (10), 1795–1803. doi:10.1681/ASN.2011050464

Suzuki, K., Honda, K., Tanabe, K., Toma, H., Nihei, H., and Yamaguchi, Y. (2003). Incidence of Latent Mesangial IgA Deposition in Renal Allograft Donors in Japan. *Kidney Int.* 63 (6), 2286–2294. doi:10.1046/j.1523-1755.63.6s.2.x

Thompson, A., Carroll, K., A Inker, L. L., Floege, J., Perkovic, V., Boyer-Suavet, S., et al. (2019). Proteinuria Reduction as a Surrogate End Point in Trials of IgA Nephropathy. *Clin. J. Am. Soc. Nephrol.* 14 (3), 469–481. doi:10.2215/CJN.08600718

Tomana, M., Novak, J., Julian, B. A., Matousovic, K., Konecny, K., and Mestecky, J. (1999). Circulating Immune Complexes in IgA Nephropathy Consist of IgA1 with Galactose-Deficient Hinge Region and Antiglycan Antibodies. *J. Clin. Invest.* 104 (1), 73–81. doi:10.1172/jci5535

Wang, J., Juan, C., Huang, Q., Zeng, C., and Liu, Z. (2013). Corticosteroid Therapy in IgA Nephropathy with Minimal Change-Like Lesions: a Single-Centre Cohort Study. *Nephrol. Dial. Transpl.* 28 (9), 2339–2345. doi:10.1093/ndt/gft211

Wang, Z., Zhang, X., Han, W., Yu, G., Ying, Z., Xu, X., et al. (2021). Immune Characteristics of Renal Allograft Donors with Mesangial IgA Deposition. *Int. Immunopharmacol.* 91, 107282. doi:10.1016/j.intimp.2020.107282

Westhoff, T. H., Waldherr, R., Loddenkemper, C., Ries, W., Zidek, W., and van der Giet, M. (2006). Mesangial IgA Deposition in Minimal Change Nephrotic Syndrome: Coincidence of Different Entities or Variant of Minimal Change Disease? *Clin. Nephrol.* 65 (3), 203–207. doi:10.5414/cnp65203

Woo, K. T., Wong, K. S., Choong, H. L., Foo, M., Chin, Y. M., and Chan, C. M. (2013). Clinicopathologic Features and Treatment Response in Nephrotic IgA Nephropathy with Minimal Change Disease. *Clin. Nephrol.* 80 (1), 79. doi:10.5414/cn108008

Wyatt, R. J., and Julian, B. A. (2013). IgA Nephropathy. *N. Engl. J. Med.* 368 (25), 2402–2414. doi:10.1056/NEJMra1206793

Yasutake, J., Suzuki, Y., Suzuki, H., Hiura, N., Yanagawa, H., Makita, Y., et al. (2015). Novel Lectin-independent Approach to Detect Galactose-Deficient IgA1 in IgA Nephropathy. *Nephrol. Dial. Transpl.* 30 (8), 1315–1321. doi:10.1093/ndt/gfv221

Zhang, H., and Barratt, J. (2021). Is IgA Nephropathy the Same Disease in Different Parts of the World? *Semin. Immunopathol* 43, 707–715. doi:10.1007/s00281-021-00884-7

Zhang, X., Xie, X., Shi, S., Liu, L., Lv, J., and Zhang, H. (2019). Plasma Galactose-Deficient Immunoglobulin A1 and Loss of Kidney Function in Patients with Immunoglobulin A Vasculitis Nephritis. *Nephrol. Dial. Transpl.* 35, 2117–2123. doi:10.1093/ndt/gfz151

Zhao, N., Hou, P., Lv, J., Moldoveanu, Z., Li, Y., Kiryluk, K., et al. (2012). The Level of Galactose-Deficient IgA1 in the Sera of Patients with IgA Nephropathy is Associated with Disease Progression. *Kidney Int.* 82 (7), 790–796. doi:10.1038/ki.2012.197

Zhu, L., Zhang, Q., Shi, S., Liu, L., Lv, J., and Zhang, H. (2013). Synergistic Effect of Mesangial Cell-Induced CXCL1 and TGF-B1 in Promoting Podocyte Loss in IgA Nephropathy. *PLoS One* 8 (8), e73425. doi:10.1371/journal.pone.0073425

# Measuring the Concentration of Serum Syndecan-1 to Assess Vascular Endothelial Glycocalyx Injury During Hemodialysis

**\*Correspondence:**
Hideshi Okada
hideshi@gifu-u.ac.jp

† These authors have contributed
equally to this work

**Keigo Kusuzawa**[1†], **Keiko Suzuki**[2†], **Hideshi Okada**[1\*†], **Kodai Suzuki**[1], **Chihiro Takada**[1], **Soichiro Nagaya**[1], **Ryu Yasuda**[1], **Haruka Okamoto**[1], **Takuma Ishihara**[3], **Hiroyuki Tomita**[4], **Yuki Kawasaki**[1], **Toru Minamiyama**[1], **Ayane Nishio**[1], **Hirotsugu Fukuda**[1], **Takuto Shimada**[1], **Yuto Tamaoki**[1], **Tomoki Yoshida**[1], **Yusuke Nakashima**[1], **Naokazu Chiba**[1], **Genki Yoshimura**[1], **Ryo Kamidani**[1], **Tomotaka Miura**[1,2], **Hideaki Oiwa**[1,5], **Fuminori Yamaji**[1], **Yosuke Mizuno**[1], **Takahito Miyake**[1], **Yuichiro Kitagawa**[1], **Tetsuya Fukuta**[1], **Tomoaki Doi**[1], **Akio Suzuki**[6], **Takahiro Yoshida**[1], **Nobuyuki Tetsuka**[2], **Shozo Yoshida**[1,5] and **Shinji Ogura**[1]

[1] Department of Emergency and Disaster Medicine, Gifu University Graduate School of Medicine, Gifu, Japan, [2] Department of Infection Control, Gifu University Graduate School of Medicine, Gifu, Japan, [3] Innovative and Clinical Research Promotion Center, Gifu University Hospital, Gifu, Japan, [4] Department of Tumor Pathology, Gifu University Graduate School of Medicine, Gifu, Japan, [5] Abuse Prevention Center, Gifu University Graduate School of Medicine, Gifu, Japan, [6] Department of Pharmacy, Gifu University Hospital, Gifu, Japan

Glycocalyx is present on the surface of healthy endothelium, and the concentration of serum syndecan-1 can serve as an injury marker. This study aimed to assess endothelial injury using serum syndecan-1 as a marker of endothelial glycocalyx injury in patients who underwent hemodialysis. In this single-center, retrospective, observational study, 145 patients who underwent hemodialysis at the Gifu University Hospital between March 2017 and December 2019 were enrolled. The median dialysis period and time were 63 months and 3.7 h, respectively. The serum syndecan-1 concentration significantly increased from $124.6 \pm 107.8$ ng/ml before hemodialysis to $229.0 \pm 138.1$ ng/ml after hemodialysis ($P < 0.001$). Treatment with anticoagulant nafamostat mesylate inhibited hemodialysis-induced increase in the levels of serum syndecan-1 in comparison to unfractionated heparin. Dialysis time and the change in the syndecan-1 concentration were positively correlated. Conversely, the amount of body fluid removed and the changes in the syndecan-1 concentration were not significantly correlated. The reduction in the amount of body fluid removed and dialysis time inhibited the change in the syndecan-1 levels before and after hemodialysis. In conclusion, quantitative assessment of the endothelial glycocalyx injury during hemodialysis can be performed by measuring the serum syndecan-1 concentration, which may aid in the selection of appropriate anticoagulants, reduction of hemodialysis time, and the amount of body fluid removed.

Keywords: hemodialysis, glycocalyx, syndecan-1, body fluid removal, nafamostat mesylate

# INTRODUCTION

Malnutrition, inflammation, and atherosclerosis are strongly associated with each other in chronic kidney disease (1), and both a malnourished state and atherosclerosis can be caused by inflammation. Moreover, chronic microinflammation is observed in patients who undergo hemodialysis (2). Several factors, such as uremia, activation of free radicals and adhesion molecules, and hemodialysis membrane, can lead to microinflammation in patients who undergo hemodialysis (3–5). Uremic substances and the hemodialysis membrane promote the production of free radicals and cytokines by stimulating neutrophils, and the resulting inflammation further causes endothelial injury. However, there is no method to quantitatively assess endothelial cell injury.

The vascular endothelium is composed of a thin monolayer of endothelial cells, and this lines the entire circulatory system, particularly the parts that are exposed to the circulating blood. The healthy endothelium is covered by a glycoprotein called glycocalyx (6–10), which plays pivotal roles in vascular homeostasis (11, 12). The endothelial glycocalyx is degraded by several factors, such as sepsis, major surgery, trauma, ischemia/reperfusion, and prolonged hyperglycemia. Persistent and diffuse alterations in the glycocalyx are associated with widespread endothelial dysfunction, changed permeability, and impaired oxygen and nutrient delivery to the cells (11, 13, 14). Several studies have revealed the relationship between endothelial glycocalyx injury and serious diseases, such as cardiovascular disease, acute kidney injury, and chronic kidney disease (15, 16). Moreover, the structure of the endothelial glycocalyx is degraded in chronic diseases, such as aging (17), diabetes (18), and hypertriglyceridemia (19).

The glycocalyx comprises cell-bound proteoglycans, glycosaminoglycan side chains, and sialoproteins (13, 20).

The proteoglycans consist of a core protein, such as a member of the syndecan protein family, to which glycosaminoglycan molecules are linked (21). Syndecan-1 is the core protein in heparan sulfate proteoglycan that is observed in the glycocalyx. It is released from the endothelium when the glycocalyx is injured, causing an increase in its concentration in circulation (22). Moreover, serum syndecan-1 has been used as an endothelial injury marker in recent clinical studies in critically ill patients (23–26).

Therefore, the present study aimed to assess endothelial injury using the serum syndecan-1 level as a marker of endothelial glycocalyx injury in patients who underwent hemodialysis. Additionally, we examined the medication type and factors that influence the concentration of syndecan-1.

# METHODS

## Patients

This was a single-center, retrospective, observational study conducted at the Gifu University Hospital, affiliated to Gifu University, Gifu, Japan. Patients, who underwent hemodialysis at the Gifu University Hospital between March 2017 and December 2019 and whose dry weight remained unchanged in the last three examinations, were enrolled. Patients aged <20 years, who underwent plasma apheresis, plasma exchange, and double filtration plasma therapy, and had not maintained their dry weight were excluded. Finally, data from 145 patients were obtained and analyzed (**Figure 1**).

## Ethics Approval and Consent to Participate

The study conformed to the principles outlined in the Declaration of Helsinki (43). Ethics approval was obtained from the Medical Ethics Committee of the Gifu University Graduate



**FIGURE 1 |** Flow diagram for the selection of study participants for data analysis.
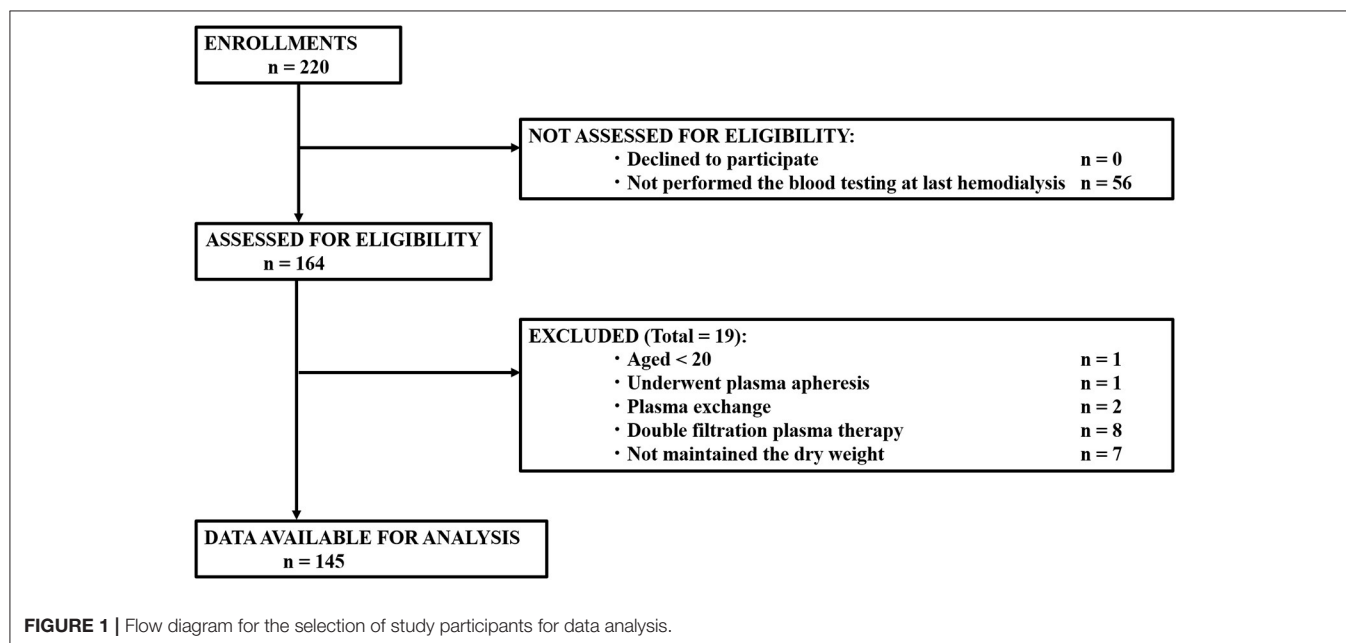
School of Medicine, Gifu, Japan (approval no.: 2021-A005). The need for informed consent from participants was waived by the medical ethics committee because of the retrospective nature of the study. Before initiation, the study was registered in the UMIN Clinical Trials Registry (registry number: UMIN000 051415).

## Data Collection and Study Design

Blood was routinely sampled before and after hemodialysis from eligible patients at the time of the last hemodialysis before being discharged from Gifu University Hospital, and data from these blood samples were used in the present study. All laboratory data (except serum syndecan-1), dry weight, and other patient demographics were extracted from the hospital's electronic medical records. The concentration of serum syndecan-1 was measured using an enzyme-linked immunosorbent assay (950.640.192; Diaclone, Besancon, Cedex, France). The data were retrospectively analyzed. As an index of the efficiency of dialysis, Kt/V was calculated as described previously (44).

## Statistical Analysis

The sample size in this study was calculated to obtain sufficient amount of data and conditions to avoid overfitting in multivariable regression analysis. It was necessary to collect at least 90 patients to estimate the parameters of the six covariates, including the interaction term in the multivariable regression model (45). Patients' baseline characteristics are presented as medians and interquartile ranges for continuous variables, and as frequencies and proportions for categorical variables. For the primary analysis, a mixed effect model was used to assess the change in the syndecan-1 levels with hemodialysis. The difference in the syndecan-1 levels before and after hemodialysis in the anticoagulant subgroup was confirmed using paired $t$-test. A multivariable linear regression analysis was performed to compare the change in the syndecan-1 levels before/after hemodialysis and treatment with anticoagulants. The covariates in the regression model were age, sex, dry weight, and dialysis period (46). These variables were selected *a priori* based on previous studies. In another model, dry weight and dialysis period were simultaneously incorporated into the linear regression model to evaluate the effect of factors during dialysis on the levels of syndecan-1. An interaction term was included in the model to confirm the effect of modification of dry weight and dialysis period on changes in the levels of syndecan-1. If the interaction term was statistically significant, the effect of the dialysis period (or dry weight) on syndecan-1 was determined to be modified by dry weight (or the dialysis period). There were no missing values in the data used in the analyses. A two-sided $P$-value $< 0.05$ was considered to be statistically significant. The study was exploratory and there were concerns concerning the low statistical power; therefore, the interaction was evaluated with a two-sided $P < 0.1$. R version 4.1.0 was used for statistical analyses (R Foundation for Statistical Computing, Vienna, Austria).

**TABLE 1 |** Patient demographics.

| Characteristics | Median (range) or number |
|---|---|
| Number of cases, $n$ | 145 |
| Age (years), mean (IQR) | 68 (60–77) |
| Sex (female/male), $n$ (%) | 44 (30.3)/101 (69.7) |
| Dialysis period (months), median (IQR) | 20.0 (1.0–87.0) |
| Dialysis time (h), median (IQR) | 4.0 (3.0–4.0) |
| Systolic blood pressure before dialysis (mmHg), median (IQR) | 136.0 (121.0–157.0) |
| Diastolic blood pressure before dialysis (mmHg), median (IQR) | 69.0 (59.0–79.0) |
| Primary illness, $n$ (%) | |
| Chronic glomerulonephritis | 29 (20.0) |
| Rapidly progressive glomerulonephritis | 4 (2.8) |
| Polycystic kidney disease | 8 (5.5) |
| Nephrosclerosis | 8 (5.5) |
| Diabetic nephropathy | 37 (25.5) |
| Nephritis with autoimmune disease | 6 (4.1) |
| Renal/urological tumor | 5 (3.4) |
| Obstructive urinary tract/urination disorders | 1 (0.7) |
| Paraproteinemia (myeloma) | 1 (0.7) |
| Acute kidney injury | 10 (6.9) |
| Congenital anomalies of the kidney and urinary tract | 1 (0.7) |
| Unknown | 33 (22.8) |
| Others | 2 (1.4) |
| Hemodialysis type, $n$ (%) | |
| HD | 133 (91.7) |
| HDF | 12 (8.3) |
| Vascular access type, $n$ (%) | |
| Arteriovenous fistula | 107 (73.8) |
| Arteriovenous graft | 8 (5.5) |
| Temporary vascular catheter | 23 (15.9) |
| Permanent vascular catheter | 7 (4.8) |
| Dialysis efficiency | |
| Kt/V | 1.20 (0.06–1.86) |
| Medication, $n$ (%) | |
| Unfractionated heparin | 101 (69.7) |
| Low-molecular-weight heparin | 24 (16.6) |
| Nafamostat mesylate | 20 (13.8) |
| Dialysis membrane, $n$ (%) | |
| Polyethersulfone | 110 (75.9) |
| Polysulfone | 34 (23.4) |
| Asymmetric triacetate | 1 (0.7) |

*HD, hemodialysis; HDF, hemodiafiltration; IQR, interquartile range.*

## RESULTS

## Characteristics of Patients

We finally enrolled 145 patients with a median age of 66 years (**Figure 1**; **Table 1**). The median dialysis period and time were 63 months and 3 h and 45 min, respectively. The most common primary illness was diabetic nephropathy, which was observed in 37 patients (25.5%).

TABLE 2 | Serum SDC-1 concentration before and after hemodialysis.

| Status | SDC-1 concentration (ng/ml) | P-value |
|--------|-----------------------------|---------|
| Before HD | 124.6 ± 107.8 | <0.001 |
| After HD | 229.0 ± 138.1 | |

*SDC-1, syndecan-1; HD, hemodialysis. P-values were obtained from a mixed-effects model.*

TABLE 3 | Serum SDC-1 concentration and anticoagulants.

| Anticoagulants | Before HD (ng/ml) | After HD (ng/ml) | P-value |
|----------------|-------------------|------------------|---------|
| Unfractionated heparin | 112.0 ± 79.8 | 235.4 ± 126.8* | <0.001 |
| Low-molecular-weight heparin | 144.1 ± 135.8 | 248.5 ± 174.1* | <0.001 |
| Nafamostat mesylate | 164.2 ± 171.1 | 173.3 ± 141.3 | 0.459 |

*SDC-1, syndecan-1; HD, hemodialysis.*
*Statistically significant (P < 0.05).*

The number of patients who underwent hemodialysis and hemodiafiltration was 133 (91.7%) and 12 (8.3%), respectively. Anticoagulation agents, such as unfractionated heparin, low-molecular-weight heparin, and nafamostat mesylate, were administered to 101, 24, and 20 patients, respectively. The median Kt/V-value, an index of dialysis efficiency, was 1.20.

## Concentration of Serum Syndecan-1 and Hemodialysis

The concentrations of serum syndecan-1 before and after hemodialysis were 124.6 ± 107.8 and 229.0 ± 138.1 ng/ml, respectively; this indicated that the serum syndecan-1 concentration significantly increased ($P < 0.001$) after hemodialysis (**Table 2**).

The concentration of serum syndecan-1 significantly increased after hemodialysis in patients who received unfractionated heparin and low-molecular-weight heparin; however, the concentration of syndecan-1 was not significantly different before and after hemodialysis in those who received nafamostat mesylate (**Table 3**).

Additionally, according to the multivariable regression analysis after adjusting for age, sex, dry weight, and dialysis period, the treatment with nafamostat mesylate inhibited the increase in the concentration of serum syndecan-1 during hemodialysis compared to treatment with unfractionated heparin and low-molecular-weight heparin (**Table 4**).

Interestingly, there was no strong relationship between the syndecan-1 levels and blood pressure (**Supplementary Table 1**), vascular access (**Supplementary Table 2**), cardiovascular disease (**Supplementary Table 3**), and primary disease (**Supplementary Table 4**) before and after dialysis.

## Association of Concentration of Serum Syndecan-1 With Dialysis Time and Body Fluid Removal

The relationship between the concentration variability of syndecan-1 and the dialysis condition, including the dialysis time

and the amount of body fluid removed, was confirmed. The amount of body fluid removal was corrected by the dry weight. The dialysis time and change in concentration of syndecan-1 showed a positive correlation ($P = 0.033$), but there was no significant association ($P = 0.111$) between the amount of body fluid removed and the syndecan-1 concentration changes (**Table 5**).

Next, we examined the modifying effect of the amount of body fluid removed on the association between the change in the concentration of syndecan-1 and dialysis time. The change in the syndecan-1 concentration before and after hemodialysis increased with respect to enhanced removal of body fluids and prolonged dialysis time ($P$ for interaction $= 0.063$, **Figure 2**). However, the change in the syndecan-1 concentration before and after hemodialysis decreased with respect to a decrease in the amount of body fluid removed and shortened dialysis time.

## DISCUSSION

The present study revealed the following: (a) the endothelial glycocalyx may be injured during hemodialysis; (b) endothelial glycocalyx injury may be attenuated by administering nafamostat mesylate as an anticoagulant; and (c) endothelial glycocalyx injury may be aggravated by an increase in the amount of body fluid removed and prolonged dialysis time.

A previous study reported that the serum syndecan-1 concentration was approximately 20 ng/ml in healthy individuals (19); in contrast, in this study, it was found to be 124.6 ± 107.8 ng/ml in patients who underwent hemodialysis. This result confirmed that the endothelial glycocalyx sustained injuries in patients who underwent hemodialysis, consistent with the findings of a previous report (27). This indicates that endothelial glycocalyx injury may be aggravated by an increasing fluid volume.

Moreover, the serum syndecan-1 concentration increased after hemodialysis compared to the corresponding value before hemodialysis. This finding suggested that the endothelial glycocalyx was injured during hemodialysis, probably because of the production of free radicals and cytokines during this procedure.

During hemodialysis, unfractionated heparin, low-molecular-weight heparin, and nafamostat mesylate were used as anticoagulating agents. Low-molecular-weight heparin and nafamostat were administered to patients that had any disease that was associated with bleeding tendencies. Our results suggested that an increase in the syndecan-1 concentration was attenuated in patients who received nafamostat mesylate.

Nafamostat mesylate, a synthetic serine protease inhibitor, is a short-acting anticoagulant (28), and is also used during hemodialysis to prevent proteolysis of fibrinogen into fibrin (29). It is a slow, tight-binding substrate that traps the target protein in the acyl-enzyme intermediate form and inhibits enzyme activity (30, 31). It was previously reported that nafamostat mesylate can inhibit the kallikrein-kinin system, which promoted vascular permeability via the produced bradykinin (32–34). In addition, nafamostat has been recently identified as a potential therapy

| Anticoagulants | Coefficient* | 95% LCL | 95% UCL | P-value |
|---|---|---|---|---|
| Low-molecular-weight heparin vs. unfractionated heparin | −18.07 | −56.776 | 20.637 | 0.358 |
| Nafamostat mesylate vs. unfractionated heparin | −116.473 | −158.442 | −74.504 | <0.001 |
| Nafamostat mesylate vs. low-molecular-weight heparin | −98.403 | −150.482 | −45.324 | <0.001 |

*LCL, lower confidence limit; UCL, upper confidence limit.*
*\*Coefficients from the multivariable linear regression model adjusted for age, sex, dry weight, and dialysis period, shown as differences in the serum syndecan-1 concentration for low-molecular-weight heparin vs. unfractionated heparin, nafamostat mesylate vs. unfractionated heparin, and nafamostat mesylate vs. low-molecular-weight heparin, respectively.*

**TABLE 5 |** Relationship between syndecan-1 concentration variability and dialysis conditions.

| Factors | Coefficient* | 95% LCL | 95% UCL | P-value |
|---|---|---|---|---|
| Body fluid removed/dry weight (per 0.01 L/kg increase) | 9.107 | 0.144 | 18.07 | 0.111 |
| Dialysis time (per 1 min increase) | 23.349 | −8.836 | 55.533 | 0.033 |

*LCL, lower confidence limit; UCL, upper confidence limit.*
*\*Coefficients from the multivariable linear regression model adjusted for age, sex, and dialysis period, shown as increment in the serum syndecan-1 concentration for a unit change in factors.*
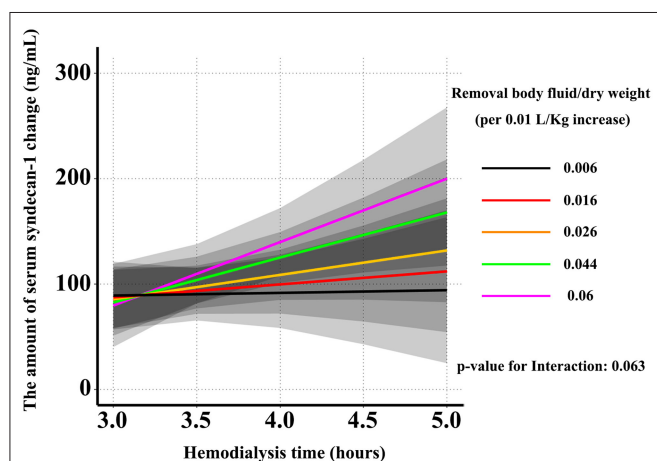


**FIGURE 2 |** Effect of dialysis time and the amount of body fluid removed on the change in the serum syndecan-1 concentration. The change in the concentration of syndecan-1 before and after hemodialysis increased with respect to the enhanced body fluid removal and prolonged dialysis time. However, the change in the concentration of syndecan-1 before and after hemodialysis decreased with respect to the decreased amount of body fluid removal and the shortened dialysis time.

against the coronavirus disease (35). Infection with severe acute respiratory syndrome coronavirus 2 induces endotheliitis due to viral involvement and inflammatory response of the host and, thus, it is associated with endothelial glycocalyx injury (21). Therefore, nafamostat mesylate may have a beneficial effect on the endothelial glycocalyx, although this is supported only by circumstantial evidence.

Extension of dialysis time is a strategy to improve prognosis (36); however, it remains controversial (36, 37). The present study identified that changes in the serum syndecan-1 levels are small in patients who have prolonged dialysis time and slow removal of body fluid. Therefore, these two strategies could prevent endothelial glycocalyx injury. Several reports have also revealed that prolonged hemodialysis was associated with improved blood pressure and fluid management (38–40). Additionally, rapid removal of body fluid is associated with a greater risk of mortality and cardiovascular events (41). Moreover, hypotension during hemodialysis is also associated with higher mortality (42).

These mechanisms may explain how lower ultrafiltration rates with prolonged hemodialysis and slow removal of body fluids may ameliorate endothelial vascular permeability via attenuation of endothelial glycocalyx injury. Therefore, we propose that slow removal of body fluids with prolonged hemodialysis can reduce hypotension during hemodialysis.

This study had some limitations. First, the hemodialysis time in most patients was <4 h. Therefore, an accurate examination of prolonged hemodialysis could not be performed. Second, less types of dialyzer were used in the present study. Third, in this study, other biomarkers of glycocalyx injury, such as the serum hyaluronan and hyaluronidase levels, were not measured. Although further studies are required, measuring the concentration of serum syndecan-1 may help assessing endothelial injury under low blood flow (e.g., chronic hemodiafiltration) and membrane compatibility by using a different type of dialyzer. Moreover, the serum syndecan-1 level is proposed to be a useful biomarker for daily monitoring of organ dysfunction, and may be an important risk factor for mortality in critically ill patients (25).

In conclusion, the study presented a method for the quantitative assessment of endothelial glycocalyx injury by measuring the concentration of serum syndecan-1 during hemodialysis. Although hemodialysis causes endothelial glycocalyx injury, it may be mitigated by maintenance of hemodialysis duration and by modulation of the amount of body fluid removed via the quantitative assessment of the serum syndecan-1 level.

## DATA AVAILABILITY STATEMENT

The raw data supporting the conclusions of this article will be made available by the authors, without undue reservation.

## ETHICS STATEMENT

Ethics approval was obtained from the Medical Ethics Committee of the Gifu University Graduate School of Medicine, Gifu, Japan (record no.: 2021-A005). Written informed consent for participation was not required for this study in accordance with the national legislation and the institutional requirements.

## AUTHOR CONTRIBUTIONS

KK and HOkad wrote the manuscript. KK, KoS, SN, HOkam, GY, RK, and TMiu collected the blood samples. FY, HOi, CT, YKa, TMin, AN, HF, TS, YT, ToY, YN, and NC measured the syndecan-1 concentration using ELISA. KeS and RY created a database. TI performed a statistical analysis. YM, TMiy, YKi, TF, TD, and TaY treated the patients. HT, SY, and SO supervised the study. HOkad and AS revised and edited the

manuscript. All authors contributed to the article and approved the submitted version.

## SUPPLEMENTARY MATERIAL

The Supplementary Material for this article can be found online at: https://www.frontiersin.org/articles/10.3389/fmed.2021.791309/full#supplementary-material

## REFERENCES

1. Stenvinkel P, Heimbürger O, Paultre F, Diczfalusy U, Wang T, Berglund L, et al. Strong association between malnutrition, inflammation, and atherosclerosis in chronic renal failure. *Kidney Int.* (1999) 55:1899–911. doi: 10.1046/j.1523-1755.1999.00422.x

2. Zimmermann J, Herrlinger S, Pruy A, Metzger T, Wanner C. Inflammation enhances cardiovascular risk and mortality in hemodialysis patients. *Kidney Int.* (1999) 55:648–58. doi: 10.1046/j.1523-1755.1999.00273.x

3. Kultz D. Hyperosmolality triggers oxidative damage in kidney cells. *Proc Natl Acad Sci USA.* (2004) 101:9177–8. doi: 10.1073/pnas.0403241101

4. Rashid G, Benchetrit S, Fishman D, Bernheim J. Effect of advanced glycation end-products on gene expression and synthesis of TNF-alpha and endothelial nitric oxide synthase by endothelial cells. *Kidney Int.* (2004) 66:1099–106. doi: 10.1111/j.1523-1755.2004.00860.x

5. Kawabata K, Nakai S, Miwa M, Sugiura T, Otsuka Y, Shinzato T, et al. CD31 expression on leukocytes is downregulated *in vivo* during hemodialysis. *Nephron.* (2001) 89:153–60. doi: 10.1159/000046062

6. Ando Y, Okada H, Takemura G, Suzuki K, Takada C, Tomita H, et al. Brain-specific ultrastructure of capillary endothelial glycocalyx and its possible contribution for blood brain barrier. *Sci Rep.* (2018) 8:17523. doi: 10.1038/s41598-018-35976-2

7. Becker BF, Chappell D, Jacob M. Endothelial glycocalyx and coronary vascular permeability: the fringe benefit. *Basic Res Cardiol.* (2010) 105:687–701. doi: 10.1007/s00395-010-0118-z

8. Inagawa R, Okada H, Takemura G, Suzuki K, Takada C, Yano H, et al. Ultrastructural alteration of pulmonary capillary endothelial glycocalyx during endotoxemia. *Chest.* (2018) 154:317–25. doi: 10.1016/j.chest.2018.03.003

9. Okada H, Takemura G, Suzuki K, Oda K, Takada C, Hotta Y, et al. Three-dimensional ultrastructure of capillary endothelial glycocalyx under normal and experimental endotoxemic conditions. *Crit Care.* (2017) 21:261. doi: 10.1186/s13054-017-1841-8

10. Rehm M, Zahler S, Lötsch M, Welsch U, Conzen P, Jacob M, et al. Endothelial glycocalyx as an additional barrier determining extravasation of 6% hydroxyethyl starch or 5% albumin solutions in the coronary vascular bed. *Anesthesiology.* (2004) 100:1211–23. doi: 10.1097/00000542-200405000-00025

11. Chelazzi C, Villa G, Mancinelli P, De Gaudio AR, Adembri C. Glycocalyx and sepsis-induced alterations in vascular permeability. *Crit Care.* (2015) 19:26. doi: 10.1186/s13054-015-0741-z

12. Woodcock TE, Woodcock TM. Revised Starling equation and the glycocalyx model of transvascular fluid exchange: an improved paradigm for prescribing intravenous fluid therapy. *Br J Anaesth.* (2012) 108:384–94. doi: 10.1093/bja/aer515

13. Salmon AH, Satchell SC. Endothelial glycocalyx dysfunction in disease: albuminuria and increased microvascular permeability. *J Pathol.* (2012) 226:562–74. doi: 10.1002/path.3964

14. Henrich M, Gruss M, Weigand MA. Sepsis-induced degradation of endothelial glycocalix. *ScientificWorldJournal.* (2010) 10:917–23. doi: 10.1100/tsw.2010.88

15. Liborio AB, Braz MB, Seguro AC, Meneses GC, Neves FM, Pedrosa DC, et al. Endothelial glycocalyx damage is associated with leptospirosis acute kidney injury. *Am J Trop Med Hyg.* (2015) 92:611–6. doi: 10.4269/ajtmh.14-0232

16. Padberg JS, Wiesinger A, di Marco GS, Reuter S, Grabner A, Kentrup D, et al. Damage of the endothelial glycocalyx in chronic kidney disease. *Atherosclerosis.* (2014) 234:335–43. doi: 10.1016/j.atherosclerosis.2014.03.016

17. Machin DR, Bloom SI, Campbell RA, Phuong TTT, Gates PE, Lesniewski LA, et al. *Advanced age results in a diminished endothelial glycocalyx Am J Physiol Heart Circ Physiol.* (2018) 315:H531–9. doi: 10.1152/ajpheart.00104.2018

18. Nieuwdorp M, van Haeften TW, Gouverneur MC, Mooij HL, van Lieshout MH, Levi M, et al. Loss of endothelial glycocalyx during acute hyperglycemia coincides with endothelial dysfunction and coagulation activation *in vivo*. *Diabetes.* (2006) 55:480–6. doi: 10.2337/diabetes.55.02.06.db05-1103

19. Oda K, Okada H, Suzuki A, Tomita H, Kobayashi R, Sumi K, et al. Factors enhancing serum syndecan-1 concentrations: a large-scale comprehensive medical examination. *J Clin Med.* (2019) 8:1320. doi: 10.3390/jcm8091320

20. Paulus P, Jennewein C, Zacharowski K. Biomarkers of endothelial dysfunction: can they help us deciphering systemic inflammation and sepsis? *Biomarkers.* (2011) 16:S11–21. doi: 10.3109/1354750X.2011.587893

21. Okada H, Yoshida S, Hara A, Ogura S, Tomita H. Vascular endothelial injury exacerbates coronavirus disease 2019: the role of endothelial glycocalyx protection. *Microcirculation.* (2021) 28:e12654. doi: 10.1111/micc.12654

22. Rehm M, Bruegger D, Christ F, Conzen P, Thiel M, Jacob M, et al. Shedding of the endothelial glycocalyx in patients undergoing major vascular

surgery with global and regional ischemia. *Circulation*. (2007) 116:1896–906. doi: 10.1161/CIRCULATIONAHA.106.684852

23. Ostrowski SR, Haase N, Müller RB, Møller MH, Pott FC, Perner A, et al. Association between biomarkers of endothelial injury and hypocoagulability in patients with severe sepsis: a prospective study. *Crit Care*. (2015) 19:191. doi: 10.1186/s13054-015-0918-5

24. Puskarich MA, Cornelius DC, Tharp J, Nandi U, Jones AE. Plasma syndecan-1 levels identify a cohort of patients with severe sepsis at high risk for intubation after large-volume intravenous fluid resuscitation. *J Crit Care*. (2016) 36:125–9. doi: 10.1016/j.jcrc.2016.06.027

25. Suzuki K, Okada H, Sumi K, Tomita H, Kobayashi R, Ishihara T, et al. Serum syndecan-1 reflects organ dysfunction in critically ill patients. *Sci Rep*. (2021) 11:8864. doi: 10.1038/s41598-021-88303-7

26. Suzuki K, Okada H, Tomita H, Sumi K, Kakino Y, Yasuda R, et al. Possible involvement of Syndecan-1 in the state of COVID-19 related to endothelial injury. *Thromb J*. (2021) 19:5. doi: 10.1186/s12959-021-00258-x

27. Berg S, Golster M, Lisander B. Albumin extravasation and tissue washout of hyaluronan after plasma volume expansion with crystalloid or hypooncotic colloid solutions. *Acta Anaesthesiol Scand*. (2002) 46:166–72. doi: 10.1034/j.1399-6576.2002.460207.x

28. Al-Horani RA, Desai UR. Recent advances on plasmin inhibitors for the treatment of fibrinolysis-related disorders. *Med Res Rev*. (2014) 34:1168–216. doi: 10.1002/med.21315

29. Sadahiro T, Yuzawa H, Kimura T, Oguchi M, Morito T, Mizushima S, et al. Current practices in acute blood purification therapy in Japan and topics for further study. *Contrib Nephrol*. (2018) 196:209–14. doi: 10.1159/000485724

30. Ramjee MK, Henderson IM, McLoughlin SB, Padova A. The kinetic and structural characterization of the reaction of nafamostat with bovine pancreatic trypsin. *Thromb Res*. (2000) 98:559–69. doi: 10.1016/S0049-3848(00)00206-1

31. Ramjee MK, Patel S. Continuous-flow injection microfluidic thrombin assays: the effect of binding kinetics on observed enzyme inhibition. *Anal Biochem*. (2017) 528:38–46. doi: 10.1016/j.ab.2017.04.016

32. Fujii S, Hitomi Y. New synthetic inhibitors of C1r, C1 esterase, thrombin, plasmin, kallikrein and trypsin. *Biochim Biophys Acta*. (1981) 661:342–5. doi: 10.1016/0005-2744(81)90023-1

33. Hitomi Y, Ikari N, Fujii S. Inhibitory effect of a new synthetic protease inhibitor (FUT-175) on the coagulation system. *Haemostasis*. (1985) 15:164–8. doi: 10.1159/000215139

34. Paques EP, Romisch J. Comparative study on the *in vitro* effectiveness of antithrombotic agents. *Thromb Res*. (1991) 64:11–21. doi: 10.1016/0049-3848(91)90201-7

35. Wang M, Cao R, Zhang L, Yang X, Liu J, Xu M, et al. Remdesivir and chloroquine effectively inhibit the recently emerged novel coronavirus (2019-nCoV) *in vitro*. *Cell Res*. (2020) 30:269–71. doi: 10.1038/s41422-020-0282-0

36. Chertow GM, Levin NW, Beck GJ, Daugirdas JT, Eggers PW, Kliger AS, et al. Long-term effects of frequent in-center hemodialysis. *J Am Soc Nephrol*. (2016) 27:1830–6. doi: 10.1681/ASN.2015040426

37. Rocco MV, Daugirdas JT, Greene T, Lockridge RS, Chan C, Pierratos A, et al. Long-term rffects of frequent nocturnal hemodialysis on mortality: the Frequent Hemodialysis Network (FHN) nocturnal trial. *Am J Kidney Dis*. (2015) 66:459–68. doi: 10.1053/j.ajkd.2015.02.331

38. Burton JO, Jefferies HJ, Selby NM, McIntyre CW. Hemodialysis-induced repetitive myocardial injury results in global and segmental reduction in systolic cardiac function. *Clin J Am Soc Nephrol*. (2009) 4:1925–31. doi: 10.2215/CJN.04470709

39. Lacson E Jr, Xu J, Suri RS, Nesrallah G, Lindsay R, Garg AX, et al. Survival with three-times weekly in-center nocturnal versus conventional hemodialysis. *J Am Soc Nephrol*. (2012) 23:687–95. doi: 10.1681/ASN.2011070674

40. Ok E, Duman S, Asci G, Tumuklu M, Onen Sertoz O, Kayikcioglu M, et al. Comparison of 4- and 8-h dialysis sessions in thrice-weekly in-centre haemodialysis: a prospective, case-controlled study. *Nephrol Dial Transplant*. (2011) 26:1287–96. doi: 10.1093/ndt/gfq724

41. Flythe JE, Kimmel SE, Brunelli SM. Rapid fluid removal during dialysis is associated with cardiovascular morbidity and mortality. *Kidney Int*. (2011) 79:250–7. doi: 10.1038/ki.2010.383

42. Flythe JE, Xue H, Lynch KE, Curhan GC, Brunelli SM. Association of mortality risk with various definitions of intradialytic hypotension. *J Am Soc Nephrol*. (2015) 26:724–34. doi: 10.1681/ASN.2014020222

43. Rickham PP. Human experimentation. Code of ethics of the World Medical Association Declaration of Helsinki. *Br Med J*. (1964) 2:177.

44. Daugirdas JT. Second generation logarithmic estimates of single-pool variable volume Kt/V: an analysis of error. *J Am Soc Nephrol*. (1993) 4:1205–13. doi: 10.1681/ASN.V451205

45. Harrell FE. *Regression Modeling Strategies: With Applications to Linear Models, Logistic and Ordinal Regression, and Survival Analysis*. New York, NY: Springer. (2015). doi: 10.1007/978-3-319-19425-7

46. Koch J, Idzerda NMA, Ettema EM, Kuipers J, Dam W, van den Born J, et al. An acute rise of plasma Na(+) concentration associates with syndecan-1 shedding during hemodialysis. *Am J Physiol Renal Physiol*. (2020) 319:F171–7. doi: 10.1152/ajprenal.00005.2020

# Advantages of publishing in Frontiers

**OPEN ACCESS**
Articles are free to read for greatest visibility and readership

**FAST PUBLICATION**
Around 90 days from submission to decision

**HIGH QUALITY PEER-REVIEW**
Rigorous, collaborative, and constructive peer-review

**TRANSPARENT PEER-REVIEW**
Editors and reviewers acknowledged by name on published articles

**Frontiers**
Avenue du Tribunal-Fédéral 34
1005 Lausanne | Switzerland

**Visit us:** www.frontiersin.org
**Contact us:** frontiersin.org/about/contact

**REPRODUCIBILITY OF RESEARCH**
Support open data and methods to enhance research reproducibility

**DIGITAL PUBLISHING**
Articles designed for optimal readership across devices

**FOLLOW US**
@frontiersin

**IMPACT METRICS**
Advanced article metrics track visibility across digital media

**EXTENSIVE PROMOTION**
Marketing and promotion of impactful research

**LOOP RESEARCH NETWORK**
Our network increases your article's readership